

Aus dem Institut für Pflanzenbau und Pflanzenzüchtung  
der Christian-Albrechts-Universität zu Kiel

**Studying the cyst nematode resistance gene *Hs4* in different  
genomic backgrounds**

Dissertation  
zur Erlangung des Doktorgrades  
der Agrar- und Ernährungswissenschaftlichen Fakultät  
der Christian-Albrechts-Universität zu Kiel

vorgelegt von

M. Sc. Annika Carolin Schildberg

aus Speyer, Germany

Kiel, 2024

---

Dekan: Prof. Dr. Tim Diekötter

1. Berichterstatter: Prof. Dr. Christian Jung

2. Berichterstatter: Prof. Dr. Remco Stam

Tag der mündlichen Prüfung: 29.01.2025



veröffentlicht mit Genehmigung der Agrar- und Ernährungswissenschaftlichen Fakultät

published with the approval of the Faculty of Agricultural and Nutritional Sciences



## Table of Contents

<b>1</b>	<b>Introduction .....</b>	<b>1</b>
1.1	The sugar beet crop .....	1
1.2	The genera <i>Beta</i> and <i>Patellifolia</i> .....	1
1.3	Plant-parasitic nematodes as important pests worldwide .....	4
1.4	The beet cyst nematode <i>Heterodera schachtii</i> .....	5
1.5	Plant-nematode interactions.....	8
1.6	Controlling the beet cyst nematode in the field .....	11
1.7	Resistance to the beet cyst nematode.....	12
1.7.1	Resistance in non-related plant species .....	14
1.7.2	The ultrastructure of syncytia in resistant host plants.....	15
1.7.3	The resistance gene <i>Hs4</i> .....	16
1.8	Aims and Objectives.....	17
<b>2</b>	<b>Homologs of the beet cyst nematode resistance gene <i>Hs4</i> are differentially expressed between <i>Patellifolia</i> and <i>Beta</i> species .....</b>	<b>18</b>
2.1	Materials and Methods .....	18
2.1.1	Plant material and growth conditions .....	18
2.1.2	DNA isolation, PCR, and Sanger sequencing .....	18
2.1.3	DNA and polypeptide sequence analysis .....	19
2.1.4	<i>In vivo</i> nematode infection assay .....	19
2.1.5	Expression analysis.....	19
2.1.6	Statistical analysis.....	20
2.2	Results .....	20
2.2.1	Verifying the <i>Hs4</i> gene structure .....	20
2.2.2	The distribution pattern of <i>Hs4</i> homologs across <i>Patellifolia</i> and <i>Beta</i> species.....	21
2.2.3	Sequence variations between <i>Hs4</i> and its homologs from <i>Patellifolia</i> and <i>Beta</i> species .....	23
2.2.4	Expression patterns of <i>Hs4</i> and its homologs across <i>Beta</i> and <i>Patellifolia</i> species .....	31
2.2.5	Nematode infection does not alter the expression of <i>Hs4</i> and its homolog.....	33
<b>3</b>	<b>The cyst nematode resistance gene <i>Hs4</i> from a wild relative of sugar beet confers resistance in a distantly related species .....</b>	<b>35</b>
3.1	Materials and Methods .....	35
3.1.1	Vector construction.....	35
3.1.2	Arabidopsis transformation and selection of homozygous lines .....	35
3.1.3	Nematode infection assays .....	35
3.1.4	Nucleic acid isolation, PCR, and RT-qPCR conditions.....	36
3.1.5	Statistical analysis.....	37
3.2	Results .....	37
3.2.1	Generating T <sub>3</sub> lines expressing the <i>Hs4</i> gene .....	37
3.2.2	Arabidopsis plants expressing <i>Hs4</i> display an altered phenotype .....	38
3.2.3	Optimizing Arabidopsis resistance tests .....	40
3.2.4	Arabidopsis plants expressing 35S:: <i>Hs4</i> show nematode resistance in an expression-dependent manner - Experiment I.....	40
3.2.5	Arabidopsis plants expressing Hs1:: <i>Hs4</i> show nematode resistance in an expression-dependent manner – Experiment II.....	42

## Table of Contents

3.2.6	Comparison of the effect of different promoters on the <i>Hs4</i> expression and the resulting resistance reaction in Arabidopsis – Experiment III.....	43
3.2.7	Determining the number of transgenes integrated.....	45
3.2.8	Testing the resistance reaction under <i>in vivo</i> conditions .....	46
<b>4</b>	<b>Ultrastructural analysis reveals differences between syncytia of wild type and <i>Hs4</i>-expressing Arabidopsis .....</b>	<b>51</b>
<b>4.1</b>	<b>Materials and Methods .....</b>	<b>51</b>
4.1.1	Plant material and nematode infection .....	51
4.1.2	Microscopic analysis .....	51
<b>4.2</b>	<b>Results .....</b>	<b>52</b>
4.2.1	Comparative analysis of non-inoculated roots .....	53
4.2.2	Syncytia induced in Col-0 .....	55
4.2.3	Syncytia induced in <i>Hs4</i> -transgenic plants.....	59
<b>4.3</b>	<b>Concluding summary .....</b>	<b>75</b>
<b>5</b>	<b>Generation of <i>Hs4</i>-expressing rapeseed .....</b>	<b>76</b>
<b>5.1</b>	<b>Materials and Methods .....</b>	<b>76</b>
5.1.1	Plant material and growth conditions .....	76
5.1.2	Vector construction.....	76
5.1.3	Rapeseed hypocotyl co-transformation .....	76
5.1.4	Genotyping of regenerating plants.....	76
5.1.5	Expression analysis.....	77
<b>5.2</b>	<b>Results .....</b>	<b>77</b>
5.2.1	Regeneration of <i>Hs4</i> -positive plants.....	77
5.2.2	<i>Hs4</i> expression verification .....	78
5.2.3	Production of T <sub>2</sub> seeds .....	79
<b>6</b>	<b>Discussion.....</b>	<b>81</b>
<b>6.1</b>	<b>Reassessing the structure of <i>Hs4</i>.....</b>	<b>81</b>
<b>6.2</b>	<b>Homologs from <i>P. procumbens</i> and <i>P. webbiana</i> show the highest sequence similarity to <i>Hs4</i> .....</b>	<b>82</b>
<b>6.3</b>	<b>Homologs of <i>BvHs4</i> are present in various <i>Beta</i> species.....</b>	<b>83</b>
<b>6.4</b>	<b><i>Hs4</i> and <i>BvHs4</i> show contrasting expression patterns .....</b>	<b>84</b>
<b>6.5</b>	<b><i>Hs4</i> confers resistance to BCN in a non-related species .....</b>	<b>86</b>
6.5.1	Investigating the function of <i>Hs4</i> under field-like conditions .....	88
<b>6.6</b>	<b>Syncytia developing under <i>Hs4</i> expression show distinct characteristics.....</b>	<b>89</b>
<b>6.7</b>	<b><i>Hs4</i>-transgenic plants can facilitate crop rotation .....</b>	<b>92</b>
<b>7</b>	<b>Summary .....</b>	<b>94</b>
<b>8</b>	<b>Zusammenfassung.....</b>	<b>96</b>
<b>9</b>	<b>Appendix .....</b>	<b>98</b>
<b>9.1</b>	<b>Supplementary Tables .....</b>	<b>98</b>
<b>9.2</b>	<b>Supplementary Figures.....</b>	<b>114</b>
<b>10</b>	<b>References .....</b>	<b>133</b>
<b>11</b>	<b>Supplementary data provided only electronically.....</b>	<b>155</b>
<b>12</b>	<b>Curriculum Vitae and Publications.....</b>	<b>156</b>

<b>12.1</b>	<b>Curriculum vitae .....</b>	<b>156</b>
<b>12.2</b>	<b>Oral and poster presentations .....</b>	<b>156</b>
<b>13</b>	<b>Publications and declaration of own contribution .....</b>	<b>157</b>
<b>14</b>	<b>Acknowledgements.....</b>	<b>158</b>

## List of Abbreviations

%	percent
°C	degree Celsius
µl	microliter
µm	micrometer
<i>A. thaliana</i>	<i>Arabidopsis thaliana</i>
<i>A. tumefaciens</i>	<i>Agrobacterium tumefaciens</i>
aa	amino acid(s)
ANOVA	analysis of variance
<i>B. vulgaris</i>	<i>Beta vulgaris</i>
BC	before Christ
BCN	beet cyst nematode
BLAST	Basic Local Alignment Search Tool
bp	base pair(s)
ca.	circa
cDNA	complementary DNA
CDS	coding sequence
cm	centimeter
Col-0	Columbia
Ct-value	cycle threshold value
cv.	cultivar
DAS	days after sowing
ddH <sub>2</sub> O	double-distilled water
DNA	deoxyribonucleic acid
dpi	days post-inoculation
DsRed2	<i>Discosoma</i> red fluorescent protein 2
ER	endoplasmic reticulum
EtOH	ethanol

gDNA	genomic DNA
GP	gene pool
<i>H. schachtii</i>	<i>Heterodera schachtii</i>
h	hour(s)
HgCl <sub>2</sub>	mercury bichloride
InDel(s)	insertion(s)/deletion(s)
ISC	initial syncytial cell
J2	second-stage juvenile
kb	kilobases
kV	kilovolts
LD	long-day
M	molar
mA	milliamperes
MA	membrane aggregation(s)
MALs	monosomic addition lines
Mb	megabases
mbar	millibar
min	minute(s)
ml	milliliter
mM	millimolar
ms	milliseconds
mya	million years ago
N.A.	not available
NaClO	sodium hypochlorite
NCBI	National Centre for Biotechnology Information
ng	nanogram
nm	nanometer
ORF	open reading frame

## List of Abbreviations

<i>P. procumbens</i>	<i>Patellifolia procumbens</i>
PCN	potato cyst nematode
PCR	polymerase chain reaction
PPN	plant-parasitic nematode(s)
PTMs	post-translational modifications
QTL	quantitative trait locus
RNA	ribonucleic acid
ROS	reactive oxygen species
rpm	rounds per minute
RT	room temperature
RT-qPCR	real-time quantitative PCR
SD	short-day
sec	second(s)
SER	smooth ER
SNP	single nucleotide polymorphism
ssp.	subspecies
T-DNA	transfer DNA
TMD	transmembrane domain(s)
TSS	transcription start site
U	unit(s)
UTR	untranslated region
v.	version
V	Volt
ZnCl <sub>2</sub>	zinc chloride
$\lambda_{\text{excitation}}$	excitation wavelength

# 1 Introduction

## 1.1 The sugar beet crop

The domestication of beets began around 8,000 BC in Mesopotamia. Ancestral forms were mainly selected for their leaves, though the plants' roots were used likewise for consumption (Biancardi et al. 2020). Even though beetroots have been known for their sweet juice for a long time, the cultivation of sugar beets as we know them today only began ca. 220 years ago in German Silesia, when the sugar obtained from beets was proven to be identical to the sugar from sugarcane. The White Silesian Beet selected and used for the first sugar extractions in 1784 is believed to be the ancestor of all present-day sugar beets (Fischer 1989). The first plant for sugar production from beets was established in 1801 (Hallmann et al. 2009). Modern sugar beet (*Beta vulgaris* subsp. *vulgaris*) is a biennial, diploid crop ( $2n = 18$ ) of the Amaranthaceae family. Owing to the constant selection, the roots' sugar content increased from 8 % to almost 20 % in the past 200 years (Biancardi et al. 2020). Upon harvest, sugar beet contains 75% water. The remaining 25% dry matter consists of 76 % sucrose, 18 % marc (insoluble cell wall components), and 6 % non-sucrose substances (Hoffmann et al. 2005). Nowadays, 80 % of the world's sugar is produced from sugar cane and the remaining 20 % comes from sugar beet, 50 % of which is produced in the European Union, making sugar beet one of the most important crops in Europe (Directorate-General for Agriculture and Rural Development 2024). In 2022, the top five sugar beet-producing countries were Russia, France, the US, Germany, and Turkey (Food and Agriculture Organization of the United Nations 2024). The by-products of sugar production are used for livestock feed and for producing biofuels (Marzo et al. 2019).

Several sugars, among them sucrose, are the main products of photosynthesis. They are produced in the leaves and transported to sink organs like flowers, seeds, and roots via the phloem. Early in the growing season, the cambium rings of the sugar beet root are formed (Hoffmann 2010). The parenchymal tissue storing the sucrose is located between those rings and the number of rings is directly correlated with the sucrose content (Milford 1976; Hoffmann and Kluge-Severin 2011). Sucrose is involved in starch biosynthesis, the regulation of anthocyanin production, and plant developmental processes where it acts as a signal molecule (Yoon et al. 2021).

As sugar beet is biennial, it grows vegetatively in the first year and switches to the reproductive phase in the second year, after being exposed to an extended period of cold, called vernalization (Biancardi et al. 2020). Bolting and ultimately flowering reduces the storage root and hence the sugar yield. Therefore, sugar beets are generally sown in spring and the roots are harvested in autumn before the plants can switch to the reproductive stage (Hoffmann and Kluge-Severin 2011; Biancardi et al. 2020). However, sowing in autumn and cultivating the plants over winter has been investigated and is even postulated to lead to a yield increase of ~30%. Winter beet cultivation is possible in the mild climate of the Mediterranean countries but not in northern Europe (Hoffmann and Kluge-Severin 2011; Loel and Hoffmann 2014).

## 1.2 The genera *Beta* and *Patellifolia*

The relationship between cultivated *Beta* species and the crop's wild relatives has been debated since the times of Hippocrates (Frese and Ford-Lloyd 2020). A widely used classification of beets was undertaken by Kadereit et al. (2006). Using internal transcribed spacers, they subclassified the Betoideae Ulbr. subfamily of the Amaranthaceae family into the Beteae, including the sections *Beta* and *Corollinae* of the genus *Beta*, and the Hablitzieae,

comprised of the other four genera *Aphanisma*, *Hablitzia*, *Oreobliton*, and *Patellifolia*. The sixth genus *Acroglochin* could not be clearly positioned (Kadereit et al. 2006). Newer analysis using nuclear, ribosomal, and chloroplast DNA has rebutted the existence of the Beteae and Hablitzieae subclasses. Instead, the subfamily Betoideae is shown to be monophyletic, consisting of five genera, excluding *Acroglochin* (Romeiras et al. 2016).

The concept of gene pools states that the primary gene pool (GP1) consists of species easily crossable with each other, including both wild and cultivated species. The secondary gene pool (GP2) includes species that can cross with GP1 species, even though crossing barriers leading to sterility might exist. Gene transfer from species of the tertiary gene pool (GP3) to GP1 species is only possible when using advanced biotechnological techniques to rescue the sterile or sublethal offspring generated (Harlan and Wet 1971).

Accordingly, the genus *Beta* can be subdivided into two sections or gene pools which diverged around 7.2 million years ago (mya). Section *Beta* resembles the first gene pool and contains the Macaronesian and Western Mediterranean species *B. macrocarpa*, *B. patula*, *B. vulgaris* ssp. *adanensis*, *B. vulgaris* ssp. *maritima*, and *B. vulgaris* ssp. *vulgaris* (Table 1) (Romeiras et al. 2016). The four cultivated beet types (sugar beet, fodder beet, garden beet, and foliage beet) are included in the species *Beta vulgaris* ssp. *vulgaris* (Ford-Lloyd and Williams 1975; Frese and Ford-Lloyd 2020). Due to the geographical proximity of the *Beta* species, gene flow between the wild species *B. vulgaris* ssp. *maritima* and domesticated forms of beet grown in the same area was possible until beets started to be cultured outside the areas where *B. vulgaris* ssp. *maritima* naturally occurred (McGrath et al. 2011). That might be the reason why there are different hypotheses about who the ancestor of the modern sugar beet varieties is. While the White Silesian beet has arisen from a fodder beet (Fischer 1989), the ‘Beta Imperialis’ grown by the German breeder Knauer and thought to be ‘the mother of modern sugarbeet’<sup>1</sup> is suggested to have originated from crosses between the Silesian beet and *B. vulgaris* ssp. *maritima* (Bosemark 1979). Others, however, believe that the Silesian beet itself was the result of a spontaneous hybridization of chard and fodder beets (Bosemark 1979; McGrath et al. 2011), a view contradicted by Jung et al. (1993) after DNA “fingerprinting”. It is commonly agreed that modern sugar beets have a genetically narrow gene pool, due to the Silesian beet as a single ancestor and continued selection to improve the production and quality traits. This bottleneck underpins the importance of crop wild relatives like the sea beet *B. vulgaris* ssp. *maritima* as a source for useful traits that can be introgressed easily into the sugar beet germplasm by crossing (Jung et al. 1993; Panella et al. 2020).

The second section of the genus *Beta* is *Corollinae*. It resembles the secondary gene pool and comprises the Eastern Mediterranean and Southwestern Asian species *B. corolliflora*, *B. intermedia*, *B. lomatogona*, *B. macrorhiza*, *B. nana*, and *B. trigyna* (Table 1) (Romeiras et al. 2016). *B. nana* has formerly been placed in a third section (*Nanae*), but recent analyses have placed it in the section *Corollinae* (Kadereit et al. 2006; Sielemann et al. 2022). This section contains species with frost tolerance, a trait not found in the section *Beta* or the genus *Patellifolia*, and has high variability in ploidy levels (Sielemann et al. 2022). Different experiments have been conducted to introduce traits from this section into *B. vulgaris* subsp. *vulgaris* (for better readability hereafter named *B. vulgaris*). Crosses with *B. corolliflora* and *B. lomatogona* led to partial or full sterility in the resulting hybrids, while fertile hybrids could be obtained from crosses with *B. macrorhiza* (Szota 1995). In conclusion, there is evidence that the species of this secondary gene pool can be used for trait introgression, even though crosses are complicated by for example insufficient chromosome pairing, reduced fertility, and a restricted seed set (Frese and Ford-Lloyd 2020).

---

<sup>1</sup> as stated by (Bosemark 1979).

**Table 1:** The taxa of the subfamily Betoideae, adapted from Kadereit et al. (2006) and Romeiras et al. (2016).

	<b>Taxon</b>	<b>Gene pool</b>
<i>Beta</i> L.		
section <i>Beta</i>		
	<i>B. macrocarpa</i>	1
	<i>B. patula</i>	
	<i>B. vulgaris</i> ssp. <i>adanensis</i>	
	<i>B. vulgaris</i> ssp. <i>maritima</i>	
	<i>B. vulgaris</i> ssp. <i>vulgaris</i>	
section <i>Corollinae</i>		
	<i>B. corolliflora</i>	2
	<i>B. intermedia</i>	
	<i>B. lomatomogona</i>	
	<i>B. macrorrhiza</i>	
	<i>B. nana</i>	
	<i>B. trigyna</i>	
<i>Patellifolia</i> A.J.Scott, Ford-Lloyd & J.T.Williams		
	<i>P. patellaris</i>	3
	<i>P. procumbens</i>	
	<i>P. webbiana</i>	

The genus *Patellifolia* was formerly described as *Beta* section *Procumbentes* Ulbr. but was revised to constitute a separate genus in the late seventies (Williams et al. 1976; Scott et al. 1977). It has diverged from the genus *Beta* around 25.3 mya (Romeiras et al. 2016). The genus forms the third gene pool and comprises three species, *P. patellaris*, *P. procumbens*, and *P. webbiana*. While the latter two species are endemic to the Macaronesian Islands, *P. patellaris* can also be found on the Iberian Peninsula, in Italy, and North Africa (Kadereit et al. 2006). The final taxonomic classification of the three *Patellifolia* species is not finally settled. First doubts about the existence of three separate species were expressed by Curtis (1968). In experiments, *P. patellaris* was found to be self-fertile, while *P. procumbens* and *P. webbiana* did not produce seeds after selfing. Rather, these two species were interfertile and led to the generation of fertile offspring, while hybridizations with *P. patellaris* were not successful. Further, *P. patellaris* was differentiated from *P. procumbens*/*P. webbiana* by its (leaf) morphology and the incomplete resistance to cyst nematodes, while those traits were found to be identical in the other two species (Curtis 1968; Szota 1995). Using a limited set of accessions, the similarities between the isozyme patterns of these two species were compared and found to be highly similar, reinforcing the idea of a single species (Wagner et al. 1989). Another important differentiation characteristic between *P. patellaris* and *P. procumbens*/*P. webbiana* was the ploidy level: *P. patellaris* is described to be tetraploid and the other two species as diploids (Curtis 1968; Kadereit et al. 2006). However, *P. patellaris* from East Andalusia was found to contain both diploid and tetraploid plants (Blanca et al. 2011), and Frese et al. (2017a) proved that *P. patellaris* and *P. procumbens* did intercross when they co-occurred in their natural habitats, leading to di-, tri- and tetraploid plants. Deploying microsatellite markers and plastome data, the most recent studies conclude that three separate species exist, even though they exhibit high morphological variation and the ability for interspecific crosses. Further, *P. procumbens* and *P. webbiana* are considered closely related and clearly separated from *P. patellaris* (Frese et al. 2019; Sielemann et al. 2022).

While cultivated beets have a narrow genetic makeup, the wild *Patellifolia* species are genetically heterogeneous and represent an important source of resistance against diverse pathogens like the fungus *Polymyxa betae* and the beet cyst nematode *Heterodera schachtii* (Panella et al. 2020). Therefore, the different species were employed extensively in crossing

experiments with various *Beta* species, but the lack of chromosome pairing and the often sterile hybrids hindered the use of the *Patellifolia* genetic resources until the first viable hybrids could be generated in the 70s. From them, diploid monosomic addition lines that functioned as bridges for the transfer of genetic traits could be produced (Savitsky 1975; van Geyt et al. 1990).

### 1.3 Plant-parasitic nematodes as important pests worldwide

The word 'nematode' is derived from the Greek word 'nema' which means thread, indicating the microscopically small, thread-like appearance of these unsegmented roundworms. Nematodes have a well-conserved basic body plan and generally undergo four molting stages during their life cycle (Decraemer et al. 2013). They belong to the ancient animal superphylum *Ecdysozoa*, which includes all molting invertebrates, uniting more than a million described species. While insects constitute the most diverse metazoan phylum, nematodes are the most abundant animals on Earth (Telford et al. 2008; Schratzberger et al. 2019). About 27,000 nematode species are described but different estimates range between 500,000 to 10 million existing species (Hugot et al. 2001; Qing et al. 2023). Among the species described, approx. 10,700 are classified as free-living and the remaining as parasitic to either vertebrate (~8,400), invertebrate (~3,500), or plant hosts (~4,100) (Hugot et al. 2001). Nematodes are found in a vast range of habitats from oceanic trenches to the peaks of mountains, where they are present at different trophic levels of the food webs in sediments and soils, contributing to nutrient mineralization, the dispersal of microorganisms, and the recycling of nutrients (Ferris 2010; Schratzberger et al. 2019).

The first nematodes evolved in marine habitats of the early Cambrian (~525 mya), most likely as insect parasites. After terrestrialization, they followed their hosts onto land and began parasitizing land plants (Rota-Stabelli et al. 2013; Qing et al. 2023). The earliest evidence of a plant-parasitic nematode dates back to the nematode *Palaeonema phyticum*, which was found in the stomatal chambers of the early Devonian (396 mya) land plant *Aglaophyton major* (Poinar 2015).

The co-evolution of plants and nematodes has since led to the formation of a diverse set of species nowadays classified as plant-parasitic nematodes (PPNs). They are known pests of major crop plants like rice, wheat, and potato, causing annual yield losses of over \$80-173 billion (Nicol et al. 2011; Elling 2013). The actual figure might be even higher, as nematode infestations are often not easily distinguished from abiotic stresses. This leads to extremely high population densities in infested fields as suitable measures are not implemented (Pires et al. 2022). All PPNs are obligate biotrophs and even though the different species feature a wide range of interactions with their hosts, they all display similar protrusible, hollow stylets or mouth spears for host cell penetration. The PPNs can be further grouped into ecto- and endoparasites, and for both migratory and sedentary forms exist. Ectoparasitic nematodes never enter the roots but migrate through the soil. They use their stylet to feed on plant tissues like root hairs, epidermis, cortex, or vascular tissues while remaining on the root surface. An important migratory ectoparasite is *Xiphinema index* which mainly feeds on grapevine. The sedentary ectoparasitic nematodes remain attached to a selected feeding location for several days, but members of this group are of little economic importance. Contrarily, endoparasitic nematodes completely enter the host. The migratory endoparasites enter the host and cause severe damage by moving through the different cell layers while searching for a suitable cell to feed on. Finally, once the feeding is complete, the feeding cell is destroyed. Important migratory genera are *Hirschmanniella*, *Pratylenchus*, and *Radopholus*. Sedentary endoparasites pose the most economically important group and include the *Meloidogyne* species (root-knot nematodes) as well as the cyst nematode species of the genera *Globodera* and *Heterodera*. They induce a particular feeding structure in the host, become sedentary, and

feed solely from it while completing their life cycle (Sijmons et al. 1994; Jones et al. 2013; Holbein et al. 2016).

#### 1.4 The beet cyst nematode *Heterodera schachtii*

Cyst nematodes belong to the most successful and specialized PPNs. They induce a nematode-specific permanent feeding site, which supplies them throughout their life cycle (Wyss 2002). The genus *Heterodera* contains some of the most devastating cyst nematodes: the soybean cyst nematode (*Heterodera glycines*), cereal cyst nematodes (*H. avenae*, *H. latipons*, and *H. filipjevi*), and the sugar beet cyst nematode (*H. schachtii*). The economically important potato cyst nematodes (*Globodera pallida* and *G. rostochiensis*) belong to the genus *Globodera* from the same family (*Heteroderidae*) (Subbotin 2013; Perry et al. 2018). The *Heterodera* species exhibit a wide geographical distribution and different crop specializations. While certain species have a rather narrow host specificity, like the carrot cyst nematode *H. carotae* that only infects carrots (Nicol et al. 2011), the beet cyst nematode *H. schachtii* is distributed globally, occurring preferably in temperate, Mediterranean, or subtropical climates, and can attack 218 plant species of 95 genera (Steele 1965; Daub 2021). It was first described by the German botanist Hermann Schacht in 1859 who observed small white dots on the roots of sugar beets showing yield reductions. Soon thereafter, Julius Kühn demonstrated that the observed “beet weariness” occurred due to infestations with the beet cyst nematode (BCN). Finally, the species was described as *Heterodera schachtii* of the new genus *Heterodera* by Adolf Schmidt in 1871, who named it after its discoverer (Hallmann et al. 2009). As stated above, *H. schachtii* has a wide host range but is reported to reproduce mainly on crops of the Brassicaceae and Amaranthaceae families. Today, *H. schachtii* can be found in all beet-growing areas. In Europe, 10-20 % of these are considered to be infested, regional infestation rates might even exceed 50 % in intensive sugar beet cultivation areas (Perry et al. 2018; Daub 2021). As the main pathogen of sugar beets, BCNs lead to estimated yield losses of \$95 million in the European Union per year (Müller 1999). The main above-ground symptoms are wilting and stunted growth, resulting from water and nutrient deficiency caused by impaired root growth. Below-ground, lateral roots are formed to compensate for the damage, leading to a “bearded root” phenotype and strong yield reductions (Figure 1). Further, interactions with other pathogens lead to enhanced infestations with different *Pythium* or *Rhizoctonia* species, causing even higher yield decreases (Harveson and Jackson 2008; Daub 2021).

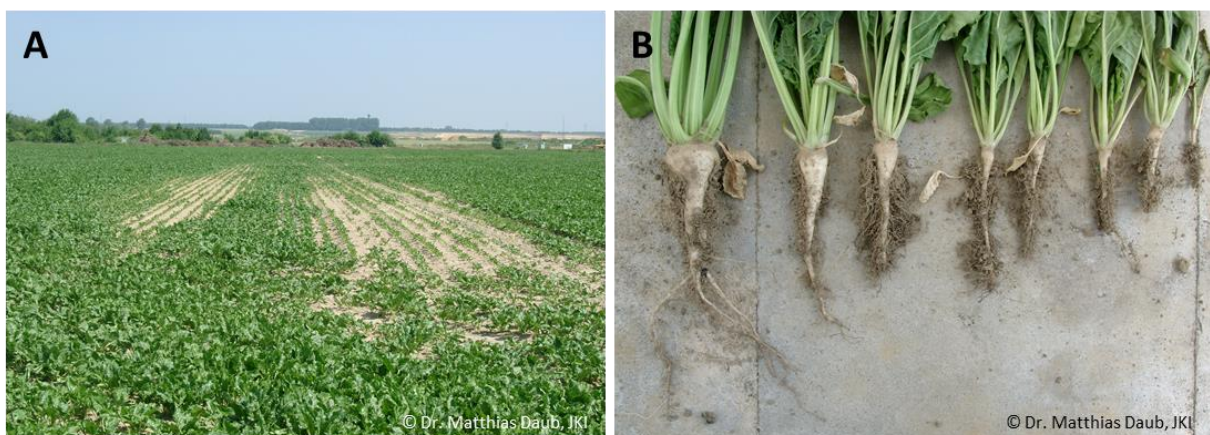


**Figure 1:** Symptoms of *H. schachtii* infestation on sugar beets. (A) The sugar beets show puny growth in field areas with high nematode densities. (B) Normal root development is impaired and increased side root development is observable under high infestation rates. The photos were taken by Dr. Matthias Daub (JKI, Elsdorf, Germany) in June 2010.

The developmental stages of the beet cyst nematode life cycle (Figure 2) and the ultrastructure of the nematode-induced feeding site, called syncytium, have been investigated broadly in the translucent roots of the model plant *Arabidopsis thaliana* using a combination of *in vivo* video light microscopy and transmission electron microscopic analysis. Even though detailed analyses of syncytia induced by *H. schachtii* have been conducted in *Arabidopsis*, syncytia analyzed in susceptible sugar beet show the same characteristics (Bleve-Zacheo and Zacheo 1987; Holtmann et al. 2000).

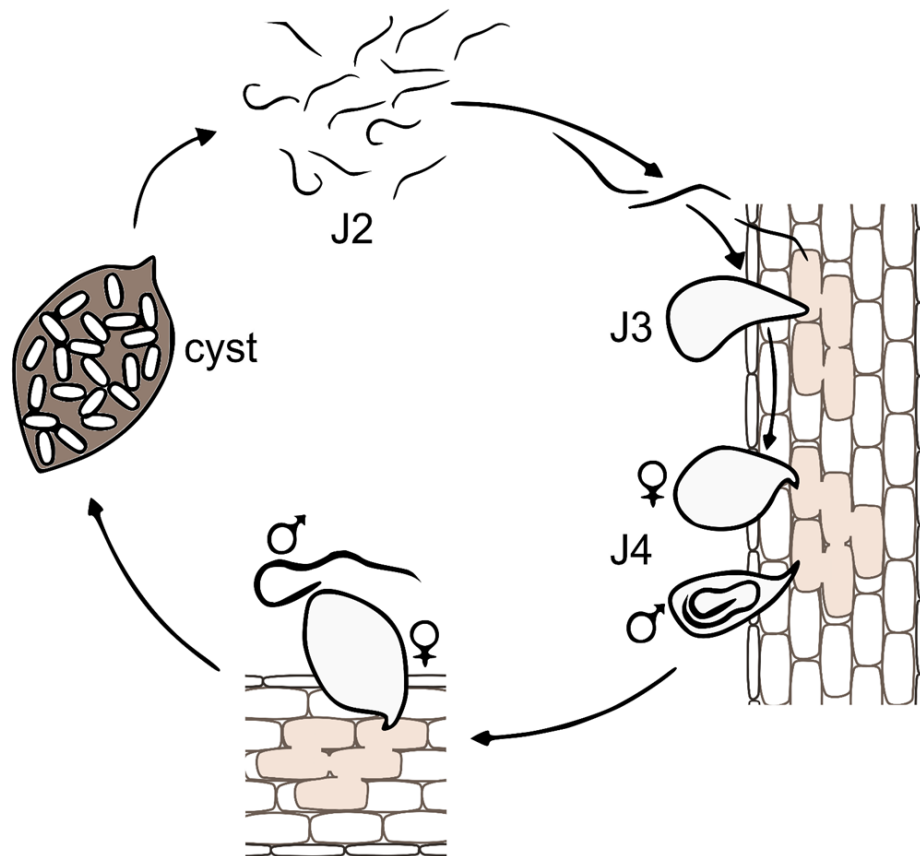


**Figure 2:** Schematic overview of the life cycle of the beet cyst nematode *H. schachtii*. The cyst contains the eggs, from which the J2 larvae hatch. They move towards the host root, induce the feeding site called syncytium, become sedentary, and molt to the J3 stage. After molting to the J4 stage, males and females can be easily differentiated. The males become mobile again and leave the root to fertilize a sedentary female. After egg production, the females die, and the cell wall hardens and forms a durable cyst. Modified from Müller and Wyss (1981).

The cyst resembles the durable form of the nematode and can contain up to 600 eggs (Sharma 1998). Inside the eggs, the larvae molt from the J1 to the J2 stage, mature cysts therefore contain eggs with infective J2 larvae (Figure 2). At this developmental stage, the larvae can remain dormant until external stimuli like root exudates lead to their hatching. They perforate the eggshell with their stylet, leave the cyst through the opening of the vulva, and migrate towards the host plant. The larvae penetrate and enter the roots, preferably in the elongation zone. They move intracellularly by deploying their stylet to cut open cell walls until they reach the pericycle (Müller and Wyss 1981; Perry et al. 2018). Here, the destructive behavior shown during migration through the root changes and becomes more exploratory and gentler. The J2 carefully inserts the stylet into root cells to determine the initial syncytial cell (ISC) for establishing the syncytium (Golinowski et al. 1997). Preferably, procambial or pericyclic cells are selected as ISC (Golinowski et al. 1996; Sobczak et al. 1997). After the successful initiation of the ISC, the J2 becomes sedentary and starts feeding from it in repeated cycles of three distinct phases. During the first phase, the nematode withdraws nutrients from the

syncytium through its inserted stylet. Then, two phases of rest and preparation follow, before the cycle begins anew (Wyss and Zunke 1986; Wyss 1992). At the site of stylet injection into the host cell, a feeding plug covered with callose-like material is formed at 12-24 h after syncytial induction. After its establishment, the continuous re-insertion of the stylet at each new feeding cycle occurs through the feeding plug exclusively (Sobczak et al. 1999). For feeding from the established syncytium, the nematode forms a feeding tube from secretions injected into the host cytoplasm through its stylet. This feeding tube is formed anew in every cycle. The feeding tube is surrounded by a zone of organelle-free cytoplasm (Wyss and Zunke 1986). Sobczak et al. (1999) observed the association of endoplasmic reticulum (ER) membranes with the feeding tube walls, which is believed to promote the uptake of sterols produced in the ER and essential to the nematode. Apart from facilitating food uptake, the feeding tube might also act as a filter, excluding molecules with a Stokes radius above 3.2 nm (Böckenhoff and Grundler 1994).

Within three hours after the J2 starts feeding, increased cytoplasmic streaming can be observed. The cytoplasm of adjacent cells shows increased activity and nuclear hypertrophy within the first 12 h of feeding (Wyss 1992). The subsequent incorporation of cells adjacent to the ISC leads to the formation of the multi-nucleate syncytium. The first fully developed cell wall openings can be observed six hours after the larvae start feeding. They are formed by the stepwise widening of plasmodesmata. Consequently, the protoplasts of the neighboring cells fuse and cytoplasmic continuity can be observed. Incorporation of cells at the terminal syncytial ends occurs similarly. The mode of cell wall degradation changes in syncytia of later stages. Here, ER membranes accumulate along the walls where the first lesions appear. These lesions extend until only the middle lamella remains. Once the middle lamella is dissolved, the cytoplasm of both cells fuses, followed by a fusion of the ER systems (Grundler et al. 1998; Sobczak and Golinowski 2011). An initial syncytium including several neighboring cells is formed 24 h after feeding has started. The syncytium then expands further in an acropetal direction inside the vascular cylinder (Wyss 1992). In the final stages, syncytia can comprise up to 200 cells with cytoplasmic continuity (Sobczak and Golinowski 2011). The outer cell walls of developed syncytia are described to be thickened and do not contain open plasmodesmata (Grundler et al. 1998). Davis et al. (2012) have analyzed the composition of syncytial cell walls. They found that secondary cell walls were absent in syncytia and the walls exhibited an increased flexibility, likely to enable the syncytium to react to changes in turgor pressure during feeding and to withstand the high turgor pressure within.

Syncytia exhibit a pronounced proliferation of the cytoplasm and hypertrophy of the syncytial elements. The central vacuole is dissolved and numerous small vacuoles are formed in its place (Sobczak and Golinowski 2011). In the early stages of syncytium development, rough ER dominates and is often arranged in parallel lines or concentric swirls. In developed syncytia, smooth ER prevails, often in the form of circular cisternae (Golinowski et al. 1996; Sobczak et al. 1997). The abundance of ER in the syncytia points to a highly active protein synthesis. The number and size of plastids in syncytia increase. In early-stage syncytia, they also contain starch grains. Similar to the plastids, the number of mitochondria and dictyosomes increases, although their structures are preserved (Sobczak and Golinowski 2011). The nuclei are highly active and contain well-visible nucleoli. In syncytial cells, cell wall ingrowths occur mainly along xylem vessels, though they have also been observed along other syncytial cell walls. These protuberances are covered by the plasma membrane, leading to an increased interface between the syncytium and the adjacent vessels. They are therefore believed to improve the short-distance transport of water and nutrients. Interestingly, the inner xylem vessel surface often appears to be coated with osmiophilic substances. Another characteristic of syncytia are invaginations of the plasma membrane often associated with paramural bodies or multivesicular bodies (MVBs). Paramural bodies can also be found in

association with cell wall remnants, and, when they detach from the cell wall, they form MVBs (Golinowski et al. 1996; Sobczak et al. 1997). The word ‘paramural’ means ‘attached to a cell wall’ and paramural bodies are described as vesicular membrane structures of apoplastic origin (Akita et al. 2017). They are formed by the deposition of cell material between the cell wall and the invaginated plasma membrane (Yang et al. 2018).

The larvae remain attached to their metabolically active syncytium and molt to the J3 and J4 stage (Figure 2). At this stage the differences between males and females become evident. The female larvae continue withdrawing food from their syncytium and swell up to form lemon-shaped females. The male larvae abort their syncytium upon their fourth molt and develop into vermiform males enclosed by the J3 skin. Using their stylet, the J4 males leave the J3 skin and migrate through the soil, attracted by sexual pheromones exuded by the females. After fertilization, the males die and the females start producing eggs that remain inside the females’ bodies. As long as the females are alive, they remain white. Once egg production is concluded, the females die and their skin hardens and turns brown, forming the cyst. Under favorable conditions, the larvae can hatch within 28 days and penetrate new roots. Usually, not all larvae hatch simultaneously, instead, the J2 larvae can survive in the cysts for several years (Müller and Wyss 1981). The syncytium induced in the roots collapses once the nematode finishes its life cycle and stops feeding. The process is marked by a decrease in cytoplasmic density and the degeneration of the ER structures. The vacuoles increase in size, and the plasma membrane detaches from the cell wall and becomes lined with osmiophilic granules, while the integrity of plastids and mitochondria is maintained longer (Golinowski et al. 1996).

### 1.5 Plant-nematode interactions

Cyst nematodes have developed a unique advancement to sustain their parasitic sedentary life stage. Due to their inability to move once the feeding site has been selected, they depend on the nourishment provided by selected cell(s) at a single location. The syncytium induced by the cyst nematode resembles a newly formed plant organ, whose functionality is tightly linked to the nematode’s survival and reproductive success. Hence, a complex molecular signal exchange leading to the reprogramming of plant cells is the basis of syncytium induction and maintenance (Juvale and Baum 2018). The mechanisms of host-parasite interaction in cyst nematodes have been studied broadly on roots of *A. thaliana*. The diploid plant comes from the Brassicaceae family, making it a close relative to important crops like rapeseed and cabbage. Its small genome size of about 125 Mb, compact growth type, and rapid life cycle have been key traits in establishing it as a model species (Wyss and Grudler 1992; Arabidopsis Genome Initiative 2000; Wang et al. 2022). Sijmons et al. (1991) demonstrated that Arabidopsis was a suitable host for different root-parasitic nematodes. Since then, detailed descriptions of the culturing conditions for nematode infection experiments, have paved the way for using Arabidopsis as a model in nematode-plant interaction studies (Sijmons et al. 1991; Bohlmann and Wieczorek 2015).

Years of co-evolution of hosts and parasites have led to the emergence of a complex network of defense- and pathogenesis-related genes and pathways. Plants have developed pattern recognition receptors (PRRs) that can identify pathogen-, microbial-, or damage-associated molecular patterns (PAMPs/MAMPs/DAMPs) released by invading pathogens or damaged plant cells. Upon detection, the PAMP-triggered immunity (PTI) responses are activated, leading to the activation of a downstream signaling cascade. Ultimately, bursts of reactive oxygen species (ROS) and calcium, protein kinase activation, cell wall reinforcement, and reprogramming of the plant cell’s transcriptome are induced, restricting pathogen development and growth. On the other hand, pathogens have evolved to overcome these defense mechanisms. They secrete so-called effector proteins into the plant cells that interfere

with PTI-induced responses and lead to effector-triggered susceptibility (ETS). Simultaneously, plants can perceive those effectors via intracellular nucleotide-binding leucine-rich repeat receptor proteins, short NLRs. Their activation leads to a defense response increased in strength and intensity, effector-triggered immunity (ETI), which often peaks in a hypersensitive response (HR) reaction causing programmed cell death (Holbein et al. 2016). The interaction of plants and pathogens like nematodes is highly complex. For example, plant-parasitic nematodes possess a small family of pheromones called ascarosides that resemble MAMPs as they can induce MAMP-triggered immunity. Plants respond to very low concentrations of the most abundant of these ascarosides, ascr#18, by activating conserved immune responses. The early recognition of this parasite pheromone thereby leads to enhanced plant resistance (Manosalva et al. 2015). Intriguingly, Manohar et al. (2020) could show that plants take up ascr#18 and convert it into smaller molecules, which in turn can be secreted by the plant to deter nematodes already in the rhizosphere.

To reach the vascular cylinder and establish the syncytium, cyst nematodes first have to move intracellularly through the root cells. They use the mechanical force of their stylet thrusts and a diverse set of secretions containing cell-wall-degrading or -modifying enzymes to dissolve the cell walls in their way (Holbein et al. 2016). One of these enzymes is polygalacturonase (PG), which has been shown to be secreted into the host by the root-knot nematode *Meloidogyne incognita* (Jaubert et al. 2002). Plants encode PG-inhibiting proteins (PGIP) that block the action of PG. Even though no PG-similar sequences were yet detected in cyst nematodes, it was demonstrated that the interaction of *Heterodera goettingiana* with its host plant pea (*Pisum sativum*) leads to the upregulation of a plant PGIP under nematode infestation. Contrarily, the repression of the plant PGIP in susceptible roots is believed to result from the successful establishment of the nematode in the root (Veronico et al. 2010).

The nematode's intracellular movement causes extensive tissue damage. Analyses showed that plant cells reacted to the wounding with the deposition of callose-like depositions and necrosis (Grundler et al. 1997). Further, Ali et al. (2013) demonstrated that an enhanced callose deposition, along with the upregulation of jasmonic acid-responsive genes, led to an improved resistance of *Arabidopsis* against *H. schachtii*. An example of how nematodes hijack the plants' defense mechanisms is the ROS production pathway, which constitutes an important mechanism of plant basal defense. While an oxidative burst of ROS could be detected in both susceptible and resistant tomato plants after infection with *M. incognita*, the most significant increase in ROS levels and a second oxidative burst, leading to a hypersensitive response, was only observed in the incompatible reaction between nematode and plant. In the compatible reaction, ROS were produced during invasion but became undetectable when the nematodes had established their feeding site (Melillo et al. 2006). Recently, two NADPH oxidases involved in ROS production (RbohD and RbohF) were shown to support the ISC establishment by leading to a local prevention of cell death. Upon expansion of the syncytium, salicylic acid-mediated plant defense responses are then suppressed by ROS signaling at the infection site (Siddique et al. 2014). Following up on this, the auxin transporter WAT1 was identified as a downstream target of the Rboh-induced ROS cascade. It promotes the initiation and establishment of the syncytium by modulating the plant indole metabolism (Chopra et al. 2021). Hewezi et al. (2010) provided evidence that the nematode effector molecule 10A06 interacts with the plant spermidine synthase 2 protein. The resulting increase in spermidine and its enhanced degradation by the polyamine oxidase forms the ROS H<sub>2</sub>O<sub>2</sub>, which acts as a signaling molecule inducing the production of antioxidants to protect the growing syncytium from the plant-generated ROS.

The initial syncytium can be observed 24 h after the nematode commences feeding (Wyss and Zunke 1986). To establish this multicellular feeding structure and overcome the plant defense

responses, the nematode uses a whole collection of effector proteins produced in the nematode's dorsal and subventral esophageal glands and secreted through the stylet into the plant cells for large-scale cellular reprogramming of the host cells (Juvale and Baum 2018). Effectors aid the nematode parasitism in various ways. In the early phases of syncytium formation, the effector *CBP* (*cellulose-binding protein*) is expressed and interacts with the pectin methylesterase protein 3 (PME3) of Arabidopsis. The interaction leads to a reduction of methylesterifications in the cell walls, which enables facilitated access to cell wall polymers for further degradations and a rapid extension of the syncytium (Hewezi et al. 2008). Other effectors mimic plant proteins to restrict the ability of the plant immune system to induce defense reactions. An example is an effector protein exhibiting a conserved C-terminal domain that mimics the domain found in plant CLAVATA3/ENDOSPERM SURROUNDING REGION-related (CLE) proteins. This CLE-like effector can bind to host receptor-like kinases to activate signaling cascades necessary for parasitism (Hewezi 2015). The CLE-like effector has another remarkable feature: after being secreted by the nematode it is translocated into the apoplast. The effector harbors a translocation signal enabling it to use the plant's ER secretory pathway. Thereby, it obtains a plant-specific glycosylation signal and is most likely aiding in priming distantly located cells for incorporation into the syncytium (Wang et al. 2021).

Another important pathway hijacked by nematode effectors is the auxin biosynthesis. The phytohormone auxin is involved in various plant developmental processes and plays a crucial role in syncytium induction. Auxin-responsive elements were detected in the promoter regions of nematode-responsive cell wall degrading enzymes required in the early stages of syncytium formation, highlighting the importance of this metabolite for nematode parasitism (Goverse and Bird 2011). The auxin transporter gene *AUX1* is induced in syncytia three days post-infection, indicating an active auxin influx upregulation by the nematodes (Mazarei et al. 2003; Grunewald et al. 2009b). Simultaneously, auxin efflux carriers are affected adversely. *PIN1* and *PIN7* are downregulated to avoid auxin efflux out of the early syncytium. In order to provide the infection site with auxin, the phytohormone has to be transported acropetally along the root, a process greatly mediated by PIN1. The inoculation of *pin1* and *pin7* knockout mutants revealed reductions in infection efficiencies of 40 % and 20 %, respectively. Two other members of the PIN family, *PIN3* and *PIN4*, were shown to be specifically upregulated in the syncytium. Strikingly, PIN3 localization changes in the feeding site and leads to a distribution of auxin to the surrounding cells. In inoculation experiments using *pin3* and *pin4* mutants, the nematodes could establish their feeding site normally but only formed very small cysts, indicating that an expansion of the syncytium was limited (Grunewald et al. 2009a).

A recent study has shown another aspect of plant-nematode interaction. The biosynthesis pathway of vitamin B5 is conserved in plants. Although animals require vitamin B5 for the metabolism of carbohydrates, proteins, and lipids, making it an essential nutrient for them, the biosynthesis pathway is absent in animals. In syncytia, genes contributing to the B5 synthesis are upregulated. Interestingly, *H. schachtii* encodes two genes for the last step of this pathway. The plant homologs are tightly regulated by feedback loops and nematode-produced proteins are believed to function inside the nematode to complement the last step of the biosynthesis pathway and guarantee a continuous vitamin B5 supply by avoiding those feedback inhibitions (Siddique et al. 2022).

In the same study, the authors showed that the *H. schachtii* genome contains numerous segmental duplications, leading to the identification of at least 209 effector genes in the predicted proteome data set (Siddique et al. 2022). Transcriptome analysis of different J2 stages and the nematode glands led to the identification of 178 putative *H. schachtii* effectors

(Elashry et al. 2020). More recently, the transcriptomic analysis of gland cells at three BCN life stages identified 717 effector gene loci, 448 of which were considered novel effectors (Molloy et al. 2024). Due to the current advances in technology, the “effectorome” of plant-parasitic nematodes will expand. With only a handful of effectors characterized to date, likely, more effectors not only suppressing the host immune responses but also altering the development and physiology of plants will be detected in the future (Molloy et al. 2023).

As *Arabidopsis* is a suitable host for *H. schachtii* and a well-established model plant, most studies focus on the interaction of the nematode with this model. While differential expression in sugar beet has been used to identify genes related to *H. schachtii* resistance (for example Samuelian et al. 2004), studies using sugar beet as a host plant for the identification of large-scale molecular interactions and the effectors employed in parasitism are scarce. Ghaemi et al. (2020) found expression changes in beet genes involved in metabolism, nutrition, hormone pathways, signal transduction, and defense responses, confirming pathways (e.g. the jasmonic acid signaling pathway as part of the defense reaction) and effectors (e.g. cell wall degrading enzymes) known to be important in parasitism from *Arabidopsis* studies. Though *Arabidopsis* and sugar beet belong to different orders of the flowering plants (Cole et al. 2019), the high conservation of genes in various pathways has been demonstrated (for example Reeves et al. 2007; Xue et al. 2024). Similarly, it can be assumed that plant-nematode interactions identified in the *Arabidopsis* background can be transferred to the parasitism of sugar beet.

## 1.6 Controlling the beet cyst nematode in the field

Different management strategies exist for controlling BCNs in the field. Soon after the discovery of *H. schachtii*, crop rotations were established to reduce population densities. Different reports from the 20<sup>th</sup> century consider field rests of five to eight years in sugar beet growth cycles (Hallmann et al. 2009). Nowadays, the cultivation of sugar beet every fourth year in the same field is regarded as the best option if *H. schachtii* infestations occur (Reuther et al. 2016). The resulting crop rotation system uses non-host crops like alfalfa, beans, corn, or small grains to reduce the nematode population through a naturally occurring decline (Harveson and Jackson 2008). Cultivating catch crops like white mustard (*Sinapis alba*) or oilseed radish (*Raphanus sativus*) in between the sugar beet cycles increases this effect. The plants stimulate the hatching of the larvae. However, after root invasion, the nematodes fail to reproduce and the whole hatched generation is eradicated. Nevertheless, weed control remains important as several weeds are suitable hosts for *H. schachtii* (Perry et al. 2018). Rapeseed is cultivated in rotation with sugar beet. Like *Arabidopsis*, rapeseed belongs to the Brassicaceae family and is, therefore, a splendid host to *H. schachtii*. The nematodes are described to be able to reproduce on rapeseed roots even better than on sugar beet itself (Nielsen et al. 2003; Daub 2020). While the cultivation of rapeseed before the planting of sugar beet does not increase BCN multiplication rates under field conditions (Kenter et al. 2014), the post-harvest emerging volunteer rapeseed has to be tightly controlled as it emerges at nematode-favorable soil temperatures and in high densities. Unlike sugar beet, rapeseed has a high tolerance for BCN infestations and does not show yield reductions. Thus, the uncontrolled growth of volunteer rapeseed enables the establishment of large nematode populations in the field (Hallmann et al. 2009; Daub 2020, 2021). Early planting is claimed to reduce the damage caused by the nematodes as they are less active at low soil temperatures and older plants can withstand the attacks better (Harveson and Jackson 2008). Further, agricultural means like soil tilling, anaerobic soil disinfection, soil solarization, and biofumigation using plants high in glucosinolates are employed. Nematodes can also be controlled by nematicides but they are largely banned in the EU. Following the ban of chemical agents, the potential of biological control agents, known since the 1930s, was rediscovered (Perry et al. 2018). Biological control agents can suppress nematodes indirectly by enhancing the plant defenses through the

provision of plant-promoting effects, like the rhizobacterium *Bacillus firmus* that colonizes *Arabidopsis* roots and protects them against nematode attacks, or directly by antagonism in the form of nematode parasitism or the production of toxins (Pires et al. 2022).

Even though an integrated management approach combining different measures shows good results against BCN infestations, it is complex and time-consuming. Hence, the cultivation of tolerant or resistant varieties is favored.

### 1.7 Resistance to the beet cyst nematode

Plants possess basal and host-specific defense reactions. The basal responses serve as a first line of defense based on recognizing the parasite (PAMP/MAMP/DAMP) and the follow-up host-specific reactions are based on effector recognition (see 1.5). Apart from physical and chemical barriers as part of the defense reaction, plants have evolved to contain specialized resistance (*R*) genes. To date, several nematode-specific *R* genes have been cloned from plants. Two genes cloned from tomato (*Mi-1* and *Hero A*) confer resistance to different species of root-knot or potato cyst nematodes. In contrast, the genes identified in potato (*Gpa2* and *Gro1-4*) exhibit highly specific pathogen recognition and confer resistance only to certain field strains of *Globodera*. The four genes belong to the nucleotide-binding site leucine-rich repeat (NBS-LRR) immune receptor class of *R* genes. While the first three contain a coiled-coil (CC) domain at their N-terminus, *Gro1-4* exhibits an N-terminal toll-interleukin receptor-like (TIR) domain. Host-specific resistance can be conferred either by single dominant *R* genes or quantitative trait loci (QTL) (Williamson and Kumar 2006; Goverse and Smant 2014). Two loci for soybean cyst nematode (SCN) resistance have been identified. The resistance locus *Rhg1* contains three genes contributing to the specific resistance reaction, though the exact mode of action remains to be elucidated (Bayless et al. 2019). In contrast, the resistance conferred by the *Rhg4* locus is based on genetic polymorphisms of the underlying serine hydroxymethyltransferase gene (Liu et al. 2012).

However, the first nematode resistance gene ever cloned, and not showing apparent similarities to the above-described *R* genes, was *HsI<sup>pro-1</sup>* conferring resistance to *H. schachtii*. It also contains LRRs, but they are imperfect, and does not show apparent sequence similarities to the above-described *R* genes (Cai et al. 1997).

Sugar beet is highly susceptible to the BCN. The sea beet *B. vulgaris* ssp. *maritima* has been reported to exhibit a polygenic partial resistance to *H. schachtii* that manifests as a strong reduction of developing females on its roots (Viglierchio 1960; Heijbroek et al. 1977; Lange et al. 1993). Yet, complete resistance to the beet cyst nematode is only found in the three species of the genus *Patellifolia* (Stewart 1950; Golden 1959; Viglierchio 1960). The larvae can invade the *Patellifolia* roots but cannot mature or reproduce. Nevertheless, developing females could occasionally be observed on *Patellifolia* plants, depending on the nematode population used (Yu 1984; Lange et al. 1993). Hybridizations between *B. vulgaris* and the different *Patellifolia* accessions were attempted frequently but the nonviability of the F1 hybrids due to a lack of root growth hampered advancements. After grafting onto sugar beet stocks was introduced, viable hybrids were obtained occasionally, though they exhibited male sterility. In 1973, crosses between diploid *P. procumbens* and tetraploid *B. vulgaris* led to the production of viable offspring harboring one chromosome from the wild beet. After backcrossing with *B. vulgaris*, four out of 6,750 plants showed nematode resistance and were found to be monosomic additions carrying one resistance-bearing *Patellifolia* chromosome (Savitsky 1973). Upon backcrossing, a spontaneous hybridization between *P. procumbens* and *B. vulgaris* led to the transfer of a segment of a resistance-bearing *P. procumbens* chromosome to a sugar beet chromosome. For the first time, diploid sugar beet plants containing the nematode resistance from *Patellifolia* arose (Savitsky 1975). Subsequently, several monosomic addition lines (MALs) of the different *Patellifolia* species have been

produced (Speckmann and Bock 1982; Heijbroek et al. 1983; Löptien 1984; Jung et al. 1986; Jung and Wricke 1987; Reamon-Ramos and Wricke 1992).

First isozyme analysis led to the conclusion that several *Patellifolia* chromosomes contained resistance genes (Jung et al. 1986). Using the monosomic *P. procumbens* addition lines, Lange et al. (1988) analyzed the phenotypes conferred by the single chromosomes. They found that all MALs showed growth reductions and grew gall-like formations on the roots. Including the isozyme analysis conducted by Van Geyt et al. (1988), the characteristics of each added chromosome were deduced. MALs containing chromosomes 1 or 7 of *P. procumbens* showed nematode resistance. The analysis of *P. webbiana* MALs highlighted the presence of resistance genes on chromosomes 1, 7, and 8 (Reamon-Ramos and Wricke 1992), while resistance in *P. patellaris* has been reported to be located only on chromosome 1 (Lange et al. 1990). Accordingly, the resistance genes were named *Hs1*, located on the homologous chromosomes 1 of all three *Patellifolia* species, *Hs2*, from the homologous chromosomes 7 of *P. procumbens* and *P. webbiana*, and *Hs3* from *P. webbiana* chromosome 8 (Thurau et al. 2010). Different independent diploid translocation lines were generated from the monosomic addition lines (Savitsky 1975; Jung and Wricke 1987) and markers for detecting the translocations were designed (Jung et al. 1990; Jung et al. 1992). Heller et al. (1996) mapped the resistance genes *Hs1<sup>pro-1</sup>*, *Hs1<sup>web-1</sup>*, and *Hs2<sup>web-7</sup>* in four non-related translocation lines and found that integrations into the sugar beet genome had occurred at the same position at the end of chromosome 9, indicating a preferred point of integration. Causative for this hotspot are homologous regions between *B. vulgaris* chromosome 9 and *P. procumbens* chromosome 1 (Schmidt et al. 1997; Kleine et al. 1998). Recently, *P. procumbens* chromosome 1 has been relabeled to chromosome 9, due to its homology with the according sugar beet chromosome (personal communication M. Arslan, PBI Kiel, based on unpublished data from Dr. Kevin Dorn, USDA, Fort Collins, USA).

The *P. procumbens* translocation line A906001 contains the smallest wild beet translocation compared to other translocation lines (Jung et al. 1992). It was used for the generation of a yeast artificial chromosome (YAC) library and a subsequent screening with the pRK643 marker identified by Jung et al. (1992), which was shown to be closely linked to the nematode resistance gene (Kleine et al. 1995). Consequently, three clones could be selected to test a cDNA library made from A906001 roots infected with *H. schachtii*. Among the resulting three cDNA clones, the 1.6 kb transcript of clone 1832 proved to be present only in the resistant plants. The expression of the 1832 cDNA in transformed wild type sugar beet roots led to an incompatible reaction as observable in the resistant A906001 translocation line. Hence, the first beet cyst nematode resistance gene (*Hs1<sup>pro-1</sup>*, for better readability named *Hs1* hereafter) was identified and cloned (Cai et al. 1997). Originally, *Hs1* was described to encode a protein of 282 amino acids, harboring an extra-cytoplasmic LRR domain that could function as a receptor for elicitor recognition. Similarities to the protein structure of the *Cf-9* resistance gene from tomato were also found (Cai et al. 1997). It was further shown to be expressed specifically in syncytia and upregulated upon nematode attack (Thurau et al. 2003). However, a few years later, detailed analysis revealed different predicted plant proteins with high similarity to *Hs1*, among them an *A. thaliana* homologue encoding a 435 amino acid protein with no function in nematode resistance. Based on these homologies, 208 additional amino acids lacking at the *P. procumbens* *Hs1* N-terminus were identified, incorporating large stretches previously identified as promoter regions. Conclusively, *Hs1* encodes a protein of 490 amino acids (McLean et al. 2007). Similar to the results from Cai et al. (1997), McLean et al. (2007) could not detect complete but only enhanced resistance after transforming soybean with the full-length *Hs1* cDNA. A recent study has demonstrated the presence of functional *Hs1*-homologous resistance genes in other plant species. In pine (*Pinus massoniana*), the homolog *PmHs1<sup>pro-1</sup>* recognizes an effector of the pine wood nematode and leads to the

activation of resistance responses (Xie et al. 2024).

Soon after *Hs1* had been identified, translocation lines exhibiting nematode resistance but lacking the identified resistance gene were described (Sandal et al. 1997; Kleine et al. 1998; Schulte et al. 2006). One of those was the line TR363 derived from the translocation line PRO4. Together with the A906001-derived translocation line TR520 containing the *Hs1* gene, it has been used extensively for identifying the second resistance gene (Tian 2003; Schulte et al. 2006; Capistrano 2009; Jäger 2012). Recently, the nematode resistance gene *Hs4* has been identified (Kumar et al. 2021), which will be highlighted in more detail in chapter 1.7.3.

Continued breeding efforts have led to the release of a broad spectrum of tolerant sugar beet germplasms (for example Richardson 2018; Todd et al. 2024). Sugar beet cultivars showing either tolerance or resistance to BCN are available. Resistant cultivars carrying the complete *P. procumbens* translocation, like Nemata, inhibit the development of nematodes but show yield penalties. As they are derived from *Patellifolia* translocation lines, they still contain large regions of the wild beet genome, leading to yield reductions. Consequently, they are only cultivated on a limited scale (Märländer et al. 2003; Reuther et al. 2017). Tolerant cultivars are still successfully infected by *H. schachtii* larvae but show an increased yield potential under infested conditions. Compared to susceptible cultivars they also exhibit lower BCN reproduction rates (Reuther et al. 2017). Likely, all modern tolerant cultivars originated from a few accessions of the beet progenitor *B. vulgaris* ssp. *maritima* sampled at the Loire Valley Estuary in France. Hence, the tolerant or partially resistant varieties based on the resistance found in *B. vulgaris* ssp. *maritima* might be closely related (Lewellen and Pakish 2005; Panella et al. 2020).

Using the tolerant beet genotype U2Bv, the nematode tolerance locus from sea beet located on sugar beet chromosome 5 was recently proven to contain a cluster of genes with high similarity to *A. thaliana* nodule inception protein-like protein 7 (NLP7) (Sielemann et al. 2023a). They examined changes in the expression profiles of four *BvNLP7* genes and found the genes *NLP7-T1* and *NLP7-T2* to be significantly lower expressed in susceptible compared to tolerant genotypes. Further, all four genes were upregulated after nematode infection, the strongest upregulation could however be observed in the tolerant genotype. Based on their findings they concluded that nematode tolerance in the U2Bv genotype might be due to a dosage effect. Even though pyramiding of resistances from *B. vulgaris* ssp. *maritima* and *Patellifolia* has been suggested (Lange and Bock 1994), cultivars available comprise either of these resistance mechanisms.

### 1.7.1 Resistance in non-related plant species

As delineated above (see 1.5), the model plant *Arabidopsis* is susceptible to BCN. In the past years, several *Arabidopsis* susceptibility genes were identified which could be exploited for enhancing nematode tolerance in related crop species. Among them are *RAP2.6*, whose overexpression leads to an expression increase in jasmonic acid-responsive genes and enhanced callose deposition (Ali et al. 2013), the TIR-domain containing *AtPP2-A3* and *AtPP2-A8*, which contribute to susceptibility when overexpressed but reduce *H. schachtii* infections when mutated (Wojszko et al. 2023), the transcription factors bHLH25 and bHLH27 aiding in nematode parasitism (Jin et al. 2011), and different transcription factors modulating the root system, thereby conferring nematode tolerance (Willig et al. 2022; Willig et al. 2024). Recently, a QTL affecting the sex ratio of developing nematodes on *Arabidopsis* has been described (Anwer et al. 2018). The latest advances in high-throughput screening of large *Arabidopsis* sets will surely assist in the identification of naturally occurring differences of nematode tolerances among *Arabidopsis* ecotypes (Kranse et al. 2022; Willig et al. 2023).

Similarly, rapeseed (*Brassica napus*) is susceptible to BCN infections and the good host qualities of the plant pose a problem in crop rotation systems. No genetic variation for BCN-resistance has been found in *B. napus* (Lelivelt 1995; Nielsen et al. 2003), but certain accessions of the two related species oil radish (*Raphanus sativus*) and white mustard (*Sinapis alba*) were shown to be resistant to BCN (Steele et al. 1983). Crosses with resistant *Raphanus* and *Sinapis* accessions resulted in hybrid offspring exhibiting high BCN resistance levels. However, chromosomal instability and sterility have hampered their use in breeding programs (Lelivelt and Krens 1992; Lelivelt et al. 1993b). De Block (1989) established a first genotype-independent *Agrobacterium*-mediated transformation protocol for rapeseed using antibiotic or herbicide resistance genes for selection. They transformed hypocotyls and obtained transformation rates of up to 30 % for the spring-type cultivar Westar. Cardoza and Stewart (2003) introduced preconditioning and an altered co-cultivation, and managed to improve the rooting efficiency of shoots arising after Westar hypocotyl transformation. Similarly, Tang et al. (2011) demonstrated that pre-culturing of hypocotyl segments could increase regeneration efficiencies from 13 % to 24 %. Utilizing this protocol, Zhong et al. (2019) transferred the two *P. procumbens* genes *cZR3* and *Hs1* to rapeseed which resulted in the activation of plant-defense-related genes and ultimately in a decrease of BCN female numbers. Even though *cZR3* has been shown to have originated from *B. vulgaris* (Jäger 2012; Kumar 2020), the observed enhanced resistance indicates the transferability of nematode resistance genes between plants from the Amaranthaceae and Brassicaceae families. Further, it demonstrated the feasibility of rapeseed hypocotyl transformation for BCN resistance gene transfer; resistance genes from *Patellifolia* might therefore be exploited to generate nematode-resistant rapeseed.

### 1.7.2 The ultrastructure of syncytia in resistant host plants

The development of resistant sugar beet translocation lines enabled the ultrastructural analysis of syncytia during the resistance reaction. The first comprehensive comparison of syncytia in regards to BCN susceptibility was conducted by Holtmann et al. (2000). They observed the same mode of root invasion and syncytium induction in both genotypes. The resistant genotype did not show signs of an early hypersensitive response. The first prominent differences arose two days post-inoculation (dpi) when membrane aggregations (MA) formed from ER membranes were observable in syncytia of the resistant genotype. The MA differed in size and could fill whole syncytial cells. On the outer tubules of these, ribosomes accumulated. Apart from the prevalence of rough ER in the resistant system, those syncytia also contained fewer but larger vacuoles. In the susceptible system, smooth ER dominated and vacuoles were abundant and smaller. Nevertheless, syncytia exhibiting MA did not show immediate degradation of cytoplasm or cell organelles. The degeneration became evident at 4 dpi though, and associated nematodes rarely reached the adult stage. Nonetheless, some female juveniles developed to advanced stages, and their syncytia remained partially intact, although MA could also be detected here (Holtmann et al. 2000). To decipher if the occurrence of MA resulted from the action of the previously described resistance gene *Hs1*, the gene was transformed into susceptible sugar beet hairy roots. However, no MA could be detected in syncytia induced in this background. The fact that the MA were formed independently of *Hs1* was further confirmed by an analysis of a population derived from the translocation line PRO3, where *Hs1* is absent. Syncytia in this genotype showed the same characteristics as those induced in the translocation line containing *Hs1*. Apart from the formation of MA, the occurrence of starch granules in plastids was a main difference to the susceptible controls (Holtmann 2000).

Comparisons between resistant and susceptible genotypes were also conducted in *Raphanus*. Similar to the observations in sugar beet, syncytia could be induced in both systems and

displayed dense cytoplasm and an increase in organelle abundance. At 3 dpi, differences between the two genotypes became apparent. The vacuoles in the resistant roots became larger than those in the susceptible ones. While smooth ER prevailed in the susceptible background, syncytia in resistant plants contained mainly rough ER and many free ribosomes in the cytoplasm. Cell wall ingrowths could be observed in both genotypes but were much more developed in the susceptible roots. Like in resistant sugar beet, the degeneration process started at 4-5 dpi. It was accompanied by the accumulation of granular material in expanding vacuoles and the occurrence of osmiophilic, lipid-like globules, resulting in a restriction of female development. However, the degenerated syncytia were able to provide sufficient nutrients for the development of males (Wyss et al. 1984).

### 1.7.3 The resistance gene *Hs4*

After several attempts to identify the second nematode resistance gene located on the *Patellifolia* translocation, the gene *Hs4* could be identified by Kumar et al. (2021) through comparative sequence analysis. Two resistant translocation lines with differently sized translocations, TR520 and TR363, and the susceptible translocation line TR659, produced by the  $\gamma$ -irradiation of TR520, were whole-genome sequenced and the comparison of the sequences resulted in the identification of a critical region present in both resistant but absent from the susceptible genotype. Within it, 33 gene models were identified, and after cross-validation with expression data from TR520 roots after nematode infection, the rhomboid-like protease *Hs4* was identified. It encodes a protein of 210 amino acids and is predicted to be ER-bound. Interestingly, homologs could be detected in sugar beet and spinach (*Spinacia oleracea*). The encoded polypeptides showed 60 % similarity to *Hs4*. The *B. vulgaris* homolog has 102 additional amino acids at the polypeptide's N-terminus. Further, Kumar et al. (2021) found that *Hs4* contains a leader sequence for the transport into the ER which is lacking in the homolog in sugar beet. Differences in subcellular localization of the two homologs are therefore highly likely.

Various proteases contributing to plant defense responses are known. Several of them function in the apoplast, the cytoplasm, or vacuoles, but endomembrane proteases are also described (Thomas and van der Hoorn 2018). Papain-like cysteine endopeptidases (CysEPs) harbor a C-terminal KDEL signal, leading to their retention at the ER. *AtCEP1* is a CysEP expressed in Arabidopsis and found to be expressed in the ER after the plants are attacked by the fungus *Erysiphe cruciferarum*. The protein accumulates specifically around the haustoria induced by the pathogen, contributing to controlled cell death to restrict the spread of the pathogen (Höwing et al. 2014; Höwing et al. 2017). A CysEP directly involved in nematode defense has been identified in tomato. The interaction of the *Globodera rostochiensis* effector Gr-VAP1 with the apoplastic protease Rcr3 results in structural perturbations of the protease's active site. This conformation change is detected by the immune receptor Cf-2 and leads to the activation of defense-related plant responses (Lozano-Torres et al. 2012).

Among the proteases, three families can catalyze intramembrane proteolysis. One of them is the family of rhomboid proteases (Urban and Dickey 2011). They were first discovered in *Drosophila*, where the ER membrane-anchored growth factor Spitz is cleaved by the intramembrane serine protease Rhomboid-1, localized in the Golgi apparatus, to enable its secretion from the cell (Urban et al. 2001). Rhomboid proteases consist of six or, in the case of eukaryotes and hence plants, often seven transmembrane domains (TMDs). They are characterized by a serine protease catalytic unit that cleaves the substrates inside the membrane. Rhomboid proteins can also lack the catalytic residues, rendering them inactive proteases, and are then classified as iRhoms. Rhomboids can be found in all domains of life: In animals, they enable cell signaling and contribute to mitochondrial fusion, mitophagy, and apoptosis (Lemberg and Freeman 2007; Freeman 2009; Urban and Dickey 2011). The

mammalian ER-located rhomboid protease RHBLD4 is activated upon ER stress and participates in recognizing and cleaving anomalous membrane proteins as part of the ER-associated degradation pathway. Surprisingly, RHBLD4 can cleave non-membrane-spanning domains of membrane-located substrates (Fleig et al. 2012). In bacteria, the rhomboid proteases are involved in population-density-dependent gene expression alteration. In eukaryotic, unicellular parasites, rhomboids enable the cleavage of adhesins important for host invasion. In yeast (*Saccharomyces cerevisiae*), the rhomboid protease Pcp1 located in the mitochondria controls the fusion of mitochondria membranes by cleaving a GTPase. Thirteen and twelve rhomboid proteases were found in Arabidopsis and rice, respectively (Lemberg and Freeman 2007; Freeman 2009; Urban and Dickey 2011). In plants, Rhomboid-1 homologues located in mitochondria and chloroplasts have been identified (Kmiec-Wisniewska et al. 2008). Recently, the involvement of plant rhomboids in the hypoxia stress reaction was described. Under conditions of oxygen and mitochondrial stress, the ER membrane-bound protease RHOMBOID-LIKE 2 (RBL2) mediates the release of the ER-located transcription factor ANAC013 to enable the transcriptional activation of hypoxia core genes in the nucleus of Arabidopsis (Eysholdt-Derzsó et al. 2023).

Kumar et al. (2021) knocked out *Hs4* in hairy roots of the resistant sugar beet variety Nemata and obtained roots highly susceptible to *H. schachtii*. Reciprocally, when they overexpressed *Hs4* in the susceptible *B. vulgaris* background, they observed hairy roots highly resistant to the BCN, depending on the gene expression level achieved. These analyses indicated that *Hs4* is the second resistance gene located on the translocation from *P. procumbens* chromosome 9.

## 1.8 Aims and Objectives

In the present study, I aimed to characterize the previously identified nematode resistance gene *Hs4* in different genomic backgrounds. The work is structured into four work packages.

In the first work package (Chapter 2), I identified homologs of *Hs4* and *BvHs4* in different *Patellifolia* and *Beta* species. Following sequencing of the homologs from various species, I evaluated the gene and resulting protein structures. Further, I determined local expression differences between the two genes in a broad set of species. Using *P. procumbens* and *B. vulgaris* I then compared the expression of the homologs over time in different tissues and under nematode infestation.

In the second work package (Chapter 3), I established Arabidopsis T<sub>3</sub> lines expressing *Hs4* under the control of either a constitutive or inducible promoter. Using a subset of the lines generated, I analyzed the resistance reaction according to the *Hs4* expression levels in this non-related species.

In work package three (Chapter 4), I examined the ultrastructure of syncytia in the roots of the transgenic Arabidopsis. I compared the results to syncytia from wild type roots as well as non-inoculated control roots of the different genotypes.

In the final work package (Chapter 5), I aspired to generate transgenic rapeseed plants expressing *Hs4* for further analysis.

The questions to answer during my study were:

1. Do homologs of *Hs4* or *BvHs4* exist in other *Patellifolia* and *Beta* species?
2. Does the expression of *Hs4* and its *Beta* homolog differ between tissues, across time, or upon nematode inoculation?
3. Does *Hs4* confer resistance in a non-related species in an expression-dependent manner?
4. Are structural differences between the syncytia of *Hs4*-expressing and wild type plants detectable? If so, do the differences correlate with nematode infestation?
5. Can transgenic rapeseed plants expressing *Hs4* be obtained?

## **2 Homologs of the beet cyst nematode resistance gene *Hs4* are differentially expressed between *Patellifolia* and *Beta* species**

### **2.1 Materials and Methods**

#### **2.1.1 Plant material and growth conditions**

Plants of different *Beta* or *Patellifolia* species available from the Plant Breeding Institute as well as accessions ordered from the Leibniz Institute of Plant Genetics and Crop Plant Research (IPK; Gatersleben, Germany), the translocation lines TR363 and TR520 and the TR520-derived variety Nemata (Supplementary Table 1) were grown in a greenhouse or a climate chamber, respectively, under long-day conditions (LD; 16 h light / 8 h dark). Plants destined for further inoculation experiments were sown and germinated in germination trays in a climate chamber under LD conditions and re-potted to sand tubes filled with quartz sand (grain size 0.1-0.4 mm) once the plantlets were ca. 11 days old and further kept under the same growing conditions.

#### **2.1.2 DNA isolation, PCR, and Sanger sequencing**

Samples of different plant tissues were taken at several time points, frozen in liquid nitrogen, and stored at -70°C until further usage. Following the grinding of the tissues, genomic DNA was isolated using the NucleoSpin Plant II kit (Macherey-Nagel, Düren, Germany) following the manufacturer's instructions or the plant DNA minipreparation protocol (Dellaporta et al. 1983). Before further usage, the genomic DNA was checked on a 1 % agarose gel (90V, 30 min or 80V, 12 min).

A non-sequenced (unresolved) region in the first *Hs4* intron was amplified from the variety Nemata (Supplementary Table 1) with a Taq polymerase (Biozym Scientific GmbH, Hessisch Oldendorf, Germany) using AK\_F2/AS\_R5 (Supplementary Table 2).

A first PCR screen for the presence or absence of *Hs4* in *Patellifolia* and its homolog in *Beta* was conducted using AS\_F7/AS\_R7 (Supplementary Table 2), which amplified a region of 1217 bp and 1499 bp, respectively. Amplification of the whole *Hs4* or the *Beta* homolog's genomic regions was done using either a Taq polymerase (Biozym Scientific GmbH) or Phusion™ High-Fidelity polymerase (ThermoFisher Scientific™, Waltham, MA, USA). For specific *Hs4* amplification, the primer combination AK\_F5/AK\_R6 (Supplementary Table 2) and for the amplification of other *Beta* homologs AS\_BvHs4\_F1/AS\_BvHs4\_R0 (Supplementary Table 2) were used. PCR results were verified on a 1 % agarose gel (90V, 30-40 min).

Using the CloneJET PCR Cloning Kit (ThermoFisher Scientific™), double bands were cloned into the pJET1.2/blunt cloning vector according to the manufacturer's instructions and transformed into competent *Escherichia coli* (strain DH5a) via the heat-shock method (Froger and Hall 2007). Following overnight incubation at 37 °C on LB plates supplemented with ampicillin (50 µg/ml), colonies were screened for the plasmid's presence by PCR. Positive colonies were cultured overnight in 5 ml LB with ampicillin on a shaker. Plasmids were then isolated using the Presto Mini Plasmid Kit (Geneaid, New Taipei City, Taiwan) or the NucleoSpin Plasmid Mini Kit (Macherey-Nagel) and used for PCR in a 1:1000 dilution.

Amplified gene fragments or whole genes were Sanger sequenced on an Applied Biosystems 3730xl DNA Analyzer (ThermoScientific™, via IKMB, Kiel University) using a set of different primers (Supplementary Table 2).

### 2.1.3 DNA and polypeptide sequence analysis

Sanger sequences were aligned to the reference sequences using the CLC Main Workbench 20 (Qiagen, Hilden, Germany). As reference, the *Hs4* sequence derived from TR520 by Kumar et al. (2021) was used for the *Patellifolia* sequences and the genomic RefBeet-1.2.2 (Dohm et al. 2014) sequence of the rhomboid-like protein 11 from sugar beet (NCBI Reference Sequence XM\_010669575.1) was deployed for all *Beta* sequences. After alignment, specific *Hs4* or *Beta* homolog sequences were generated for each accession sequenced using the CLC Main Workbench. Using the CLC-incorporated tool for protein translation, the respective polypeptide sequences were generated. These were aligned using the MUSCLE algorithm and a maximum-likelihood phylogenetic tree (500 bootstraps) was generated from the alignment using MEGA11 (Tamura et al. 2021). Alignments were visualized using pyBoxshade v. 1.2 (mdbaron42 2021).

For DNA sequence comparisons, the blastn suite (Camacho et al. 2009) of the National Center for Biotechnology Information (Sayers et al. 2022) was deployed.

The localization and conformation of single polypeptides were predicted using DeepLoc2.1 (Ødum et al. 2024) and DeepTMHMM (Hallgren et al. 2022), respectively.

### 2.1.4 *In vivo* nematode infection assay

The *H. schachtii* strain ‘Schach 0’ was propagated on susceptible sugar beet or rapeseed in sand-filled tubes in a greenhouse under LD conditions. Larvae of *H. schachtii* were hatched from cysts in 3 mM ZnCl<sub>2</sub> in a Baermann-funnel aperture. The J2 larvae were concentrated to the desired density of 150 larvae per ml and used for the inoculation.

Plants of *B. vulgaris* and *P. procumbens* were grown as described (see 2.1.1). Circa two weeks after the transfer to sand tubes, the plants were inoculated with a 2 ml suspension containing 300 J2 larvae of *H. schachtii* using a Muto syringe. Developing females were assessed four weeks later.

### 2.1.5 Expression analysis

In addition to the accessions used for the sequence analysis, further accessions of *P. patellaris*, *B. adanensis*, and *B. vulgaris* ssp. *martima* were included. All plants were grown in the greenhouse as described above (see 2.1.1). For the initial expression test, leaf and root samples of three biological replicates per accession were taken. For the spatiotemporal expression analysis, samples of plant roots (R), hypocotyls (H), cotyledons (C), and leaves (L) were taken after germination (R, H, C), upon the development of the first true leaves (R, C, L), 21 days after germination (R, L), before inoculation (R, L) as well as at three and 28 dpi (R, L). The samples were frozen in liquid nitrogen and total RNA was isolated using the Universal RNA Kit (roboklon, Berlin, Germany), according to the manufacturer’s instructions. The RNA quality was checked using a NanoDrop2000 spectrophotometer (ThermoFisher Scientific™) and agarose gel electrophoresis (2 % gel, 100V, 12 min).

100 ng of RNA were incubated with 1 U DNase (ThermoFisher Scientific™) at 37°C for 30 min. Subsequently, the DNase was inactivated by adding 1 µl EDTA (50 mM) followed by incubation at 65°C for 10 min. Then, the cDNA was generated using the First Strand cDNA Synthesis Kit (ThermoFisher Scientific™), following the manufacturer’s instructions. Using the GAPDH primer combination for *Beta* (BvGAPDH\_F/BvGAPDH\_R, Supplementary Table 2) or *Patellifolia* (AS\_BvPp\_GAPDH\_F/AS\_BvPp\_GAPDH\_R, Supplementary Table 2), respectively, the cDNA quality was assessed by PCR.

Following the manufacturer's instructions, two  $\mu\text{l}$  cDNA were used for quantitative reverse transcription PCR (RT-qPCR) deploying the Platinum<sup>TM</sup> SYBR<sup>TM</sup> Green qPCR SuperMix-UDG (Invitrogen<sup>TM</sup>, ThermoFisher Scientific<sup>TM</sup>). For gene expression normalization, the *GAPDH* gene was used. For detection of *Hs4* and its *Beta* homolog the primer combination AK\_F7/AK\_R5 and AS\_BvHs4\_F1/AS\_BvHs4\_R7 (Supplementary Table 2), respectively, was used. The primer combination AS\_Hs1\_F/AS\_Hs1\_R (Supplementary Table 2) was used for detection of *Hs1*. Employing the Pfaffl method (Pfaffl 2001), the obtained Ct-values (cycle threshold) were evaluated.

### 2.1.6 Statistical analysis

Normally distributed data were statistically analyzed by a one-way analysis of variance (ANOVA) using Microsoft Excel (Microsoft Corporation, Redmond, WA, USA). The non-normally distributed data were statistically analyzed by the Kruskal-Wallis rank sum test, followed by a Hochberg-corrected Dunn post-hoc test using the online calculator Astatsa (Vasavada 2016) and the open-source statistical computing software R version 4.3.3 (R Core Team 2024) using the package "PMCMRplus" (Pohlert 2023).

## 2.2 Results

### 2.2.1 Verifying the *Hs4* gene structure

A first *in silico* analysis of the *Hs4* gene described the genomic region to cover 5786 bp (Kumar 2020) or 5664 bp (Kumar et al. 2021), containing five exons and five introns. The cDNA of 633 bp encodes a protein of 210 amino acids (Kumar 2020; Kumar et al. 2021). Due to these variations, I first verified these data before starting my analysis of the *Hs4* variation in different accessions and across species. The TR520-based *Hs4* sequence obtained from Avneesh Kumar consisted of 5857 bases, including the 5'- and 3'-untranslated regions (UTRs). The gene harbored six exons and five introns, out of which five exons were protein-coding (Figure 3). The sequence I obtained contained a large stretch (964 bp) of unknown nucleotides (NNN) in the first intron. I used the primer AK\_F2/AS\_R5 (Supplementary Table 2) for amplifying the 1885 bp large region containing the N-stretch from the translocation-derived hybrid variety Nemata. In the consequent agarose gel electrophoresis, the amplified PCR fragment was already smaller than expected with an approximate size of 1000 bp (data not shown). I sequenced the generated fragment using AK\_F2, AS\_R5, AS\_F1, and AS\_R6 (Supplementary Table 2) and found that all primers had an overlapping region. Consequently, I could resolve the large N-stretch region to contain 107 bp, thereby reducing the genomic region of *Hs4* to 4999 bp. The composition of the cDNA and the resulting protein remained unchanged.

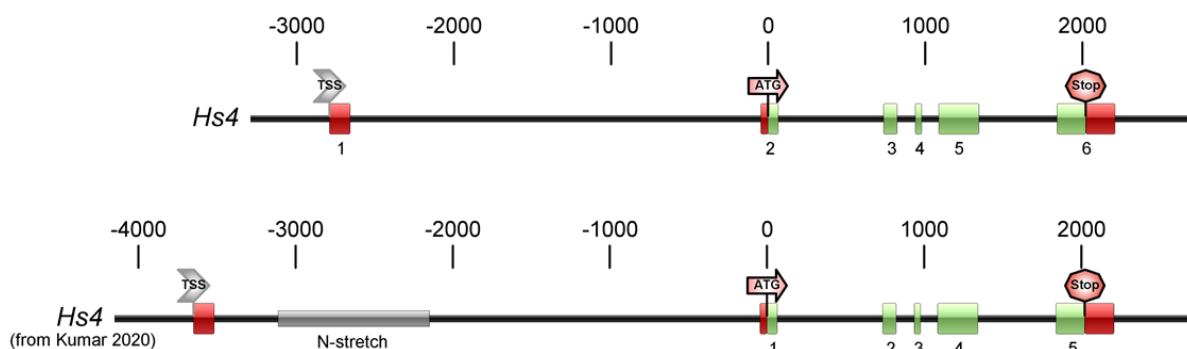


**Figure 3:** Comparison of the *Hs4* sequence verified in the current study and the previous *Hs4* sequence obtained from Kumar (2020). The genomic region of *Hs4* spans 4999 bp and contains six exons and five introns.

Contrastingly, *Hs4* as annotated by Kumar (2020) spans 5857 bp and has five exons. It also harbors an unidentified sequence region (N-stretch). Colors differentiate the protein-coding exons (green) from the UTR-containing exons or exon parts (red). The exons are numbered with 1-6 accordingly. The start (ATG) and stop (Stop) codon, and the transcription start site (TSS) of the gene are indicated. The figure was generated using the Illustrator for Biological Sequences software (Liu et al. 2015).

### 2.2.2 The distribution pattern of *Hs4* homologs across *Patellifolia* and *Beta* species

The *Hs4* gene was cloned from a translocation line (TR520) derived from a monosomic addition line that arose after hybridization between *Beta vulgaris* and *Patellifolia procumbens*. As all *Patellifolia* species are described as resistant to the BCN, I hypothesized that *Hs4* was present in the three different *Patellifolia* species. Hence, I investigated if homologs of *Hs4* could be detected in different accessions of these species. Additionally, as *B. vulgaris* has a homolog of *Hs4* (hereafter named *BvHs4*), I hypothesized that a similar homolog might be present in other *Beta* species as well. Accordingly, I screened several *Beta* species for homologous sequences to *BvHs4*. Hence, I designed a primer pair (AS\_F7/AS\_R7, Supplementary Table 2) that amplifies both homologs in both genera. I chose a conserved protein region between *Hs4* and *BvHs4* (Supplementary Figure 1A) to locate the primer set, expecting a low variation at the sequence level. Still, a mismatched nucleotide was bridged with a wobble base in the reverse primer's sequence to guarantee perfect primer binding (Supplementary Figure 1B). The primer set is expected to amplify 1217 bp of *Hs4* and 1499 bp of *BvHs4* (Figure 4A). Homologs showing sequence similarities to any of the two genes should therefore be amplified with the homology primers.

Using the homology primer set AS\_F7/AS\_R7, I screened the genomic DNA of the different *Patellifolia* accessions. I could detect *Hs4* homologs in all five *P. procumbens*, six *P. webbiana*, and three *P. patellaris* accessions analyzed (Figure 4B). The homologs detected in the different *Patellifolia* species will accordingly be named *PpHs4* from *P. procumbens*, *PwHs4* from *P. webbiana*, and *PpatHs4* from *P. patellaris* for simplicity reasons, while *Hs4* refers to the original coding gene sequence identified by Kumar et al. (2021). Additionally, I screened the translocation lines TR363 and TR520 and the hybrid variety Nemata with the same primer set. As the primers also bind to the exons of *BvHs4* (Figure 4A), double bands could be observed in the resistant sugar beets (Figure 4B). While the lower band resembles *Hs4* from the *P. procumbens* translocation, the upper band at 1499 bp delineates *BvHs4* from the *B. vulgaris* background.

The bands obtained for the *Patellifolia* species were Sanger sequenced to see if they were *Hs4*-homologous sequences. Indeed, the sequencing results revealed that all accessions contained a *Hs4* homolog with a high sequence similarity to *Hs4* (data not shown).

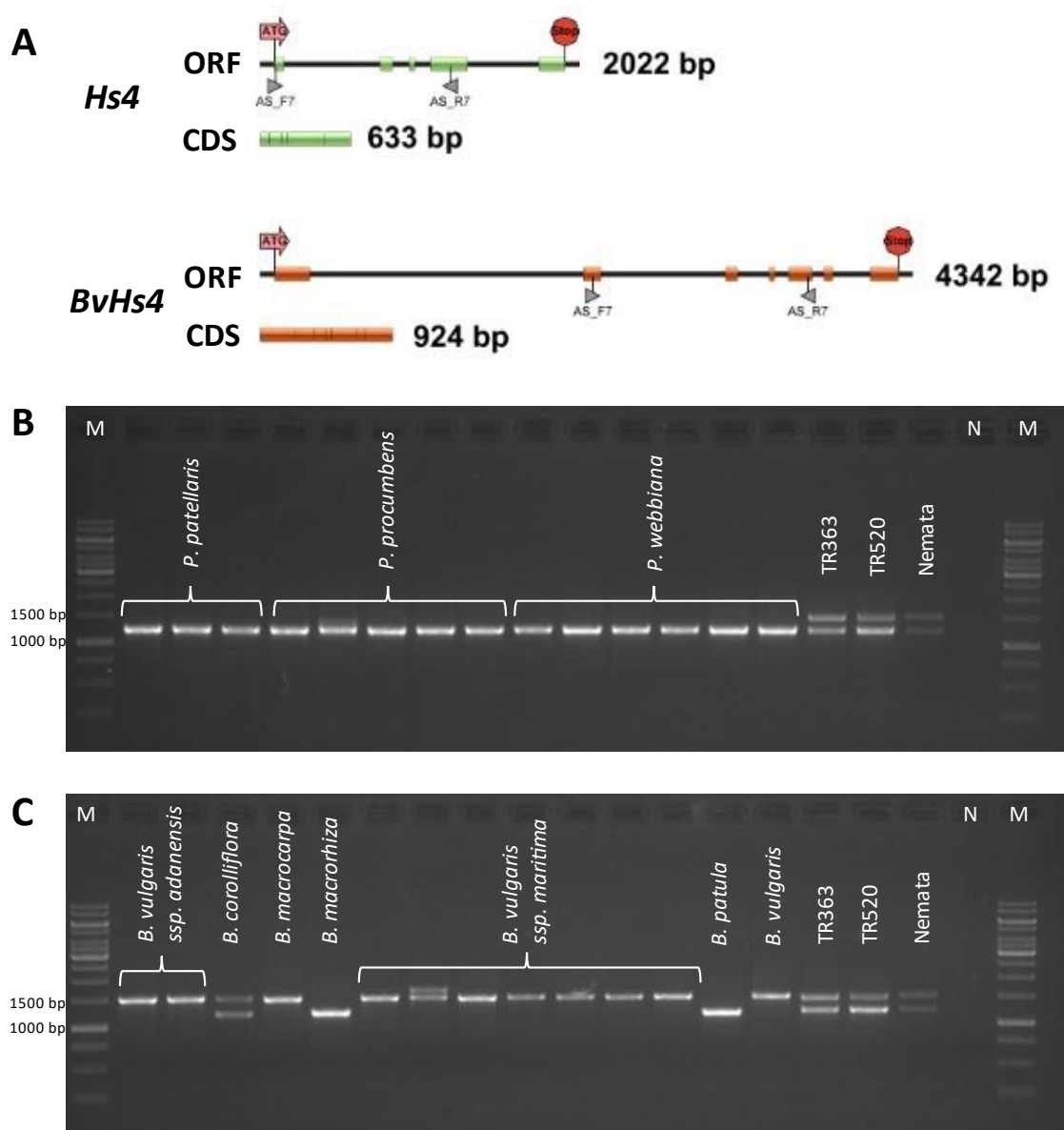


**Figure 4:** (A) Gene structure of *Hs4* and the *Beta* homolog (*BvHs4*) open reading frames (ORF) and the according coding sequence (CDS) derived from the genomic DNA. Exons are shown in green (*Hs4*) and orange (*BvHs4*), respectively. The start codon (ATG) as well as the stop codon are indicated. The positions of the homology primers (AS\_F7/AS\_R7) used for the amplification of both genes across the species are shown. (B and C) Agarose gel electrophoresis (1 %, 90V, 40 min) of a PCR amplifying *Hs4* and its *Beta* homolog. Using the same set of primers, a single band at 1217 bp was amplified in all *Patellifolia* species (B), while in most *Beta* samples a band at 1499 bp was generated (C). Single *Beta* species show a deviation in the form of double or lower bands. The translocation lines (TR363 and TR520) and the resistant cultivar Nemata serve as controls, containing both *Hs4* and its *Beta* homolog and showing a clear double-band. M: 1 kb ladder, N: negative control. The gene structures were generated using the Illustrator for Biological Sequences software (Liu et al. 2015).

To determine if a *BvHs4* homolog was present in different *Beta* species, I used the species *B. vulgaris ssp. adanensis*, *B. corolliflora*, *B. macrocarpa*, *B. macrorhiza*, *B. vulgaris ssp. maritima*, *B. patula*, and *B. vulgaris* (Supplementary Table 1). As for the *Patellifolia* species, I wanted to grow several accessions per species. Due to the bad germination rates of several accessions, I could only use single accessions of *B. corolliflora*, *B. macrocarpa*, *B. macrorhiza*, and *B. patula* for the following sequence analysis. I also aimed to obtain DNA for *B. nana*, however, the seeds did not germinate and the material had to be excluded from further analysis.

Using the homology primers, I screened the different *Beta* accessions. I could detect bands at a similar size as *BvHs4* (1499 bp) in eleven of thirteen accessions (Figure 4C). Following the homolog designation of the *Patellifolia* species, the *Beta* homologs will be named *BaHs4* (*B. vulgaris* ssp. *adanensis*), *BcHs4* (*B. corolliflora*), *BmcHs4* (*B. macrocarpa*), *BmrHs4* (*B. macrorrhiza*), *BmHs4* (*B. vulgaris* ssp. *maritima*), and *BpHs4* (*B. patula*). For *BcHs4* (Figure 4C) a double band was obtained. While the upper band was in the size range of the *BvHs4* gene's expected size, the lower band was smaller than the *Hs4*-expected size (1217 bp), whose size was represented by the lower bands of the translocation lines used as reference. For one *B. vulgaris* ssp. *maritima* accession (seed code 190649) a second band slightly above *BvHs4* was detected. *B. macrorrhiza* and *B. patula* showed single bands located below the expected size of a *BvHs4* homolog. However, the primer set used spans a huge intronic area, where sequence deviations, including deletions leading to smaller bands, are likely.

The obtained single bands were sequenced to see if their sequence was similar to that of *BvHs4*. All single bands analyzed showed high sequence similarity to the homolog from *B. vulgaris* (data not shown). As only a fraction of the complete gene had been amplified and the single bands were clear homologs of *BvHs4*, I did not analyze the double bands further.

### 2.2.3 Sequence variations between *Hs4* and its homologs from *Patellifolia* and *Beta* species

After it had been demonstrated that all *Patellifolia* and *Beta* species analyzed contained homologs of *Hs4* and *BvHs4*, respectively, I investigated if sequence variations among existing homologs were present. I selected single accessions of each species, based on the clarity of the first sequencing data, to amplify the whole genomic region from start to stop codon (Figure 4A) using gene-specific primers for both homologs separately (see 2.1.2). This region contains the protein-coding exons 2-6 of *Hs4* which spans 2022 bp (exon 1 resembles the 5' untranslated region separated from the start codon by 2658 bp), and exons 1-7 in *BvHs4*, spanning 4342 bp.

As *Hs4* was identified from a translocation line derived from a monosomic addition line that arose after hybridization of *B. vulgaris* and *P. procumbens*, I expected genes identified from *P. procumbens* to exhibit the closest sequence similarity to *Hs4*. Due to the close relatedness of *P. procumbens* and *P. webbiana* (see 1.2), I hypothesized to find highly similar sequences in the accessions of those two species while *P. patellaris* homologs were expected to show more deviations from *Hs4*.

Based on the phylogeny of the genus *Beta* (see 1.2), I expected to detect high *BvHs4* sequence similarity in homologs found in the species *B. macrocarpa*, *B. patula*, *B. vulgaris* ssp. *adanensis*, and *B. vulgaris* ssp. *maritima*. Higher sequence divergence was anticipated in the homologs of *B. corolliflora* and *B. macrorrhiza* as they belong to the genus *Corollinae*.

#### 2.2.3.1 Variations at the DNA level

As a first step, I analyzed *Hs4* homologs from all *Patellifolia* accessions available. The *Hs4* gene from the translocation lines TR363/TR520 and Nemata was also sequenced. Additionally, I used the first *P. procumbens* draft genome made available (personal communication A. Kumar and K. Dorn, USDA, Fort Collins, USA) for *Hs4* sequence analysis. The alignment of the different *Hs4* sequences revealed that *Hs4* and its homologs are highly conserved across all *Patellifolia* species and the regions of the protein-coding exons 2-6 present in *Hs4* (Figure 4A) could be transferred to *PpHs4*, *PwHs4*, and *PpatHs4*. Nevertheless, single nucleotide polymorphisms (SNPs) as well as insertions/deletions (InDels) were detected (Figure 5A, Supplementary Figure 2). Even though the *Hs4* homolog

sequences differ from each other, all *Patellifolia Hs4* genes examined are highly similar (Table 2). The reference sequence based on the *Hs4* sequence obtained from Kumar et al. (2021) (and derived from the translocation line TR520) was detected with high sequence similarity in three of the five *P. procumbens* accessions (95-99 %), the five *P. webbiana* accessions (99 %), the *P. procumbens* draft genome (*PpHs4<sub>Draft</sub>*; 99 %), the translocation lines (*Hs4<sub>TR363/TR520</sub>*; 100 %), and *Nemata* (*Hs4<sub>Nemata</sub>*; 100 %). Among the *Patellifolia* species, the highest *Hs4* similarity across all accessions analyzed was detected in *P. webbiana*, while in *P. procumbens* the similarity values varied by 4 % between different accessions (Table 2). The sequences of the *P. patellaris* accessions (and two *P. procumbens* accessions) showed a higher divergence from *Hs4* with a maximum of 95 % sequence identity. Further, they exhibited 1% gaps and the gene sequence was extended by 29-30 bp (Table 2). Accordingly, the majority of SNPs detected were shared by these accessions.

**Table 2:** DNA sequence identities of different *Hs4* sequences compared to the reference *Hs4* sequence of 2022 bp. Single *Hs4* homologs from the same species are demarcated by their seed code or other identifier. Similarities were calculated with the blastn suite (Camacho et al. 2009).

Query sequence	Length	Identity [%]	Gaps [%]
<i>PpHs4<sub>100810</sub></i>	2051	95	1
<i>PpHs4<sub>100820</sub></i>	2052	95	1
<i>PpHs4<sub>100821</sub></i>	2032	97	0
<i>PpHs4<sub>IPK419</sub></i>	2022	99	0
<i>PpHs4<sub>IPK951</sub></i>	2025	99	0
<i>PwHs4<sub>100002</sub></i>	2022	99	0
<i>PwHs4<sub>100832</sub></i>	2024	99	0
<i>PwHs4<sub>100833</sub></i>	2022	99	0
<i>PwHs4<sub>IPK526</sub></i>	2025	99	0
<i>PwHs4<sub>IPK927</sub></i>	2025	99	0
<i>PpatHs4<sub>100012</sub></i>	2052	95	1
<i>PpatHs4<sub>930065</sub></i>	2052	95	1
<i>PpatHs4<sub>IPK10</sub></i>	2052	95	1
<i>PpHs4<sub>Draft</sub></i>	2025	99	0
<i>Hs4<sub>TR363</sub></i>	2022	100	0
<i>Hs4<sub>TR520</sub></i>	2022	100	0
<i>Hs4<sub>Nemata</sub></i>	2022	100	0

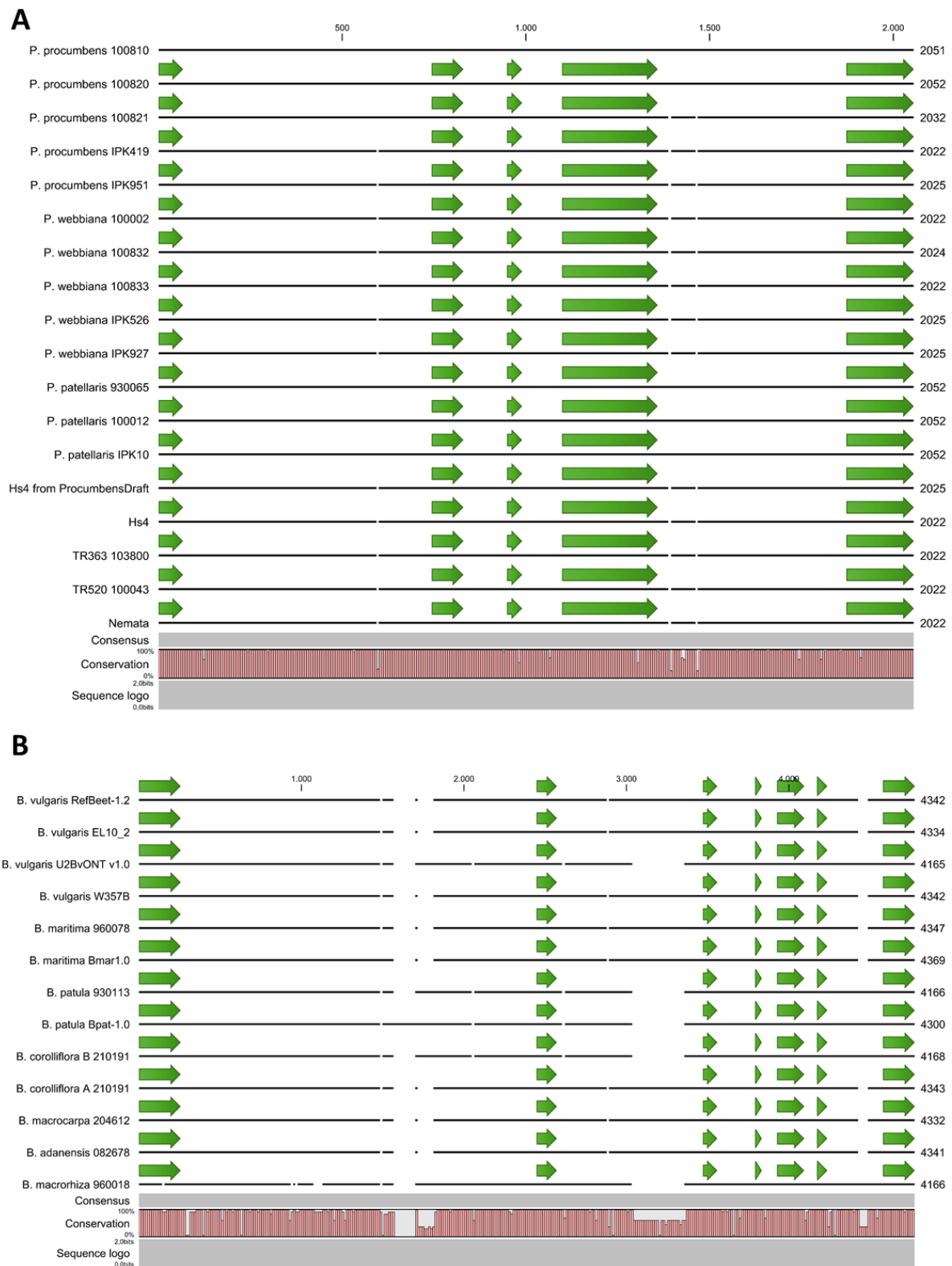


**Figure 5:** Alignment of genomic *Hs4* and *BvHs4* homologous sequences. (A) Comparison of the original *Hs4* with the *Hs4* homologs from the *Patellifolia* species, the *P. procumbens* draft genome (ProcumbensDraft), the translocation lines (TR363 and TR520), and the variety Nemata. (B) Comparison of the *BvHs4* homologous sequences from different *Beta* species and accessions. All sequences were compared to the RefBeet-1.2 reference sequence. The *B. corolliflora* genes were cloned into pJET1.2 and isolated from different *E. coli* colonies before sequencing. Hence, the two different genes encountered are distinguished by “A” and “B”. The whole genomic region is shown as a black line and the exons are highlighted in green. Gaps in the genomic region are represented by gaps in the alignment and sequence deviations can be inferred from the “Conservation” bar at the bottom. Numbers at the end give the whole sequence length from start to stop codon. The graphic was created using the CLC Main Workbench 20.

Four of the InDels found are located in intronic regions, therefore not impacting the protein derived from the sequence (Table 3). However, a 3 bp insertion at position 1302 in exon 5 leads to the addition of one amino acid to the protein (orange box in Supplementary Figure 6). This integration is present in four *P. procumbens* accessions, two *P. webbiana* accessions, all *P. patellaris* accessions analyzed, and the draft genome sequence of *P. procumbens*. Most interestingly, the integration is absent from one *P. procumbens* and three *P. webbiana* accessions, the *Hs4* sequence, the translocation lines, and Nemata (orange box in Supplementary Figure 2).

**Table 3:** InDels found between *Hs4* homologs in different *Patellifolia* species. The position is given in Supplementary Figure 2.

Position	bp	Genomic region	Genes with insertion	Genes with deletion
593	6	intron	<i>PpHs4</i> <sub>100810</sub> , <i>PpHs4</i> <sub>100820</sub> , <i>PpHs4</i> <sub>100821</sub> , <i>PpatHs4</i> <sub>930065</sub> , <i>PpatHs4</i> <sub>100012</sub> , <i>PpatHs4</i> <sub>IPK10</sub>	<i>PpHs4</i> <sub>IPK419</sub> , <i>PpHs4</i> <sub>IPK951</sub> , <i>PwHs4</i> <sub>100002</sub> , <i>PwHs4</i> <sub>100832</sub> , <i>PwHs4</i> <sub>100833</sub> , <i>PwHs4</i> <sub>IPK526</sub> , <i>PwHs4</i> <sub>IPK927</sub> , <i>PpHs4</i> <sub>Draft</sub> , <i>Hs4</i> , <i>Hs4</i> <sub>TR363</sub> , <i>Hs4</i> <sub>TR520</sub> , <i>Hs4</i> <sub>Nemata</sub>
873	3	intron	<i>PpHs4</i> <sub>100810</sub> , <i>PpHs4</i> <sub>100820</sub> , <i>PpatHs4</i> <sub>930065</sub> , <i>PpatHs4</i> <sub>100012</sub> , <i>PpatHs4</i> <sub>IPK10</sub>	<i>PpHs4</i> <sub>100821</sub> , <i>PpHs4</i> <sub>IPK419</sub> , <i>PpHs4</i> <sub>IPK951</sub> , <i>PwHs4</i> <sub>100002</sub> , <i>PwHs4</i> <sub>100832</sub> , <i>PwHs4</i> <sub>100833</sub> , <i>PwHs4</i> <sub>IPK526</sub> , <i>PwHs4</i> <sub>IPK927</sub> , <i>PpHs4</i> <sub>Draft</sub> , <i>Hs4</i> , <i>Hs4</i> <sub>TR363</sub> , <i>Hs4</i> <sub>TR520</sub> , <i>Hs4</i> <sub>Nemata</sub>
1302	3	exon	<i>PpHs4</i> <sub>100810</sub> , <i>PpHs4</i> <sub>100820</sub> , <i>PpHs4</i> <sub>100821</sub> , <i>PpHs4</i> <sub>IPK951</sub> , <i>PwHs4</i> <sub>IPK526</sub> , <i>PwHs4</i> <sub>IPK927</sub> , <i>PpatHs4</i> <sub>930065</sub> , <i>PpatHs4</i> <sub>100012</sub> , <i>PpatHs4</i> <sub>IPK10</sub> , <i>PpHs4</i> <sub>Draft</sub>	<i>PpHs4</i> <sub>IPK419</sub> , <i>PwHs4</i> <sub>100002</sub> , <i>PwHs4</i> <sub>100832</sub> , <i>PwHs4</i> <sub>100833</sub> , <i>Hs4</i> , <i>Hs4</i> <sub>TR363</sub> , <i>Hs4</i> <sub>TR520</sub> , <i>Hs4</i> <sub>Nemata</sub>
1387	8	intron	<i>PpHs4</i> <sub>100810</sub> , <i>PpHs4</i> <sub>100820</sub> , <i>PpatHs4</i> <sub>930065</sub> , <i>PpatHs4</i> <sub>100012</sub> , <i>PpatHs4</i> <sub>IPK10</sub>	<i>PpHs4</i> <sub>100821</sub> , <i>PpHs4</i> <sub>IPK419</sub> , <i>PpHs4</i> <sub>IPK951</sub> , <i>PwHs4</i> <sub>100002</sub> , <i>PwHs4</i> <sub>100832</sub> , <i>PwHs4</i> <sub>100833</sub> , <i>PwHs4</i> <sub>IPK526</sub> , <i>PwHs4</i> <sub>IPK927</sub> , <i>PpHs4</i> <sub>Draft</sub> , <i>Hs4</i> , <i>Hs4</i> <sub>TR363</sub> , <i>Hs4</i> <sub>TR520</sub> , <i>Hs4</i> <sub>Nemata</sub>
1461	6	intron	<i>PpHs4</i> <sub>100810</sub> , <i>PpHs4</i> <sub>100820</sub> , <i>PpatHs4</i> <sub>930065</sub> , <i>PpatHs4</i> <sub>100012</sub> , <i>PpatHs4</i> <sub>IPK10</sub>	<i>PpHs4</i> <sub>100821</sub> , <i>PpHs4</i> <sub>IPK419</sub> , <i>PpHs4</i> <sub>IPK951</sub> , <i>PwHs4</i> <sub>100002</sub> , <i>PwHs4</i> <sub>100832</sub> , <i>PwHs4</i> <sub>100833</sub> , <i>PwHs4</i> <sub>IPK526</sub> , <i>PwHs4</i> <sub>IPK927</sub> , <i>PpHs4</i> <sub>Draft</sub> , <i>Hs4</i> , <i>Hs4</i> <sub>TR363</sub> , <i>Hs4</i> <sub>TR520</sub> , <i>Hs4</i> <sub>Nemata</sub>

Next, I compared the *BvHs4* sequences from one *B. vulgaris* ssp. *adanensis* (082678), one *B. vulgaris* ssp. *maritima* (960078), and the *B. patula*, *B. corolliflora*, *B. macrocarpa* and *B. macrorrhiza* accessions available. The *BvHs4* sequence from RefBeet-1.2. (Dohm et al. 2014) was used as a reference. Furthermore, I included the reference sequences available for *B. vulgaris*, EL10\_2 (McGrath et al. 2022) and W357B v1.0 (Dorn 2022), for *B. patula*, Bpat-1.0 (Rodríguez del Río et al. 2019), and *B. vulgaris* ssp. *maritima*, Bmar1.0 (Rodríguez del Río et al. 2019), respectively. Finally, I also included the genomic sequence of a nematode-tolerant beet genotype, U2BvONT v1.0, recently generated (Sielemann et al. 2023a).

When analyzing the PCR amplicons by gel electrophoresis, *B. corolliflora* was the only species showing a clear double band for the whole genomic *BvHs4* region (Supplementary Figure 3A). The upper band had a size similar to *BvHs4* while the lower band at ~2.3 kb was much smaller. To analyze both sequences, I cloned them into pJET1.2 and sequenced the resulting plasmids after colony PCR and plasmid isolation. However, BLAST analysis revealed that the lower band's sequence did not match any known gene from *B. vulgaris* (data not shown). Interestingly, when sequencing different plasmids containing the larger *BcHs4* band, I obtained various sequences. One sequence (*BcHs4<sub>A</sub>*) was a perfect match to *BvHs4* known from RefBeet-1.2, while another sequence (*BcHs4<sub>B</sub>*) showed several SNPs, small InDels, and a prominent insertion of 97 bp starting after position 1,522 of the RefBeet sequence. Blasting these 97 bp at NCBI perfectly matched the sequence of the *BvHs4* homolog from the tolerant *B. vulgaris* genotype U2Bv. Both the *BcHs4<sub>B</sub>* and *BvHs4<sub>U2Bv</sub>* sequences also show a matching 312 bp deletion, starting at the RefBeet position 2,713, compared to the *BcHs4<sub>A</sub>* sequence (Supplementary Figure 3B). When comparing the genomic sequence of the *BvHs4* homologs across several *Beta* species, I could detect the 97 bp insertion also in *B. patula* and *B. macrorhiza*. Those species also contained the 312 bp deletion. Further, the sequences of these species contained the same small InDels compared to the other *Beta* species. Single SNPs were shared by *BpHs4*, *BcHs4<sub>B</sub>*, and *BvHs4<sub>U2Bv</sub>* but not *BmrHs4<sub>960018</sub>*. Occasionally, the small variations were shared by *BmHs4* (Supplementary Figure 4). A prominent shared insertion is the additional 3 bp at position 57 in exon 1 (Supplementary Figure 5). However, all large sequence deviations detected lie in the intronic region of the gene and do not affect the protein composition (Figure 5B, Supplementary Figure 3B).

Overall, the *BvHs4* homologs sequenced from the different *Beta* species showed high similarity across the whole gene sequence (Table 4). The sequences having sequence identity values of 97 % or below were those found to contain the 97 bp insertion and 312 bp deletion. The known exons of *BvHs4* were annotated analogously in the newly derived sequences.

**Table 4:** DNA sequence identities of different *BvHs4* homolog sequences compared to the reference *BvHs4* sequence of 4342 bp and the *Hs4* sequence of 2022 bp, respectively. When required, individual *BvHs4*-homologs are demarcated by their seed code or the reference sequence they were retrieved from. Similarities were calculated with the blastn suite (Camacho et al. 2009).

Query sequence	Length	compared to <i>BvHs4</i>		compared to <i>Hs4</i>	
		Identity [%]	Gaps [%]	Identity [%]	Gaps [%]
<i>BaHs4</i>	4341	99	0	77	4
<i>BcHs4<sub>A</sub></i>	4343	99	0	76	4
<i>BcHs4<sub>B</sub></i>	4168	97	0	77	4
<i>BmHs4</i>	4347	99	0	77	4
<i>BmHs4<sub>Bmar1.0</sub></i>	4369	99	0	77	4
<i>BmcHs4</i>	4332	99	0	77	4
<i>BmrHs4<sub>960018</sub></i>	4166	90	3	76	4
<i>BpHs4</i>	4166	97	0	77	4
<i>BpHs4<sub>Bpat-1.0</sub></i>	4300	97	0	77	4
<i>BvHs4<sub>EL10_2</sub></i>	4334	99	0	77	4
<i>BvHs4<sub>W357B</sub></i>	4342	100	0	76	4
<i>BvHs4<sub>U2Bv</sub></i>	4165	97	0	77	4
<i>Hs4</i>	2022	76	4	-	-

All *BvHs4* homologs analyzed were highly similar to *BvHs4* and there was no evidence that one of the genes found had more similarities to *Hs4* than *BvHs4* (Table 4). In conclusion, none of the *BvHs4* homologs seem to be genes conferring resistance to *H. schachtii* based on the sequencing results.

### 2.2.3.2 Variations at the polypeptide level

Using the exonic regions from *Patellifolia* and *Beta* species, I generated the open reading frame sequences for each gene separately. Additionally, I extracted the sequences of rhomboid-like proteins of quinoa (*Chenopodium quinoa*, LOC110702170 and LOC110705623), mung bean (*Vigna radiata*, LOC106763922), and spinach (*Spinacia oleracea*, LOC110775063) from the NCBI protein database (Sayers et al. 2022). They showed high homologies to *BvHs4* and were used as outgroups for the following phylogenetic analysis. Utilizing the CLC Main Workbench tool, the corresponding polypeptide sequences were translated. I aligned all polypeptides of the *Patellifolia* and *Beta* species and the four outgroups.

The polypeptides from the *Patellifolia* species showed high conservation (Supplementary Figure 6) even though I had observed differences at the DNA sequence level (Supplementary Figure 2). Nevertheless, small amino acid substitutions were visible. Two substitutions at positions 98 (from arginine in Hs4 to serine) and 126 (arginine in Hs4 to threonine) were present in four *P. procumbens*, two *P. webbiana*, and all *P. patellaris* accessions and the *P. procumbens* draft genome sequence. The substitution at position 124 (arginine in Hs4 to serine) was present only in three *P. procumbens* and all *P. patellaris* accessions. Similarly, the substitution at position 163/164 (asparagine in Hs4 to aspartic acid) was present in those accessions, with the exception of one *P. procumbens* accession that showed the same amino acid as the Hs4 sequence at this position. The insertion of an additional amino acid after the 132<sup>nd</sup> position was present in various accessions of all three *Patellifolia* species but absent from three *P. webbiana* accessions, the Hs4 sequence, the translocation lines, and Nemata.

Further, the amino acid sequence ‘LLRDRCPDN’ located right before the additional amino acid and described as highly Hs4-specific and absent in the sugar beet homolog (Kumar 2020) was not highly conserved across the different *Patellifolia* species. The sequence described could only be found in three *P. webbiana* accessions (100002, 100832, 100833), one *P. procumbens* accession (IPK419), the translocation lines, and Nemata. The other homologs analyzed displayed either the sequence ‘ALSDTCPDN’ or ‘ALRDTCPDN’. As two more amino acids at the 3’-end of this sequence are present in all *Patellifolia* but absent from the *Beta* samples, the highly conserved sequence can be revised to ‘CPDNKE’.

The polypeptides from the *Beta* species were highly similar to each other and also to the outgroup proteins (Supplementary Figure 6). Interestingly, stretches of up to fifteen amino acids (aa) were also conserved across the two genera. A prominent difference was the addition of roughly 100 aa at the N-terminus of the protein in all *Beta* species, giving rise to an additional exon at the beginning of *BvHs4* (Figure 4A). Hs4, in turn, shows an integration of 9-10 aa (position 123; R/S D R/T CPDNKE+V) in the region of exon 5, which is the conserved region described above, and a second one of two aa (position 163/164; V N/D) in the exon 6 region. Upon comparing the polypeptide sequences, it became evident that *B. macrorhiza* showed strong deviations from the remaining *Beta* species, even though it exhibited high similarity at the coding sequence level (Supplementary Figure 5). The small sequence variations led to the formation of a putatively non-functional polypeptide with several premature stop codons and many amino acid exchanges. The first stop codon terminates the polypeptide after position 141 (Supplementary Figure 6).

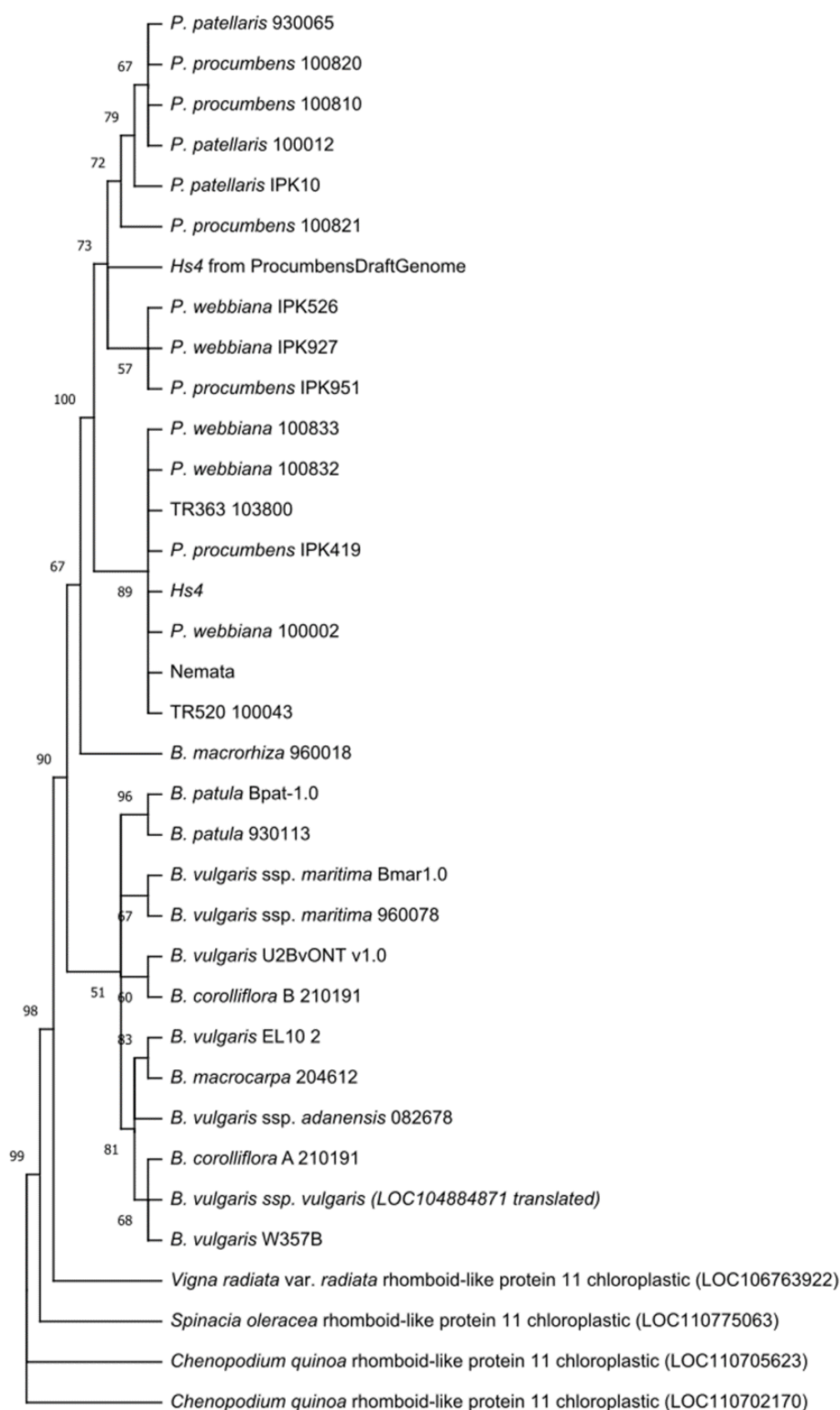


**Figure 6:** Phylogenetic tree of polypeptide sequences from different *Patellifolia* and *Beta* species and accessions. The tree was constructed with MEGA11 (Tamura et al. 2021), using the maximum likelihood method. Bootstrapping was conducted with 500 replicates. Quinoa (*C. quinoa*), spinach (*S. oleracea*), and mung bean (*V. radiata*) were used as outgroups.

I used the polypeptide sequences generated to create a maximum likelihood tree in MEGA11 (Figure 6). The BvHs4 homologs cluster closest to the outgroup proteins, and the *Patellifolia* polypeptides are grouped further away, indicating their distant relationship. Interestingly, quinoa groups as the furthest outgroup, and the mung bean polypeptide sequence has the highest similarity to the *Beta* species. The *Beta* species form a distinct clade supported by a high bootstrap value of 90 at the point of divergence. However, *B. macrorhiza*, which showed strong deviations from BvHs4 at the polypeptide level, is an exception to the *Beta* clade. Due to the differences found in BmrHs4, it groups apart from the other *Beta* species. In the *Beta* clade of the tree, the polypeptides obtained by sequencing *B. patula* and *B. vulgaris* ssp. *maritima*, respectively, group together with the BpHs4 and BmHs4 polypeptides derived from the according reference sequences. The high similarity observed between BcHs4<sub>B</sub> and U2Bv could be verified in the phylogenetic tree, as they group together. The polypeptides of the different *B. vulgaris* reference genomes, BmcHs4, BaHs4, and BcHs4<sub>A</sub> are part of a subclade of the tree, whose node is supported by a high bootstrap value of 81.

The divergence point towards the *Patellifolia* polypeptides is supported by a very high bootstrap value of 100, indicating that this clade is distinct from the *Beta* and outgroup proteins. Conclusively, the original Hs4 polypeptide groups with the translocation lines and Nemata, which are all derived from each other. Additionally, one PpHs4 and three PwHs4 polypeptides are part of that subclade. Interestingly, the remaining PpHs4 and PwHs4 polypeptides form a distinct small subclade. The polypeptide derived from the *P. procumbens* draft genome is rather distantly related to Hs4. Unexpectedly, three *P. procumbens* accessions group together with the *P. patellaris* accessions.

Finally, I analyzed the predicted localization and conformation of the polypeptides Hs4 (reference sequence), PpHs4<sub>100810</sub>, and BvHs4 from RefBeet1.2. I used DeepLoc2.1 (Ødum et al. 2024) to predict the subcellular localization as well as membrane associations for each protein. As described by Kumar et al. (2021), Hs4 is predicted to be localized at the ER as a transmembrane protein (Table 5). The conformation prediction using DeepTMHMM (Hallgren et al. 2022) revealed that Hs4 constitutes a protein with six transmembrane domains (Supplementary Table 3). The addition of one amino acid in PpHs4<sub>100810</sub> does not change its subcellular localization. Contrarily, the probability of an ER localization increased from 0.7973 for Hs4 to 0.8184 for PpHs4<sub>100810</sub> (Table 5). The additional valine leads to a slight conformation change. Five amino acids assigned to a transmembrane domain beforehand are now predicted to be part of a loop located in the lumen and hence the proximate fourth transmembrane domain is slightly decreased in size (Supplementary Table 3). BvHs4, in turn, is predicted to be plastid-localized with a high prediction value of 0.9158 (Table 5). Nevertheless, it is also a transmembrane protein exhibiting six transmembrane domains. The main conformation difference lies in its long cytosolic N-stretch, which is much shorter in Hs4 and PpHs4<sub>100810</sub> (Supplementary Table 3). Interestingly, using the AlphaFold Protein Structure Database (Varadi et al. 2022; Varadi et al. 2024), I found that Arabidopsis contains an Hs4 homolog with 57 % and 71 % protein similarity to Hs4 and BvHs4, respectively. The protein is classified as rhomboid-like protease 11 (AtRBL11, UniProt identifier: Q84MB5) and located in the plastids, like BvHs4. It also has six transmembrane domains (Supplementary Table 3).

**Table 5:** Probabilities of predicted localization and membrane association for the *P. procumbens*-derived polypeptides Hs4 and PpHs4<sub>100810</sub>, the latter with an additional amino acid, BvHs4 from *B. vulgaris* and the *A. thaliana* AtRBL11. The probability values were calculated using DeepLoc2.1 (Ødum et al. 2024).

	<b>Hs4</b>	<b>PpHs4<sub>100810</sub></b>	<b>BvHs4</b>	<b>AtRBL11</b>
<b>Localization</b>	<b>Prediction probability</b>			
cytoplasm	0.0667	0.0695	0.0707	0.0796
nucleus	0.0761	0.0790	0.0566	0.0689
extracellular	0.1902	0.1712	0.0209	0.0218
cell membrane	0.1334	0.1330	0.0505	0.0623
mitochondrion	0.3080	0.2782	0.2748	0.3320
plastid	0.1721	0.2045	0.9158	0.9346
endoplasmic reticulum	0.7973	0.8184	0.2247	0.1656
lysosome/vacuole	0.4065	0.4335	0.0581	0.0521
Golgi apparatus	0.4089	0.4283	0.0673	0.0372
peroxisome	0.0274	0.0371	0.1004	0.1345
<b>Membrane association</b>				
peripheral	0.1530	0.1580	0.2850	0.3000
transmembrane	0.9670	0.9680	0.9580	0.9610
lipid anchor	0.0740	0.0770	0.0590	0.0550
soluble	0.1430	0.1450	0.1220	0.1130

#### 2.2.4 Expression patterns of *Hs4* and its homologs across *Beta* and *Patellifolia* species

Once it had been established that *Hs4* or a homolog was present in several *Patellifolia* and *Beta* species, I wanted to see if they were differentially expressed between tissues in those genera. Based on the predicted protein localizations I expected to find spatial expression differences.

In the *Patellifolia* species and the translocation line-derived *B. vulgaris* plants, *Hs4* and its homologs were always strongest expressed in the roots (Figure 7A). The highest difference between expression in leaves and roots was observed in the translocation line TR520 with 26.6-fold higher expression in roots compared to leaves. The variety Nemata derived from this translocation line showed an 18.9-fold expression difference. Among the *Patellifolia* species, *PpatHs4* was expressed 14.6-20.3x, *PwHs4* 0.9-6.9x, and *PpHs4* 6.2-26.6x higher in roots versus leaves, respectively. TR363 showed a 5.2x higher gene expression in roots.

Contrastingly, the *BvHs4* homologs showed the highest expression levels in leaves in all *Beta* species analyzed (Figure 7B). These findings are in line with the subcellular localization predictions. The leaf-to-root expression ratio was similar among the different species. The highest upregulation in leaves was observed in *BmHs4* with up to 6x higher expression. It was followed by *BmcHs4* with 5.7x and *BaHs4* with up to 5.2x higher expression in leaves. The remaining homologs showed between 1.4- (*BvHs4*) to 3.2-fold (*BcHs4* and TR363) upregulation in leaves compared to roots.

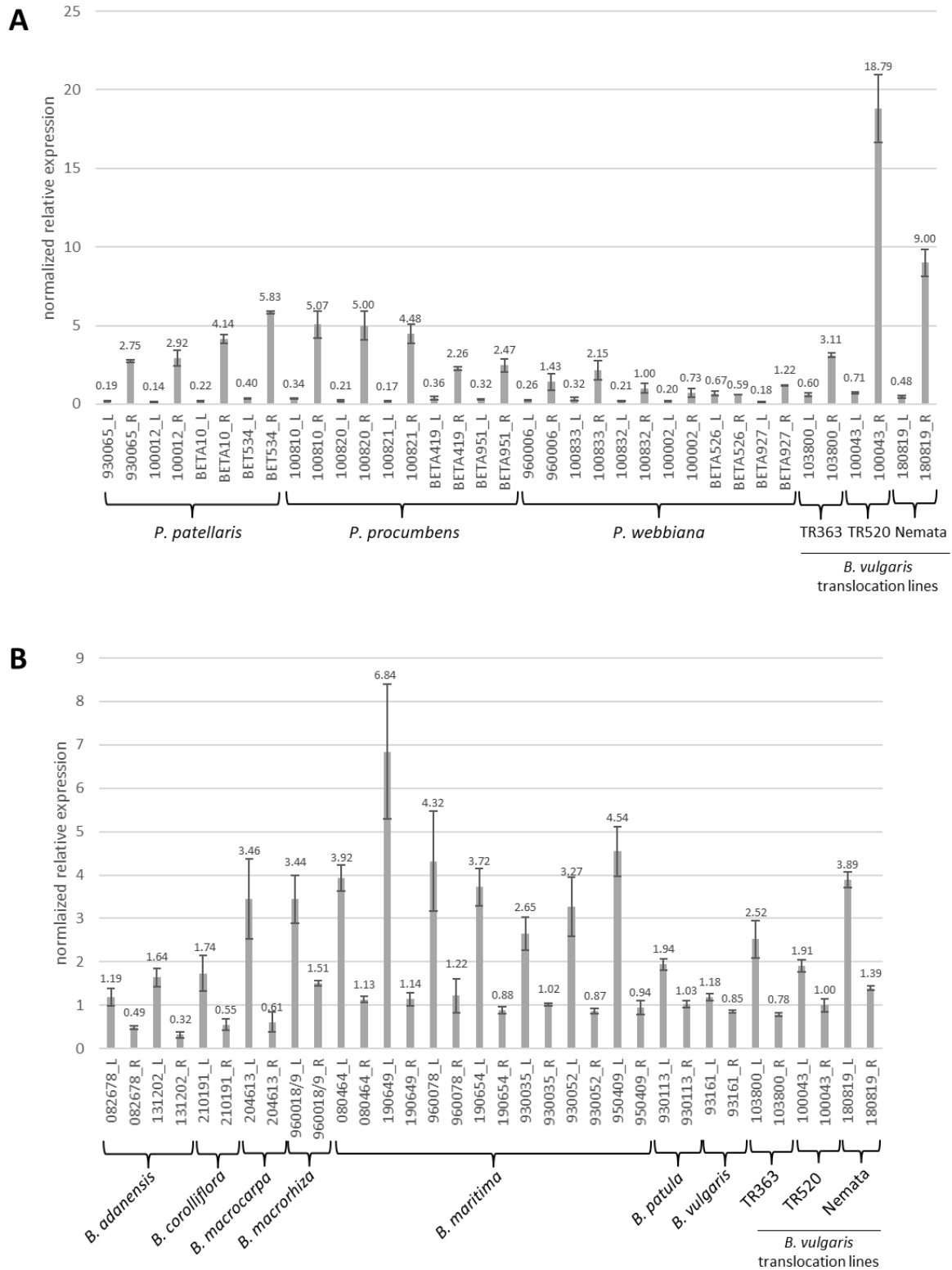


**Figure 7:** Bar plots showing the expression levels of *Hs4* and its homologs in leaf (L) and root (R) tissues of diverse *Patellifolia* (A) and *Beta* (B) species as determined by RT-qPCR (primer: AK\_F7/AK\_R5 for *Patellifolia* and BvHs4\_F1/BvHs4\_R7 for *Beta*; reference gene: *GAPDH*). (A) Expression of *Hs4* in different *Patellifolia* species. The different accessions within one species are given with their unique identifier (seed code). In all samples, expression was higher in the root compared to leaf samples. (B) Expression of *BvHs4* homologs across different *Beta* species. The accessions within one species are differentiated by their seed code. Due to a lack of biological replicates, the expression data of two different *B. macrorrhiza* accessions were pooled in this analysis. The gene's expression was proven to be continuously higher in the leaf compared to root tissues. Standard deviations are given as SEM.

### 2.2.5 Nematode infection does not alter the expression of *Hs4* and its homolog

The nematode resistance gene *Hs4* shows a contrasting expression pattern to its homolog from sugar beet across leaf and root tissues (see 2.2.4). I wanted to analyze how the expression patterns of both genes changed over time in different tissues and if nematode inoculation had an effect on the genes' expressions. Four weeks after inoculation, the number of females developing on the roots of five replicates for both species were assessed. No developing females were observed on *P. procumbens*. On *B. vulgaris* roots, female numbers ranged between a minimum of 54 and a maximum of 119 (mean: 83.4).

In *P. procumbens* an expression pattern resembling the pattern discovered in a broad set of *Patellifolia* species (see 2.2.4) was observed. Across all sampling points the plants showed the highest *Hs4* expression in roots (Figure 8). While the expression level in roots was quite stable over the first weeks it showed a slight increase in the older plants, even though this increase was not statistically significant. The highest expression differences between leaves and roots were observed in the older plants. The non-inoculated plants had a 16.1x higher expression in roots compared to leaves upon female counting and the inoculated plants showed a similar value of 15.8x higher expression in roots. In the early plant developmental phases, the expression differences between leaves and roots were very similar. Directly after germination, roots had a 6.5x higher expression compared to the cotyledons. This value slightly increased in the first true leaves, where roots had 8.1x higher expression than the cotyledons while it was 4.6x higher compared to leaves. The expression relative to the leaves remained stable three weeks after germination and then dropped slightly to 3.1x before inoculation. Three days post-inoculation, the difference had already slightly increased to 6.5x in non-inoculated and 6.8x in inoculated plants. Even though a trend of continuous expression in leaves and an increasing expression level in roots is showing, a statistically significant upregulation after nematode inoculation could not be observed (Figure 8).

The nematode resistance gene *Hs1*, which also comes from *Patellifolia*, was found to be upregulated at four weeks after nematode inoculation (Cai et al. 1997). Hence, I screened the *P. procumbens* accession used for *Hs4* expression analysis to test if I could detect an upregulation of *Hs1* at 28 dpi in the inoculated compared to the non-inoculated samples. The mean expression of 7.43 in the non-inoculated and 8.28 in the inoculated sample (Supplementary Figure 7) was not significantly different as determined by a one-way ANOVA ( $F(1, 4) = 7.71, p = 0.79$ ).

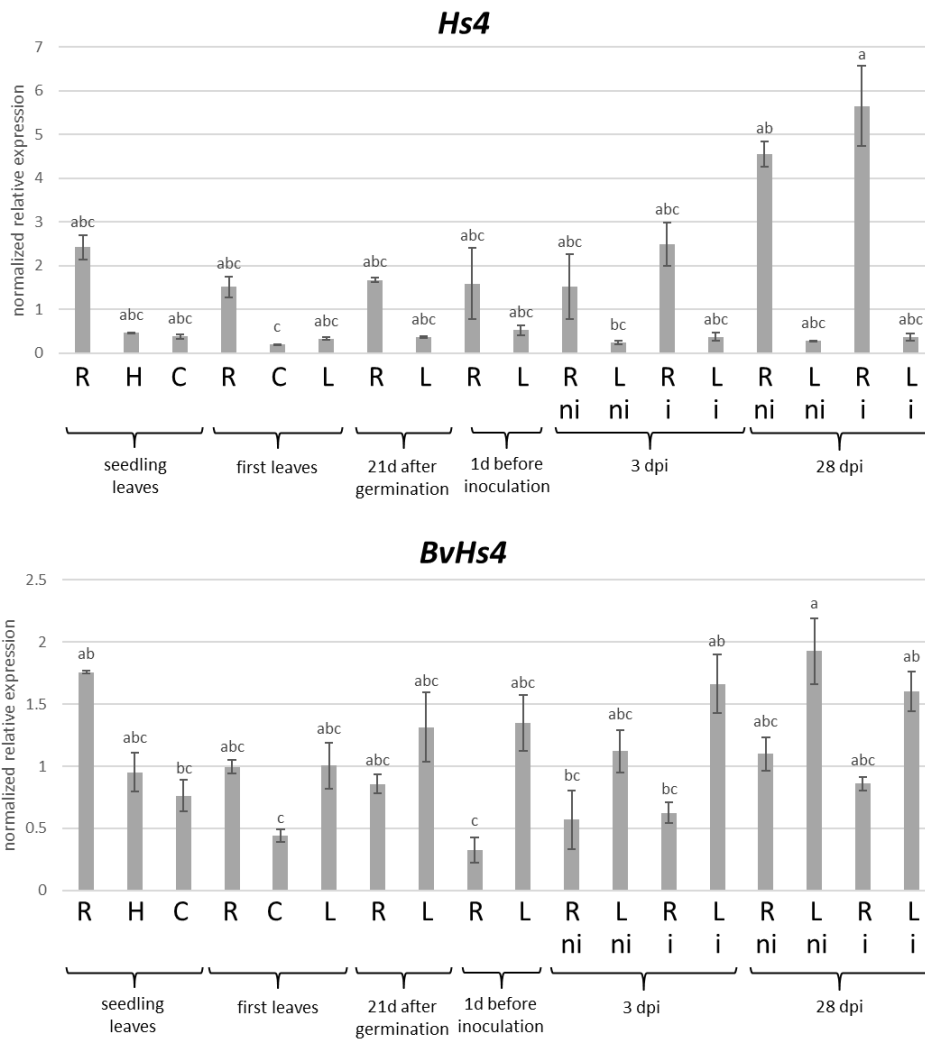


**Figure 8:** Bar plots showing the RT-qPCR results of the expression analysis of *Hs4* in *P. procumbens* (primer: AK\_F7/AK\_R5; reference gene: *GAPDH*) and its *Beta* homolog in *B. vulgaris* (primer: AS\_BvHs4\_F1/AS\_BvHs4\_R7; reference gene: *GAPDH*) over time and under different treatments (i: inoculated, ni: non-inoculated) in root (R), hypocotyl (H), cotyledon (C), or leaf (L) tissues. (A) A Kruskal-Wallis test ( $p < 0.05$ ) was performed for the *P. procumbens* samples and significant differences between groups were calculated using the Hochberg-corrected Dunn post-hoc test ( $p < 0.05$ ). Statistical significances between *B. vulgaris* samples were calculated using a one-way ANOVA, followed by the Tukey HSD Test. Standard deviations are given as SEM.

In *B. vulgaris* the higher *BvHs4* expression in leaves compared to roots was not evident in the very early samples (Figure 8). Contrarily, expression was higher in roots compared to leaves directly after germination, where expression in cotyledons was 0.4x that of the root. Interestingly, the ratio of cotyledon-to-root expression remained the same upon the development of the first true leaves, while *BvHs4* expression in leaves and roots was balanced. Starting with the sampling point three weeks after germination, *BvHs4* was always higher expressed in leaves than roots. The largest difference could be seen directly before inoculation, where leaves showed 4.1x higher expression than roots. No statistically significant differences were observed when comparing the inoculated and non-inoculated samples at 3 and 28 days post-inoculation. The ratio of leaf-to-root expression also remained stable with up to about 2-fold higher expression in leaves compared to roots. Nematode inoculation did not lead to an increase in *BvHs4* expression.

### 3 The cyst nematode resistance gene *Hs4* from a wild relative of sugar beet confers resistance in a distantly related species

#### 3.1 Materials and Methods

##### 3.1.1 Vector construction

The vectors pBin35SRed-*Hs4* (hereafter named 35S::*Hs4*) and pBin35SRed-pHs1::*Hs4* (hereafter named Hs1::*Hs4*) containing the *Hs4* open reading frame from cDNA of the sugar beet cultivar Nemata was used (Leineweber 2020; Kumar et al. 2021). In the 35S::*Hs4* plasmid, the *Hs4* gene is under the transcriptional control of the constitutive 35S promoter while it is expressed from the inducible Hs1 promoter (Thurau et al. 2003) in Hs1::*Hs4*. The pBin35SRed vector (Pidkowich et al. 2007) contains a constitutively expressed *DsRed2* gene for plant selection.

The 35S::*Hs4* plasmid was introduced into *Agrobacterium tumefaciens* strain GV3101 (Hellens et al. 2000) via a modified heat-shock method (Höfgen and Willmitzer 1988). Finally, 200 µl of the bacteria were plated on LB plates containing selective antibiotics (50 µg/ml kanamycin, 50 µg/ml gentamycin, 50 µg/ml rifampicin) and incubated at 28°C for two days. Positive colonies were identified by colony PCR using the primer combination AK\_F7/AK\_R5 (Supplementary Table 2).

The transformation of *A. tumefaciens* (strain GV3101) with the Hs1::*Hs4* plasmid was conducted by Johanna Leineweber (2020).

##### 3.1.2 Arabidopsis transformation and selection of homozygous lines

The *Agrobacteria* containing the 35S::*Hs4* plasmid were used for floral dip transformation of *A. thaliana* Col-0 (Supplementary Table 1) as described (Clough and Bent 1998). The plants were cultivated in a climate chamber under LD conditions (16 h light/8 h dark, 22°C) for 4-6 weeks. *A. tumefaciens* carrying 35S::*Hs4* were grown as overnight cultures (28°C, 180 rpm) and centrifuged at 4,000 rpm for 10 min. The bacterial pellets were resuspended in a 5 % sucrose solution containing 0.01 % Silwett (Kurt Obermeier GmbH, Bad Berleburg, Germany). The plant inflorescences were immersed in the bacterial suspension for 20-30 seconds. The plants were then kept under short-day conditions (SD; 8 h light/16 h dark, 24°C) for one night, before they were grown in a climate chamber under LD conditions (16 h light/8 h dark, 24°C) until T<sub>1</sub> seeds were harvested ca. 6 weeks later.

Transgenic T<sub>1</sub> seeds displaying red fluorescence were identified under a Nikon SMZ25 microscope equipped with a Nikon Intensilight C-HGFI fluorescence unit with a Nikon Texas Red bandpass filter cube ( $\lambda_{\text{excitation}}$  560 nm; Nikon, Tokyo, Japan) using a 600 ms exposure time. Pictures were taken with a DS-Fi3 camera mounted onto the microscope using the NIS-Elements BR software (both Nikon, Tokyo, Japan). In the following generations (T<sub>2</sub>, T<sub>3</sub>), transgenic seeds were selected accordingly, and heterozygous and homozygous seed families could be distinguished (Supplementary Table 5 and Supplementary Table 6).

The *A. thaliana* plant material transformed with Hs1::*Hs4* was received as T<sub>3</sub> seeds from Johanna Leineweber (2020).

##### 3.1.3 Nematode infection assays

Following surface sterilization with 2.6 % NaClO for 5 min and three washes with sterilized water, the *Arabidopsis* seeds were placed either in 9 cm Petri dishes or in 6-well plates

containing B5 medium. After stratification for 2 days at 4°C, the plants were grown for approximately two weeks in a climate chamber (16 h light/8 h dark). *H. schachtii* strain 'Schach 0' (Müller and Klinke 1996) cysts were incubated in 3 mM ZnCl<sub>2</sub> for 3-4 days to induce hatching of the larvae. The J2 larvae were surface-sterilized in 0.05 % HgCl<sub>2</sub> for 35 sec, followed by three washing steps in sterile tap water, and then resuspended in 0.6 % gelrite (Duchefa, Haarlem, Netherlands). The nematode suspension was adjusted to a concentration of 10-12 larvae in 10 µl and 240-300 µl were applied to each plantlet using Pasteur pipettes. Plants were further grown for ca. 3 weeks in a climate chamber under long-day conditions. Finally, the developing females were counted under a Zeiss Stemi SV 11 stereomicroscope (Zeiss, Oberkochen, Germany).

For *in vivo* nematode infection assays, Arabidopsis plants were grown in large sand tubes filled with a mixture of sieved soil and sand (volume ratio 75 %:25 %) under LD conditions (16 h light/8 h dark, 24°C) for up to four weeks. They were fertilized with Steiner solution (Steiner 1968) every week. *H. schachtii* larvae were harvested as described. The larvae were concentrated and kept in sterile tap water; surface sterilization was omitted. Using pipette tips, the plants were inoculated with a 2 ml solution containing 250-500 J2 larvae. Developing females were assessed four weeks post-inoculation.

*In vivo* nematode infection assays were also carried out under semi-sterile conditions. Here, the sand-soil mixture (volume ratio 75 %:25 %) was heated to 80°C for ca. 5 h before being filled into sand tubes rinsed with 80 % ethanol. Arabidopsis seeds were surface-sterilized and transferred to the sand tubes using autoclaved pipette tips. The plants were grown for up to four weeks under LD conditions (16 h light/8 h dark, 24°C) in a previously ozone-gassed climate chamber and watered with autoclaved tap water. They were fertilized every week using a sterile Steiner solution. Using autoclaved pipette tips, the plants were inoculated with 2 ml nematode suspension containing 250 surface-sterilized J2 larvae in sterile tap water. Developing females were counted four weeks after inoculation.

### 3.1.4 Nucleic acid isolation, PCR, and RT-qPCR conditions

Leaf samples were frozen in liquid nitrogen. DNA was isolated with the NucleoSpin Plant II mini kit (Macherey-Nagel, Düren, Germany) or as described (Dellaporta et al. 1983). The DNA quality was checked on a 1 % agarose gel (90V, 30 min) before further usage.

RNA was isolated from Arabidopsis roots using the Universal RNA Kit (Roboklon, Berlin, Germany), following the manufacturer's instructions. The roots were first washed clean from the agar using a sieve and then frozen in liquid nitrogen. The samples were collected at three sampling points (one day before inoculation, 3 dpi, and 21 dpi). The RNA quality was assessed using agarose gel electrophoresis and a NanoDrop2000 spectrophotometer (ThermoFisher Scientific<sup>TM</sup>). 100-300 ng RNA was incubated with 1 U DNase (ThermoFisher Scientific<sup>TM</sup>) for 30 min at 37°C. Then, the DNase was inactivated by adding 1 µl EDTA (50 mM) followed by incubation at 65°C for 10 min. Subsequently, the cDNA was synthesized using the First Strand cDNA Synthesis Kit (ThermoFisher Scientific<sup>TM</sup>) according to the manufacturer's instructions.

The cDNA quality was assessed by PCR using *GAPDH* primers (B349/B350, Supplementary Table 2). Two µl cDNA were used for quantitative reverse transcription PCR (RT-qPCR) employing the Platinum<sup>TM</sup> SYBR<sup>TM</sup> Green qPCR SuperMix-UDG (Invitrogen<sup>TM</sup>, ThermoFisher Scientific<sup>TM</sup>) according to the manufacturer's instructions. The *GAPDH* gene was used as a reference for gene expression normalization. For transgene detection, the primer combination AK\_F7/AK\_R5 (Supplementary Table 2) was utilized. The obtained Ct-values were evaluated using the Pfaffl method (Pfaffl 2001). The mean of the Col-0 Ct values for

*GAPDH* and *Hs4* were utilized as a non-treated control (for *Hs4* expression the value was artificially set to 40 cycles).

### 3.1.5 Statistical analysis

Normally distributed data were statistically analyzed by a one-sample t-test or a parametric one-way analysis of variance (ANOVA) using the R-based MVApp (Julkowska et al. 2019). Significant differences were then calculated based on Tukeys's pairwise comparison using the MVApp and the online calculator Astatsa (Vasavada 2016). If the data were not normally distributed, the Kruskal-Wallis rank sum test was applied, followed by a Hochberg-corrected Dunn post-hoc test using Astatsa and the open-source statistical computing software R version 4.3.3 (R Core Team 2024) using the package "PMCMRplus" (Pohlert 2023).

## 3.2 Results

### 3.2.1 Generating T<sub>3</sub> lines expressing the *Hs4* gene

Two expression vectors containing the *Hs4* cDNA under the control of the constitutive 35S (35S::*Hs4*) and the inducible Hs1 (Hs1::*Hs4*) promoter, respectively, were constructed (Leineweber 2020). The Arabidopsis transformation with the Hs1::*Hs4* construct was conducted by Johanna Leineweber (2020) and T<sub>3</sub> seeds of this plant material were received at the beginning of the experiment. To allow for better comparison, the number of transformed plants and fluorescing seeds per generation were reevaluated in the context of this study. The 35S promoter was previously found to cause lethality when driving *Hs4* expression (Leineweber 2020; Kumar et al. 2021). However, I could detect transgenic seeds when I repeated the plant transformation with freshly prepared competent *A. tumefaciens*.

After *A. tumefaciens*-mediated transformation of 7 (35S::*Hs4*) and 26 (Hs1::*Hs4*) T<sub>0</sub> plants, respectively, T<sub>1</sub> seeds were bulk-harvested for each construct separately (Supplementary Figure 8). As the *DsRed2* gene is integrated into the vector backbone as a selection marker, the harvested seeds were screened under a fluorescence microscope for the transgene's presence. From the seeds screened, 73 (35S::*Hs4*) and 39 (Hs1::*Hs4*) displayed red fluorescence (Supplementary Table 4). For the 35S::*Hs4* construct, 15 T<sub>1</sub> seeds and for Hs1::*Hs4* all 39 T<sub>1</sub> seeds were selected and sown to generate T<sub>2</sub> seeds, which were harvested separately and subjected to another red fluorescence selection cycle. Seed fluorescence could be observed in 6 out of 8 35S::*Hs4* and 9 out of 12 Hs1::*Hs4* T<sub>2</sub> families. For each T<sub>2</sub> family showing red fluorescence, seven to nine T<sub>3</sub> plants were grown to produce the next generation (Supplementary Table 4). Here, T<sub>3</sub> seeds of 47 35S::*Hs4* T<sub>2</sub> plants and 62 Hs1::*Hs4* T<sub>2</sub> plants could be harvested. All T<sub>3</sub> populations were screened for fluorescence. Six and eleven populations, respectively, exhibited uniformly fluorescing red seeds (Supplementary Table 5 and Supplementary Table 6). As *DsRed2* and *Hs4* are completely linked, a correlation between fluorescence intensity and *Hs4* gene expression levels, depending on the integration site of the transgenes, was expected. Similarly, homogeneous red fluorescence was anticipated to point to homozygous *Hs4* expression. Thus, T<sub>3</sub> populations showing homogeneous red fluorescence were designated homozygous lines and chosen for further experiments.

The six 35S::*Hs4* T<sub>3</sub> lines were directly used for an initial infection test (see 3.2.4). The eleven Hs1::*Hs4* T<sub>3</sub> lines were considered too many genotypes for large-scale experiments. An initial inoculation experiment in 9 cm Petri dishes was conducted with these eleven lines and developing females were assessed three weeks post-inoculation. Eight of the eleven transgenic lines displayed lower female numbers than Col-0 (Supplementary Table 7). Six

lines with a higher mean female number than the control were excluded from further analysis and five lines with values below the control were selected for further work (see 3.2.5).

### 3.2.2 Arabidopsis plants expressing *Hs4* display an altered phenotype

The terms ‘fluorescence’ and ‘coloration’ are used when describing the plant phenotypes. While ‘fluorescence’ implies the red fluorescence only observable under fluorescence-stimulating light ( $\lambda_{\text{excitation}}$  560 nm), the word ‘coloration’ describes root or leaf colors observable under white light without any fluorescence-stimulating light (by naked eye).

The phenotypes of six 35S::*Hs4* and five Hs1::*Hs4* T<sub>3</sub> lines with homogeneous red fluorescence were assessed (Supplementary Figure 8). Upon screening the T<sub>3</sub> seeds it became evident that the seed fluorescence levels varied across the different T<sub>3</sub> lines while the intensity was uniform within the individual lines. The 35S::*Hs4* lines 228934 and 228936 showed the overall strongest red seed fluorescence (Supplementary Figure 9). Line 210637 exhibited the strongest red seed fluorescence of the five Hs1::*Hs4* lines analyzed. Among both genotypes, lines with barely visible seed fluorescence levels were detectable, i.e. lines 228944 and 228956 of 35S::*Hs4* and line 210659 of Hs1::*Hs4* (Supplementary Figure 9).

The T<sub>3</sub> lines were then grown in Petri dishes. At all developmental stages, differences in fluorescence intensities could be observed between but not within the lines (Figure 9). The most prominent fluorescence of leaf and root tissues was present in the lines exhibiting the strongest seed fluorescence before sowing (228934, 228936, 210636, 210637; Figure 9). Additionally, several lines showed pink coloration of root parts during plant development (Supplementary Figure 10). This coloration was most dominantly visible in line 228934, which also showed the strongest red fluorescence signal. The coloration was not uniformly distributed, instead, the points of lateral root branching showed strong pink colors, and the pinkness was reduced towards the root tips (Supplementary Figure 11). Pink roots were never observed in Col-0. Similar observations were made when the plants were grown in a sand-soil mixture for *in vivo* resistance tests (see 3.2.8). Here, the roots exhibited a stronger pink coloration than under *in vitro* conditions. Further, a red coloration could be observed in the leaves of the different genotypes. However, it was not uniformly distributed among plants of single T<sub>3</sub> lines. A correlation between inoculation and leaf reddening was also not ascertainable. Further, this discoloration was also visible in Col-0 leaves. Leaf reddening can therefore be attributed to the plant stress in tissue culture.

Arabidopsis lines with stronger red fluorescence and root coloration showed a lower germination rate compared to lines with less red fluorescence and non-red roots. Line 228934 exhibited the poorest germination efficiency with 82 % (Supplementary Table 9).



When the plants were grown on soil, differences in flowering time could be observed. The exact flowering times were not assessed, but the lines with the strongest red fluorescence flowered ca. two weeks later than those with lower red fluorescence intensities or the wild type. They also formed more leaves compared to Col-0. Line 210637 for example formed between 21-25 leaves before flowering, while Col-0 only produced 17-21 leaves.

Taken together, the transgenic lines with the strongest red fluorescence signals showed the most severe root coloration. They flowered later than the other lines with weaker fluorescence signals and less discolored roots.

### 3.2.3 Optimizing Arabidopsis resistance tests

In the Plant Breeding Institute, normal-sized 9 cm Petri dishes have been used for resistance tests of sugar beet hairy roots as well as Arabidopsis. Their handling is laborious and time-consuming as every plate has to be opened individually for the plants' inoculation and then sealed again. Six-well plates, on the other hand, increase the handling efficiency by being able to treat six plants at once. Therefore, I investigated if a switch to 6-well plates was affecting the formation of females on the Arabidopsis roots. I used Col-0 and inoculated seven individual Petri dishes and eleven plants in 6-well plates with 200 J2 larvae. The developing females were assessed three weeks later.

**Table 6:** Developing females 21 dpi on roots of Col-0 plants grown either in 9 cm Petri dishes or 6-well plates. Plants were inoculated with 200 *H. schachtii* J2 larvae.

Replicate #	Petri dish	6-well plate
1	6	6
2	6	1
3	8	1
4	5	0
5	10	3
6	8	9
7	10	15
8		8
9		4
10		7
11		4
mean	7.57	5.27
SD	1.99	4.4

A t-test for independent samples was conducted to compare the number of developing females between the two culturing systems. There was no statistically significant difference in female number means between the two systems,  $t(15) = 1.52$ ,  $p = 0.15$  (two-tailed). As the female numbers were similar but the 6-well plates were much easier for handling large sample sets, they were used for all further resistance tests.

### 3.2.4 Arabidopsis plants expressing 35S::*Hs4* show nematode resistance in an expression-dependent manner - Experiment I

In a first experiment, I wanted to test whether a constitutive expression of *Hs4* could confer resistance to *H. schachtii* in Arabidopsis. I analyzed if the transgenic lines expressing 35S::*Hs4* varied in their expression levels and if there was a correlation to the level of BCN resistance. For this purpose, the six 35S::*Hs4* T<sub>3</sub> lines showing homogeneous red fluorescence were grown in 6-well plates and inoculated with 250 *H. schachtii* J2 larvae. Developing

females were counted at 21 dpi and whole root samples were taken before and three days after inoculation from non-inoculated and inoculated plants to verify the transgene's expression under the constitutive promoter. To determine the lines' general *Hs4* expression level, the data over the different time points were pooled.

All transgenic lines tested showed significantly lower female numbers than Col-0 (Figure 10). The different transgenic lines varied significantly in their female number means (Kruskal-Wallis rank sum test,  $p = 1.81e-11$ ). Line 228934 exhibited the lowest female numbers with a mean of 6.5 females compared to 26.6 females on the Col-0 roots. Though the females developing on the roots of the transgenic plants often appeared smaller than those observed on Col-0, they were usually filled with eggs.

I analyzed each line's expression per time point and treatment separately and then combined all the expression data to generate the overall *Hs4* expression per line. The housekeeping gene *GAPDH* was used for normalization and all samples were normalized against the mean Cq values of the Col-0 samples. Interestingly, the transgene expression was not consistent in all lines across the different time points and treatments (Supplementary Figure 12). Lines 228921, 228924, 228934, and 228936 did not show statistically significant differences (Kruskal-Wallis rank sum test,  $p = 0.06e-4$ ) between the expression measured in the non-inoculated and inoculated samples before and three days after the inoculation. Line 228944, however, showed an increase in *Hs4* expression in the non-inoculated samples from 0 to 3 dpi, and the gene was more strongly expressed in the inoculated plants. In line 228956, the non-inoculated samples showed an expression increase from 0 to 3 dpi, while there was no difference between inoculated and non-inoculated samples at 3 dpi.

When pooling the expression data across timepoints and treatments, line 228934 showed the highest transgene expression (Figure 10). It was also the line with the lowest number of developing females.

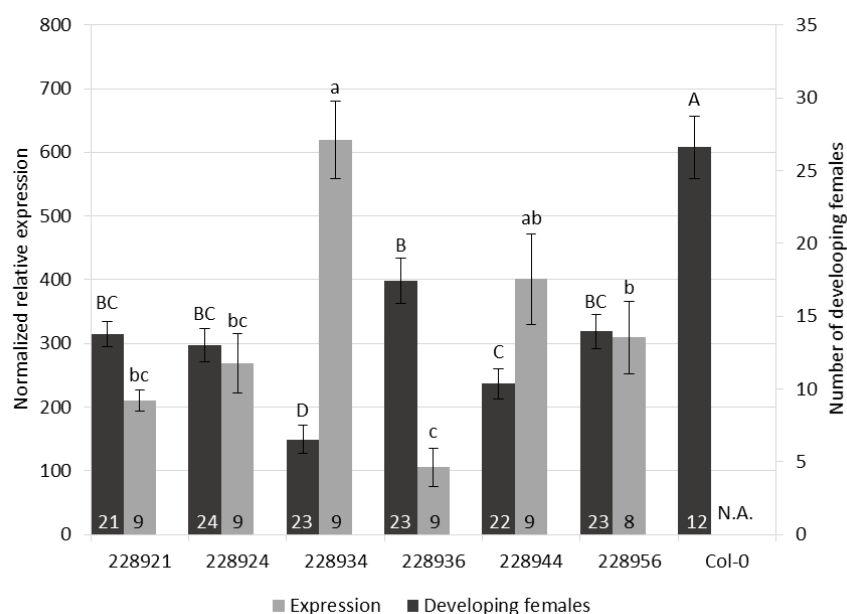


**Figure 10:** Bar plot showing the results of different 35S::*Hs4*-transgenic lines and Col-0 tested in sterile 6-well plates in experiment I. The overall *Hs4* expression level as determined by RT-qPCR (primer: AK\_F7/AK\_R5; reference gene: *GAPDH*) is shown as grey bars (left y-axis). The number of developing females counted at 21 dpi is indicated by black bars (right y-axis). The expression was calculated based on pooled data from two different sampling points (one day before inoculation and 3 dpi) and across treatments (inoculated and non-inoculated). The number of biological replicates is given at the bottom of each bar. Statistical significances were calculated using the Kruskal-Wallis rank sum test at  $p < 0.05$ , followed by a Hochberg-corrected Dunn test. Error bars represent the SEM.

### 3.2.5 Arabidopsis plants expressing Hs1::*Hs4* show nematode resistance in an expression-dependent manner – Experiment II

In a second experiment, the five selected Hs1::*Hs4* lines (see 3.2.1) were screened similarly to the 35S::*Hs4* plants to determine if an inducible expression of *Hs4* could also confer resistance to BCN. The plants were grown in 6-well plates and inoculated with 250 *H. schachtii* larvae. The developing females were counted at 21 dpi and whole root samples were taken one day before, three, and 21 days after inoculation. Again, expression levels obtained from the different time points were pooled to generate the general lines' transgene expression rate.

Two transgenic lines did not show significantly lower developing female numbers compared to Col-0 (Kruskal-Wallis rank sum test,  $p = 4.47e-11$ ; Figure 11). The other three lines showed a significant reduction in developing female numbers. Again, the females that developed were filled with eggs.

I compared the individual expression levels across the different time points and treatments (Supplementary Figure 13). All except line 210636 showed significant differences between the individual expression levels determined. Nevertheless, the differences did not occur between treatments (i.e. inoculated and non-inoculated) but rather across time points. In line 210637 the samples from 21 dpi showed higher *Hs4* expression than samples from 0 or 3 dpi. Contrastingly, line 210654 displayed higher expression levels in the early time points and a reduction at 21 dpi. Lines 210659 and 210678 showed no clear trend, instead, the expression levels were lower or higher at individual sampling points. Upon analyzing the individual expression levels, the large difference in scale sizes (Supplementary Figure 13) became apparent. The *Hs4* expression was much higher in lines 210636, 210637, and 210654 compared to the other two.

This trend was verified when looking at the overall expression per line (Kruskal-Wallis rank sum test,  $p = 1.94e-30$ ). Lines 210636 and 210637 exhibited the highest transgene expression, and accordingly the lowest numbers of developing females. Line 210654 showed a lower *Hs4* expression and a slightly higher number of females. In comparison, lines 210659 and 210678 had almost no expression. They also exhibited female numbers comparable to Col-0.

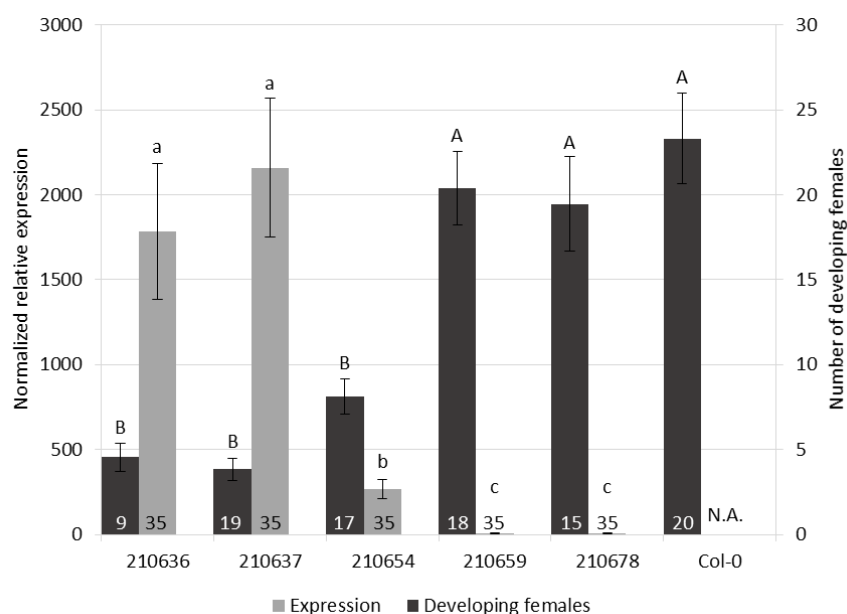


**Figure 11:** Bar plot showing the results of different Hs1::*Hs4*-transgenic lines and Col-0 tested in sterile 6-well plates in experiment II. The overall *Hs4* expression level as determined by RT-qPCR (primer: AK\_F7/AK\_R5; reference gene: *GAPDH*) is shown as grey bars (left y-axis). The number of developing females counted at 21 dpi is indicated by black bars (right y-axis). The expression was calculated based on pooled data from three different sampling points (one day before inoculation, 3 dpi, and 21 dpi) and across treatments (inoculated and non-inoculated). The number of biological replicates is given at the bottom of each bar. Statistical significances were calculated using the Kruskal-Wallis rank sum test at  $p < 0.05$ , followed by a Hochberg-corrected Dunn test. Error bars represent the SEM.

### 3.2.6 Comparison of the effect of different promoters on the *Hs4* expression and the resulting resistance reaction in Arabidopsis – Experiment III

In order to directly compare the results obtained in the first two experiments and define if one promoter construct outperformed the other, I selected the best-performing lines, i.e. those with the highest transgene expression and lowest female numbers, from the previous experiments. Hence I chose lines 228934 and 228944 containing the 35S::*Hs4* construct and lines 210636, 210637, and 210654 expressing Hs1::*Hs4* for a third experiment. I expected to see highly similar performances of each line in experiment III compared to the previous experiments I and II.

All lines were grown simultaneously in 6-well plates and inoculated with the same *H. schachtii* inoculum (250 larvae). The developing females were counted at 21 dpi and whole roots were collected one day before, three, and 21 dpi for expression verification. The overall expression was determined by pooling all samples per line.

All lines chosen for experiment III showed statistically significantly lower female numbers in experiments I and II, respectively. The direct comparison revealed that only three of the five lines showed female numbers significantly different from Col-0 (Kruskal-Wallis rank sum test,  $p = 2.74e-11$ ; Figure 12), contradicting the significance levels calculated in experiments I and II. When comparing the results from experiment III to experiments I and II, differences in female numbers can be observed. The female counts rely on the inoculum, which is different in each experiment, and the maximum female numbers observed on Col-0 roots in experiment III (mean 16) were lower than in experiments I and II (means 26.6 and 23.3, respectively). Nevertheless, the mean female numbers remained stable in the different transgenic lines across the different experiments. Accordingly, the female means of the 35S ( $r = 1$ ) and Hs1

( $r = 0.99$ ) lines, respectively, were highly correlated between both experiments. Similar to the results from experiments I and II, lines 228934, 210636, and 210637 outperformed lines 228944 and 210654.

When looking at the expression per time point and treatment, significant differences were only present in the 35S::*Hs4* lines but not in the Hs1::*Hs4* lines (Supplementary Figure 14). The differences found in the 35S::*Hs4* lines did not occur between treatments from the same sampling point but across time points. In both cases, the expression before inoculation was significantly lower than the expression measured in the inoculated samples 21 dpi. Similar to the results from experiments I and II, lines 210636, 210637, and 228934 also showed the highest overall transgene expression in this third experiment (Kruskal-Wallis rank sum test,  $p = 0.52e-4$ ; Figure 12). Their strong *Hs4* expression was consistent with the significant reduction in female numbers. Nevertheless, the lower-expressing Hs1-line 210654 showed lower female numbers than the 35S-line 228944, even though the latter had a higher overall transgene expression. Furthermore, line 228934 exhibited expression levels similar to the high-expressing Hs1-lines, but it still showed statistically significantly higher female numbers than line 210637. Across the three experiments, the expression data can show variation due to the calculation method used for normalizing the data. The expression values measured are normalized against Col-0 values determined individually in each experiment, which are therefore inconsistent. Nevertheless, the expression trends observed in experiments I and II were also evident in experiment III and high correlations between the line means across experiments were observed ( $r = 1$  for 35S,  $r = 0.997$  for Hs1).

Although the 35S promoter is expected to lead to a constantly high expression level, the Hs1::*Hs4*-transformed *Arabidopsis* plants performed better in terms of expression rates and developing female numbers.

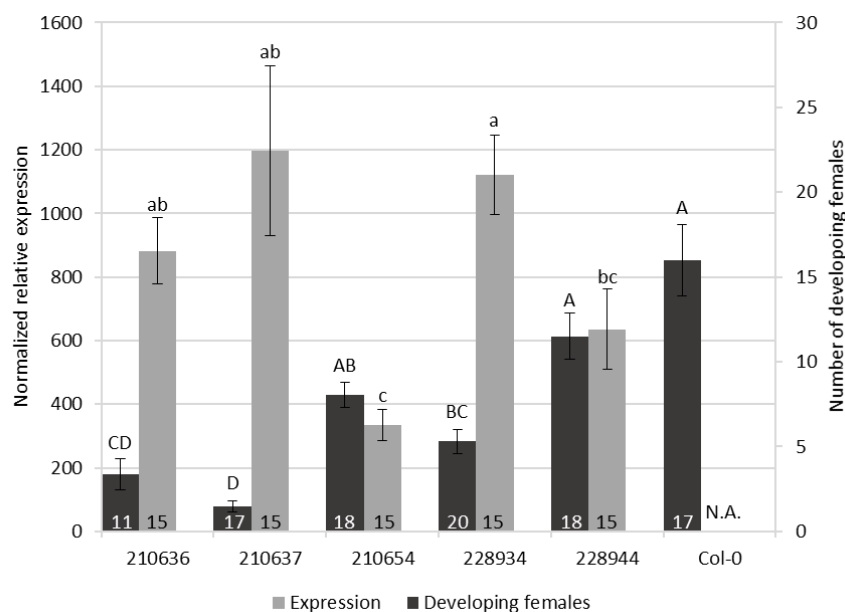


**Figure 12:** Bar plot showing the results of different Hs1::*Hs4*-transgenic (210636, 210637, 210654) and 35S::*Hs4*-transgenic (228934, 228944) lines and Col-0 tested in sterile 6-well plates in experiment III. The overall *Hs4* expression level as determined by RT-qPCR (primer: AK\_F7/AK\_R5; reference gene: *GAPDH*) is shown as grey bars (left y-axis). The number of developing females counted at 21 dpi is indicated by black bars (right y-axis). The expression was calculated based on pooled data from three different sampling points (one day before inoculation, 3 dpi, and 21 dpi) and across treatments (inoculated and non-inoculated). The number of biological replicates is given at the bottom of each bar. Statistical significances were calculated using the Kruskal-Wallis rank sum test at  $p < 0.05$ , followed by a Hochberg-corrected Dunn test. Error bars represent the SEM.

### 3.2.7 Determining the number of transgenes integrated

The assumption that the T<sub>3</sub> plant material resembled ‘lines’ was based on the homogeneous red seed fluorescence that was expected to correlate with a homogeneous *Hs4* expression level. However, in the *in vitro* tests I detected substantial expression variations between individuals of the transgenic T<sub>3</sub> lines. To test if true homozygous T<sub>3</sub> lines were at hand, I screened four T<sub>2</sub> families per construct for the presence of the *Hs4* gene using the AK\_F7/AK\_R5 primer combination (Supplementary Table 2). I expected a genotypic segregation of 3:1 (*Hs4*-positive:*Hs4*-negative) in the case of a single transgene integration. If a population harbored two transgene integration sites, I expected a segregation ratio of 15:1. Forty randomly selected seeds per family were sown and all arising plants were tested for *Hs4* presence. Segregation ratios of three 35S::*Hs4* and two Hs1::*Hs4* families were not statistically different from a 3:1 ratio, indicating a single insertion of the *Hs4* transgene (Supplementary Table 8). The 35S::*Hs4* family 226883, a single seed of which gave rise to the T<sub>3</sub> line 228934, had poor germination rates and could not be evaluated. For two Hs1::*Hs4* families (206178 and 206181) the null hypothesis of a 3:1 ratio could be rejected. The alternative null hypothesis (15:1 segregation ratio) was not rejected (Supplementary Table 8), indicating two transgene insertions. Single seeds from those families gave rise to the T<sub>3</sub> lines 210636, 210637, and 210654. Hence, the test revealed that several T<sub>3</sub> lines harbored two transgene integrations.

In the case of a single integration, the T<sub>3</sub> lines selected are truly homozygous as no non-fluorescing T<sub>3</sub> seeds were detected and hence the transgene cannot have been in a heterozygous state in the selected T<sub>2</sub> seed (Table 7).

**Table 7:** Segregation in the T<sub>2</sub> (and a heterozygous T<sub>3</sub>) generation in the case of a single transgene integration. The transgene is indicated by ‘T’ and the wild type allele by ‘WT’.

	<i>T</i> <sub>1</sub>	<i>WT</i> <sub>1</sub>
<i>T</i> <sub>1</sub>	<i>T</i> <sub>1</sub> <i>T</i> <sub>1</sub>	<i>T</i> <sub>1</sub> <i>WT</i> <sub>1</sub>
<i>WT</i> <sub>1</sub>	<i>WT</i> <sub>1</sub> <i>T</i> <sub>1</sub>	<i>WT</i> <sub>1</sub> <i>WT</i> <sub>1</sub>

In the case of two transgene integrations, different genotypes showing the same phenotype (red seed fluorescence) are possible. The segregation in the T<sub>2</sub> generation is depicted in Table 8. The phenotypical selection can lead to the selection of eight different genotypes showing the red seed fluorescence phenotype. When T<sub>2</sub> material heterozygous for both transgenes is selected and propagated, the resulting T<sub>3</sub> seeds show a phenotypic segregation into fluorescing and non-fluorescing seeds. However, the homozygous ‘lines’ selected in the T<sub>3</sub> generation did not contain non-fluorescing seeds. Therefore, it can be assumed that T<sub>2</sub> seeds homozygous for at least one transgene have been selected. In that case, the homozygous transgene will always be inherited in a homozygous state and the second transgene can be present in a homozygous or heterozygous state, or as homozygous wild type allele (like the segregation in Table 7). The selected seeds will, accordingly, always display red fluorescence, though it might be possible that differences in fluorescence intensity are observable depending on the segregation of the second transgene. Differences in fluorescence intensity were not encountered between seeds of single T<sub>3</sub> populations. Therefore, in material with one homozygous transgene, the state of the second transgene could not be determined in the T<sub>3</sub> generation. Nevertheless, double homozygous material could also have been selected by chance. The expression variations observed between individual plants of one seed code do, however, point to a differently segregating second transgene.

Conclusively, even though some T<sub>3</sub> Arabidopsis lines were most likely segregating populations, the term ‘lines’ was employed for them for simplicity reasons. Still, the strong seed fluorescence detected in the selected lines was correlated with a strong *Hs4* expression

level, as determined under *in vitro* conditions (see 3.2.4, 3.2.5, and 3.2.6). Further, the strong expression was in accordance with the observed stronger resistance reaction to *H. schachtii*.

**Table 8:** Segregation in the T<sub>2</sub> generation in the case of two transgene integrations. The transgene is indicated by ‘T’ and the wild type allele by ‘WT’ and the two different loci are distinguished by ‘1’ and ‘2’.

	$T_1T_2$	$T_1WT_2$	$WT_1T_2$	$WT_1WT_2$
$T_1T_2$	$T_1T_1T_2T_2$	$T_1T_1T_2WT_2$	$T_1WT_1T_2T_2$	$T_1WT_1T_2WT_2$
$T_1WT_2$	$T_1T_1T_2WT_2$	$T_1T_1WT_2WT_2$	$T_1WT_1T_2WT_2$	$T_1WT_1WT_2WT_2$
$WT_1T_2$	$T_1WT_1T_2T_2$	$T_1WT_1T_2WT_2$	$WT_1WT_1T_2T_2$	$WT_1WT_1T_2WT_2$
$WT_1WT_2$	$T_1WT_1T_2WT_2$	$T_1WT_1WT_2WT_2$	$WT_1WT_1T_2WT_2$	$WT_1WT_1WT_2WT_2$

### 3.2.8 Testing the resistance reaction under *in vivo* conditions

To verify if the resistance reaction was also observable under more field-like conditions, I conducted the inoculation experiments with the lines characterized under *in vitro* conditions under *in vivo* conditions in a sand-soil mixture in a climate chamber.

In a preliminary experiment, it was determined that the germination rate of Arabidopsis seeds on pure quartz sand was very low, but it was much improved when the sand was mixed with soil (data not shown). However, due to the fine structure of the Arabidopsis roots, a high percentage of soil hindered the washing of the roots for a subsequent nematode female number assessment. Hence, a mixture of 75 % sieved potting soil, with the largest particles removed, and 25 % sand was considered the best option.

#### Comparison of *in vivo* and *in vitro*

I started by testing one transgenic line under both *in vivo* and *in vitro* conditions for comparison of the two systems. I chose the Hs1::*Hs4* line 210637 due to its good performance under *in vitro* conditions and the seed availability.

The plants tested under *in vivo* conditions in a climate chamber were sown first because they required more time to establish themselves on the sand-soil mixture. Two weeks later, the *in vitro* plants were sown under sterile conditions. Approximately two weeks thereafter, the sterile *in vitro* plants were inoculated first and the same surface-sterilized inoculum was used for inoculating the *in vivo* plants the following day. Concurrently, I inoculated the plants in both setups with 200, 300, or 400 J2 larvae, respectively, to determine differences in the resistance reaction under different larval concentrations. The number of developing females was assessed at different time points in both systems: Under *in vitro* conditions, the females can be easily distinguished three weeks after inoculation, while in the sand-soil mixture, it is necessary to wait another week for the females to be properly attached to the roots to be able to wash them clean from the substrate. I also took root samples before and four days after inoculation as well as upon the counting of the females at 21 and 28 dpi, respectively.

Upon counting the females, the plant phenotypes were briefly assessed. The *in vitro* plants looked like the ones observed before (see 3.2.2). The leaves showed either green or red colorations, independent of the genotype or treatment (inoculated or non-inoculated). The roots of Col-0 were whitish-green, while the roots of 210637 exhibited pink coloration. Under *in vivo* conditions, the canopy of both genotypes was darker green with hints of purple. The Col-0 plants were already flowering properly upon counting, while the 210637 plants had just started forming the first floral shoot. The color of the Col-0 roots was similar to the *in vitro* conditions. The roots of 210637, however, exhibited a much stronger pink coloration than under *in vitro* conditions (data not shown).

I assessed the number of developing females in both cultivation systems. The *in vitro* plants showed significantly lower female numbers at all three larval densities tested (Kruskal-Wallis rank sum test,  $p = 0.52e-4$ ; Figure 13A). The *in vivo* tested plants, however, showed female numbers similar to Col-0 (Kruskal-Wallis rank sum test,  $p = 0.07$ ; Figure 13B). I then analyzed the expression from every sampling point individually. Even though the *in vitro* plants showed the strongest expression at 4 dpi, regardless of the number of larvae used, the differences were not significant (Supplementary Figure 15). The only significant difference between sampling points could be observed in the non-inoculated plants where *Hs4* expression increased drastically between 0 and 4 dpi. The *in vivo* plants did not show significant differences in expression over time or between treatments. However, samples taken at 28 dpi showed a higher expression than the earlier time points (Supplementary Figure 15). The samples were then pooled to generate the overall expression per time point and treatment. Here, no statistically significant differences were observable between non-inoculated or differently inoculated plants neither in the *in vitro* ( $p = 0.76$ ) nor the *in vivo* plants ( $p = 0.82$ ; Figure 13). Interestingly, the mean expression in *in vivo* plants was up to 27 times higher than under *in vitro* conditions.

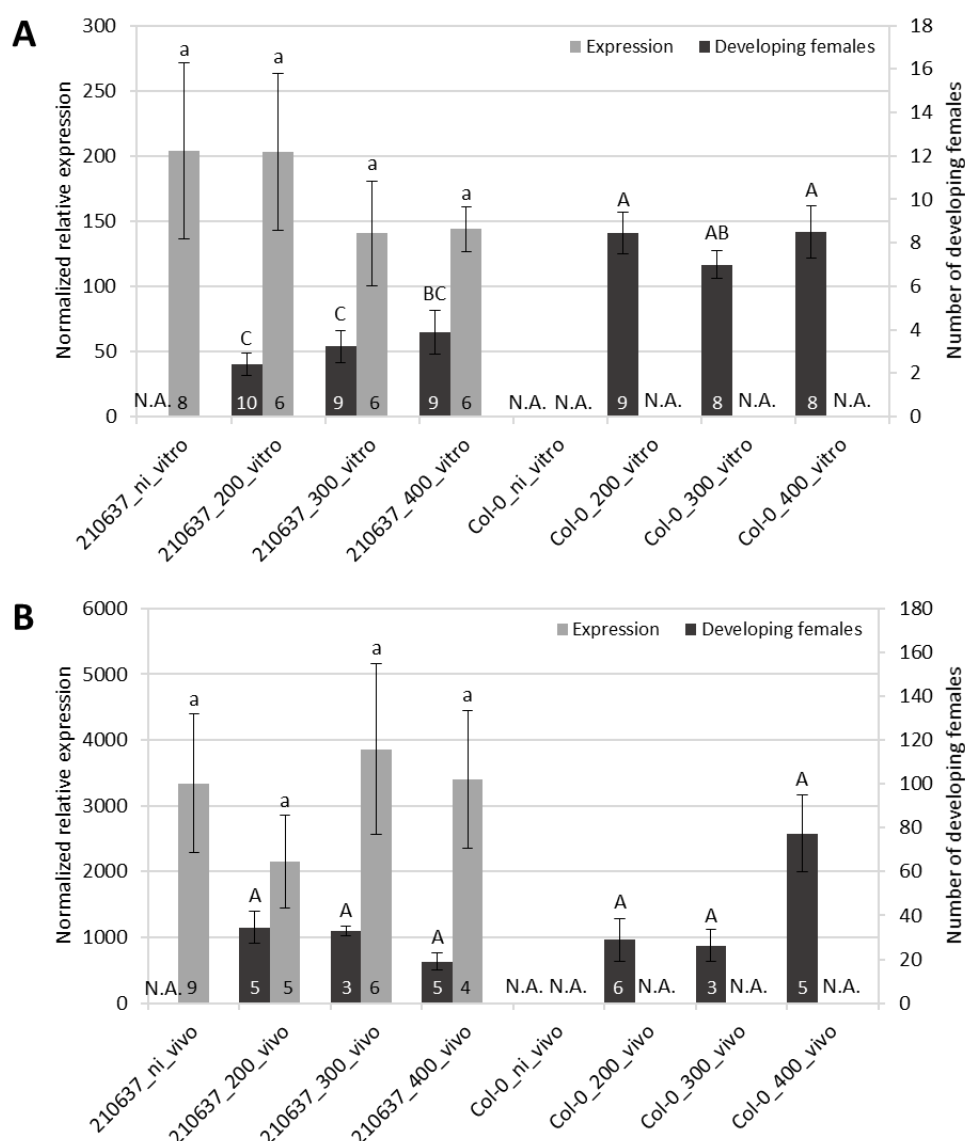


**Figure 13:** Bar plots showing the *Hs4* expression level (grey bars, left y-axis) as determined by RT-qPCR (primer: AK\_F7/AK\_R5; reference gene: *GAPDH*) and the number of developing females (black bars, right y-axis) of the *Hs1::Hs4*-transgenic line 210637 and Col-0 counted at 21 dpi under sterile *in vitro* (A) and at 28 dpi under non-sterile *in vivo* (B) conditions. The different numbers of larvae used for the inoculation (200, 300, 400)

and non-inoculated (ni) samples are indicated. The number of biological replicates is indicated at the bottom of the bars. Statistical significances were calculated using the Kruskal-Wallis rank sum test at  $p < 0.05$ , followed by a Hochberg-corrected Dunn test. Error bars represent the SEM.

### **A preliminary experiment under semi-sterile *in vivo* conditions**

As a resistance reaction could be observed under the sterile *in vitro* but not the non-sterile *in vivo* conditions, I used the same line, 210637, for a semi-sterile *in vivo* test. I expected to see a resistance reaction similar to the sterile *in vitro* results, as any microbes enhancing or reducing nematode fitness were excluded. Before sowing, the climate chamber was gassed with ozone to eliminate any residing pests, and the sand-soil mixture was heated to 80°C for four hours before using it to fill sand tubes washed in ethanol. The *Arabidopsis* seeds were also surface-sterilized and sown wearing gloves and using sterile pipette tips. The plants were watered with autoclaved tap water. The inoculum was surface-sterilized, as was the case in the prior test. I counted the developing females four weeks after inoculation and could see a clear resistance reaction. On average, 14 females were developing on the roots of line 210637 and the maximum was 24 females in the five replicates (Supplementary Table 10). On the control roots, 49 females were developing on average and the maximum reached 70 females in the six replicates analyzed.

### **Large-scale *in vivo* resistance tests under semi-sterile and non-sterile conditions**

As a clear resistance reaction in line 210637 could be observed under semi-sterile conditions in the sand-soil mixture, I tested the two 35S::*Hs4* and three Hs1::*Hs4* lines characterized under *in vitro* conditions in two simultaneous *in vivo* experiments. The first experiment was conducted under semi-sterile conditions as described above. The second experiment was performed under non-sterile conditions, using an inoculum that was not surface-sterilized. Apart from the sterility, the plants were treated the same. For example, they were watered with the same tap water, but autoclaved and not autoclaved, respectively. I expected to see the results obtained with line 210637 verified in this larger setup, i.e. a resistance reaction under semi-sterile conditions and no or only a limited resistance reaction under non-sterile conditions. As the differences between the transgenic lines were determined *in vitro*, I hypothesized to observe the same differences under *in vivo* conditions.

As briefly described above, the naked-eye coloration of the roots observed upon female counting was more extreme under *in vivo* conditions compared to *in vitro* conditions. The strongest pink coloration and the strongest fluorescence intensity were observed in the roots of the Hs1::*Hs4* lines 210636 and 210637 (Figure 14C-D), followed by the 35S::*Hs4* line 228934 (Figure 14A). Lines 228944 and 210654 had roots of a lighter pink color and exhibited less strong fluorescence (Figure 14B and E). The roots of Col-0 were whitish-green (Figure 14F). Conclusively, Col-0 did not show any fluorescence while all transgenic roots displayed red fluorescence (Figure 14). The differences in fluorescence intensity between the transgenic lines matched previous observations (see 3.2.2).

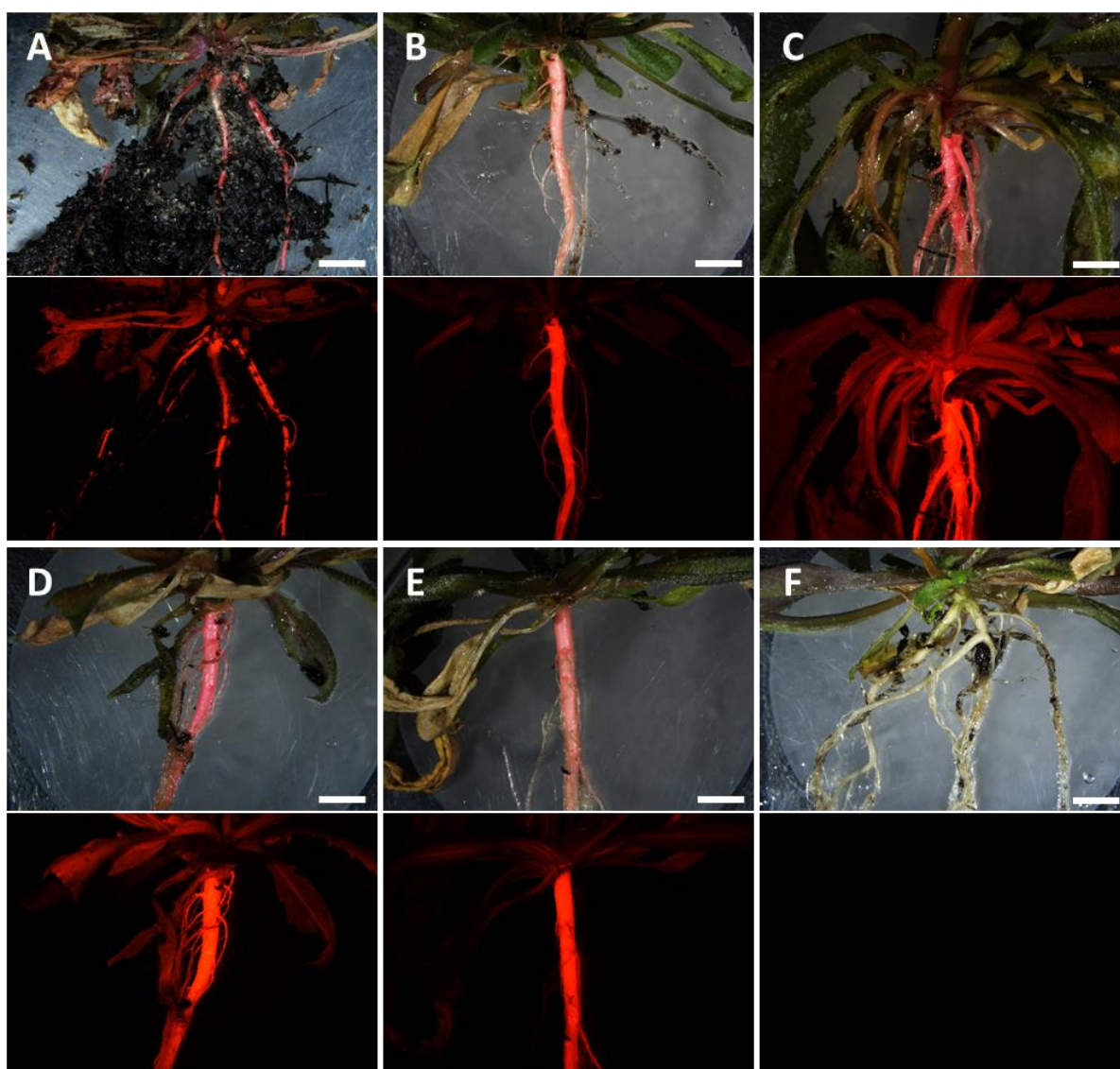


**Figure 14:** Phenotypes of the 35S::*Hs4* lines 228934 (A) and 228944 (B), the Hs1::*Hs4* lines 210636 (C), 210637 (D), and 210654 (E) and Col-0 (F) grown in a sand-soil mixture at 32 dpi. The root and leaf coloration (upper picture) was assessed under bright light and the fluorescence intensity (lower picture) was analyzed at 600 ms exposure time and  $\lambda_{\text{excitation}}$  560 nm. Bars: 0.5 cm.

The developing females were assessed at 32 dpi in both setups. Under semi-sterile *in vivo* conditions, only line 210636 had female numbers significantly lower than the control (Figure 15A). Even though the means of lines 210637 (38), 210654 (35.4), and 228934 (32.9) were below the control mean of 53.8, the differences were not statistically significant (Kruskal-Wallis rank sum test,  $p = 0.32e-2$ ). Line 228944 was the only line exhibiting a mean female value (54) even above the control. Under non-sterile conditions, none of the lines exhibited female numbers statistically different from Col-0 (Kruskal-Wallis rank sum test,  $p = 0.02$ ; Figure 15B). The female number means of the Hs1::*Hs4* lines 210636 (17.2), 210637 (22.5), and 210654 (21.7) were slightly below the mean female number observed in Col-0 (23.4). The 35S::*Hs4* lines 228934 (27.4) and 228944 (37.4) had mean values above the control. It is noteworthy that the mean female numbers developing on the Col-0 roots differed by thirty females between the semi-sterile and non-sterile setup.

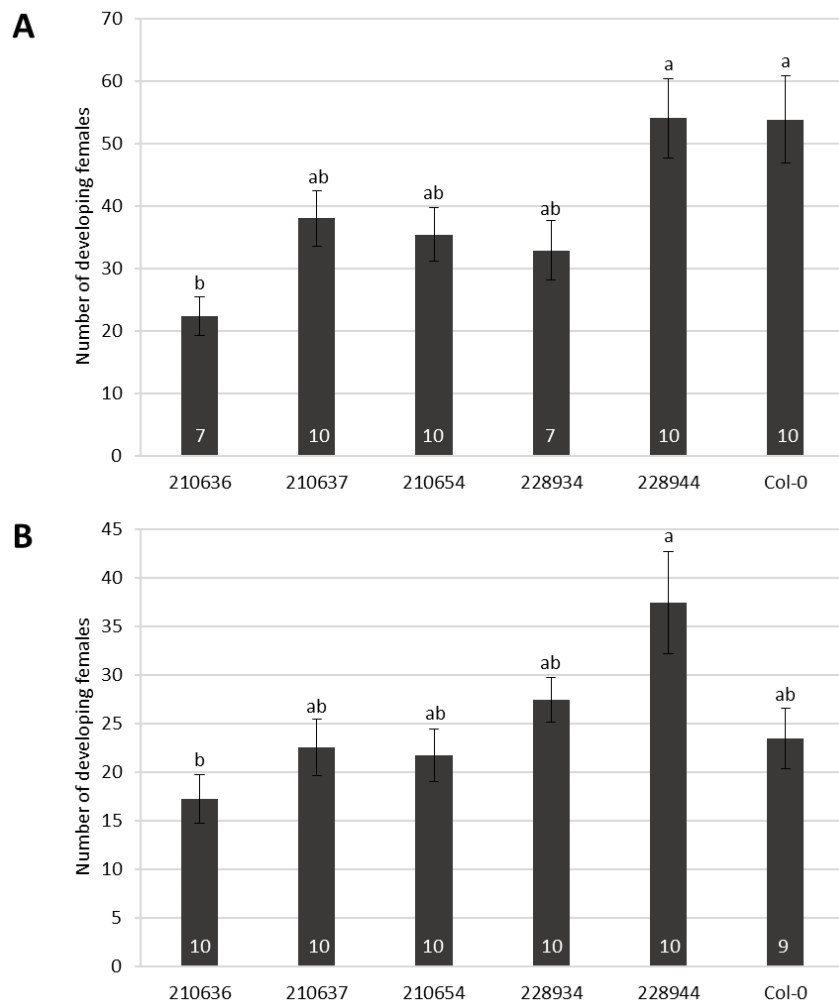


**Figure 15:** Bar plots showing the number of developing females counted at 32 dpi on different Arabidopsis lines inoculated with 250 *H. schachtii* larvae under semi-sterile (A) or non-sterile (B) *in vivo* conditions. The number of biological replicates is indicated at the bottom of the bars. Statistical significances were calculated using the Kruskal-Wallis rank sum test at  $p < 0.05$ , followed by a Hochberg-corrected Dunn test. Error bars represent the SEM.

## 4 Ultrastructural analysis reveals differences between syncytia of wild type and *Hs4*-expressing Arabidopsis

### 4.1 Materials and Methods

#### 4.1.1 Plant material and nematode infection

*A. thaliana* Col-0 (Supplementary Table 1) and the *Hs4*-expressing Arabidopsis T<sub>3</sub> lines 228934 (35S::*Hs4*) and 210637 (Hs1::*Hs4*) generated (see 3.1.2) were grown on B5 medium in 6-well plates in a climate chamber under long-day conditions (16 h light/8 h dark, 22°C) as described in chapter 3.1.3.

Two weeks after sowing, the plants were inoculated with 250 J2 larvae of the *H. schachtii* strain 'Schach 0' (Müller and Klinke 1996) as specified in chapter 3.1.3.

#### 4.1.2 Microscopic analysis

Inoculated Arabidopsis roots were sampled at 5, 8, 9, 11, and 26 dpi, respectively. The roots were observed daily under a light microscope and putative syncytia, identified by an attached nematode, were marked (workflow depicted in Supplementary Figure 16). The marked putative syncytia and associated nematodes were monitored every day. Once I could be certain that the nematode had indeed established a syncytium and would not detach from the root again, I sampled the syncytium. The sterile 6-well plates were opened and, after the roots were freed from the medium, the syncytial area was generously excised from the roots and transferred to the fixation solution. Afterward, the plates were sealed again and kept for observations on the following days (Supplementary Table 11).

The sampled root segments were fixed in a 2.5 % glutaraldehyde/0.1 M phosphate buffer (pH 7; both Carl Roth GmbH + Co. KG, Karlsruhe, Germany) solution for 1-2 h. At the beginning of the fixation, vacuum was applied for 7 min, then released and applied for another 7 min. Afterward, the samples were kept at room temperature for the remaining incubation time. The samples were then kept in the fridge in a 0.5 % glutaraldehyde (GA; Carl Roth) solution until further usage.

Samples were rinsed in a 0.1 M phosphate buffer solution and contrasted with a 0.5 % osmium tetroxide solution (Carl Roth) for 2 h, followed by four washes in double-distilled water and overnight incubation in a 1 % uranyl acetate (Science Services GmbH, Munich, Germany) solution. The samples were dehydrated using an acetone gradient of 50 %, 75 %, and 99.7 % acetone (Carl Roth). The embedding medium was prepared using the Epoxy Embedding Medium kit (Sigma-Aldrich, St. Louis, MO, USA). Ten milliliter epoxy resin was mixed with 8 ml of the hardener DDSA (dodecenylsuccinic anhydride) and 4 ml of the hardener MNA (methyl nadic anhydride). Then, 15 µl/ml of the accelerator BDMA (benzyltrimethylamine) were added. The samples were infiltrated with a 1:1 mixture of embedding medium and 99.7 % acetone on a rotator for 2 h. Further, the samples were infiltrated overnight with pure embedding medium. Finally, the infiltrated samples were placed in molds of a block form filled with embedding medium and polymerized for 48 h at 60°C.

Semi-thin (1 µm) as well as ultra-thin (80 nm) sections were prepared using a UC7 ultramicrotome (Leica, Wetzlar, Germany) equipped with a diamond knife. Semi-thin sections were transferred to a glass slide. The slide was covered with Richardson's stain and kept on a heated plate (86°C) for one minute before the stain was rinsed off with distilled water.

Richardson's stain was prepared as a 1:1 mixture of an aqueous solution containing 1 % methylene blue (Sigma-Aldrich) and 1 % di-sodium tetraborate (Carl Roth) with an aqueous 1 % Azure II (Carl Roth) solution. After drying, the sections were observed under a light microscope (Primostar, Zeiss). Later, the semi-thin sections were mounted under a cover glass using embedding medium and photographed with a DS-Ri2 camera mounted onto a Nikon Eclipse Ni microscope using the NIS-Elements BR software (Nikon, Tokyo, Japan).

Once a syncytium became visible in the semi-thin sections observed under the light microscope, ultra-thin sections were prepared. Following the standardized procedure from the central microscopy, blocks were sectioned at different depths. After the first semi-thin and ultra-thin sections, 25-60  $\mu\text{m}$  were removed from the top of the block, and the preparation of semi-thin and ultra-thin sections was repeated at the new site. Ultra-thin sections were transferred to glow-discharged copper slot grids. The slot grids (slot size 1mm x 2mm; Science Services GmbH) were coated with a Formvar support film (1 % solution in chloroform; Science Services GmbH) and glow-discharged at 0.6 mbar vacuum and a current of 10 mA for 20 sec in a CCU-010 compact coating unit to reduce folds (Safematic, Zizers, Switzerland). The slot grids containing the sections were contrasted with saturated uranyl acetate for 10 s, washed on water drops, and then transferred to Reynolds lead citrate (Reynolds 1963) for 1 min, followed by another wash on water drops. The sections were then analyzed on a Philips CM10 (Philips/FEI, Hillsboro, OR, USA) or a FEI Tecnai G2 Spirit BioTWIN (FEI/ThermoFisher Scientific<sup>TM</sup>) transmission electron microscope operated at 80 kV using the TEM User interface v. 4.2 and equipped with a LaB6 filament. Images were recorded with a MegaView III or MegaView III G2 CCD camera using the iTEM v. 5 software (all Olympus Soft Imaging Solutions, EMSIS GmbH, Münster, Germany). Photos were merged with the open-source software Hugin Panorama photo stitcher (d'Angelo 2023).

## 4.2 Results

I wanted to know if differences in the ultrastructure of syncytia between Col-0 and *Hs4*-expressing Arabidopsis plants could be observed. I expected to see more and smaller vacuoles, smooth ER, and higher cytoplasmic density in syncytia induced in wild type roots (see 1.4). Contrarily, I expected to find more and larger vacuoles, rough ER, and less dense cytoplasm in the transgenic plants' syncytia. Further, I hypothesized to detect membrane aggregations in syncytia in *Hs4*-expressing plants (see 1.7.2).

The plants were grown in 6-well plates and inoculated with *H. schachtii* J2 larvae two weeks after sowing. Samples of syncytia induced in Col-0 and transgenic roots were taken at different time points. Directly after selecting the ISC, the nematode starts its feeding cycle with the preparation phase. The early-stage syncytium, demarcated by cell wall openings and hence the incorporation of adjacent cells, is formed 18 h later (Grundler et al. 1998). Holtmann et al. (2000) started examining syncytia at 4 dpi. They also found main differences between translocation line and wild type material at 8 dpi and 11 dpi. Therefore, I aimed to examine syncytia sampled at similar time points. Additionally, I examined established syncytia at 26 dpi. The inoculated plants were inspected daily to detect syncytia formation (Supplementary Figure 16). After samples had been taken, the plates were re-sealed for further observations. Therefore, samples for 5, 8, and 11 dpi come from the same set of plants (one plant was lost after the 5 dpi sampling point; Supplementary Table 11), while the plants for the 9 dpi and 26 dpi sampling point were grown and inoculated separately. The excised syncytial area was embedded and semi-thin (1  $\mu\text{m}$ ) and ultra-thin (80 nm) sections of selected blocks (Supplementary Table 11) were generated and analyzed under a light or transmission electron microscope, respectively. I selected the blocks under a light microscope, based on the orientation of the root segment containing the syncytium, i.e., planarity to the sectioning plane.

As ultra-thin sections were prepared at different depths (see 4.1.2), all blocks investigated here, except the ones containing non-inoculated samples, were examined at a minimum of two sectioning depths. Sections from a second layer are only reported here if new findings were observable, compared to the first section. Differences between syncytia induced in resistant and susceptible plants are well characterized (see 1.4 and 1.7.2). As I was interested in examining putative differences between syncytia induced in transgenic and wild type *Arabidopsis* roots, I compared sections from those samples once a syncytium was encountered and did not section deeper to detect the nematode's site of attachment. However, the nematode was often observable as a round black shape next to the root in semi-thin sections (see Figure 17). As the embedding protocol was not optimized to infiltrate the nematodes, their shape was not conserved in ultra-thin sections and the nematodes detected under the electron transmission microscope are therefore not shown here.

#### 4.2.1 Comparative analysis of non-inoculated roots

First, I screened a non-inoculated control root sampled 25 days after sowing (DAS; equivalent to 11 dpi). The Col-0 *Arabidopsis* root was clearly separated into epidermis, cortex, endoderm, and pericycle. The row of xylem vessels surrounded by procambial cells was distinguishable in the middle of the root, both under the light microscope (Figure 16A) and the transmission electron microscope (Figure 16B).

To see if the root morphology in the transgenic line 228934 expressing 35S::*Hs4* was different from Col-0, a non-inoculated root sampled at 22 DAS (equivalent to 8 dpi) was examined. The general structure of epidermis, cortex, endoderm, and pericycle was detected (Figure 16C-D). The xylem vessels, however, were arranged in a bundle instead of a row (compare Figure 16B and D). The cells contained larger plastids, as observable under the electron microscope (Figure 16D). Otherwise, no differences to the Col-0 root were detected.

Similarly, a non-inoculated root of the transgenic line 210637 expressing Hs1::*Hs4* sampled at 25 DAS (equivalent to 11 dpi) was examined. Again, the normal root structure of epidermis, cortex, endoderm, and pericycle was found (Figure 16E-F). Similar to the root from line 228934, the xylem vessels were arranged in a bundle instead of a row (compare Figure 16D and F). Furthermore, many cells contained pronounced plastids (Figure 16F). No other differences to Col-0 were detected.

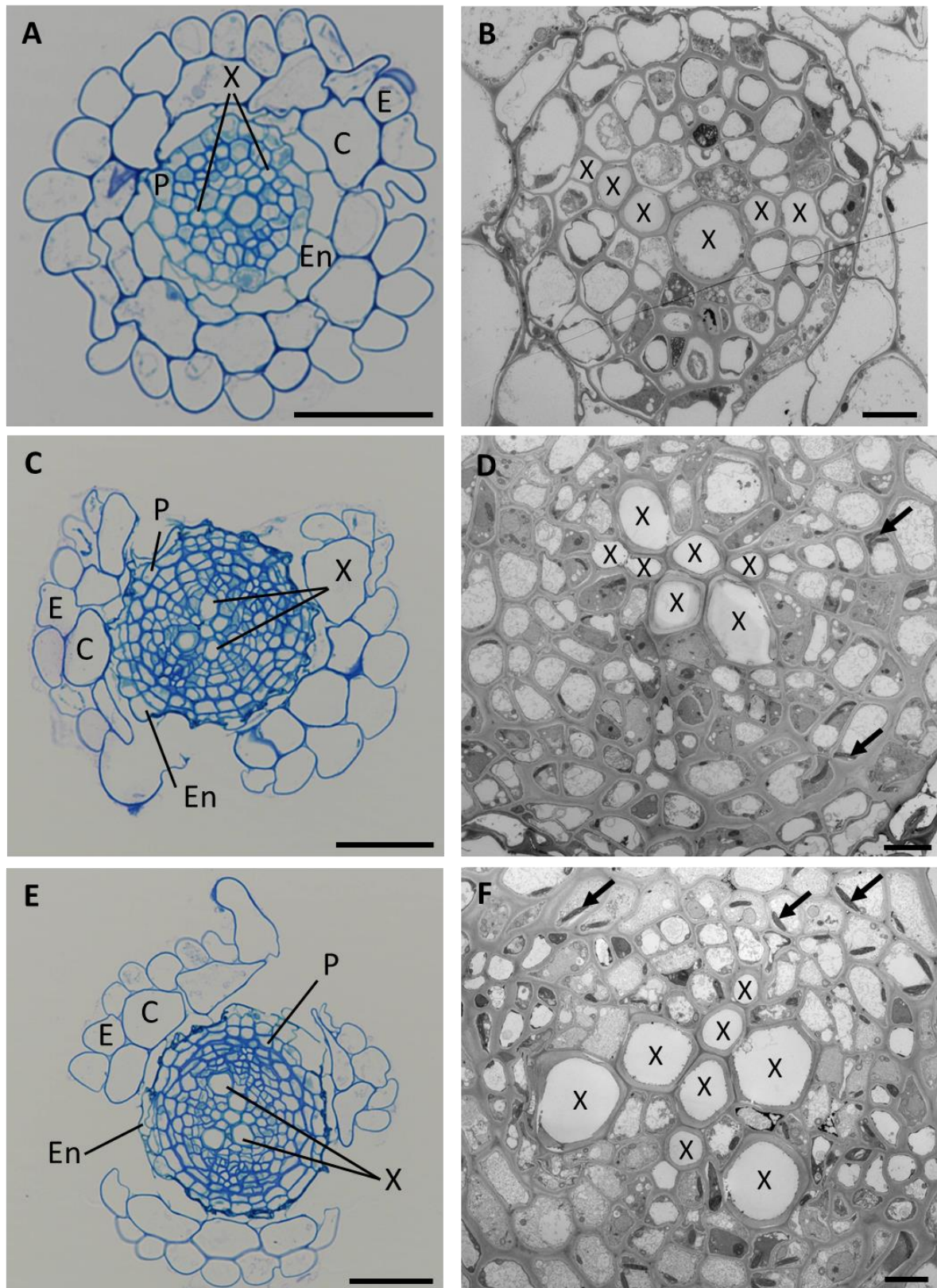


**Figure 16:** Cross sections of non-inoculated roots observed as semi-thin sections, dyed with Richardson's stain, under the light microscope (A, C, E; bar: 100  $\mu$ m) or as ultra-thin sections under the transmission electron microscope (B, D, F; bar: 5  $\mu$ m), respectively. (A-B) Non-inoculated Col-0 root (25 DAS, equivalent to 11 dpi). C: Cortex, E: epidermis, En: endodermis, P: pericycle, X: xylem elements. (C-D) Non-inoculated root of the 35S::*Hs4* transgenic line 228934 (22 DAS, equivalent to 8 dpi). C: Cortex, E: epidermis, En: endodermis, P: pericycle, X: xylem elements, arrows: plastids. (E-F) Non-inoculated root of the Hs1::*Hs4* transgenic line 210637 (25 DAS, equivalent to 11 dpi). C: Cortex, E: epidermis, En: endodermis, P: pericycle, X: xylem elements, arrows: plastids. The transmission electron microscopic pictures were generated by stitching 10, 35, and 30 individual photos, respectively.

### 4.2.2 Syncytia induced in Col-0

In Col-0, syncytia from 9 dpi and 26 dpi were analyzed. Before preparing ultra-thin sections for transmission electron microscopy, semi-thin sections of the roots were screened under a light microscope to reliably identify the syncytia (Figure 17).

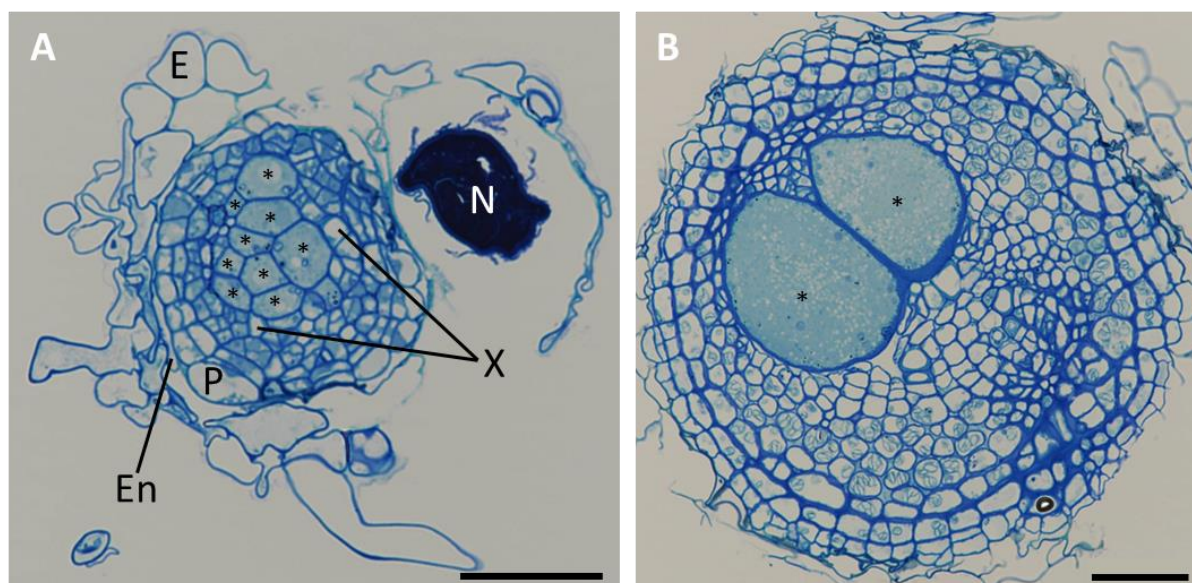


**Figure 17:** Stained semi-thin cross sections of Col-0 roots. (A) Cross section of an infected root 9 dpi with a syncytium (asterisks) distinguishable. A nematode (N) is visible next to the root. Bar: 100  $\mu$ m. E: epidermis, En: endodermis, P: pericycle, X: xylem elements. (B) Cross section of an infected root 26 dpi. The syncytium consists of two large syncytial elements (asterisks) connected in another layer. Bar: 100  $\mu$ m.

#### *Syncytium at 9 dpi*

I analyzed one syncytium sampled 9 days after inoculation from Col-0. The syncytium was already observable under the light microscope (Figure 17A). Syncytial elements were identifiable by their light-blue staining and the filled appearance. The syncytial cells were much larger than the other root cells not integrated into the syncytium. The root morphology looked disrupted. The epidermis was no longer continuous, and the cells of cortex, endoderm, and pericycle seemed compressed compared to the non-inoculated control sample. Whether these morphological differences occurred during the sample preparation or due to the infection with the nematode could not be determined. Next to the root, a nematode stained dark blue could be observed. The analysis of the embedded block showed that the nematode was positioned with its head away from the front of the block, hence the sectioning started at the nematode's tail visible here (Figure 17B).

Similar to the light microscopic observations, syncytial cells of the 9-day-old syncytium could easily be differentiated from other root cells not incorporated into the syncytium under the transmission electron microscope (Figure 18A). The syncytium was located between the xylem vessels and exhibited dense cytoplasm and several cell wall openings. The central vacuole had been degenerated, instead, various smaller vacuoles could be observed. Several nuclei and numerous mitochondria were also present, hinting at the active stage of the syncytium. Additionally, the syncytium contained plastids with large starch grains. Paramural bodies budding off the cell walls could be identified (Figure 18B-C). They form by the deposition of cell material between the cell wall and plasma membrane (see 1.4). Many small endoplasmic reticulum (ER) vesicles were visible in the cytoplasm (Figure 18B), though some rough ER could also be detected, with ribosomes on the surface of the membranes (Figure 18C).

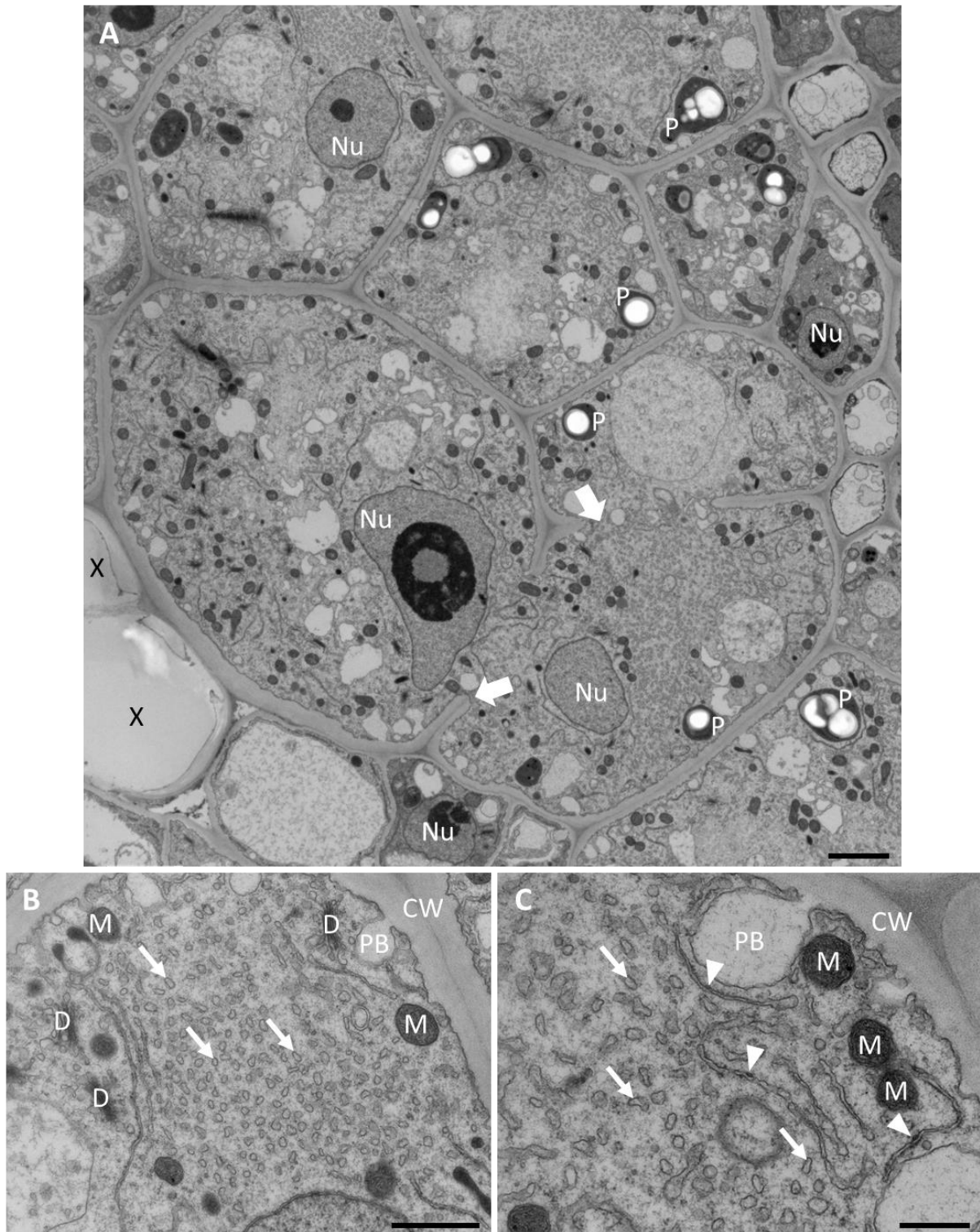


**Figure 18:** Transmission electron microscopic analysis of a syncytium from Col-0 sampled at 9 dpi. (A) The syncytial elements contain dense cytoplasm with numerous mitochondria and several nuclei (Nu). Cell wall degradations are visible (bold arrows). The picture was generated by stitching 25 individual photos. Bar: 2  $\mu$ m. P: plastid, X: xylem. (B) The syncytium contains many smooth ER vesicles (arrows). Bar: 1  $\mu$ m. CW: cell wall, D: dictyosomes, M: mitochondria, PB: paramural body. (C) Apart from the smooth ER (arrows), rough ER with single ribosomes (arrow heads) could occasionally be observed. Bar: 500 nm. CW: cell wall, M: mitochondria, PB: paramural body.

### *Syncytium at 26 dpi*

Two syncytia sampled at 26 dpi, demarcated by a clearly swollen female attached to the feeding site, were analyzed. They were well-developed and distinct in their morphology compared to non-incorporated root cells and could already be identified under the light microscope (Figure 17B). Both syncytia were found between xylem vessels, though their general appearance differed. In one syncytium analyzed, single cells were still evident, though they were joined by cell wall openings (Figure 19A). Here, strong cell wall ingrowths were observed around the xylem elements, protruding far into the syncytial cells. The xylem vessels were partly coated with osmiophilic substances or contained floccular material. The cytoplasm of this syncytium was dominated by vesicular ER. Seldomly, tubular ER structures with ribosomes were detected. Several mitochondria were present, though they were not as abundant as at the earlier time point. The plastids did not contain starch grains.

The second syncytium analyzed appeared much larger compared to the first syncytium. It did not contain any distinguishable single cells or cell wall openings. The surrounding cells were very small. The syncytium had a highly condensed cytoplasm with numerous small vacuoles accumulating in the middle (Figure 19B). Cell wall ingrowths could also be observed along the xylem elements, though they were less prominently developed. The differently pronounced development of cell wall ingrowths could, however, be caused by the different lengths in shared cell walls between syncytium and xylem elements evident between those two syncytia. The second syncytium displayed only a few vesicular ER structures, but many ER cisternae (Figure 19C), and seldomly ribosomes. Interestingly, several small, electron-dense vesicles were observed, that co-localized with those ER cisternae or the cell wall ingrowths. The mitochondria in this syncytium appeared degenerated, based on their translucent lumen. The plastids, many of them also found in cells around the syncytium (Figure 19B), contained visible starch grains.

The structural differences between both syncytia from the same sampling point might have arisen from different time points of syncytium induction. The second syncytium analyzed appeared much more advanced, on the verge of being degraded, while the first still seemed highly functional and active.

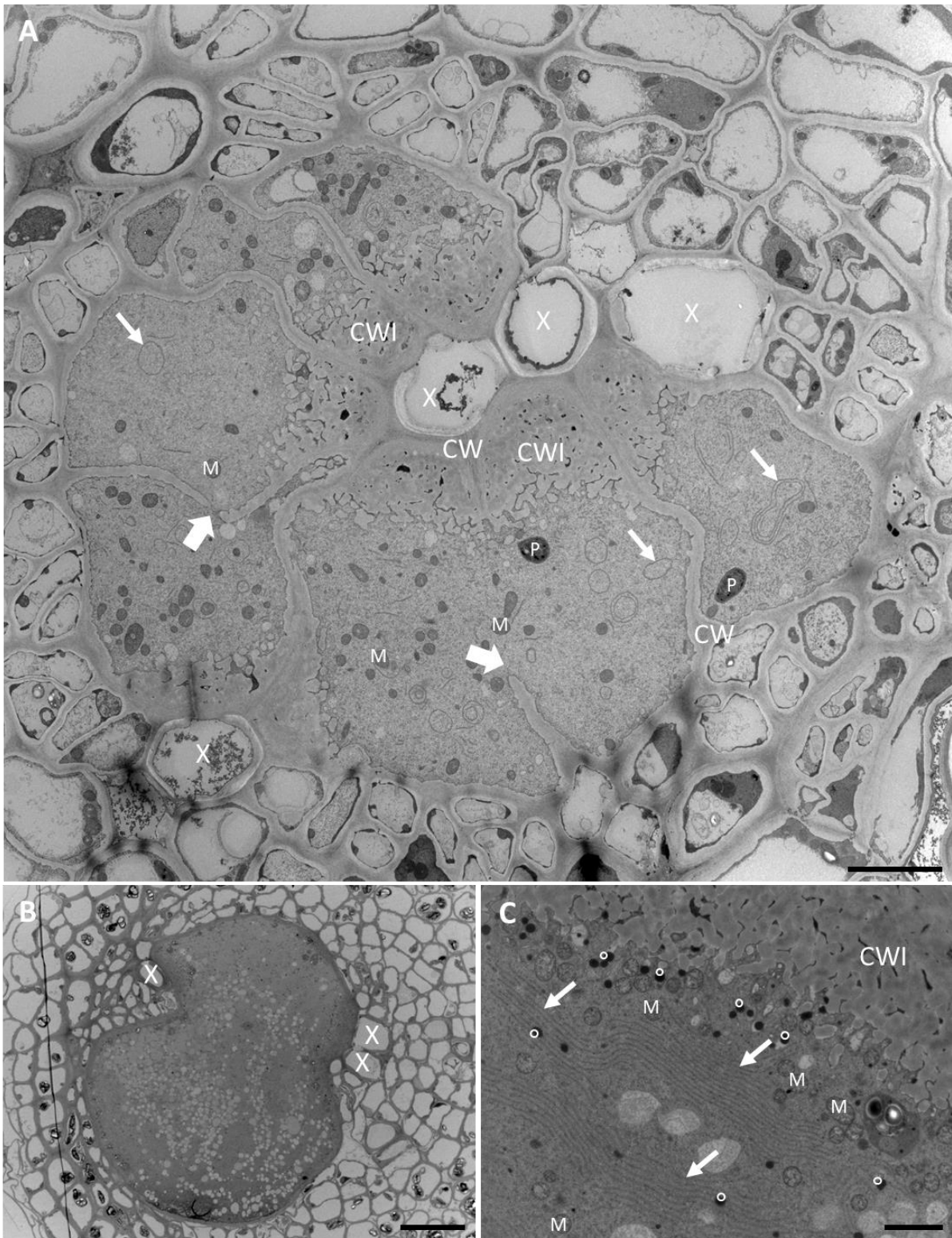


**Figure 19:** Transmission electron microscopic analysis of syncytia at 26 dpi in the susceptible system. (A) Overview of a syncytium with evident cell wall degradations (bold arrows) and cell wall ingrowths (CWI) starting around the xylem vessels (X). The syncytium contains numerous mitochondria (M), many smooth ER (SER) vesicles, and some circularly arranged tubular SER (arrows). The picture was generated by stitching 26 individual photos. Bar: 5  $\mu$ m. CW: cell walls, P: plastids. (B) A second syncytium from the same sampling point contains no internal cell walls and several vesicles. Cell wall ingrowths starting at the xylem elements (X) are visible. Bar: 20  $\mu$ m. (C) View of the cell wall ingrowths (CWI) and SER cisternae (arrows) found in the second syncytium. Additionally, electron-dense, putative secretory vesicles (circles) are present close to the SER and the cell wall ingrowths. Bar: 2  $\mu$ m. M: mitochondria.

When comparing the earlier and later developmental time points, the growth of the syncytium over time becomes evident. Structures present in Col-0 syncytia at 9 dpi were also observed in the later stages. The main finding is the smooth ER present at both time points. The numerous mitochondria supporting the active state of the syncytium were also persistent between the two stages, although their degradation process seems to have started in the later stage. Cell wall ingrowths flanking the adjacent xylem vessels were only observed in more developed syncytia. Additionally, the cell walls were thicker in later-stage syncytia.

### 4.2.3 Syncytia induced in *Hs4*-transgenic plants

For comparison of syncytia in the *Hs4*-expressing *Arabidopsis* plants, one high-expressing line (see 3.2.6) per promoter-gene combination was selected. Hence, syncytia of the 35S::*Hs4* line 228934 at 11 dpi and the Hs1::*Hs4* line 210637 at 5, 8, 11, and 26 dpi were analyzed. Prior to the preparation of ultra-thin sections for transmission electron microscopy, semi-thin sections of the roots were screened under a light microscope to reliably identify the syncytia.

#### 4.2.3.1 Line 228934 expressing 35S::*Hs4*

Upon sampling, syncytia in the 228934 line were hardly identifiable, considering an attached nematode as a criterium. Therefore, only a limited number of samples with putative syncytia from two time points were available (see Supplementary Table 11). In the root sampled at 9 dpi, no syncytium could be detected in ultra-thin sections even though a nematode was attached to the root (data not shown). Therefore, the block was excluded from further analysis and two reliably identified syncytia from 11 dpi were screened.

#### *Syncytium at 11 dpi*

Similar to Col-0, the eleven-day-old syncytia could already be identified in the semi-thin sections under the light microscope (Figure 20). The syncytial cells were light-blue stained and appeared opaque, while the remaining root cells were translucent. Furthermore, cell wall openings could be observed between the syncytial cells.

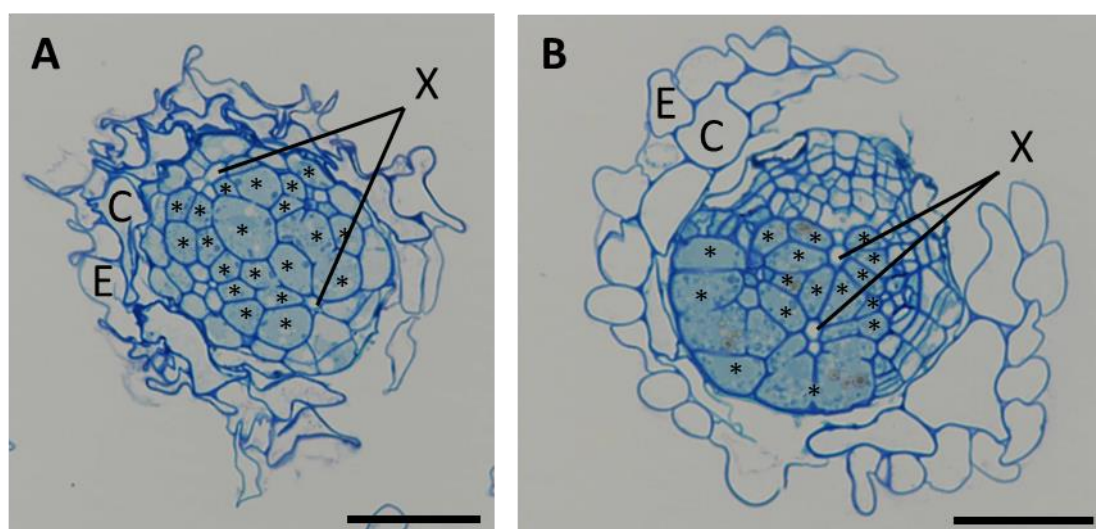


**Figure 20:** Stained semi-thin cross sections of two infected roots of the 35S::*Hs4* transgenic line 228934 at 11 dpi. In both roots, syncytia (asterisks) are visible. Bars: 100  $\mu$ m. C: cortex, E: epidermis, X: xylem vessels.

The two syncytia from 11 dpi were then analyzed under the electron microscope. The first syncytium was positioned between the xylem elements and covered almost the whole root area in that section (Figure 20A, Figure 21A). Its cells were easily distinguishable

by their dense cytoplasm and the degradation of single cell walls. The central vacuoles had been degenerated and several smaller vacuoles were present. The syncytium contained numerous mitochondria and some plastids, though they did not contain starch grains as was the case in Col-0. Most strikingly, the whole syncytium was filled with sheets of membrane structures that appeared tubular based on the thin layer examined (Figure 21B-C). These ER sheets were devoid of ribosomes. They were highly abundant in the cells and other organelles like nuclei or mitochondria were encircled by them. The vesicular ER observed in the susceptible syncytium was only rarely found here (black arrows in Figure 21B).

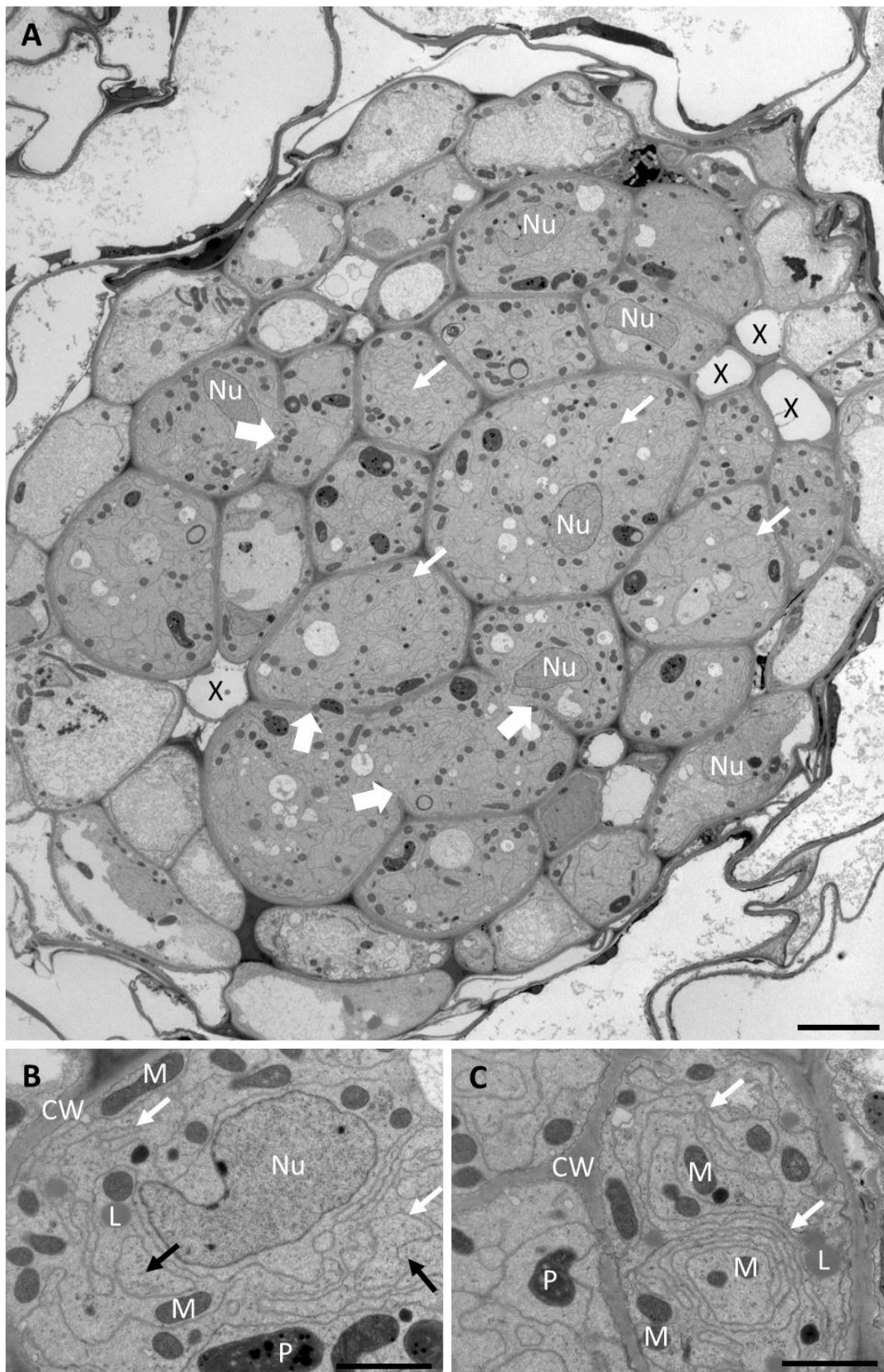


**Figure 21:** Transmission electron microscopic analysis of a syncytium in the transgenic line 228934 at 11 dpi. (A) Overview of the whole root. The syncytium contains dense cytoplasm with numerous mitochondria and several cell wall openings (bold arrows). Interestingly, ample ER sheets (white arrows) running through all syncytial cells can be observed. The picture was generated by stitching 31 individual photos. Bar: 5  $\mu$ m. Nu: nuclei, X: xylem vessels. (B and C) The membrane structures (arrows) found in the transgenic syncytium stretch through all syncytial cells and encircle other organelles like nuclei (Nu) or mitochondria (M). Only individual vesicular ER structures (black arrows) are found. Bars: 2  $\mu$ m. CW: cell walls, L: lipid droplets, P: plastids.

The second syncytium was also easily separable from the normal root cells (Figure 20B, Figure 22A). It again displayed a highly dense cytoplasm and was multi-nucleate (Figure 22B). Further, it contained many small vacuoles and numerous mitochondria. Several multivesicular bodies enclosing vesicular structures could also be identified (Figure 23F). Cell wall degradations were evident. Some cell walls were degraded to an extent that only small stubs remained where a complete wall once separated the cells. As before, the syncytium was located between the xylem elements. The cell wall ingrowths were not very pronounced though identifiable along the xylem elements' walls (Figure 23A). The main difference to the other syncytium from 228934 was the absence of ER in the form of vesicles or sheets. Instead, membrane aggregations of different sizes were detected (Figure 22B, Figure 23B-E). Once identified, the membrane aggregations were already discernible in the large-scale view of the whole root (Figure 22A) as grey electron-dense shapes. The larger aggregations spanned over two or more former cells (Figure 22B), while the smallest ones were the size of a mitochondrion (Supplementary Figure 17B). The membrane aggregations were formed by ER-derived tubules, as ribosomes were localized on the outer tubules (Figure 23E). While the outer tubules could be identified precisely, showing a double membrane and an enclosed lumen, the inner regions consisted of hundreds of membranes entangled and stacked over each other. The membrane aggregations were continuous between different layers analyzed.

To ascertain that the membrane aggregations were not just a local phenomenon in the sectioning layer analyzed, a second section 30  $\mu\text{m}$  deeper into the syncytium was investigated. The largest membrane aggregations detected in the first section could also be identified in this second layer (Supplementary Figure 17A). Further, the second layer displayed a necrotic region along the syncytium's border (Supplementary Figure 17A). Using the continuous xylem elements between the two sections as a reference, I could trace the location of the necrotic region back to the first section, where no signs of necrosis were evident in that area. 30  $\mu\text{m}$  further in, however, the bespoken region was devoid of organelles or any recognizable tissues. Instead, a black membranous substance filled the cell (Supplementary Figure 17C). The cell walls were also in a state of degradation. The middle lamella was no longer discernible and the walls looked porous and electron-translucent. Interestingly, the cell walls facing adjacent cells were intact as were the neighboring cells themselves.

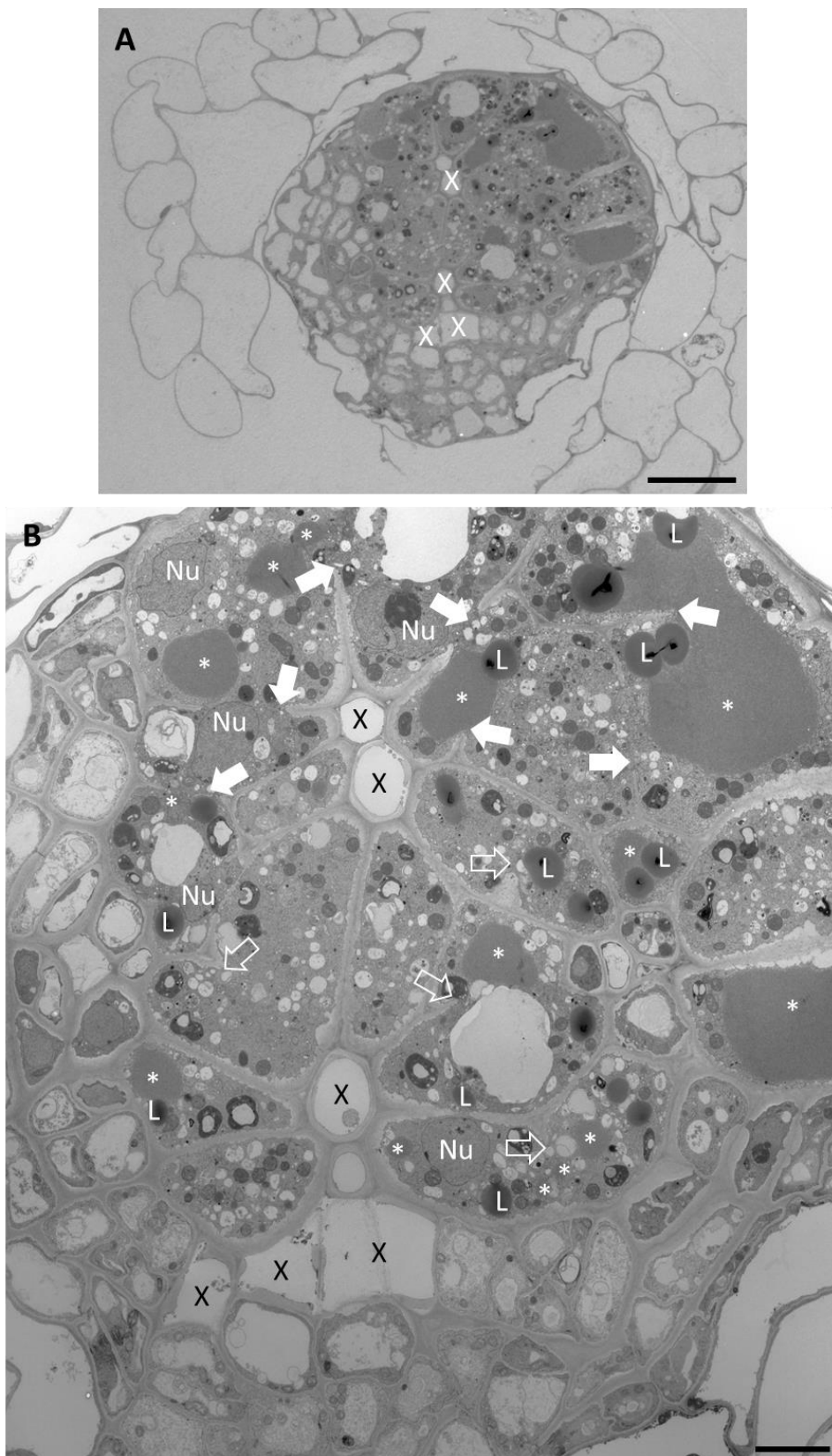


**Figure 22:** Transmission electron microscopic analysis of a second syncytium in line 228934 at 11 dpi. (A) Overview of the whole root. The syncytial elements can be easily distinguished from the surrounding non-incorporated root cells by their denser cytoplasm. Bar: 20  $\mu\text{m}$ . X: xylem vessels. (B) Detailed overview of the syncytium from (A) located between the xylem vessels (X). Several cell wall openings are visible (bold arrows), and partly the remaining cell wall stubs are hardly identifiable (empty bold arrows). The syncytium contains several nuclei (Nu), numerous mitochondria, and plenty of lipid droplets (L). Membrane aggregations (asterisks) of different sizes are present in the syncytial cells. The picture was generated by stitching 33 individual photos. Bar: 5  $\mu\text{m}$ .

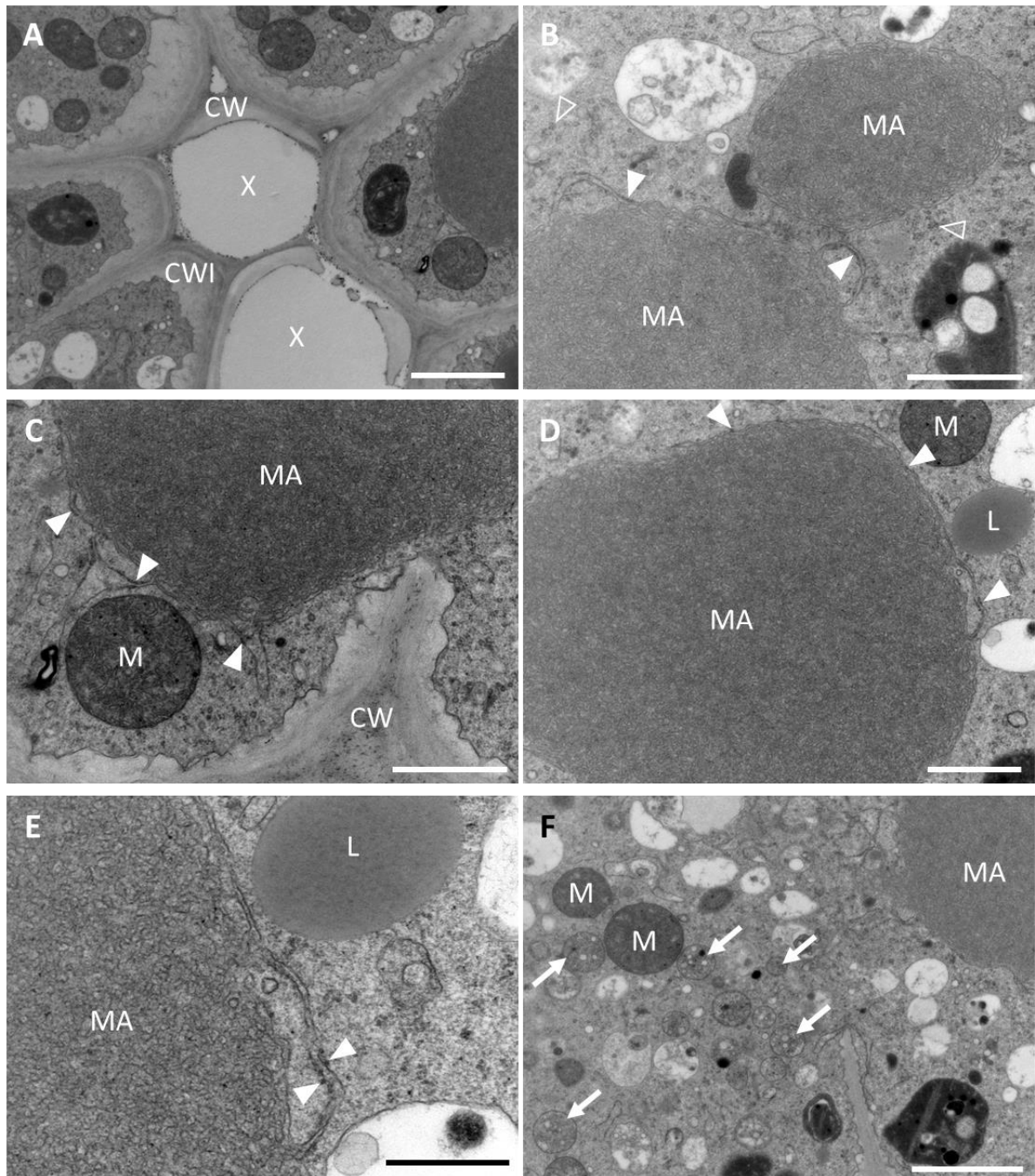


**Figure 23:** Details of the syncytium from Figure 22. (A) Beginning cell wall ingrowths (CWI) can be found along the xylem elements (X). Bar: 2  $\mu\text{m}$ . CW: cell wall. (B-D) The membrane aggregations (MA) are differently sized, their tubular structure is well visible. On the outer membranes of the MA, ribosomes (arrowheads) can be observed, while polyribosomes (empty arrowheads) are found in the cytoplasm. Bar: 1  $\mu\text{m}$ . CW: cell wall, L: lipid droplet, M: mitochondria. (E) Detail of the outer tubules of the membrane aggregation (MA) from (D), with the ribosomes (arrowheads) visible. Bar: 500 nm. L: lipid droplet. (F) Multivesicular bodies (arrows) filled with small vesicles are abundant in the syncytium. Bar: 2  $\mu\text{m}$ . M: mitochondria, MA: membrane aggregation.

#### 4.2.3.2 Line 210637 expressing Hs1::*Hs4*

Sampling in the Hs1::*Hs4* expressing line 210637 was easier compared to line 228934. The syncytia were more abundant and could be identified reliably at earlier stages. Accordingly, I could analyze syncytia from 5, 8, 11, and 26 dpi (Supplementary Table 11).

*Syncytium at 5 dpi*

At the earliest time point, 5 dpi, the syncytium analyzed was still rather small and harder to identify in the semi-thin sections (Figure 24A). Even under the transmission electron microscope the clear demarcation to the non-incorporated root cells was difficult (Figure 25A).

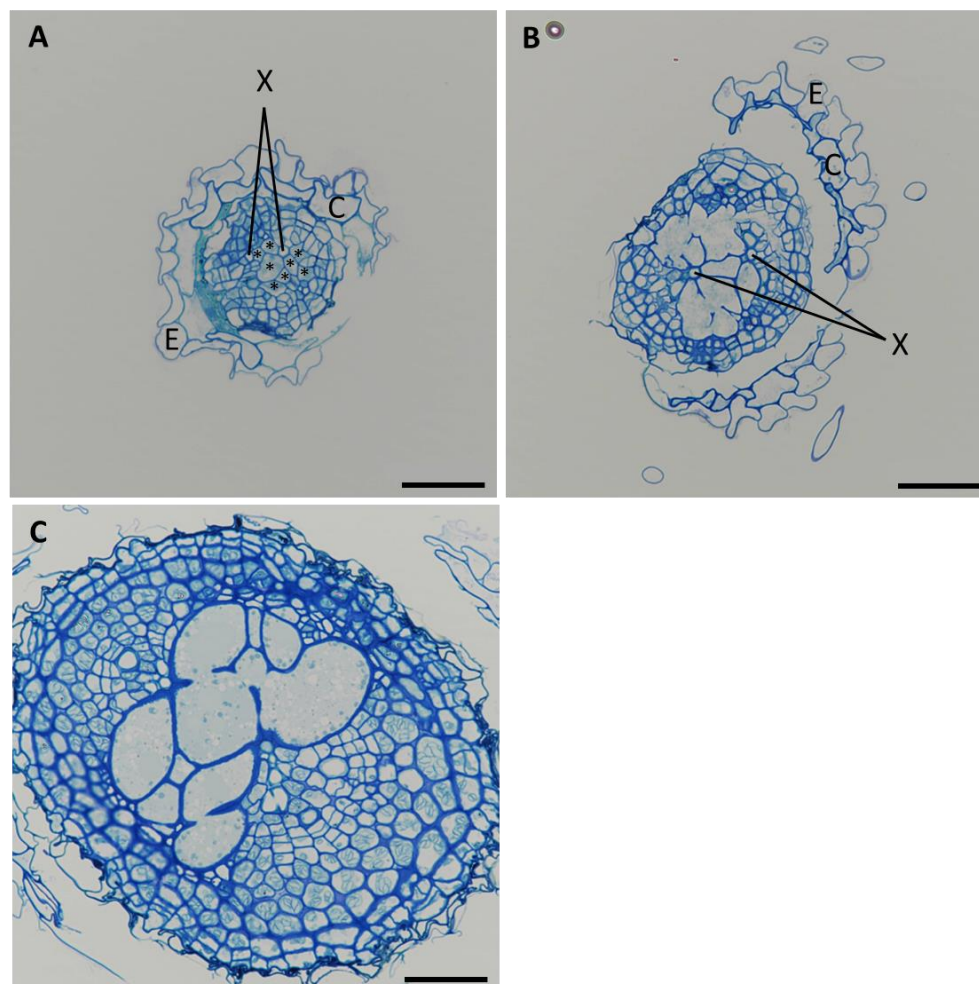


**Figure 24:** Stained semi-thin cross sections of roots of the Hs1::Hs4 transgenic line 210637. (A) An infected root 5 dpi with a syncytium (asterisks). Bar: 100  $\mu$ m. C: cortex, E: epidermis, X: xylem vessels. (B) An infected root at 11 dpi with a large syncytium discernible between the xylem vessels (X). Bar: 100  $\mu$ m. E: epidermis, C: cortex. (C) A root 26 dpi with a huge syncytium in its middle. Bar: 100  $\mu$ m.

The syncytium was located between the xylem vessels and the syncytial cells were enlarged compared to the normal root cells. The central vacuoles were still present in parts of the syncytium (Figure 25B). Nevertheless, single syncytial cells also showed signs of vacuolization with many small vesicles forming. Some multivesicular bodies, enclosing former organelles, were also present (Figure 25F). No cell wall degradations were observable in this first sectioning layer. The cell wall exhibited an anomalous composition. In Figure 25C the putative middle lamella can be seen as a darker grey continuous strand and the cell wall around it appears almost empty. Usually, cell walls have an even, light-grey appearance under the electron microscope (compare Figure 18B-C) and the middle lamella is observable as a thin strand in its middle. Here, however, the cell wall was much lighter and contained fibrous structures (Figure 25C) or even larger callose-like depositions (Figure 25E). Along the plasmalemma, electron-dense granules accumulated. Most strikingly, adjacent cells not incorporated into the syncytium still possessed a normal light-grey appearing cell wall and a

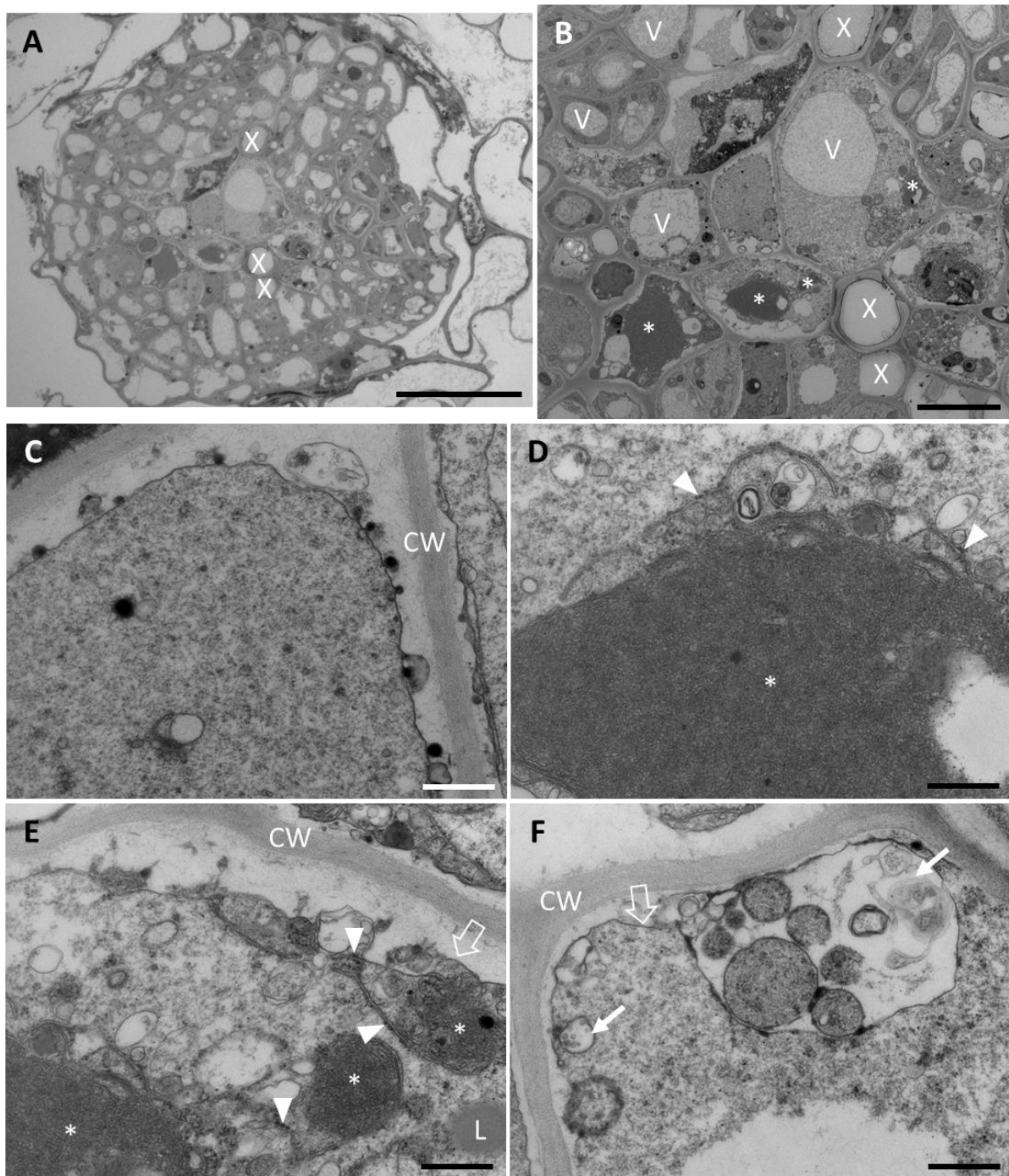


**Figure 25:** Transmission electron microscopic analysis of a syncytium in the transgenic line 210637 at 5 dpi. (A) Overview of the root and the barely distinguishable syncytium located between the xylem vessels (X). Bar: 20  $\mu\text{m}$ . (B) In the sectioning layer, no cell wall degradations are evident. However, the syncytial cells show abnormal cell organization patterns with strong vacuolization in some cells and membrane structure accumulations between the plasma membrane and middle lamella in others. Membrane aggregations (asterisks) are observable in different syncytial cells. The picture was generated by stitching 10 individual photos. Bar: 5  $\mu\text{m}$ . V: vacuoles, X: xylem vessels. (C) Electron-dense vesicles between the plasma membrane and middle lamella. Bar: 500 nm. CW: cell wall. (D) The membrane aggregations (asterisk) consist of ER tubules and carry ribosomes (arrowheads) on their outer tubules. Bar: 500 nm. (E) Membrane aggregations can have different sizes (asterisks) and ribosomes (arrowheads) on the outer tubules. The cell wall looks enlarged (empty arrow), and depositions accumulate in the widened space. Bar: 500 nm. CW: cell wall, L: lipid droplet. (F) Multivesicular bodies (arrows) with different contents are present in the syncytium. Again, the cell wall appears enlarged (empty arrow). Bar: 500 nm. CW: cell wall.

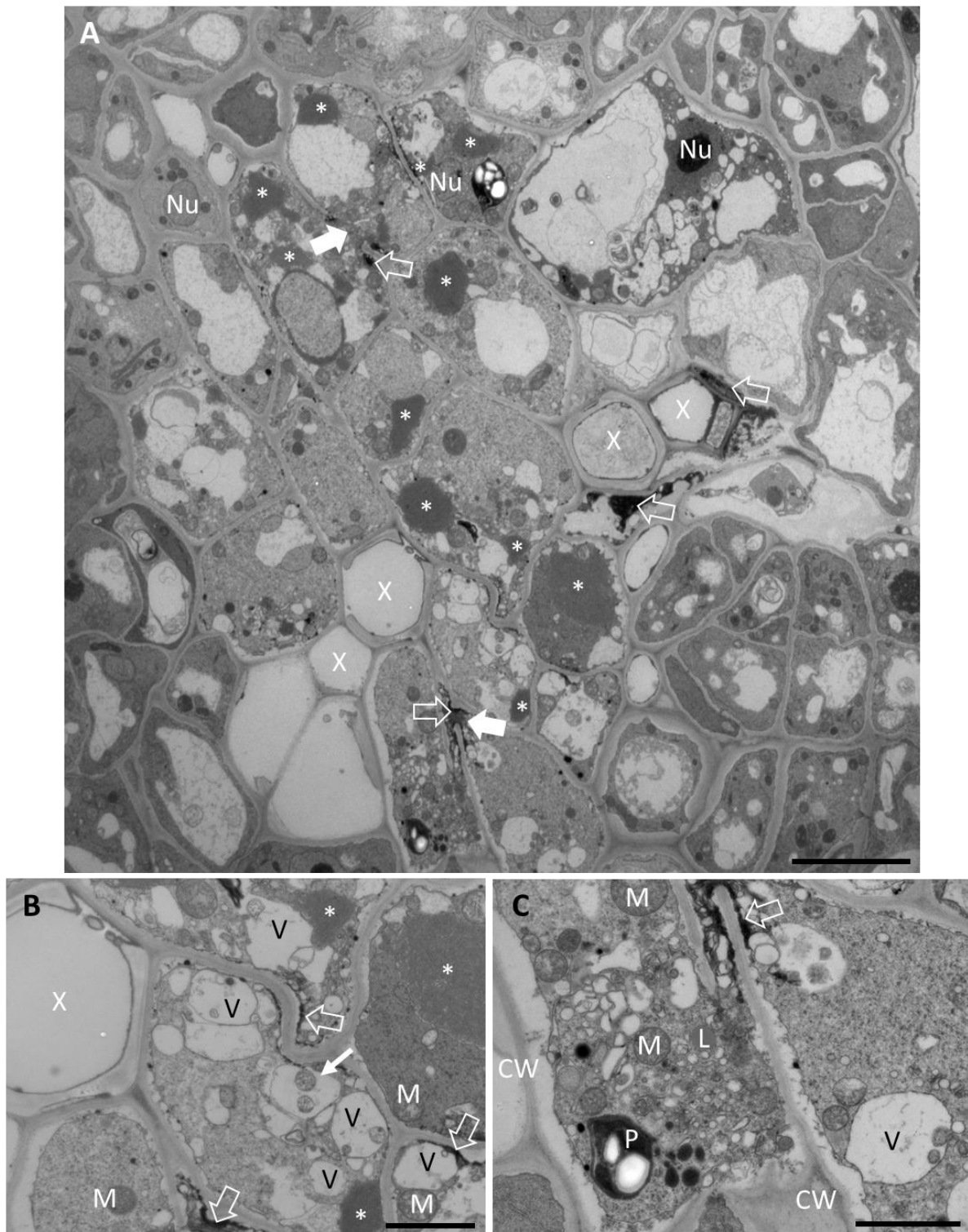


**Figure 26:** Transmission electron microscopic analysis of a second section 60  $\mu\text{m}$  deeper into the syncytium depicted in Figure 25. (A) Several membrane aggregations (asterisks) can be seen. Accumulations of electron-dense material (empty arrows) are observed. A few atypical cell wall degradations (bold arrows) are present. The picture was generated by stitching 6 individual photos. Bar: 5  $\mu\text{m}$ . X: xylem vessels. (B-C) Details of the vacuolization and accumulation of electron-dense material observed in the syncytium. Some vacuoles (V) are filled with former cell organelles (arrow). The electron-dense material accumulates mainly along the cell walls (empty arrows). Bars: 5  $\mu\text{m}$ . CW: cell walls, L: lipid droplet, M: mitochondria, V: vacuoles, X: xylem vessels, asterisks: membrane aggregations.

discernible middle lamella (lower left cell in Figure 26C). The membrane aggregations detected in syncytia of line 228934 were also found in this syncytium. They were constituted of various tubular membrane systems joined together to form the larger structures. Though they were present in different sizes and shapes, they mainly adopted circular shapes. On the outer tubules, ribosomes could be observed (Figure 25D and E).

To clarify if the same abnormal cell wall structures and the accumulation of electron-dense material were present in another layer of the syncytium, I analyzed a second section made 60  $\mu\text{m}$  deeper. Here, some cell wall degradations (bold arrows in Figure 26A) were present. The vacuolization only scarcely observed in the first layer was more evident here. It led to the formation of both organelle-filled vacuoles as well as membrane structures overlapping and joining each other (Figure 26B-C). Electron-dense material accumulated along syncytial cell walls, next to a cell wall opening as well as in adjacent cells (empty arrows in Figure 26A-C). Xylem elements adjacent to the accumulation sites of this material were partly lined with osmiophilic matter and filled with flocculent material. Additionally, even more membrane aggregations could be identified in this layer.

### *Syncytium at 8 dpi*

The syncytium sampled at 8 dpi could be identified precisely in the semi-thin sections by its translucent nature (data not shown). Under the electron microscope, it showed clear signs of necrosis. Its empty-appearing cells could be easily distinguished from the functional, non-incorporated root cells (Figure 27A). The syncytium had developed around the xylem vessels, but unlike the wild type syncytium at a comparable time point, no cell wall ingrowths had developed yet. Numerous cell wall openings could be observed (Figure 27B), indicating that the syncytium was very large and many individual cells were incorporated. Instead of being filled with dense cytoplasm, all syncytial cells showed a strong vacuolization and the formation of membrane structures (Figure 27B-D). The organelles appeared degenerated. The mitochondria looked degraded, based on their unstructured, translucent lumen (Figure 27C-D). Only some plastids remained to look functional (Figure 27C). In the upper part of the syncytium, the accumulation of electron-dense, necrotic material could be observed (Figure 27E). The plasma membrane was found to be detached from the cell wall at several locations (Figure 27F). Contrastingly, root cells not incorporated into the syncytium showed a dense cytoplasm, functional nuclei, and normal organelles. They were separated from the disrupted syncytium by thickened cell walls (Figure 27C). The plasma membrane detachment observed in the syncytium was not found in the normal root cells (Figure 27F).

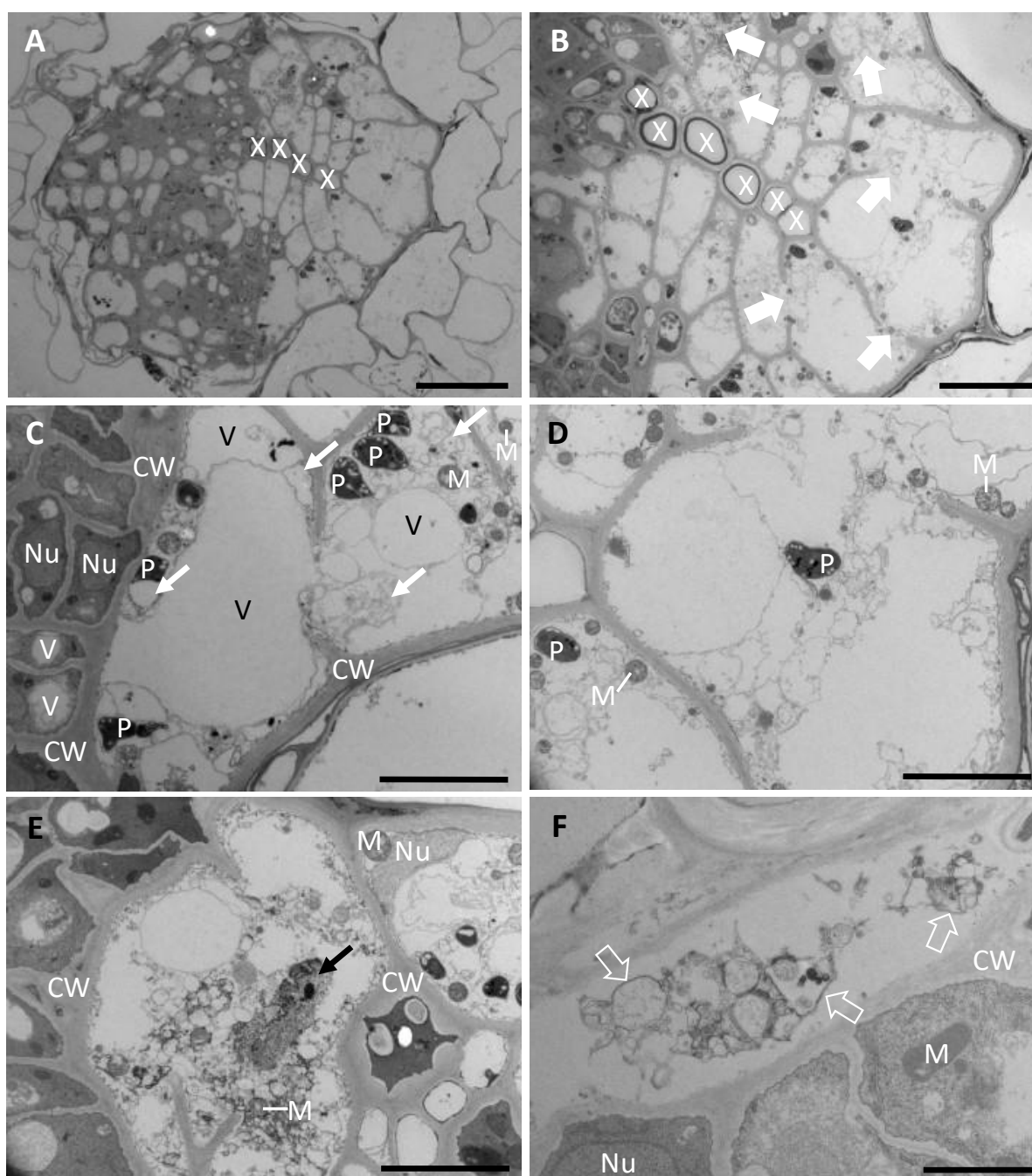


**Figure 27:** Transmission electron microscopic analysis of a degenerated syncytium in line 210637 at 8 dpi. (A) The syncytium can be clearly differentiated from the remaining, functional root cells by its translucent nature. It is situated around the xylem vessels (X). Bar: 20  $\mu\text{m}$ . (B) The syncytium is filled with membranous structures instead of dense cytoplasm. Several cell wall openings (bold arrows) are visible. Bar: 10  $\mu\text{m}$ . X: xylem vessels. (C) The necrotic syncytium contains some functional-appearing plastids (P). The mitochondria (M) look degenerated. Several vacuolar or membranous structures (arrows) can be observed. The cell wall (CW) separating the syncytium from the functional root cells is enlarged. The adjacent root cells show normal vacuoles (V) and nuclei (Nu). Bar: 5  $\mu\text{m}$ . (D) Detailed view of the membranous structures filling the syncytium. Bar: 5  $\mu\text{m}$ . P: plastids, M: mitochondria. (E) The degenerated syncytium also contains a region of electron-dense material entwined with membranes (arrow). Not only the mitochondria (M) but also the nucleus (Nu) have started degrading. Bar: 5  $\mu\text{m}$ . (F) The plasma membrane has detached from the cell wall (empty arrows). This detachment is only observable in the syncytium, never in the non-incorporated root cells. Bar: 2  $\mu\text{m}$ . CW: cell wall, M: mitochondrion, Nu: nucleus.

### *Syncytium at 11 dpi*

I analyzed two syncytia from 11 dpi. They were discernible in the semi-thin sections by their translucent appearance and the cell wall degradations (exemplary syncytium in Figure 24B). Like the other syncytia analyzed, they were induced between the xylem vessels (Figure 28, Figure 29C). Under the electron microscope, the two syncytia showed structures depicting an intermediate stage between the 5 and the 8 dpi syncytium already investigated. The first syncytium was distinguishable from the surrounding root cells by its translucent cytoplasm and the apparent cell wall degradations (Figure 28A). The organelles appeared functional, only the mitochondria exhibited atypical shapes and lumen structures. Membrane aggregations were observable in several syncytial cells.

In order to verify these observations, I analyzed a second section of the syncytium, appr. 30  $\mu\text{m}$  deeper (Figure 28B). The cell wall openings were coherent between the two layers (the second section is turned by 180 degrees relative to the first section). The membrane aggregations were also evident here, though they did not seem to be continuous between the sections. Instead, the second section contained fewer but partly larger-appearing membrane aggregations. Again, the membrane aggregations consisted of ER tubules with ribosomes on the outer tubules (Figure 29A-B). Often, lipid droplets were encountered in close vicinity to the aggregations.

The second syncytium analyzed was more advanced in the degeneration process compared to the first one (Figure 29C). The syncytium was strongly necrotized and filled with numerous membranes instead of dense cytoplasm. The mitochondria looked degenerated (Figure 29D-E). The membrane aggregations were also present in this syncytium. Interestingly, they colocalized with osmiophilic granules (Figure 29D-E). These electron-dense granules had a diffuse border, unlike the well-defined plastoglobules found in plastids (arrowheads in Figure 29D). The granules were also observed along the border of the plasma membrane (Figure 29F). Unlike the syncytium in Figure 25, the cell wall looked normal here, with the middle lamella silhouetted against the grey even structure of the cell wall. As an enlargement of the cell wall can therefore be excluded, the plasma membrane is assumed to have detached from the wall at this stage of necrosis.

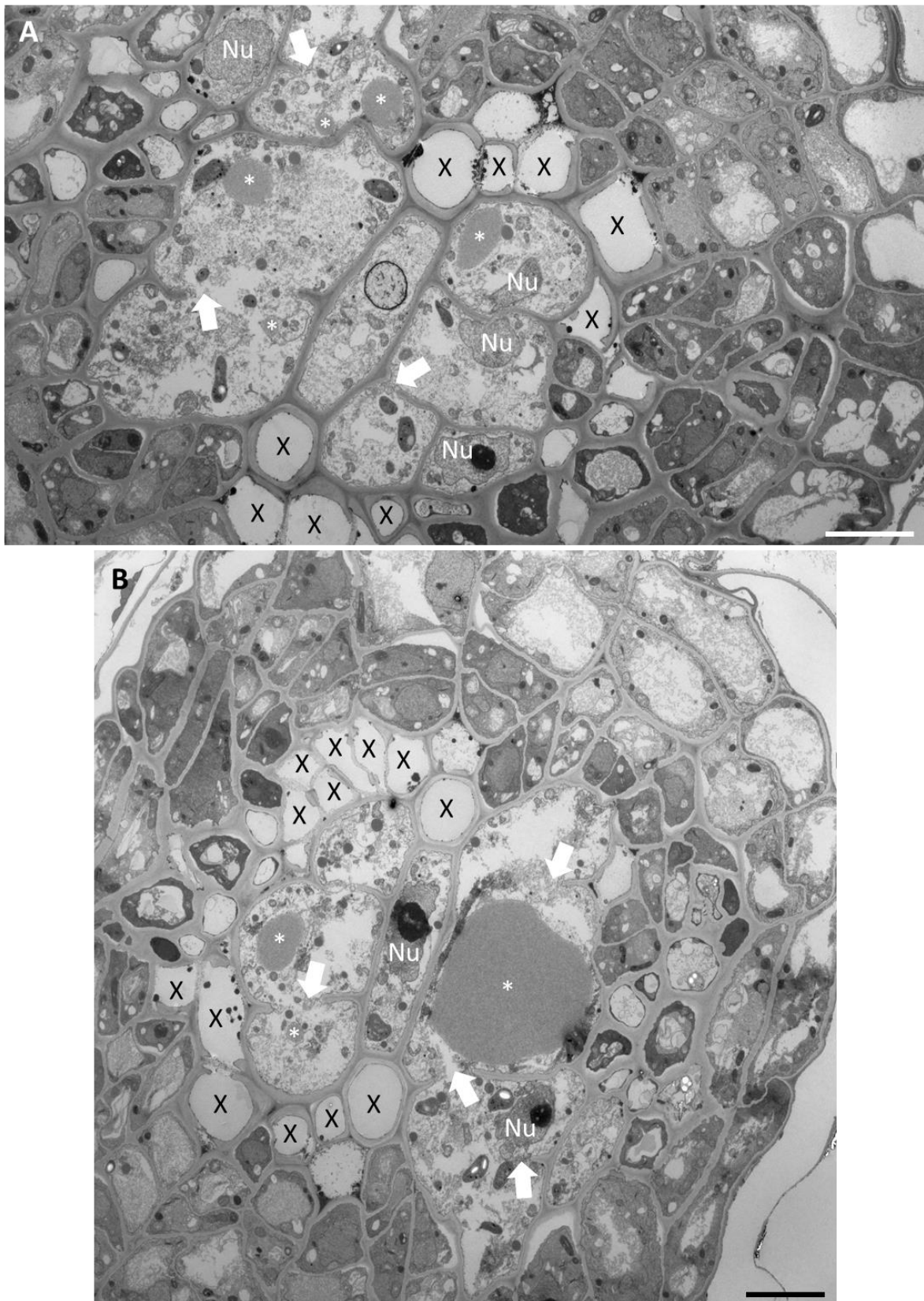


**Figure 28:** Transmission electron microscopic analysis of two sectioning layers of a syncytium from the transgenic line 210637 at 11 dpi. (A) The syncytium lies between the xylem elements (X) and has a translucent cytoplasm. Cell wall openings (bold arrows) and several nuclei (Nu) are evident. Membrane aggregations (asterisks) can be encountered in various cells of the syncytium. The picture was generated by stitching 23 individual photos. Bar: 5  $\mu$ m. (B) A second section appr. 30  $\mu$ m further into the syncytium. The positions of the cell wall openings (bold arrows) follow the previous section's (turned by 180 degrees). A large and some small membrane aggregations (asterisks) are present. The figure was generated by stitching 27 individual photos. Bar: 5  $\mu$ m. Nu: nuclei, X: xylem vessels.

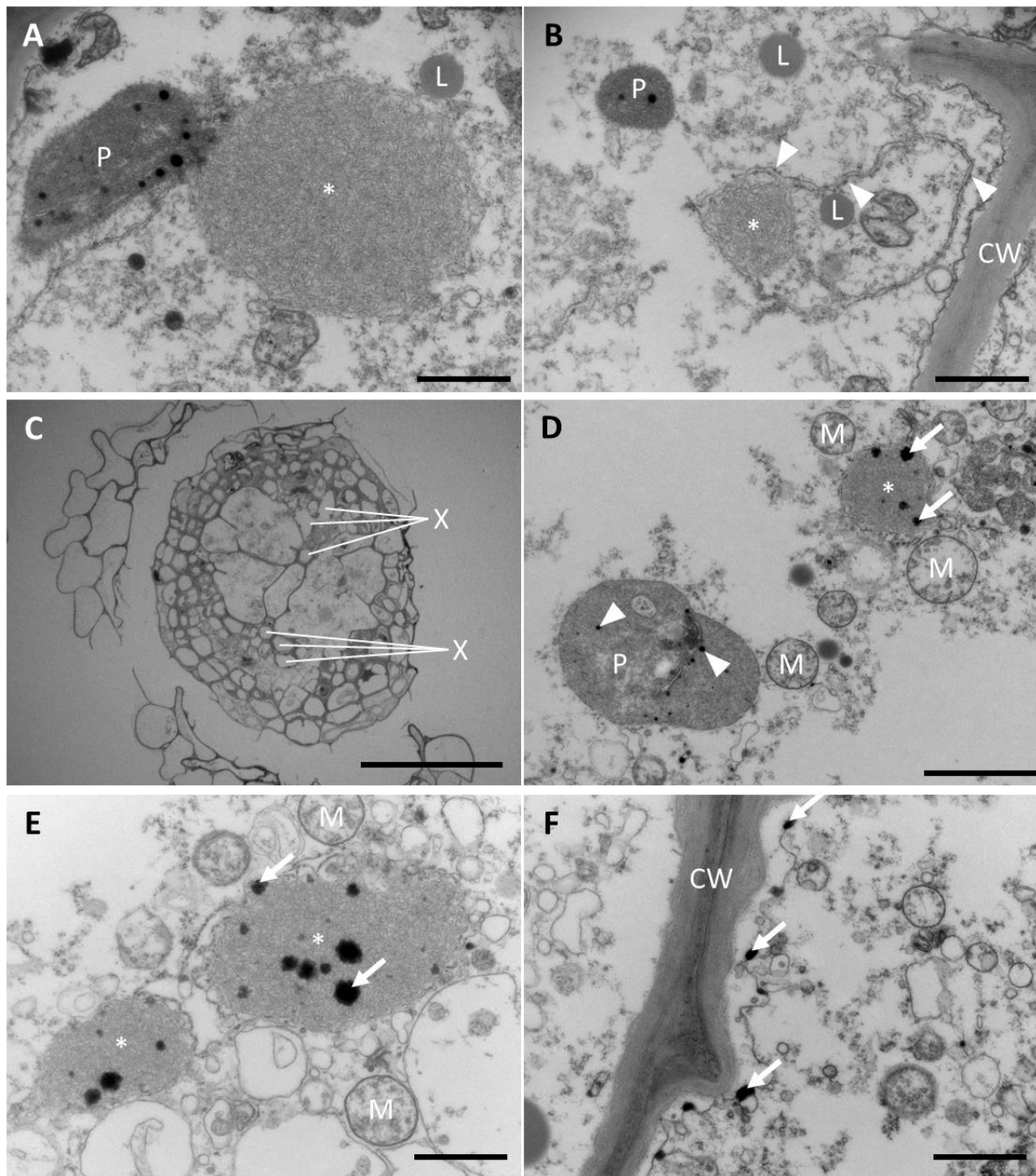


**Figure 29:** Transmission electron microscopic analysis of different syncytia at 11 dpi. (A-B) Details of the differently-sized membrane aggregations (asterisks) found in the syncytium shown in Figure 28. Ribosomes (arrowheads) are present on the outer tubules. Bars: 1  $\mu$ m. CW: cell wall, L: lipid droplets, P: plastids. (C) The second syncytium from 11 dpi analyzed is in an advanced degenerative stage. The huge syncytium located between the xylem elements (X) has a translucent cytoplasm. Bar: 50  $\mu$ m. (D-F) The syncytium contains no functional organelles. Instead, the syncytial cells are filled with vacuoles and membranes and the mitochondria (M) seem degenerated. Membrane aggregations (asterisks) can be found. Electron-dense, osmiophilic granules (arrows) co-localize with these aggregations and the detached plasma membrane. Bars: 1  $\mu$ m. CW: cell wall, P: plastid, arrowheads: plastoglobules.

### *Syncytium at 26 dpi*

I analyzed two syncytia from the later developmental stage (26 dpi). Both syncytia were sampled based on the visibly swollen root (where the syncytium is located) and the attachment of a well-developed female adhering to the feeding site. One syncytium investigated appeared completely electron-dense and no cell structures were discernible even

though different layers were examined (data not shown). I supposed that the whole syncytium was highly necrotic. Still, as I could not exclude the formation of artifacts due to bad infiltration at that time point, the syncytium was not further analyzed.

The other syncytium examined had increased significantly in size, compared to earlier stage syncytia, and was well visible in the semi-thin sections, with obvious cell wall degradations and a translucent cytoplasm (Figure 24C). The cell wall openings could also be observed under the electron microscope (Figure 30A). At one position, a cell wall remnant, being disconnected from all cell walls surrounding it, could be detected freely in the cytoplasm (Figure 30C). Even though the syncytium was located between xylem vessels, the cell wall ingrowths observed (Figure 30A) were less pronounced than in Col-0 syncytia at 26 dpi. The syncytial cytoplasm was still filled and appeared functional. It was not in an advanced necrotic stage as the syncytia from earlier time points. Numerous small vacuoles were present in the syncytium (Figure 30B). Several plastids and nuclei could also be found. The mitochondria, however, showed signs of degeneration. They were very small and did not contain normal cristae structures (Figure 30F). The plastids still appeared functional and only rarely contained starch granules. Interestingly, the plastids of root cells not incorporated into the syncytium included many starch grains (Figure 30A). ER vesicles or cisternae were almost completely absent in this syncytium, in contrast to the Col-0 syncytia from similar developmental stages. The membrane aggregations were present abundantly in several syncytial cells (Figure 30A). They occurred in different sizes but were always more or less spherical (Figure 30D). Again, they consisted of ER tubules (Figure 30E). Lipid droplets could often be found in close vicinity to the aggregations (Figure 30C).

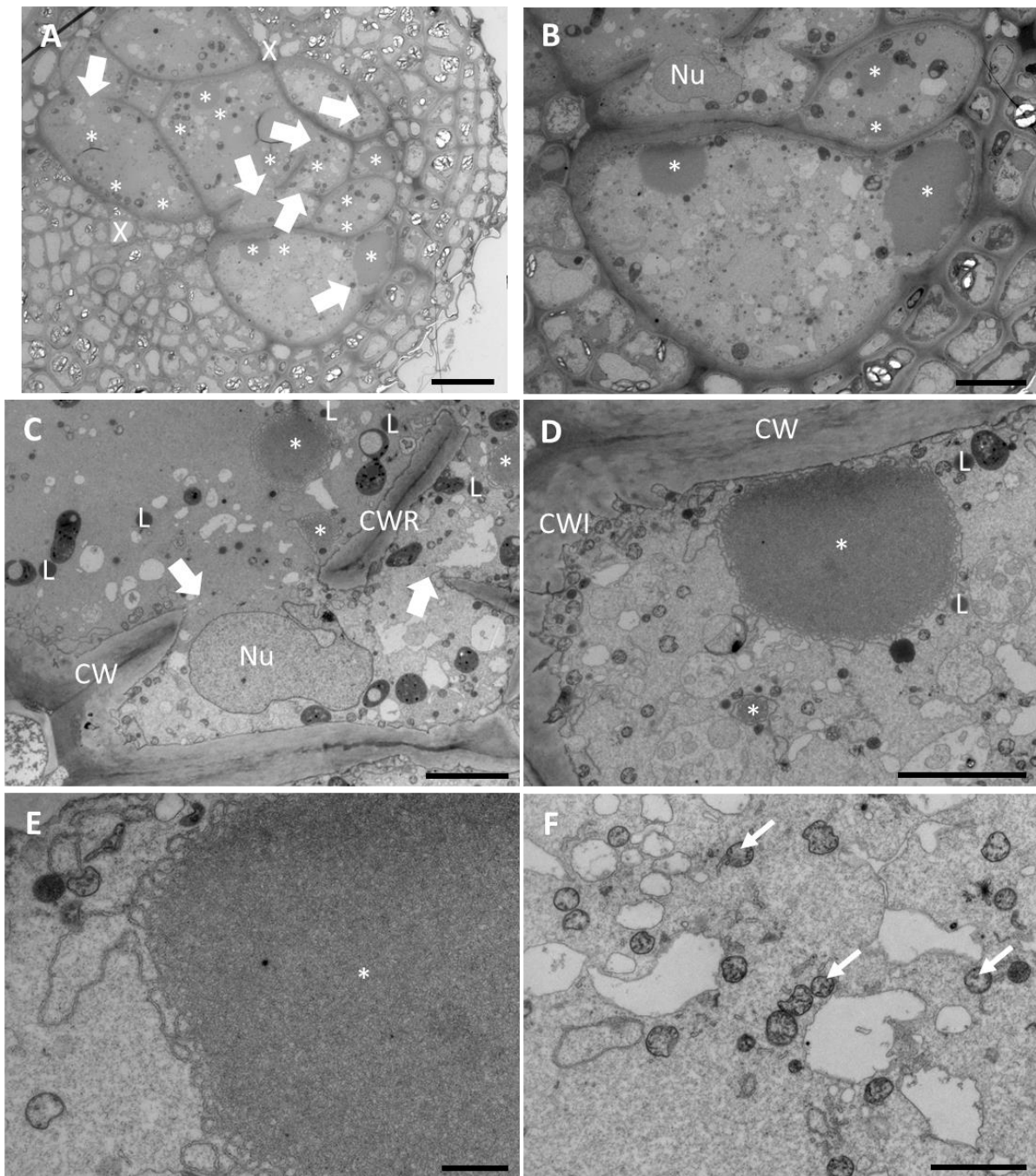


**Figure 30:** Transmission electron microscopic analysis of a syncytium from line 210637 at 26 dpi. (A) The syncytial cells are enlarged, have several cell wall openings (bold arrows), and contain numerous membrane aggregations (asterisks). The figure was generated by stitching 12 individual photos. Bar: 20  $\mu\text{m}$ . X: xylem vessels. (B) Apart from the membrane aggregations (asterisks), the syncytium contains many vacuoles and very small mitochondria. Bar: 10  $\mu\text{m}$ . Nu: nucleus. (C) Detailed view of cell wall degradations (bold arrows), leading to a cell wall remnant (CWR) not attached to the cell walls (CW). Bar: 5  $\mu\text{m}$ . L: lipid droplets, Nu: nucleus, asterisks: membrane aggregations. (D) Some poorly developed cell wall ingrowths (CWI) can be observed. Bar: 5  $\mu\text{m}$ . CW: cell wall, L: lipid droplets, asterisks: membrane aggregations. (E) The tubular structure of the membrane aggregation (asterisks) is evident. Bar: 1  $\mu\text{m}$ . (F) The mitochondria in the syncytium appear degenerated (arrows). Bar: 2  $\mu\text{m}$ .

### 4.3 Concluding summary

In conclusion, syncytia in non-transgenic as well as *Hs4*-transgenic plants were always induced between the xylem vessels and characterized by cell wall degradations.

In Col-0, the syncytia contained dense cytoplasm, small vacuoles, functional organelles, and numerous smooth ER vesicles. Further, the analysis of syncytia from 26 dpi revealed pronounced cell wall ingrowths along xylem elements. Degradation processes were only observable in the late-stage syncytia. At this point, some organelles like mitochondria started to appear degenerated while the cytoplasm was still intact.

In syncytia induced in the transgenic roots, the cytoplasm appeared dense but granular. Necrosis and callose accumulations could be observed as early as 5 dpi and the first degenerated syncytia were found three days later. Those syncytia contained translucent cytoplasm filled with numerous vacuoles and membrane structures. The first degenerated organelles were detected at 8 dpi. In several syncytia analyzed, the vacuoles were larger compared to Col-0. Most importantly, smooth ER vesicles were absent in syncytia in *Hs4*-transgenic roots. Instead, membrane aggregations consisting of ER tubules and harboring ribosomes on the outer surface were detected. The cell wall ingrowths found in Col-0 syncytia were also observable in late-stage syncytia in *Hs4*-transgenic roots though they were less pronounced.

## 5 Generation of *Hs4*-expressing rapeseed

### 5.1 Materials and Methods

#### 5.1.1 Plant material and growth conditions

Rapeseed plants of the spring-type cultivar Westar were used for the transformation (Supplementary Table 1). For seed production, transformed plants were grown in a climate chamber under long-day conditions (16 h light/8 h dark, 20°C) until seeds could be harvested.

#### 5.1.2 Vector construction

The pBin35SRed-*Hs4* plasmid constructed and transformed into *A. tumefaciens* GV3101 (Hellens et al. 2000) as described under 3.1.2 was used for rapeseed co-transformation. It contains the *Hs4* open reading under the control of a 35S promoter.

For co-transformation, agrobacteria (GV3101) containing the plasmid B425p9o-LH-35s-o-*SDR* (*SHOOT DEVELOPMENTAL REGULATOR*), kindly provided by Kea Ille (Plant Developmental Biology and Physiology Department, Kiel University, Germany), were used. This plasmid induces the regeneration of plants from the transformed hypocotyls.

#### 5.1.3 Rapeseed hypocotyl co-transformation

The co-transformation protocol recently developed by K. Ille was used for hypocotyl transformation (personal communication K. Ille). In brief, Westar seeds were sterilized by rinsing them in 70 % EtOH for 5 min, followed by incubation in 6 % NaClO for 20 min. Then, the seeds were washed thoroughly with ddH<sub>2</sub>O and sown on a germination medium. 11-day-old hypocotyls, cut into 1 cm explants, were used for transformation. *A. tumefaciens* ON cultures containing pBin35SRed-*Hs4* and B425p9o-LH-35s-o-*SDR*, respectively, were mixed 1:1 and adjusted to an OD<sub>600</sub> of 0.1. The hypocotyl explants were incubated in the bacterial suspension for 5-10 min, briefly dried, and moved to a co-cultivation medium. After two days, the hypocotyl pieces were washed in a buffer with 0.1 % Timentin (400 mg/ml) and transferred to a regeneration medium. Two weeks later they were moved to a regeneration medium with reduced 6-benzylaminopurine (BAP) content. Emerging shoots were transferred to a root-inducing medium. Regenerated *Hs4*-positive plants were transferred to soil and grown in a climate chamber as described (see 5.1.1).

#### 5.1.4 Genotyping of regenerating plants

The plants developing roots in the tissue culture were screened for the presence of *Hs4*, *DsRed2*, and *SDR*. DNA was isolated from leaves frozen in liquid nitrogen as described (Dellaporta et al. 1983). The DNA quality was checked on a 1 % agarose gel (90V, 30 min) before further usage.

The functionality of the isolated DNA was assessed via PCR with the primer combination Bnapus\_GAPDH\_F/Bnapus\_GAPDH\_R (Supplementary Table 2). Subsequently, the presence of *Hs4*, *DsRed2*, and *SDR* was tested with the primers AK\_F7/AK\_R5, AS\_dsRed\_F/AS\_dsRed\_R, and SDR\_F/SDR\_R (Supplementary Table 2), respectively. PCR amplicons were analyzed on a 1 % agarose gel (100V, 11 min).

### 5.1.5 Expression analysis

After transfer to soil, leaves were sampled and frozen in liquid nitrogen. RNA was isolated using the Universal RNA Kit (Roboklon, Berlin, Germany), according to the manufacturer's instructions. The RNA quality was assessed using a NanoDrop2000 spectrophotometer (ThermoFisher Scientific™) and agarose gel electrophoresis (2 % gel, 100V, 12 min).

300 ng RNA was incubated with 1 U DNase (ThermoFisher Scientific™) at 37°C for 30 min. Then, the DNase was inactivated by adding 1 µl EDTA (50 mM) followed by a 10 min incubation at 65°C. The cDNA was synthesized using the First Strand cDNA Synthesis Kit (ThermoFisher Scientific™) following the manufacturer's instructions.

The cDNA quality was assessed by PCR using the *GAPDH* primer combination (Bnapus\_GAPDH\_F/Bnapus\_GAPDH\_R, Supplementary Table 2). For detection of the different transgenes, the primer combinations AK\_F7/AK\_R5 (*Hs4*), AS\_dsRed\_F/AS\_dsRed\_R (*DsRed2*), and SDR\_F/SDR\_R (*SDR*) were utilized (Supplementary Table 2).

## 5.2 Results

Rapeseed is a good host to BCN and the emergence of volunteer rapeseed in rotation systems with sugar beet leads to an increase in nematode population densities, thereby increasing the nematode infestation pressure for sugar beets (see 1.7.1). Therefore, resistant rapeseed is of interest to control the nematodes in the soil. If they cannot find a suitable host, their populations will decline and sugar beets cultivated in the same fields will suffer less yield losses. As *Hs4* is active in Arabidopsis, another plant of the Brassicaceae family, I hypothesized that *Hs4* would also confer resistance in rapeseed.

### 5.2.1 Regeneration of *Hs4*-positive plants

Following the protocol by K. Ille (pers. communication), approximately 800 hypocotyls (Table 9) of the spring-type rapeseed Westar were co-transformed with pBin35SRed-*Hs4* and B425p9o-LH-35s-o-*SDR*. While B425p9o-LH-35s-o contains a kanamycin resistance gene, the pBin35SRed vector only has the *DsRed2* gene for plant selection. Therefore, 435 of the hypocotyls were cultivated on medium with and 355 on medium without kanamycin. I expected emerging shoots on the kanamycin-containing medium to contain *SDR*, which I selected for, and by chance also *Hs4*. Shoots emerging on the medium without kanamycin could be completely transgene-free due to the lack of selection pressure. Within two weeks, the hypocotyls on the two different media showed clear differences. The hypocotyls placed on kanamycin-containing medium bleached out, only seldomly green remnants were visible (Figure 31A). The hypocotyls on the medium without antibiotics remained green (Figure 31B). Some of them started to produce roots at an early stage. Later on, they exhibited stronger callus growth (Figure 31D) and an increased shoot emergence rate compared to the hypocotyls cultivated on the selective medium (Figure 31C).

**Table 9:** Rapeseed transformation data.

# hypocotyl explants	# rooted shoots	<i>SDR</i> positive shoots	<i>SDR/Hs4</i> positive shoots	# plants trans-planted to soil	# plants showing expression in leaves (seed code)	# T <sub>2</sub> seeds harvested (seed code)
800	66	2	2	2	1 (230004)	740 (241086)



**Figure 31:** Transformed hypocotyls of *B. napus* cv. Westar on regeneration medium with (A) and without (B) kanamycin 15 days after the transformation. Bars: 1 cm. At 57 days after the transformation, the hypocotyls cultivated on medium with (C) or without (D) kanamycin showed callus production and regenerating shoots. Bars: 0.5 cm.

On the selective medium, only one shoot emerged and could be transferred to the rooting medium. On the antibiotic-free medium, over 65 shoots emerged and could be transferred to the rooting medium (Table 9). Because of the lack of selection during the shoot growth, all shoots surviving and making roots on the rooting medium were screened for the presence of the transgenes before being transferred to soil. As the vector containing *Hs4* contained *DsRed2* as a selection marker, I first attempted to select the regenerating shoots based on an emitted red fluorescence, but neither hypocotyls nor early-stage shoots showed any red fluorescence signals. Once they had been transferred to the rooting medium, the boxes in which the plants were kept were too large for observations under the microscope. Hence, DNA from leaf pieces of all 66 regenerating plants was isolated and tested for the presence of the three different transgenes. Four plants contained *SDR*, two of which were also positive for *Hs4*. Interestingly, only one of the *Hs4*-positive plants (out of all 66 plants) showed a band for *DsRed2*.

Accordingly, the *Hs4*-positive plants #35 (genotype *Hs4*+, *SDR*+, *DsRed2*-) and #66 (genotype *Hs4*+, *SDR*+, *DsRed2*+) were transferred to soil for seed production.

## 5.2.2 *Hs4* expression verification

After the plants had been transferred to soil, DNA was isolated from five different leaves per plant to decipher if the plants were completely transgenic or chimeric. Plant #35 was *Hs4*-positive in three of the five leaves. None of those showed bands for *DsRed2* but all were *SDR*-positive (L1-L5 in Figure 32A-B). Plant #66 contained *Hs4* in all five leaves tested. The leaves were also all positive for *DsRed2* and *SDR* (L6-L10 in Figure 32A-B).

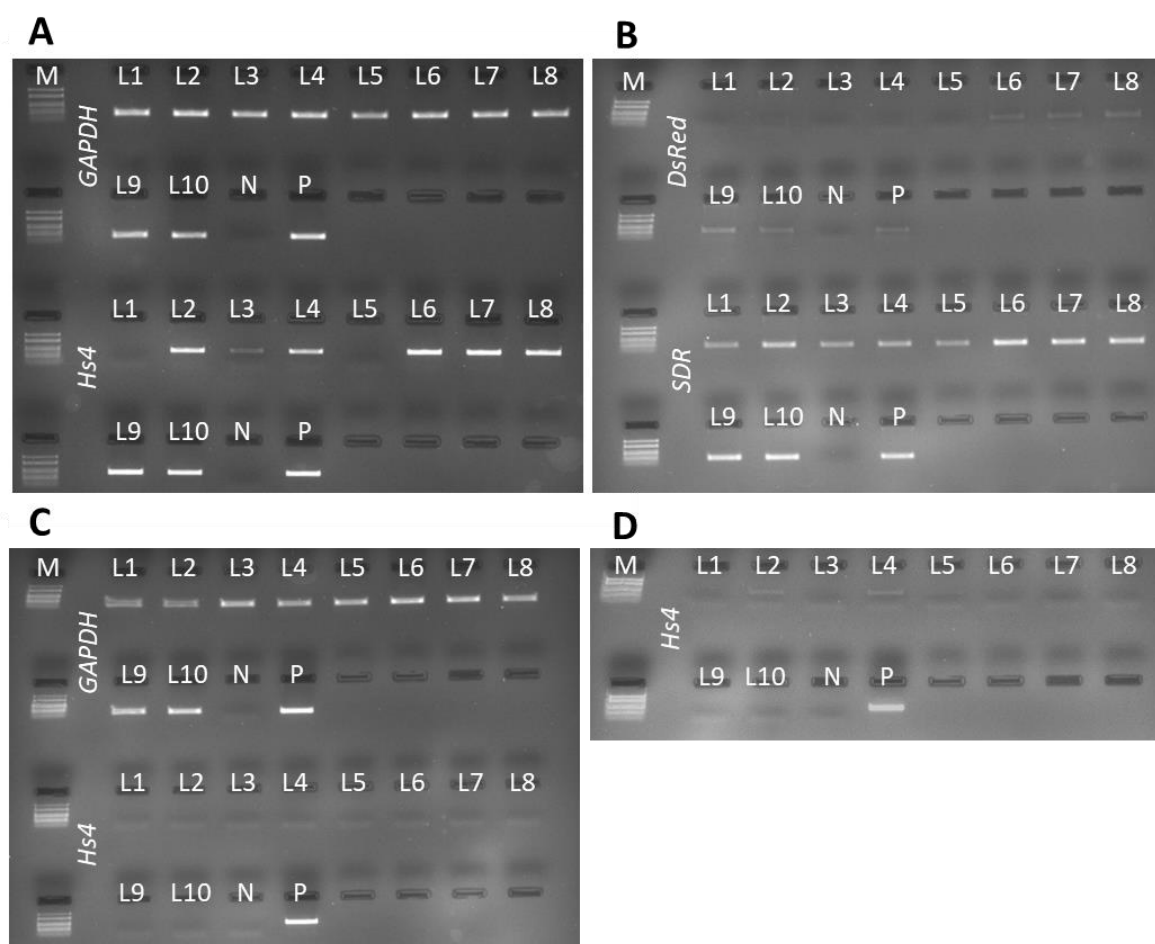


**Figure 32:** Agarose gel electrophoresis of PCR products of transgenic rapeseed plants. (A-B) DNA was isolated from five different leaves of plants #35 (L1-L5) and #66 (L6-L10) and amplified with *GAPDH*, *Hs4*, *DsRed2*, and *SDR* primers. 1 % gel, 100V, 11 min. (C-D) The cDNA of the leaves of plants #35 (L1-L5) and #66 (L6-L10) was amplified with *GAPDH* and *Hs4* primers. An initial screen was done using diluted cDNA (C), afterwards, undiluted cDNA was used (D). 2 % gels, 80V, 11 min. M: marker (low-range FastRuler; 50-200-400-850-1500bp), N: negative control, P: positive control.

After verifying that plant #35 was chimeric for *Hs4* and plant #66 was completely *Hs4*-positive, I tested if the transgene was also expressed in those leaves. Using a 1:10 diluted cDNA as a template, the expression of the housekeeping gene *GAPDH* and the transgene *Hs4* was tested. While strong bands were observed in all leaves for *GAPDH*, no *Hs4* expression could be detected (Figure 32C) in any of the leaves tested. As the cDNA was only generated with 300 ng of RNA, the PCR was repeated using the undiluted cDNA as a template. Here, faint bands for two leaves of plant #35 were observable. None of the leaves from plant #66 showed *Hs4* expression (Figure 32D). The leaves were also tested for expression of *DsRed2* and *SDR*. Surprisingly, plant #35 showed bands for *DsRed2* in two leaves, even though it did not exhibit bands in the gDNA PCR. Plant #35 did, however, show expression of *SDR* in all five leaves tested. Plant #66 showed faint bands in two of the five leaves for both *DsRed2* and *SDR* (data not shown).

### 5.2.3 Production of T<sub>2</sub> seeds

Plant #66 showed no expression of the resistance gene *Hs4* and was therefore discarded. In contrast, plant #35 showed partial *Hs4* expression and was propagated to obtain T<sub>2</sub> seeds. It had already formed floral buds in the tissue culture before it was moved to soil. The flowers opened 11 days after transplanting (Figure 33A). The plant showed no anomalous phenotype

and flowered normally. Only the lower-most leaves did not have a typical Brassica shape but were more rounded instead (Figure 33B). Within three months, the siliques ripened (Figure 33C) and could be harvested. In total, plant #35 yielded 740 T<sub>2</sub> seeds.

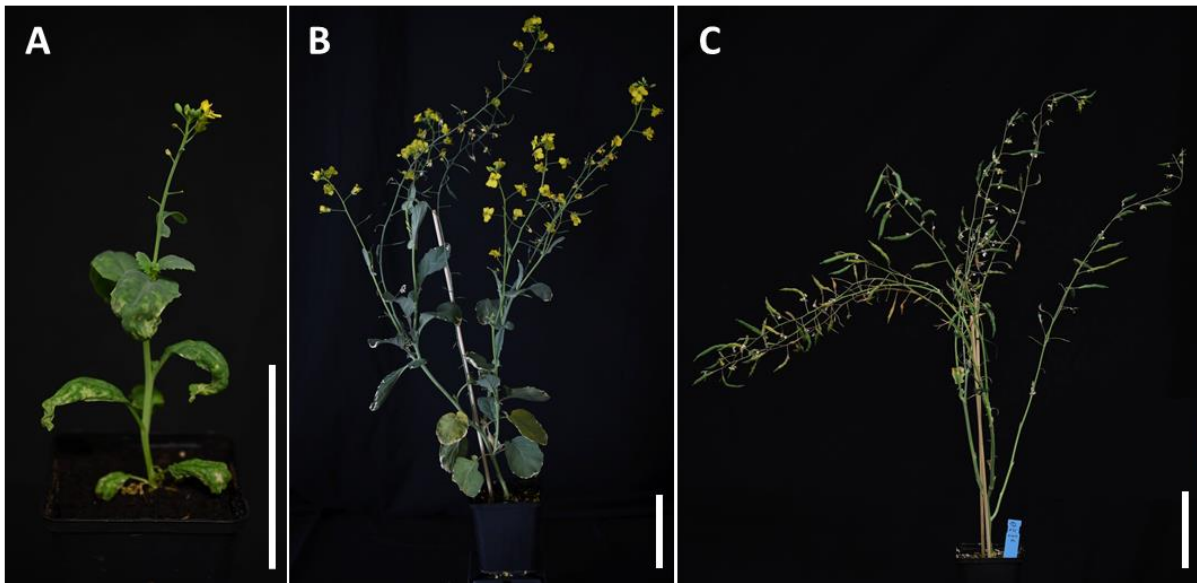


**Figure 33:** Different developmental stages of plant #35 after transfer to soil. (A) Upon transfer from tissue culture to soil the plant had already developed floral buds which opened 11 days after the transfer to soil. (B) At 37 days after transplanting, all shoots were flowering. (C) About a month later, at 64 days after the transfer, the last siliques were forming. The photos were taken by K. Ille (CAU Kiel, Germany). Bars: 10 cm.

The analysis of the T<sub>2</sub> plants is currently being conducted as part of a master's thesis.

## 6 Discussion

The beet cyst nematode (BCN) *Heterodera schachtii* belongs to the sedentary endoparasitic plant parasites. It establishes a feeding site, called syncytium, in the host roots by incorporating up to two hundred cells via cell wall degradations. The syncytium poses a new plant tissue that ensures the successful survival of the nematodes to finish their life cycle. Complete resistance to BCNs is not found in the genus *Beta*. However, the three species of the genus *Patellifolia* show BCN resistance and have been used extensively for hybridization with sugar beet (*Beta vulgaris*) to transfer the resistance. The resulting translocation lines were assessed to identify the resistance genes *HsI<sup>pro-1</sup>* and *Hs4* from *P. procumbens*. *Hs4* has been shown to confer resistance in the sugar beet background but its mode of action and the possibility of conferring resistance in a non-related species were unknown.

In this study, I started by verifying the genomic *Hs4* sequence. I then analyzed variations among homologs of *Hs4* occurring in *Patellifolia* species and of the *B. vulgaris* homolog *BvHs4*, which exhibits 60 % protein similarity to *Hs4*, in different *Beta* species. I demonstrated that all species assessed contain homologs of *Hs4* and *BvHs4*, respectively. Further, the genes showed contrasting expression patterns in *Patellifolia* and *Beta* species and were not upregulated upon nematode infestations (Chapter 2). I characterized transgenic Arabidopsis lines expressing *Hs4* from different promoters and found that they exhibited BCN resistance. The intensity of the resistance reaction was correlated to the respective transgene expression level (Chapter 3). Using the generated transgenic lines, I investigated the ultrastructure of syncytia and compared it to syncytia induced in the wild type. I detected membrane aggregations appearing specifically in *Hs4*-transgenic plants under nematode infection conditions. These results help to further elucidate the role of *Hs4* in the resistance reaction (Chapter 4). Finally, I generated transgenic rapeseed plants expressing *Hs4*. Transferring the nematode resistance to rapeseed can facilitate crop rotation systems with sugar beet (Chapter 5).

### 6.1 Reassessing the structure of *Hs4*

The genomic sequence of *Hs4* has been described to span 5664 bp (Kumar et al. 2021). After sequencing an unresolved region of 964 bp in the first intron, I found that *Hs4* comprises 4999 bp. Kumar et al. (2021) claimed the gene to consist of five exons and introns each, disregarding the untranslated regions (UTRs) they had annotated (see Figure 3). Exons do not necessarily have to be protein-coding, instead, UTRs are also considered exonic regions, though non-coding (Aspden et al. 2023). Hence, *Hs4* consists of six exons and five introns.

Further, *Hs4* is described as a rhomboid protein with five transmembrane domains (Kumar 2020). According to Urban and Dickey (2011), the smallest catalytically active unit of rhomboid proteases consists of six transmembrane domains (TMD). These basic TMD are mainly found in bacteria and partly in eukaryotes, though eukaryotes often have a seventh TMD (Urban and Dickey 2011). However, many eukaryotic rhomboids belong to the secretase subfamily which can be divided into two clades: secretase-A rhomboids exhibit seven TMDs, and secretase-B rhomboids contain only the core region of six TMDs. Further, these two clades are differentiated by distinct sequences around the catalytic serine S106. In the secretase-A clade, proteins contain a highly conserved GxSxGVYA, while B-class secretases show a less stringent GxSxxxF sequence (Lemberg and Freeman 2007). When I analyzed *Hs4* using DeepTMHMM, I found the protein to consist of six TMDs which is conclusive with its classification as a rhomboid protease. Further, *Hs4* (and all related proteins analyzed in the current study) harbors the GxSxxxF sequence, indicating its affiliation with the secretase-B clade.

## 6.2 Homologs from *P. procumbens* and *P. webbiana* show the highest sequence similarity to *Hs4*

While sugar beets are highly susceptible to *H. schachtii*, all *Patellifolia* species are described as resistant (Viglierchio 1960; Biancardi et al. 2020). One of the underlying nematode resistance genes, *Hs4*, was first isolated from the sugar beet translocation line TR520, harboring a translocation from *P. procumbens* chromosome 9 (Kumar et al. 2021). Hence, I hypothesized that all *Patellifolia* species contained *Hs4* homologs and that *Hs4* from *P. procumbens* showed the highest sequence similarity to the *Hs4* reference sequence generated by Kumar et al. (2021).

As hypothesized, I detected highly similar homologs in all *Patellifolia*-derived material analyzed. Confirming my expectations, variations in the genomic sequence could be observed between the species. However, I also found variations between the accessions within a species. Sequences perfectly matching *Hs4* were detected in the translocation lines and the hybrid variety Nemata, reassuring the origin of the *Hs4* sequence. None of the *Patellifolia* accessions sequenced harbored a homolog with 100 % sequence identity to *Hs4*. However, *PpHs4<sub>IPK419</sub>*, *PpHs4<sub>IPK951</sub>*, and all *PwHs4* homologs exhibited the highest similarity to *Hs4* (99 %). Surprisingly, the majority of deviations detected occurred in the same set of accessions and several single nucleotide polymorphisms (SNPs) and insertions/deletions (InDels) were shared by three *P. procumbens* and *P. patellaris* accessions. However, a 3 bp integration in exon 5, resulting in the addition of a valine to the *Hs4* protein, could be detected in all three species, though the *P. procumbens* and *P. webbiana* accessions differed among each other and the only consistency was found in *P. patellaris*, where all accessions analyzed contained the additional three bases. Nonetheless, I found that the additional amino acid changes neither the localization of *Hs4* to the ER nor its TMD structure.

The relationship among the different *Patellifolia* accessions has long since been discussed. While the diploid *P. procumbens* and *P. webbiana* were previously considered two extreme ecotypes of a single species (Curtis 1968; Wagner et al. 1989), recent phylogenetic analyses based on plastome data have pointed to the clear separation into two distinct albeit closely related species. The tetraploid *P. patellaris* is more distantly related to these two diploid *Patellifolia* species (Sielemann et al. 2022). In my analysis, two *PpHs4* and all *PwHs4* homologs showed high sequence similarity to *Hs4*. Nevertheless, three *PpHs4* homologs showed several deviations from *Hs4*, together with the *PpatHs4* homologs. Considering the relationship between the *Patellifolia* species, similarities between *P. procumbens* and *P. patellaris* appear peculiar. However, though *P. procumbens* and *P. webbiana* are more closely related, the genus itself is described as very diverse. Even plant morphologies differ within each species, depending on sampling locations (Frese et al. 2017a). The genetic diversity of *P. procumbens* is high, based on single sequence repeat marker analysis (Nachtigall et al. 2016) and naturally occurring populations show higher variations than the accessions kept in gene banks (Frese et al. 2017a). Frese et al. (2017a) were able to name standard accessions that can be considered as a reference for *P. procumbens* (BETA 951) and *P. patellaris* (BETA534), respectively. Including these reference accessions, Sielemann et al. (2022) produced phylogenetic trees for *Beta* and *Patellifolia* species based on plastome data and using different approaches. When using assembly-based phylogenies for tree modeling, *P. procumbens* and *P. webbiana* were located in one clade and *P. patellaris* formed a separate clade. I included the *P. procumbens* and *P. webbiana* reference accessions in my *Hs4* sequence analysis. Similar to the assembly-based phylogenies reported by Sielemann et al. (2022), the two accessions formed a clade in the phylogenetic tree based on *Hs4* protein sequences. Sielemann et al. (2022) encountered the formation of contrasting clades when basing the phylogenetic tree on kmer-based phylogenies: *P. webbiana* formed a distinct clade, and *P.*

*procumbens* and *P. patellaris* were joined in the other clade. The relationship to the *P. patellaris* reference accession BETA534 deployed in their study could not be analyzed during my work as it failed to germinate in an initial sowing and was not used for *PpatHs4* sequencing. Nevertheless, the close relationship between *P. procumbens* and *P. patellaris* was reflected by the highly supported *P. procumbens/P. patellaris* subclade forming in my analysis.

Further, even though the level of ploidy separates *P. procumbens/P. webbiana* from *P. patellaris*, observations on di-, tri-, and tetraploid offspring formed by naturally co-occurring *P. procumbens* and *P. patellaris* showed that the boundaries between these species are not as strict as long assumed (Frese et al. 2017a; Frese et al. 2019). Additionally, Jassem et al. (1992) reported the generation of self-fertile tetraploid *P. procumbens* which showed high morphological similarities to *P. patellaris*. Actually, *P. procumbens* might be one of the ancestors of the allopolyploid *P. patellaris* (Frese et al. 2017b). Hence, the genus *Patellifolia* exhibits cryptic diversity, and the occurring interspecific hybridization events generate new genetic variation within the genus, contributing to the species' survival (Frese et al. 2017a; Frese et al. 2019). Such hybridizations could have impacted the diversification of *Hs4* between accessions of individual *Patellifolia* species and led to high similarities of *Hs4* homologs from single *P. procumbens* accessions and *P. patellaris*.

Interestingly, a pan-genome study of late deployed the *Hs4* gene for characterizing variant frequencies in pooled sequencing data of different *Patellifolia* (Reeves and Richards 2022). They identified haplotypes of short genomic regions, so-called short haplotype (SH) loci, that contain at least one SNP and segregate between species or accessions. Per SH locus they identified 0.16-3.36 variants between *Hs4* homologs. Of these loci, 20 % contained single- or multi-nucleotide polymorphisms, and the remaining 80 % InDels. Strikingly, Reeves and Richards (2022) detected differences in exonic variants at several *Hs4* SH loci across accessions within the same species, similar to the results found in my analysis. However, I found a major InDel located in exon 5, resulting in the addition of valine in several *P. procumbens*, *P. patellaris*, and *P. webbiana* accessions. The occurrence of this variant is not reported in their study. Instead, four SH loci with differing major variants in or around exon 5 were encountered, which, in turn, I could not detect in the *Hs4* sequences generated here. However, as exon 5 was formerly considered exon 4 (Kumar et al. 2021), it remains doubtful whether Reeves and Richards (2022) analyzed the same exon as I did.

Due to the high similarities between the *Hs4* and *P. webbiana* sequences, a working hypothesis was that *Hs4* might have come from *P. webbiana* instead of *P. procumbens*. My data demonstrate that *Hs4* is unequivocally derived from a *Patellifolia* species, but the exact species cannot be inferred from the sequence data at hand. The complex relationships within the genus account for the differences in *Hs4* sequences observed.

A second resistance gene is located on chromosome 7 of *P. procumbens* and *P. webbiana* (Lange et al. 1988; Lange et al. 1993). Using the primers matching *Hs4*, no other *Hs4* homologous sequence could be amplified from the *Patellifolia* species. It can therefore be assumed that the resistance gene located on chromosome 7 has no homology to *Hs4*.

### 6.3 Homologs of *BvHs4* are present in various *Beta* species

The genera *Patellifolia* and *Beta* have diverged 25 mya (Romeiras et al. 2016). *B. vulgaris* has a homolog to *Hs4* with 60 % protein similarity (Kumar et al. 2021), the presence of which is not unexpected, as the sugar beet genome is described to contain around 75 % homologous sequences to *Patellifolia* (Reeves and Richards 2022). As expected, I detected a highly similar *BvHs4* homolog in *B. vulgaris* ssp. *maritima*. Further, and despite multiple differentiation

events in the genus *Beta* (Romeiras et al. 2016), all other *Beta* species analyzed also contained highly similar homologs to *BvHs4*.

While all species and accessions sequenced contained only one detectable homolog, *B. corolliflora* was found to have two *BvHs4*-homologous sequences that varied at several sites. As *B. corolliflora* is a tetraploid species (Sielemann et al. 2023b), the presence of two varying *BcHs4* copies is not unexpected. While the *BcHs4<sub>A</sub>* homolog resembled *BvHs4*, the *BcHs4<sub>B</sub>* homolog had a prominent insertion of 97 bp and a deletion of 312 bp, both of which were also present in *B. patula* and *B. macrorhiza*. Matching these results, *B. macrorhiza* is believed to be a parental species of *B. corolliflora* (Sielemann et al. 2023b). Blasting the insertion yielded high congruency with the *BvHs4* homolog from the tolerant sugar beet genotype U2Bv. This genotype is characterized as nematode tolerant based on the expression of two *BvNLP7* genes that are located on chromosome 5 (Sielemann et al. 2023a) and which do not show any resemblance to the nematode resistance gene *Hs4* whose *Beta* homolog is located on chromosome 2. As both *BcHs4* variants lie in the intron, they do not affect the resulting protein. Further, these sequences did not show higher similarity to *Hs4* than *BvHs4* and are not expected to contribute to nematode resistance.

Overall, the genomic sequences of eleven *BvHs4* homologs from different *Beta* species showed sequence similarities to *BvHs4* above 97 %. An exception was the homolog from *B. macrorhiza* which only exhibited 90 % similarity to *BvHs4*. The sequences of *BvHs4* and *Hs4* show 76 % identity and none of the homologs detected in the other *Beta* species exhibited a significantly higher resemblance to *Hs4*. This finding indicates that no *BvHs4* homolog identified in the current study has a function in nematode resistance.

Except for *B. macrorhiza*, whose sequence variations led to the formation of a premature stop codon in the protein sequence, terminating the polypeptide at position 142, the high similarity of *BvHs4* homologous proteins is reflected in the phylogenetic tree, where all *Beta* homologs are located within one clade. The clade is subdivided into individual *B. patula*, *B. vulgaris* ssp. *maritima*, and *B. vulgaris* U2Bv/*B. corolliflora* “B” clades, respectively, and a clade including the different *B. vulgaris* reference genomes, *B. vulgaris* ssp. *adanensis*, *B. corolliflora* “A”, and *B. macrocarpa*. After splitting from *Patellifolia*, beets underwent several divergence events. At 7.2 mya, the western Mediterranean species, including *B. vulgaris* ssp. *maritima*, *B. macrocarpa*, *B. patula*, and *B. vulgaris*, split from the eastern species *B. corolliflora*, *B. nana*, and *B. trigyna*. The western group diverged further and *B. macrocarpa* split off 0.3 mya. *B. vulgaris* ssp. *maritima*, *B. patula*, and *B. vulgaris* are estimated to have diverged from their last common ancestor around 0.9 mya (Romeiras et al. 2016). Hence, the western Mediterranean species are expected to be related more closely to each other than to the eastern group. Based on *BvHs4*-homologous polypeptides, distinct clades of *B. patula* and *B. vulgaris* ssp. *maritima* can be separated from *B. vulgaris*. The two *B. corolliflora* homologs are, however, located together with the tolerant beet genotype U2Bv or with two other sugar beet reference genomes, respectively. A separation due to a divergence of eastern and western Mediterranean species cannot be observed here. *B. vulgaris* ssp. *maritima* is considered the ancestor of all cultivated beets (Biancardi et al. 2020). Nonetheless, it does not form a higher-order clade incorporating the cultivated beet types in the current analysis. Interestingly, *B. patula* is described to be closely related to *B. vulgaris* ssp. *maritima* (Frese and Ford-Lloyd 2020), which is observable in certain variations that are present in the homolog sequences of both species.

#### 6.4 *Hs4* and *BvHs4* show contrasting expression patterns

After having determined that *Hs4*-homologous genes were present in all *Patellifolia* and a broad set of *Beta* species, I analyzed their expression in leaves and roots. In addition to the

accessions used for homolog sequencing, I included further accessions of *P. patellaris*, *B. vulgaris* ssp. *adanensis*, and *B. vulgaris* ssp. *maritima*. Matching my expectations based on the predicted protein localizations, I found contrasting expression patterns for *Hs4* and its homologs compared to *BvHs4* and the homologs thereof.

*Hs4* is a functional nematode resistance gene (Kumar et al. 2021) and has higher expression levels in roots compared to leaves. The fact that nematodes are soil-borne pathogens can account for the elevated expression of the gene in roots. Noteworthy, I found the highest expression levels in the translocation line TR520 and the hybrid variety Nemata derived from it. Interestingly, a second translocation line, TR363, did not show enhanced *Hs4* expression levels. This inconsistency might partly be explained by a finding in maize, where an important factor controlling expression and phenotype differences associated with the selective sweep region *tb1* is located several thousand kb upstream of the transcribed gene's sequence (Clark et al. 2006). TR363 harbors a much smaller translocation than TR520 and important regulatory *cis*-elements might be lacking in its sequence, leading to differences in expression intensities.

*BvHs4*, on the other hand, is expressed strongly in leaves. Interestingly, it is predicted to be plastid-bound. Plastids can be found in their non-green form in roots and seeds, while green chloroplasts, responsible for light-requiring photosynthesis, are mainly encountered in leaves (Rolland et al. 2018). Yet, it is not known which plastids *BvHs4* is associated with. As the different species of the genus *Beta* are highly susceptible to BCN (Steele 1965), *BvHs4* does not seem to function as a nematode resistance gene and hence does not require strong expression in the roots where this pathogen attacks. However, as all *Beta* species analyzed contained and expressed homologs of *BvHs4*, it would be fascinating to identify the function of this highly conserved gene. Interestingly, the Arabidopsis protein RBL11 sharing 57 % protein identity with *Hs4* and 71 % with *BvHs4*, respectively, has been described to be involved in the cold-induced degradation of the FATTY ACID EXPORT PROTEIN1 (FAX1). FAX1 mediates the export of fatty acids from the chloroplast to the ER, where they are required for lipid biosynthesis. Under cold conditions, the reduction in FAX1 abundance by RBL11-mediated cleavage is important to balance the lipid levels, ultimately preserving membrane fluidity (John et al. 2024). Whether *BvHs4* has evolved to perform similar functions remains to be explored.

For the nematode resistance gene *Hs1<sup>pro-1</sup>*, specific upregulation after nematode infestations was demonstrated. While Cai et al. (1997) observed an upregulated state four weeks after inoculation, Thureau et al. (2003) described that *Hs1* already got induced at 1 dpi and continuously elevated levels were detectable until 11 dpi. Therefore, I tested whether *Hs4* in *P. procumbens* and *BvHs4* in *B. vulgaris* were differentially expressed over time in different tissues, including sampling points at 3 and 28 dpi. Matching the *Hs4* expression results from the broad set of accessions, *Hs4* was more strongly expressed in roots compared to leaves at all sampling points. However, using RT-qPCR, I could not detect significant expression changes after nematode inoculation. This finding confirmed previous analyses by Kumar et al. (2021). Nevertheless, *Hs4* expression was elevated in the 28 dpi samples under both treatments (inoculated and non-inoculated), indicating that the gene expression might increase with the plants' age. The phenomenon of age-related resistance is described for different plant-pathogen interactions (for example between Arabidopsis and the bacterium *Pseudomonas syringae*, Kus et al. 2002). Most importantly, this increase in resistance is also described for the interaction of *Patellifolia* species with *H. schachtii* (Yu 1984). To test whether *Hs4* itself is conferring stronger resistance in an age-dependent manner, additional tests are necessary.

Further, I tested the *P. procumbens* samples from 28 dpi for an upregulation of *Hs1* as previously demonstrated using Northern blot analysis (Cai et al. 1997). However, I could not find a significant upregulation between inoculated and non-inoculated samples. Apart from the difference in detection methods, the plant material also differed between my analysis and previous studies. While I have used a *P. procumbens* accession, Cai et al. (1997) used the translocation line TR520. Astonishingly, my data indicated strong *Hs4* expression differences between the *Patellifolia* accessions and TR520. Therefore, it might be of interest to analyze both genes in the translocation background as well.

### 6.5 *Hs4* confers resistance to BCN in a non-related species

I assessed whether the resistance conferred by the nematode resistance gene *Hs4* coming from the amaranthaceous *Patellifolia* could confer resistance in the brassicaceous species *Arabidopsis thaliana*. Heterologous expression of genes in a non-related species is widely applied in functional gene analysis and the transfer of genes from prokaryotic species to eukaryotic plants has, for instance, enabled the transmission of resistance to glyphosate and insect pests into plants (Watts et al. 2021). *Arabidopsis* is a suitable host and highly susceptible to *H. schachtii* (Sijmons et al. 1991) and therefore predestined for the investigation of nematode resistance genes. Here, I tested the resistance reaction conferred by *Hs4* and its correlation with the transgene's expression level in *Arabidopsis* T<sub>3</sub> plants. The gene's expression was either driven by the constitutive 35S or the inducible Hs1 promoter.

As expected, I found transgenic lines with significantly lower female numbers for both promoter constructs used. However, some developing females were still observable, even in the best-performing lines. Even in the resistant *Patellifolia* species, nematodes are still able to enter the roots and form a syncytium, the resistance acts postinfectious, and developing females are still observable occasionally (Yu 1984). The females found on the transgenic *Arabidopsis* roots often appeared smaller than the females on wild type roots but still contained eggs, hinting at the successful completion of their life cycle. The sex of invading J2 larvae is not defined yet, instead, the quality and amount of nutrients available are believed to determine sex differentiation which begins at the end of the J2 stage (Golinowski et al. 1997). Accordingly, differences in the site of syncytium induction and the final syncytia sizes can be observed between male and female nematodes developing on *Arabidopsis* roots (Golinowski et al. 1996; Sobczak et al. 1997). Additionally, Anjam et al. (2020) found that female nematodes grew faster than males starting from 3 dpi. Consequently, females are described as consuming 29 times more food than males (Müller et al. 1981). A restriction in female growth due to a restriction in syncytium size by the action of a nematode resistance gene could therefore be expected. The transformation of sugar beet roots with the resistance gene *Hs1* led to the stagnation of female development (Cai et al. 1997). Additionally, inoculation experiments with sporamin-expressing sugar beet roots led to either a reduction in female numbers or reduced female sizes, though the females often contained no eggs (Cai et al. 2003). In the cereal cyst nematode *H. avenae* a direct correlation between female size and egg numbers was found (Cook 1977). Even though the *H. schachtii* females detected on transgenic roots were smaller, the number of eggs produced by them was not determined. Nevertheless, a correlation between *Hs4* expression and female nematode size reduction is apparent.

The lines with the lowest number of developing females detected here also showed the highest expression levels of *Hs4*, indicating that the resistance reaction is expression-dependent. These results are in line with the previous characterization of *Hs4* in sugar beet (Kumar et al. 2021). However, the highest-expressing lines were later found to be segregating populations with two transgene integrations. As I selected the T<sub>3</sub> lines based on homogeneous red seed fluorescence, at least one transgene copy has to be present in a homozygous state.

However, the state of the second transgene could not be determined in the T<sub>3</sub> generation. Therefore, it can be present in a homo- or heterozygous state or the homozygous wild type allele might be present at that locus. Based on the different genotypes possible, differences in the *Hs4* expression levels and hence the variations between biological replicates from individual lines observed can be explained. Nevertheless, I could show that the assumption of *Hs4*-expression-dependent *H. schachtii* resistance in Arabidopsis remains untouched.

For both constructs, I also obtained lines that did not show significantly lower female numbers. These results were congruent with results obtained by Johanna Leinweber (2020) who analyzed the Hs1::*Hs4* T<sub>2</sub> families. She found Arabidopsis families exhibiting differently strong BCN resistances, though the correlation between the strength of the resistance reaction and the transgene expression was not examined in her work. Furthermore, she detected root discoloration in the transgenic plants and enhanced stress symptoms compared to the wild type. Tying in with these results, the T<sub>3</sub> lines with the highest *Hs4* expression levels and the strongest red fluorescence showed enhanced pink root colors. First, I assumed that this root coloration was correlated to plant stress based on *Hs4* expression, as lines with the highest expression exhibited the strongest discoloration. However, the naked-eye coloration was also clearly correlated with the fluorescence intensity observed under stimulating light. As described above (see 3.2.1), the expression of *Hs4* and the red fluorescence marker *DsRed2* are linked. The fluorescent dye DsRed was discovered in *Discosoma* sp. as drFP583 (Matz et al. 1999). Since then, several alterations have been made (Clontech Laboratories, Inc. 2003). DsRed itself can lead to a pink coloration of *E. coli* colonies under non-fluorescence stimulating conditions (Multamäki et al. 2022). The altered version DsRed2, which was modified to exhibit a more rapid appearing red fluorescence and have increased solubility (Clontech Laboratories, Inc. 2003), is incorporated in the pBin35SRed vector (Pidkowich et al. 2007). DsRed2 is characterized to be visible to the naked eye and overexpression in Arabidopsis resulted in a red seed coat and red root coloration (Kong et al. 2023). The color, described by them as ‘red’ but which could also be termed ‘pink’, is highly similar to the coloration observed in the *Hs4*-transgenic Arabidopsis. Hence the root discoloration observed in single T<sub>3</sub> lines exhibiting the highest *Hs4* expression results from the similarly increasing expression of the *DsRed2* selection marker.

The direct comparison of the transgenic lines with the different promoters driving *Hs4* expression revealed that lines with the inducible promoter were outperforming the constitutively expressing lines. The pBin35SRed vector contains the constitutive 35S promoter which was previously thought to cause lethality when driving *Hs4* expression in Arabidopsis (Kumar et al. 2021). When I repeated the transformation, I obtained 73 red fluorescing Arabidopsis seeds harboring the 35S::*Hs4* construct. However, contrasting reports on the activity of this promoter in syncytia exist. Goddijn et al. (1993) reported a strong downregulation when using this promoter to drive *GUS* expression in syncytia induced in Arabidopsis. Soon thereafter, analysis with GFP in Arabidopsis demonstrated that the 35S promoter was active until 27 dpi in syncytia, but downregulation of GFP could be observed within 10 dpi in female-associated syncytia (Urwin et al. 1997). Bertioli et al. (1999) infected transgenic tobacco plants transformed with various 35S-*GUS* constructs with a cyst and a root-knot nematode, respectively, and found that the promoter was active in root-knot nematode feeding sites but exhibited inactivity in 70 % of the cyst nematode-induced syncytia analyzed. In the remaining 30 % they detected activity of the 35S promoter though they observed decreasing activity with increasing maturity of the syncytia. More recently, Ali and Abbas (2016) showed that 35S::*GUS* expression in syncytia in Arabidopsis was reduced faster than 35S::*DsRed* expression. They observed downregulation of *GUS* at 10 dpi and almost complete inactivity at 15 dpi, while *DsRed* expression did not decrease before 15 dpi. Nevertheless, the constitutive 35S promoter has been used widely, also for the expression of

## Discussion

nematode resistance genes (Cai et al. 1997; Chen et al. 2006; Fuller et al. 2008; Kumar et al. 2021). In light of these findings, the inferior performance of the 35S lines is explicable, especially since no syncytium-specific expression of *Hs4* was measured.

The *Hs1* promoter incorporated in the second construct comes from *P. procumbens*. Previous analysis showed a specific activation of the promoter region in syncytia (Thurau et al. 2003). Through deletion analysis, they determined that one enhancer element was located between -1199 and -705 bp, and *cis*-acting elements required for syncytium-specific expression were located between -355 and +247. However, these regulatory *cis*-elements were later claimed to be part of the *Hs1* gene itself when sequence comparisons led to an extension of the gene's 5'-region and a shift of the translation start point by 621 bp (McLean et al. 2007). Even though the *Hs1* promoter used in my work incorporates the enhancer described, it does not incorporate the important *cis*-element specified. In plants expressing *Hs1::Hs4*, I could not detect a specific upregulation after nematode inoculation. Nevertheless, plants expressing *Hs1::Hs4* outperformed the transgenic plants constitutively expressing *Hs4*.

### 6.5.1 Investigating the function of *Hs4* under field-like conditions

The resistance reaction of Arabidopsis to nematodes is mainly tested under sterile *in vitro* conditions (for example Cai et al. 1997; Anwer et al. 2018; Hawamda et al. 2022) and only a few reports about inoculation experiments under *in vivo* conditions in sand or soil exist (Noureddine et al. 2022; Willig et al. 2023; Willig et al. 2024). The nematode resistance gene *Hs1* was mainly tested in sterile setups (Cai et al. 1997; Zhong et al. 2019), though its expression in soybean grown on soil also showed a significant reduction in developing soybean cyst nematodes (McLean et al. 2007). Accordingly, I also tested the new nematode resistance gene *Hs4* under *in vivo* conditions expecting to find the *in vitro* results confirmed.

However, when I examined the transgenic lines under *in vivo* conditions in a sand-soil mixture, I found strong deviations from the *in vitro* results. The resistance reaction observable under *in vitro* conditions was not evident under *in vivo* conditions. When comparing the relative *Hs4* expression across environments, the *in vivo* plants exhibited higher *Hs4* expression than the *in vitro* plants. The upregulation in *Hs4* expression did, however, not correlate with increased resistance. Differential expression between *in vitro* and *in vivo* conditions has for example been demonstrated for cyanobacteria (Leibroek et al. 2022) and a rice-pathogenic bacterium (Ibrahim et al. 2012). Cai et al. (2003) demonstrated that the sporamin protein SpTI-1, which has serine-protease- and trypsin-inhibitory activity, had nematode-suppressing properties in sugar beet hairy roots *in vitro*. Most importantly, they showed that there was no correlation between transcript levels and protein accumulation, and further, they detected hairy root clones where the protein was present but no inhibitory activity could be measured, resulting in susceptibility to BCN. An explanation could be post-translational modifications (PTMs) which can occur offhandedly depending on the cell status, including ROS accumulation (Friso and van Wijk 2015), which are produced by the plant as part of the defense mechanism but can also be employed by nematodes to their benefit (Siddique et al. 2014). Further, Labudda et al. (2016) determined that the activity of serine proteases was significantly reduced in Arabidopsis roots infected with *H. schachtii*. Interestingly, rhomboid proteases are classified as serine proteases (Urban and Dickey 2011). Consequently, whether PTMs influence the function of *Hs4* or if this protease is downregulated specifically under *in vivo* conditions remains to be elucidated.

An important difference between *in vitro* and *in vivo* tests is the microbiome of the sand-soil mixture, which is absent under tissue culture conditions. To see if the microbiome of the sand-soil mixture was influencing the nematode infestation rate positively, I tested the *Hs1::Hs4*-expressing line 210637 under semi-sterile *in vivo* conditions in heat-sterilized sand-

soil. Here, I observed significantly lower numbers of developing females on the transgenic plants compared to the control, hinting at a nematode-repressing microbiome under semi-sterile conditions. Accordingly, to further verify the hypothesis of a nematode-supporting microbiome under non-sterile conditions, I tested the resistance reaction of the five previously *in vitro*-characterized Arabidopsis lines under semi-sterile and non-sterile *in vivo* conditions. I could not verify the resistance reaction exhibited by 210637 plants in the second semi-sterile experiment. Nevertheless, all but one transgenic line showed reduced numbers of developing females compared to the control under semi-sterile but not under non-sterile conditions.

In the experiments conducted *in vivo*, different microbiomes have to be considered. Firstly, there is the rhizosphere which can contain a huge microbial community including plant-growth-promoting bacteria and fungi. Different interactions of Arabidopsis with these beneficial microbes have been reported (Zamioudis and Pieterse 2012). In *B. vulgaris* monocultures, *H. schachtii* populations face highly suppressive soils after a few cropping cycles (Topalović and Heuer 2019; Eberlein et al. 2020) and several rhizobacteria were shown to prevent nematode infection or penetration of sugar beet roots (Oostendorp and Sikora 1989). In Arabidopsis, characterizations of mutants have highlighted the importance of phytohormones (Sikder et al. 2021) and secondary metabolites (Sikder et al. 2022) for plant resistance or susceptibility to invasion of *Meloidogyne* species. Additionally, plants have been found to shape their root-associated microbiome which can support nematode suppression (Elhady et al. 2021). Mycorrhizal fungi are shown to be plant-beneficial and the mycorrhiza-induced resistance conferred by them can enhance nematode resistance (Li et al. 2006; Hao et al. 2012; Cameron et al. 2013). However, it has been demonstrated that many Brassicaceae, among them Arabidopsis, are not colonized by these fungi (Demars and Boerner 1996). Whether and which of those interactions were already established in the short-term cultivated plants reported here remains elusive. Nevertheless, nematode-protective bacteria have also been reported (Topalović et al. 2023). This leads to the second microbiome to consider: the nematode-native gut microbiome. In the model nematode species *Caenorhabditis elegans*, the gut microbiome contains a broad range of bacterial taxa dominated by Proteobacteria (Dirksen et al. 2016). Interestingly, Dirksen et al. (2016) revealed that the higher taxonomic level of bacteria shaping the microbiome remained stable across different geographical isolates of *C. elegans*. Variations in the gut microbiome of the different *H. schachtii* larvae used between the experiments are therefore highly unlikely. Further, the gut microbiome is not expected to differ between the semi-sterile and non-sterile experiments as the *H. schachtii* larvae were always only surface-sterilized. Differences between the two *in vivo* conditions can therefore not be attributed to the gut microbiome.

Even though the microbiome is the main difference between the heat-sterilized and non-treated soil environments in the *in vivo* experiments conducted, it cannot be claimed with certainty if a plant- or rather nematode-promoting microbiome prevailed in the setup and led to the current findings. Contrary to the results from Martínez-Soto and Ruiz-Herrera (2016), who found elevated resistance of maize plants to the pathogen *Ustilago maydis* in non-sterile soil compared to *in vitro* culture or sterile soil, the *Hs4* resistance was much enhanced under completely sterile *in vitro* conditions compared to the semi-sterile or non-sterile *in vivo* conditions, even though the *Hs4* expression levels detected were lower. Then again, I did not find any studies directly comparing sterile *in vitro* resistance tests to resistances observed under *in vivo* conditions. Clarifying where the differences in the resistance reaction come from can only be achieved after resolving the mode of action of *Hs4*.

## 6.6 Syncytia developing under *Hs4* expression show distinct characteristics

*Hs4* is predicted to be ER-bound and Kumar et al. (2021) hypothesized that the rhomboid protease gets activated after the nematode attack and leads to the destruction of the plant ER

## Discussion

and, subsequently, the syncytium, resulting in nematode death. Importantly, the ER close to the nematode stylet is directly connected to the feeding tube required for feeding from the established syncytium (Sobczak et al. 1999). Nematodes cannot produce the essentially required sterols *de novo* and PPNs therefore rely on the sterols produced in the plant ER (Hartmann and Benveniste 1987; Chitwood and Lusby 1991), which might explain the association of ER and feeding tube. Further, Holtmann et al. (2000) detected changes in syncytial ER structures between resistant translocation lines and susceptible sugar beet. While smooth ER prevailed in the susceptible genotype, they detected mainly rough ER and membrane aggregations formed from ER membranes in the resistant genotype. These differences were shown not to be linked to the by-then-characterized resistance gene *Hs1* (Holtmann 2000). Based on these findings, I hypothesized that the structural changes in ER conformation observed in previous studies were associated with the nematode resistance gene *Hs4*. To verify this hypothesis, I analyzed the ultrastructure of syncytia from *Hs4*-expressing Arabidopsis plants and compared them to syncytia formed on wild type roots.

First, I analyzed the syncytia of Col-0 at 9 and 26 dpi. My findings were in line with reports on syncytia induced by *H. schachtii* in roots of Arabidopsis (Golinowski et al. 1996; Sobczak et al. 1997; Grundler et al. 1998), susceptible sugar beet (Bleve-Zacheo and Zacheo 1987; Holtmann et al. 2000), and susceptible *Raphanus* (Wyss et al. 1984).

The nematodes could induce the syncytium successfully also in the resistant Arabidopsis lines and the analyzed syncytia were marked by extensive cell wall degradations. Those findings are in agreement with results from studies on resistant sugar beet translocation lines (Holtmann et al. 2000) and resistant *Raphanus* (Wyss et al. 1984).

At 5 dpi, I could still identify central vacuoles, but at later stages, they were often dissolved and, similar to the wild type syncytia, several smaller vacuoles were present. Mitochondria were abundant in the syncytia and the plastids contained no starch grains. The cell wall ingrowths and paramural bodies were less developed compared to the wild type. Most pronounced was the reduction of vesicular smooth ER. Rather, I detected sheets of tubular ER in one 228934 syncytium and numerous membrane aggregations (MAs) in the other syncytia of the transgenic plants. The occurrence of smooth ER tubes spread across the cells has been reported for the compatible interaction of Arabidopsis with *H. schachtii* (Golinowski et al. 1996; Anjam et al. 2020), but also for the incompatible interaction with *H. glycines* (Grunder et al. 1997). Whether the tubular ER observed in a syncytium of line 228934 formed due to a compatible or an incompatible reaction cannot be determined. The membrane aggregations detected consisted of ER tubules, as ribosomes were observed to accumulate on the outer tubule membranes. The inner regions of the membrane aggregations were devoid of ribosomes and only consisted of coils of tubules. Strikingly, the same observations were made in resistant sugar beet translocation lines lacking the resistance gene *Hs1* but containing the at that time not yet identified second resistance gene *Hs4* (Holtmann 2000).

Membrane aggregations were never observed in the syncytia induced in Arabidopsis wild type roots, neither by me nor by other authors (Golinowski et al. 1996; Grundler et al. 1997; Sobczak et al. 1997), and also never in non-inoculated *Hs4*-transgenic roots investigated by me. Therefore, a direct connection between the expression of *Hs4* and the formation of the membrane aggregations can be assumed. Additionally, *Hs4* is predicted to be bound to the ER (Kumar et al. 2021), the same organelle that forms the membrane aggregations detected. The ER is responsible for the correct folding and subsequent transport of proteins. Under stress conditions, the equilibrium between protein synthesis and processing in the ER lumen is disturbed, leading to ER stress. If homeostasis cannot be restored, the ER stress ultimately leads to the affected plant cells' programmed cell death (PCD) (Simoni et al. 2022). The direct association between nematode and plant ER has been shown for two root-knot nematode

species. The effector MiEFF12 from *Meloidogyne incognita* was shown to target plant ER-based bap-like proteins controlling the correct folding of antimicrobial pathogenesis-related proteins, thereby inhibiting the initiation or strong expression of the PTI response (Soulé et al. 2024). Liu et al. (2024) demonstrated that the *M. graminicola* effector MgCRT1 binds to an ER-localized rice protein, preventing its interaction with its natural counterpart, and suppressing the activation of defense-related genes in the nucleus in rice. In the interaction of the fungus *Erysiphe cruciferarum* with Arabidopsis, AtCEP1 becomes expressed in the ER and accumulates around the fungus-produced haustoria, ultimately resulting in PCD (Höwing et al. 2014).

I detected signs of plant cell death in syncytia of the *Hs4*-expressing roots containing membrane aggregations. At 5 dpi, the earliest stage investigated, I observed callose-like depositions along the cell walls and hence a seemingly detached plasma membrane. The accumulation of callose-like material has been reported in syncytia for both compatible as well as incompatible reactions (Grundler et al. 1997; Sobczak et al. 1999). First signs of degradation in other resistant species were also observed starting from 4-5 dpi (Wyss et al. 1984; Kim et al. 1987; Holtmann et al. 2000), and in line with findings from these species, I detected strong vacuolization and necrotic regions in syncytia induced in transgenic Arabidopsis roots. Some vacuoles might have resembled lytic vacuoles as they contained cell organelles (van Doorn et al. 2011). In advanced syncytia, the cytoplasm appeared translucent and the mitochondria looked disintegrated and non-functional, with a translucent lumen and no longer well-developed cristae. Contrarily, the plastids often remained intact. The described deposition of starch grains in plastids in resistant syncytia (Golinowski et al. 1997) could not be observed here. The early loss of plasma membrane integrity and subsequently the shrinkage of the protoplast are associated with necrotic cell death (van Doorn et al. 2011). Hence, the detachment of the plasma membrane from the cell wall detected in syncytia induced in *Hs4*-expressing roots is indicative of the necrotic stage of the syncytium.

I also observed osmiophilic granules that co-localized with the plasma membrane or the membrane aggregations in disintegrating syncytia. Wyss et al. (1984) described the occurrence of lipid-like, osmiophilic globules upon cytoplasm disintegration in resistant *Raphanus*. In Arabidopsis, electron-dense accumulations along the plasma membrane have been characterized to be associated with the degradation of the syncytium once the nematodes cease feeding (Golinowski et al. 1996). The electron-dense, osmiophilic granules observed here are therefore most likely correlated with the degradation process of the examined syncytia. Similar to results from resistant soybean (Kim et al. 1987; Kim et al. 2012), I also found necrotic regions at the borders of the syncytium.

While at 26 dpi the disintegration of cell organelles like mitochondria in the otherwise intact syncytium is associated with the feeding cessation and the concurrent disintegration of the syncytium (Golinowski et al. 1996), the disintegration processes observed in syncytia of transgenic roots at early time points can most probably be attributed to the action of the *Hs4* resistance gene. In order to verify the association of *Hs4* with the ER and determine its role in the formation of the membrane aggregations, fusion proteins, colocalization analysis or detection assays of *Hs4* in isolated ER membranes by immunoblotting can be conducted. For instance, it would be intriguing to decipher whether *Hs4* action directly leads to the fusion of existing ER membranes to form membrane aggregations, similar to the process of ER membrane fusion initiated by ER-bound GTPases (Hu and Rapoport 2016). Rhomboid proteases are also described to cleave ER-localized transcription factors, releasing them under stress conditions to alter gene expression (Ng et al. 2013; Eysholdt-Derzso et al. 2023). *Hs4* as rhomboid protease could therefore also be activated after nematode infestation and the cleavage of its substrate could initiate genes reprogramming the cellular ER structure.

Further, the formation of membrane aggregations did not always result in syncytium abortion. The late-stage syncytia analyzed were most likely functional as they were selected based on the presence of an attached, normally developed nematode. At 26 dpi, developing females were easy to distinguish by their swollen lemon-shaped form and no syncytia from abnormally developing females were excised or analyzed. How the nematodes can circumvent the lack of nutrients imposed by the restructured ER could not be determined in the current work. Additionally, it would be enthralling to define the mechanism by which the virulent *H. schachtii* pathotype Schach1 is able to overcome the combined resistance of *Hs1* and *Hs4* from *P. procumbens* chromosome 9 in translocation lines (Müller and Klinke 1996; Müller 1998). The *H. schachtii* effector 4E02 is able to re-localize the plant papain-like cysteine protease RD21A usually translocated from the vacuole to the apoplast under stress conditions to the cytoplasm or nucleus instead, thereby interfering with its defense-related function (Pogorelko et al. 2019). Whether virulent BCN pathotypes possess effectors capable of similar changes could be a starting point for investigation. Otherwise, if *Hs4* functions as a protease releasing a transcription factor, the BCN could have evolved to exhibit an effector competing with the original substrate and inhibiting downstream signaling, similar to the *M. incognita* effector MgCRT1 (Liu et al. 2024). Bearing in mind the different resistance reaction intensities observed under *in vivo* conditions, it would also be interesting to analyze syncytia from *Hs4*-expressing Arabidopsis grown *in vivo* to see if the formation of membrane aggregations is restricted or inhibited.

### 6.7 *Hs4*-transgenic plants can facilitate crop rotation

At times, rapeseed (*Brassica napus*) is used in crop rotation systems with sugar beet. As *B. napus* is tolerant to *H. schachtii* infestations and an excellent host to the pest, the nematodes can easily reproduce on rapeseed roots (Nielsen et al. 2003; Daub 2020). Therefore, the post-harvest emerging rapeseed, which enables high BCN multiplication rates at times crucial for sugar beet development, has to be tightly controlled. For example, a management tool for the effective temperature-dependent control of volunteer rapeseed was developed (Daub 2020; Landwirtschaftlicher Informationsdienst Zuckerrübe by Pfeifer & Langen 2020).

However, the cultivation of susceptible rapeseed, enabling the emergence of volunteer rapeseed that exhibits optimal reproduction prerequisites for BCN, poses a risk for sugar beet production in the same fields. Transferring resistances from *Raphanus sativus* (Lelivelt and Krens 1992) or *Sinapis alba* (Lelivelt et al. 1993b) has been attempted. Finally, crosses between *R. sativus* and *B. rapa* successfully transferred the resistance to the *Brassica* gene pool. The resultant hybrid Raparadish exhibits nematode resistance but has a low agricultural value (Lange et al. 1989; Lelivelt et al. 1993a; Daub 2020). Transferring the *Hs1* gene to rapeseed led to significantly reduced developing female numbers (Zhong et al. 2019), indicating that the resistance from *Patellifolia* is transferrable to *Brassica* crops. It is therefore intriguing to transform rapeseed plants with the nematode resistance gene *Hs4*, which has no structural similarities to *Hs1* and most likely functions differently, to see if it can also reduce female numbers. The transgenic plant generated during my studies shows chimeric *Hs4* expression. The offspring are expected to show homogenous *Hs4* expression levels across all tissues as the gene is expressed from the 35S promoter. Characterizing the next generation under *in vitro* and *in vivo* conditions will reveal whether *Hs4* expression driven by the often debated 35S promoter (for example Goddijn et al. 1993; Urwin et al. 1997; Ali and Abbas 2016) can confer resistance to BCN in rapeseed in different environments. Especially the resistance under field-like conditions should be examined, keeping in mind the ambiguous data obtained with transgenic Arabidopsis plants inoculated in a sand-soil mixture. Further, it might be of interest to generate plants expressing the resistance gene from the *Hs1* promoter which proved to be more beneficial for conferring resistance in Arabidopsis plants.

When *Hs1*-expressing rapeseed plants were tested *in vitro*, complete nematode resistance was not observed (Zhong et al. 2019). Combining both known resistance genes in rapeseed might confer complete nematode resistance, similar to *Patellifolia*.

Ultimately, an introduction of *Hs4* into sugar beet, putatively also in combination with *Hs1*, is favorable. The cultivation of completely resistant sugar beets would diminish intercropping conflicts with good BCN host species. To date, tolerant sugar beet varieties outperform the available resistant ones (Reuther et al. 2017), most likely due to the comparably large wild beet background in the translocation-line-derived resistant varieties. Whether the direct transfer of the known nematode resistance genes confers a similarly strong resistance reaction and leads to yields matching the tolerant varieties remains to be explored.

However, cultivating resistant varieties always bears risks. The introgression of the resistance gene *H1* into cultivated potato conferred lasting resistance to the potato cyst nematode (PCN) *Globodera rostochiensis*. Nevertheless, the extensive cultivation of the resistant varieties in Britain led to the selection of the other PCN, *G. pallida*, for which resistance breeding is much more complicated (Jones et al. 2011). The use of resistant cultivars should therefore be closely monitored. Before its use in the field, the *Hs4*-conferred resistance should be tested against other *H. schachtii* field populations and also closely related nematodes like the yellow beet cyst nematode *H. betae*. While the *Patellifolia* species are described to be resistant to this nematode species, accessions derived from *B. vulgaris-procumbens* hybrids were shown to be highly susceptible (Steele et al. 1983). Therefore, the search for further resistance genes on the other *Patellifolia* chromosomes should also be pursued.

## 7 Summary

Plant-parasitic nematodes are economically important threats to globally produced crops. Sugar beet (*Beta vulgaris*) suffers from beet cyst nematode (BCN, *Heterodera schachtii*) infestations. While only tolerances against this pest can be found among the *Beta* species, the genus *Patellifolia*, constituting a third gene pool, shows complete resistance. Spontaneous hybridization events have led to the formation of resistant translocation lines with a short region of *Patellifolia procumbens* chromosome 9 attached to the homologous sugar beet chromosome. To date, two resistance genes located on this translocation have been described, *HsI<sup>pro-1</sup>* and *Hs4*, both of which have been shown to confer resistance to BCN in sugar beet. Further, it has been shown that the nematode feeding structures (syncytia) induced in translocation lines exhibit unusual endoplasmic reticulum (ER) membrane aggregations. In this study, I aimed to further characterize the nematode resistance gene *Hs4* in *Beta* and *Patellifolia* species, and in the non-related species *Arabidopsis thaliana* and rapeseed (*Brassica napus*).

My work was structured into four work packages. In my first work package, I screened a large set of *Patellifolia* and *Beta* species for *Hs4* homologs. All *Patellifolia* species contained highly similar *Hs4* homologs. Single nucleotide polymorphisms (SNPs) and insertions/deletions (InDels) between the accessions and species could be detected. I found an exonic integration of 3 bases resulting in the addition of one amino acid. Interestingly, this variant was present in single accessions of all three *Patellifolia* species. Both the localization and the structure of the protein were not changed by the additional amino acid. *B. vulgaris* contains an *Hs4* homolog (*BvHs4*) with 60 % protein identity to *Hs4*. *BvHs4* homologs were present in all *Beta* species analyzed. When examining the expression patterns of *Hs4* and *BvHs4* homologs, I identified substantial differences between species. While *Hs4* homologs are more strongly expressed in roots, *BvHs4* homologs are expressed mainly in leaves. Examining the spatio-temporal expression of *Hs4*, no response to nematode inoculation was observable.

In my second work package, I characterized *Arabidopsis* T<sub>3</sub> lines expressing *Hs4* from either the constitutive 35S promoter or the inducible Hs1 promoter. I found lines exhibiting significant nematode resistance compared to the susceptible control under *in vitro* conditions. The resistance was correlated with the *Hs4* expression level. Hence, lines with low *Hs4* expression levels showed female numbers similar to the control. When comparing the best-performing plants of both promoter constructs, I could demonstrate that expression of *Hs4* from the Hs1 promoter led to higher BCN resistance levels than from the 35S promoter. Under semi-sterile conditions in a heat-sterilized sand-soil mixture, one *Arabidopsis* line exhibited a significant reduction in female nematode numbers. However, when the plants were tested under non-sterile *in vivo* conditions, no line was significantly different from the control but the female numbers observed on all plants were below the numbers from the semi-sterile setup. Therefore, a defense priming under non-sterile conditions can be assumed.

In the third work package, I analyzed the ultrastructure of the syncytia in high-expressing 35S::*Hs4*- and Hs1::*Hs4*-transgenic *Arabidopsis* lines. As expected, syncytia in susceptible non-transgenic *Arabidopsis* were filled with dense cytoplasm, many functional mitochondria, small vacuoles, and numerous smooth ER vesicles. In contrast, in the resistant roots, necrosis of the initial syncytial cell started five days post-inoculation and completely degraded syncytia were detectable three days later. The cytoplasm was filled with large, translucent membranous structures and vacuoles. Furthermore, callose accumulated along the cell walls. In many cases, the plasma membrane was detached from the cell wall, and plastids and mitochondria were degraded. Most strikingly, I observed the formation of spherical ER-

derived membrane aggregations with ribosomes on the outer tubules, while smooth ER, required by the nematodes for the synthesis of sterols, was almost completely absent. The aggregations were present in syncytia of transgenic roots at different time points but they were never found in adjacent root cells. Only few initial syncytial cells turned into syncytia, allowing the nematode to develop regularly. Even these syncytia contained characteristic membrane aggregations. Based on these findings it can be assumed that the rhomboid-protease Hs4, upon attack by the nematode, leads to the formation of membrane aggregations. How the function of the Hs4-encoded protease is altered upon nematode attack remains elusive.

Rapeseed is a good host for *H. schachtii*, and the generation of BCN-resistant rapeseed could facilitate crop rotation systems with sugar beet in the future. Therefore, I transformed rapeseed with a 35S::*Hs4* construct. I obtained one transgenic plant, however with barely detectable *Hs4* transcripts. Seeds were harvested for future studies.

## 8 Zusammenfassung

Pflanzen-parasitäre Nematoden sind ökonomisch wichtige Schädlinge weltweit angebaute Kulturpflanzen. Die Zuckerrübe (*Beta vulgaris*) leidet unter Infektionen mit dem Rübenzystennematoden (RZN, *Heterodera schachtii*). Innerhalb der Gattung *Beta* kann nur Nematodentoleranz gefunden werden, während Arten des Genus *Patellifolia*, die den dritten Genpool bildet, vollständige Resistenz aufweisen. Spontane Hybridisierung führte zur Bildung resistenter Translokationslinien, die eine kurze Region des *Patellifolia procumbens* Chromosom 9 am Ende des homologen Zuckerrübenchromosoms tragen. Bisher wurden zwei Resistenzgene aus dieser Translokation beschrieben, *Hs1<sup>pro-1</sup>* und *Hs4*, die beide Resistenz gegen RZN in Zuckerrübe vermitteln. Des Weiteren konnte gezeigt werden, dass das durch die Nematoden induzierte Nährgewebe (Synzytium) in Translokationslinien ungewöhnliche Membranaggregationen von endoplasmatischem Retikulum (ER) aufweist. In meiner Arbeit wollte ich das Nematodenresistenzgen *Hs4* in *Beta* und *Patellifolia* Spezies und in den nicht-verwandten Arten *Arabidopsis thaliana* und Raps (*Brassica napus*) näher untersuchen.

Meine Arbeit war in vier Arbeitspakete unterteilt. Im ersten Arbeitspaket habe ich mehrere *Patellifolia*- und *Beta*-Spezies auf *Hs4*-Homologe überprüft. Alle *Patellifolia*-Arten enthielten sehr ähnliche *Hs4*-Homologe. Punktmutationen und Insertionen/Deletionen zwischen den einzelnen Akzessionen und Arten konnten entdeckt werden. Ich habe eine exonische Integration von 3 Basen entdeckt, die zur Addition einer Aminosäure führte. Interessanterweise war diese Insertion in einzelnen Akzessionen aller drei *Patellifolia* Arten vorhanden. Weder die Proteinlokalisierung noch -struktur wurden durch die zusätzliche Aminosäure beeinflusst. *B. vulgaris* kodiert für ein *Hs4*-Homolog (*BvHs4*) mit 60 % Ähnlichkeit auf Proteinebene. *BvHs4*-Homologe konnten in allen analysierten *Beta*-Arten gefunden werden. Bei der Analyse der Expressionsmuster von *Hs4*- und *BvHs4*-Homologen konnte ich substantielle Unterschiede zwischen den Spezies der zwei Gattungen feststellen. Während *Hs4*-Homologe stärker in Wurzeln exprimiert sind, sind *BvHs4*-Homologe vor allem in Blättern aktiv. Bei der Untersuchung der räumlich-zeitlichen Expressionsveränderung von *Hs4* konnte keine Aktivierung nach Nematodenbefall festgestellt werden.

In meinem zweiten Arbeitspaket habe ich *Arabidopsis T<sub>3</sub>* Linien, in denen *Hs4* entweder vom konstitutiven 35S- oder induzierbaren *Hs1*-Promoter gesteuert wurde, charakterisiert. Ich habe Linien mit signifikanter Nematodenresistenz im Vergleich zur anfälligen Kontrolle unter *in vitro*-Bedingungen gefunden. Die Resistenz war mit dem *Hs4*-Expressionslevel korreliert. Dementsprechend habe ich auch Linien mit niedriger *Hs4*-Expression und Weibchenzahlen ähnlich zur Kontrolle entdeckt. Als ich die besten Pflanzen beider Promoterkonstrukte miteinander verglichen habe, konnte ich zeigen, dass die *Hs1*-Promoter-gesteuerte *Hs4*-Expression zu höheren Nematodenresistenzleveln führt als die Genexpression vom 35S-Promoter. Unter semisterilen Bedingungen in hitzesteril gemachter Sand-Erde zeigte eine *Arabidopsis*-Linie eine signifikante Reduktion in RZN-Weibchenzahlen. Als die Linien jedoch unter nicht-sterilen *in vivo* Bedingungen analysiert wurden, zeigte keine Linie signifikante Weibchenreduktionen, während die Weibchenzahlen an allen Pflanzen niedriger waren als unter semisterilen Bedingungen. Daher kann von einer Stärkung der Pflanzenabwehr unter nicht-sterilen Bedingungen ausgegangen werden.

Im dritten Arbeitspaket habe ich die Ultrastruktur von Synzytien in hoch-exprimierenden 35S::*Hs4*- oder *Hs1*::*Hs4*-transgenen *Arabidopsis*-Linien analysiert. Wie erwartet waren Synzytien in anfälligen nicht-transgenen *Arabidopsis* mit dichtem Zytoplasma gefüllt, enthielten viele funktionale Mitochondrien, kleine Vakuolen und eine Vielzahl an glatten ER-Vesikeln. Im Gegensatz dazu begann die Bildung von Nekrosen in den resistenten Wurzeln bereits fünf Tage nach Inokulation und komplett degenerierte Synzytien konnten drei Tage

später entdeckt werden. Das Zytoplasma war mit großen, durchscheinenden Membranstrukturen und Vakuolen gefüllt. Weiterhin sammelte sich Kallose entlang der Zellwände. In vielen Fällen löste sich die Plasmamembran von der Zellwand und die Plastiden und Mitochondrien waren degradiert. Am auffälligsten war die Bildung sphärischer Membranaggregationen aus ER-Membranen mit Ribosomen entlang der äußeren Tubuli, während glattes ER, das von den Nematoden für die Synthese von Sterolen benötigt wird, fast komplett abwesend war. Die Aggregationen waren in unterschiedlich alten Synzytien in den transgenen Wurzeln auffindbar, wurden aber nie in benachbarten Wurzelzellen gefunden. Nur wenige Synzytiuminitialzellen entwickelten sich zu Synzytien und erlaubten es dem Nematoden, sich normal zu entwickeln. Sogar diese Synzytien enthielten charakteristische Membranaggregationen. Basierend auf diesen Ergebnissen kann angenommen werden, dass die Rhomboid-Protease Hs4 nach Nematodenbefall zur Bildung von Membranaggregationen führt. Wie die Funktion der *Hs4*-kodierte Protease durch Nematodenbefall verändert wird, konnte nicht geklärt werden.

Raps ist ein guter Wirt für *H. schachtii* und die Erzeugung RZN-resistenter Rapspflanzen könnte Fruchtfolgesysteme im Wechsel mit Zuckerrübe zukünftig vereinfachen. Daher habe ich Raps mit einem 35S::*Hs4*-Konstrukt transformiert. Ich erhielt eine transgene Pflanze, jedoch mit kaum nachweisbaren *Hs4*-Transkripten. Samen für zukünftige Studien wurden geerntet.

## 9 Appendix

All supplementary tables and figures are also provided electronically.

### 9.1 Supplementary Tables

**Supplementary Table 1:** Wild type plant material used in this study.

Species	Seed code	Other Code	Geographical Origin	Derived gene
<i>A. thaliana</i>	206176	Col-0		
<i>B. vulgaris</i> ssp. <i>adanensis</i>	082678	B0126	Turkey	<i>BaHs4</i> <sub>082678</sub>
	131202	BETA 1050	Turkey	<i>BaHs4</i> <sub>131202</sub>
<i>B. corolliflora</i>	210191	960025		<i>BcHs4</i>
<i>B. macrocarpa</i>	204612			<i>BmcHs4</i>
<i>B. macrorhiza</i>	960018	61245	Russia	<i>BmrHs4</i> <sub>960018</sub>
	960019	61254	Russia	
<i>B. vulgaris</i> ssp. <i>maritima</i>	080464	PI 546394	USA	<i>BmHs4</i> <sub>080464</sub>
	190649	BETA 1460	Greece	<i>BmHs4</i> <sub>190649</sub>
	960078		Tunisia	<i>BmHs4</i> <sub>960078</sub>
	190654		Spain	<i>BmHs4</i> <sub>190654</sub>
	930035	164/92	South Italy	<i>BmHs4</i> <sub>930035</sub>
	930052	255/90	Spain	<i>BmHs4</i> <sub>930052</sub>
<i>B. patula</i>	950409		Spain	<i>BmHs4</i> <sub>950409</sub>
	930113	56782	Madeira	<i>BpHs4</i>
<i>B. vulgaris</i>	93161			<i>BvHs4</i>
	940043	A906001; TR520		
	100043	A906001; TR520		<i>Hs4</i> <sub>TR520</sub>
	103800	Pro 4; TR363		<i>Hs4</i> <sub>TR363</sub>
	180819	Nemata		<i>Hs4</i> <sub>Nemata</sub>
<i>B. nana</i>	231995	W6 33921	Greece	
<i>Brassica napus</i>	230004	Westar		
<i>P. patellaris</i>	930065			<i>PpatHs4</i> <sub>930065</sub>
	100012	Ames4447		<i>PpatHs4</i> <sub>100012</sub>
	231993	BETA 10; IPK10	GDR	<i>PpatHs4</i> <sub>IPK10</sub>
	231994	BETA 534; IPK534	Spain	
<i>P. procumbens</i>	100810		Spain	<i>PpHs4</i> <sub>100810</sub>
	100820	B0623	Spain	<i>PpHs4</i> <sub>100820</sub>
	100821	B0624	Spain	<i>PpHs4</i> <sub>100821</sub>
	231990	BETA 419; IPK419	Spain	<i>PpHs4</i> <sub>IPK419</sub>
	231989	BETA 951; IPK951	Spain	<i>PpHs4</i> <sub>IPK951</sub>
	960006			<i>PwHs4</i> <sub>960006</sub>
<i>P. webbiana</i>	100832	B0596	Spain	<i>PwHs4</i> <sub>100832</sub>
	100833	B0602	Spain	<i>PwHs4</i> <sub>100833</sub>
	100002	BETA 0927	Spain	<i>PwHs4</i> <sub>100002</sub>
	231991	BETA 526; IPK526		<i>PwHs4</i> <sub>IPK526</sub>
	231992	BETA 927; IPK927	Spain	<i>PwHs4</i> <sub>IPK927</sub>

**Supplementary Table 2:** Primer sequences used for PCR, RT-qPCR, and sequencing. For the primers used only for sequencing of the different genes, no annealing temperature was determined.

<b>Purpose</b>	<b>Primer names</b>	<b>Sequence (5'-3')</b>	<b>Orientation</b>	<b>Annealing temperature (°C)</b>
clarification of intronic N-stretch in <i>Hs4</i>	AK_F2	AGGCACAGTGTTACTTTCACA	forward	58
	AS_R5	TGGGTATCTTCCACACTTGC	reverse	
amplification of <i>Hs4</i> and <i>BvHs4</i> simultaneously	AS_F7	GCAGTATTCTGGATTATTCTT	forward	58
	AS_R7	GAAAACAGCACCAGAGGCTCC	reverse	
specific amplification of whole <i>Hs4</i>	AK_F5	ATGGAGGCAGTATTCTGGAT	forward	58
	AK_R6	TCAGGGTGGCAAACAATTATTCA	reverse	
specific amplification of whole <i>Beta</i> homolog	AS_BvHs4_F1	ATGGCACAAGTCCAGCAACT	forward	62
	AS_BvHs4_R0	TTAACGGTTCCTATCAGGCTTC	reverse	
<i>GAPDH</i> in <i>Beta</i> species	BvGAPDH_F	GCTTTGAACGACCACTTCGC	forward	61
	BvGAPDH_R	ACGCCGAGAGCAACTTGAAC	reverse	
<i>GAPDH</i> in <i>Patellifolia</i> species	AS_BvPp_GAPDH_F	TTCCCACCGTTGATGTCTCT	forward	58
	AS_BvPp_GAPDH_R	ACCCCATTCGTTGTCATACCA	reverse	
<i>Hs4</i> amplification	AK_F7	CAGAACCCTATACTTGATCCA	forward	58
	AK_R5	CCTTTGTAACACAAAATGACCT	reverse	
<i>BvHs4</i> amplification	AS_BvHs4_F1	ATGGCACAAGTCCAGCAACT	forward	58
	AS_BvHs4_R7	AAAAGGGGATGGACGAGAGG	reverse	
<i>Hs1</i> amplification	AS_Hs1_F	CAGTACCAGTAATTTCCGGCG	forward	58
	AS_Hs1_R	TATGTACGGTCTAGCGTCCG	reverse	
<i>GAPDH</i> in <i>Arabidopsis</i>	B349	CTAGCTGCACCACTAACTGC	forward	54
	B350	CGTTAAGAGCTGGAAGCACC	reverse	
<i>GAPDH</i> in <i>B. napus</i>	Bnapus_GAPDH_F	CCGCTTCCTTCAACATCATT	forward	58
	Bnapus_GAPDH_R	ACGCCGAGAGCAACTTGAAC	reverse	
<i>DsRed2</i> amplification	AS_dsRed_F	AGTTCATGCGCTTCAAGGTG	forward	58
	AS_dsRed_R	TCTTGTAGTCGGGGATGTCTG	reverse	
<i>SDR</i> amplification, designed by K. Ille	SDR_F	TTCCTCTCTTCCCAATGCAC	forward	58
	SDR_R	AGGGAGGTATTCCCACCATT	reverse	
	AK_F2	AGGCACAGTGTTACTTTCACA	forward	N.A.

## Appendix

sequencing (clarification) of intronic N-stretch	AS_F1	TGGATCTTGTTTGATTTGTCTCG	forward	N.A.
	AS_R5	TGGGTTATCTTCCACACTTGC	reverse	N.A.
	AS_R6	CGTTACCTTTCCACCCCACT	reverse	N.A.
<i>Hs4</i> sequencing	AK_F6	GGAGGCAGTATTCTGGATTATT	forward	N.A.
	AK_F7	CAGAACCCTATACTTGATCCA	forward	N.A.
	AK_F9	GGAAGCTCGTCGAAGAGGAA	forward	N.A.
	AS_F7	GCAGTATTCTGGATTATTCTT	forward	N.A.
	AS_F8	GTACCTAGTACCTACAAGGCCA	forward	N.A.
	AS_F9	GGTGCAGTAGTTGGGATGAG	forward	N.A.
	AK_R1	GAGGCATGATAACCTGACCCT	reverse	N.A.
	AK_R2	GCAGAGGTCACAAATTGGTACC	reverse	N.A.
	AK_R3	CCAATTATAATGACAAAATGCAG	reverse	N.A.
	AK_R4	GTACAGAAAGAATAGGTTGTTG	reverse	N.A.
	AK_R5	CCTTTGTAACACAAAATGACCT	reverse	N.A.
	AK_R6	TCAGGGTGGCAAACAATTATTCA	reverse	N.A.
	AS_R7	GAAAACAGCACCAGAGGCTCC	reverse	N.A.
	AS_Hom_R1	TAGATGTGCTATGTGATTAAC	reverse	N.A.
	<i>Beta</i> homolog sequencing	AS_BvHs4_F1	ATGGCACAAGTCCAGCAACT	forward
AS_BvHs4_F2		CCTGTGCAATATTGTCATCTGTT	forward	N.A.
AS_BvHs4_F3		GAGGCTGCTGTTATCTTGCG	forward	N.A.
AS_BvHs4_F4		TTAGCTGTTAGATGCGTTCCA	forward	N.A.
AS_BvHs4_F5		TACTACTCCCTCCGTCCCAA	forward	N.A.
AS_BvHs4_F6		TTGTGACTGCTGCGTTTTGT	forward	N.A.
AS_F7		GCAGTATTCTGGATTATTCTT	forward	N.A.
AS_Hom_F1		CTTATATTAGGCCAATTCGTG	forward	N.A.
AS_Hom_F2		GGGAAGCTTGTGGAAGAGGAA	forward	N.A.
AS_BvHs4_R0		TTAACGGTTCCTATCAGGCTTC	reverse	N.A.
AS_BvHs4_R1		GGGATGGGACTGTTTCGAGAA	reverse	N.A.
AS_BvHs4_R2		GCTCTTTCACCAATTACTCCCC	reverse	N.A.
AS_BvHs4_R3		AGTTGCATGTCTCTCCACCA	reverse	N.A.
AS_BvHs4_R4		TGAGTGAACAAAGGAAACAAGTG	reverse	N.A.

AS_BvHs4_R7	AAAAGGGGATGGACGAGAGG	reverse	N.A.
AS_Hom_R1	TAGATGTGCTATGTGATTAAC	reverse	N.A.

**Supplementary Table 3:** Protein topology predictions for Hs4, a *P. procumbens* Hs4 (from accession 100810) with an additional amino acid, BvHs4, and Arabidopsis AtRBL11 as calculated by DeepTMHMM (Hallgren et al. 2022).

	<b>Hs4</b>	<b>PpHs4<sub>100810</sub></b>	<b>BvHs4</b>	<b>AtRBL11</b>
<b>Localization</b>	<b>Amino acid position</b>			
cytosol	1-2	1-2	1-106	1-84
transmembrane helix	3-17	3-17	107-123	85-101
lumen	18-53	18-53	124-155	102-133
transmembrane helix	54-65	54-65	156-167	134-145
cytosol	66-74	66-74	168-176	146-154
transmembrane helix	75-96	75-96	177-198	155-176
lumen	97-102	97-107	199-202	177-182
transmembrane helix	103-119	108-117	203-221	183-199
cytosol	120-136	118-137	222-228	200-204
transmembrane helix	137-155	138-156	229-248	205-226
lumen	156-174	157-175	249-268	227-246
transmembrane helix	175-195	176-196	269-286	247-264
cytosol	196-210	197-211	287-307	265-280

**Supplementary Table 4:** Results of the Arabidopsis floral dip transformation experiments. The Hs1::*Hs4* seeds until T<sub>3</sub> generation were produced by Johanna Leineweber (2020).

Vector	<b>35S::<i>Hs4</i></b>	<b>Hs1::<i>Hs4</i></b>
Dipped plants (T <sub>0</sub> )	7	26
Fluorescing seeds (T <sub>1</sub> )	73	39
T <sub>1</sub> plants harvested	8	12
T <sub>2</sub> families showing red fluorescence	6	9
T <sub>3</sub> families screened for fluorescence	47	62
Homozygous (homogenously fluorescing) T <sub>3</sub> families (T <sub>3</sub> lines)	6	11

**Supplementary Table 5:** Transgenic Hs1::*Hs4* Arabidopsis material generated in this study. Homogeneous means that the T<sub>3</sub> seeds showed homogeneous red fluorescence intensities (indicated in bold italics), whereas heterogeneous means that the T<sub>3</sub> seed fluorescence was not homogeneous. T<sub>3</sub> seeds not tested for fluorescence or germination rates are indicated by N.A. (not available).

Seed code T <sub>1</sub>	T1 plant	Seed code T <sub>2</sub>	T <sub>2</sub> plant	Seed code T <sub>3</sub>	T <sub>3</sub> seed fluorescence	T <sub>3</sub> germination rate	Comments
206177	206177/1	206178	206178/1	210632	heterogeneous	N.A.	
206177	206177/1	206178	206178/2	210633	heterogeneous	N.A.	
206177	206177/1	206178	206178/3	210634	heterogeneous	N.A.	
206177	206177/1	206178	206178/4	210635	heterogeneous	N.A.	
206177	206177/1	206178	206178/5	210636	<b>homogeneous</b>	85 %	
206177	206177/1	206178	206178/6	210637	<b>homogeneous</b>	100 %	
206177	206177/1	206178	206178/7	210638	heterogeneous	N.A.	
206177	206177/3	206179	206179/1	210639	<b>homogeneous</b>	100 %	no <i>Hs4</i> detectable in DNA
206177	206177/3	206179	206179/2	no seeds	N.A.	N.A.	
206177	206177/3	206179	206179/3	210640	no fluorescence	N.A.	
206177	206177/3	206179	206179/4	210641	no fluorescence	N.A.	
206177	206177/3	206179	206179/5	210642	no fluorescence	N.A.	
206177	206177/3	206179	206179/6	210643	heterogeneous	N.A.	
206177	206177/3	206179	206179/7	210644	heterogeneous	N.A.	
206177	206177/7	206180	206180/1	210645	<b>homogeneous</b>	100 %	no <i>Hs4</i> detectable in DNA
206177	206177/7	206180	206180/2	210646	heterogeneous	N.A.	
206177	206177/7	206180	206180/3	210647	<b>homogeneous</b>	100 %	no <i>Hs4</i> detectable in DNA
206177	206177/7	206180	206180/4	210648	heterogeneous	N.A.	
206177	206177/7	206180	206180/5	210649	heterogeneous	N.A.	
206177	206177/7	206180	206180/6	210650	heterogeneous	N.A.	
206177	206177/7	206180	206180/7	210651	<b>homogeneous</b>	100 %	no <i>Hs4</i> detectable in DNA
206177	206177/9	206181	206181/1	210652	heterogeneous	N.A.	
206177	206177/9	206181	206181/2	210653	heterogeneous	N.A.	
206177	206177/9	206181	206181/3	210654	<b>homogeneous</b>	95 %	
206177	206177/9	206181	206181/4	210655	heterogeneous	N.A.	
206177	206177/9	206181	206181/5	210656	heterogeneous	N.A.	
206177	206177/9	206181	206181/6	210657	<b>homogeneous</b>	95 %	no <i>Hs4</i> expression
206177	206177/9	206181	206181/7	210658	<b>homogeneous</b>	100 %	

206177	206177/10	206182	206182/1	210659	<i>homogeneous</i>	100 %	
206177	206177/10	206182	206182/2	210660	heterogeneous	N.A.	
206177	206177/10	206182	206182/3	210661	heterogeneous	N.A.	
206177	206177/10	206182	206182/4	210662	heterogeneous	N.A.	
206177	206177/10	206182	206182/5	210663	heterogeneous	N.A.	
206177	206177/10	206182	206182/6	210664	heterogeneous	N.A.	
206177	206177/10	206182	206182/7	210665	heterogeneous	N.A.	
206177	206177/11	206183	206183/1	210666	heterogeneous	N.A.	
206177	206177/11	206183	206183/2	210667	heterogeneous	N.A.	
206177	206177/11	206183	206183/3	210668	heterogeneous	N.A.	
206177	206177/11	206183	206183/4	210669	heterogeneous	N.A.	
206177	206177/11	206183	206183/5	210670	heterogeneous	N.A.	
206177	206177/11	206183	206183/6	210671	heterogeneous	N.A.	
206177	206177/11	206183	206183/7	210672	heterogeneous	N.A.	
206177	206177/13	206184	206184/1	210673	heterogeneous	100 %	
206177	206177/13	206184	206184/2	210674	heterogeneous	N.A.	
206177	206177/13	206184	206184/3	210675	heterogeneous	N.A.	
206177	206177/13	206184	206184/4	210676	heterogeneous	N.A.	
206177	206177/13	206184	206184/5	210677	heterogeneous	N.A.	
206177	206177/13	206184	206184/6	210678	<i>homogeneous</i>	100 %	
206177	206177/13	206184	206184/7	210679	heterogeneous	N.A.	
206177	206177/15	206185	206185/1	210680	heterogeneous	N.A.	
206177	206177/15	206185	206185/2	210681	heterogeneous	N.A.	
206177	206177/15	206185	206185/3	210682	heterogeneous	N.A.	
206177	206177/15	206185	206185/4	210683	heterogeneous	N.A.	
206177	206177/15	206185	206185/5	210684	heterogeneous	N.A.	
206177	206177/15	206185	206185/6	210685	heterogeneous	N.A.	
206177	206177/15	206185	206185/7	210686	heterogeneous	N.A.	
206177	206177/17	206186	206186/1	210687	heterogeneous	N.A.	
206177	206177/17	206186	206186/2	210688	heterogeneous	N.A.	
206177	206177/17	206186	206186/3	210689	heterogeneous	N.A.	
206177	206177/17	206186	206186/4	210690	heterogeneous	N.A.	
206177	206177/17	206186	206186/5	210691	heterogeneous	N.A.	

Appendix

206177	206177/17	206186	206186/6	210692	heterogeneous	N.A.	
206177	206177/17	206186	206186/7	210693	heterogeneous	N.A.	

**Supplementary Table 6:** Transgenic 35S::*Hs4* Arabidopsis material generated in this study. Homogeneous means that the T<sub>3</sub> seeds showed homogeneous red fluorescence intensities (indicated in bold italics), whereas heterogeneous means that the T<sub>3</sub> seed fluorescence was not homogeneous. T<sub>3</sub> seeds not tested for fluorescence or germination rates are indicated by N.A. (not available).

Seed code T <sub>1</sub>	T <sub>1</sub> plant	Seed code T <sub>2</sub>	T <sub>2</sub> plant	Seed code T <sub>3</sub>	T <sub>3</sub> seed fluorescence	T <sub>3</sub> germination rate	Comments
226880	226880/1	226882	226882/1	228921	<i>homogeneous</i>	100 %	
226880	226880/1	226882	226882/2	228922	heterogeneous	N.A.	
226880	226880/1	226882	226882/3	228923	heterogeneous	N.A.	
226880	226880/1	226882	226882/4	228924	<i>homogeneous</i>	100 %	
226880	226880/1	226882	226882/5	228925	heterogeneous	N.A.	
226880	226880/1	226882	226882/6	228926	heterogeneous	N.A.	
226880	226880/1	226882	226882/7	228927	heterogeneous	N.A.	
226880	226880/4	226883	226883/1	228928	heterogeneous	N.A.	
226880	226880/4	226883	226883/2	228929	heterogeneous	N.A.	
226880	226880/4	226883	226883/3	228930	heterogeneous	N.A.	
226880	226880/4	226883	226883/4	228931	heterogeneous	N.A.	
226880	226880/4	226883	226883/5	228932	heterogeneous	N.A.	
226880	226880/4	226883	226883/6	228933	heterogeneous	N.A.	
226880	226880/4	226883	226883/7	228934	<i>homogeneous</i>	75 %	
226880	226880/6	226885	226885/1	228935	heterogeneous	N.A.	
226880	226880/6	226885	226885/2	228936	<i>homogeneous</i>	90 %	
226880	226880/6	226885	226885/3	228937	heterogeneous	N.A.	
226880	226880/6	226885	226885/4	228938	heterogeneous	N.A.	
226880	226880/6	226885	226885/5	228939	heterogeneous	N.A.	
226880	226880/6	226885	226885/6	228940	heterogeneous	N.A.	
226880	226880/6	226885	226885/7	228941	heterogeneous	N.A.	
226880	226880/6	226885	226885/8	228942	heterogeneous	N.A.	
226880	226880/6	226885	226885/9	228943	heterogeneous	N.A.	
226880	226880/7	226886	226886/1	228944	<i>homogeneous</i>	100 %	
226880	226880/7	226886	226886/2	228945	heterogeneous	N.A.	
226880	226880/7	226886	226886/3	228946	heterogeneous	N.A.	
226880	226880/7	226886	226886/4	228947	heterogeneous	N.A.	

Appendix

226880	226880/7	226886	226886/5	228948	heterogeneous	N.A.	
226880	226880/7	226886	226886/6	228949	heterogeneous	N.A.	
226880	226880/7	226886	226886/7	228950	heterogeneous	N.A.	
226880	226880/7	226886	226886/8	228951	heterogeneous	N.A.	
226880	226880/8	226887	226887/1	228952	heterogeneous	N.A.	
226880	226880/8	226887	226887/2	228953	heterogeneous	N.A.	
226880	226880/8	226887	226887/3	228954	heterogeneous	N.A.	
226880	226880/8	226887	226887/4	228955	heterogeneous	N.A.	
226880	226880/8	226887	226887/5	228956	<b>homogeneous</b>	100 %	
226880	226880/8	226887	226887/6	228957	heterogeneous	N.A.	
226880	226880/8	226887	226887/7	228958	heterogeneous	N.A.	
226880	226880/8	226887	226887/8	228959	heterogeneous	N.A.	
226880	226880/8	226887	226887/9	228960	heterogeneous	N.A.	
226880	226880/9	226888	226888/1	228961	heterogeneous	N.A.	very low fluorescence intensity
226880	226880/9	226888	226888/2	228962	heterogeneous	N.A.	very low fluorescence intensity
226880	226880/9	226888	226888/3	228963	heterogeneous	N.A.	very low fluorescence intensity
226880	226880/9	226888	226888/4	228964	heterogeneous	N.A.	very low fluorescence intensity
226880	226880/9	226888	226888/5	228965	heterogeneous	N.A.	very low fluorescence intensity
226880	226880/9	226888	226888/6	228966	heterogeneous	N.A.	very low fluorescence intensity
226880	226880/9	226888	226888/7	228967	heterogeneous	N.A.	very low fluorescence intensity

**Supplementary Table 7:** Number of developing females counted 21 dpi at roots of eleven homozygous *Hs1::Hs4* T<sub>3</sub> lines and Col-0 as control. The plants were grown in 9 cm Petri dishes under sterile conditions and inoculated with 200 *H. schachtii* J2 larvae.

Biological replicate	T <sub>3</sub> seed code											Col-0
	210636	210637	210639	210645	210647	210651	210654	210657	210658	210659	210678	
1	1	0	23	4	7	10	4	4	0	2	9	6
2	0	0	0	11	4	3	2	3	3	6	6	6
3	2	0	12	20	11	5	0	11	8	7	2	8
4	3	1	5	5	4	4	3	2	5	6	15	5
5	1	0	11	12	4	8	6	5	1	1	1	10
6	0		6	9	2	14	2	10	0	1	2	7
7				9		0		2		0		10
8										1		6
9												1
10												1
11												0
12												3
13												9
14												15
15												8
16												4
17												7
18												4
<b>mean</b>	1.7	0.2	9.5	10	5.3	6.3	2.8	5.3	2.8	3	5.8	6.1

Appendix

**Supplementary Table 8:** Genotypic segregation for *Hs4* in the transgenic Arabidopsis T<sub>2</sub> generation. N.A. indicates test data not generated.

Genotype	T <sub>2</sub> seed code	Total number of plants	<i>Hs4</i> <sup>+</sup>	<i>Hs4</i> <sup>-</sup>	$\chi^2$ test for H <sub>0</sub> = 3:1 ( <i>Hs4</i> <sup>+</sup> vs. <i>Hs4</i> <sup>-</sup> ) <sup>a</sup>	$\chi^2$ test for H <sub>0</sub> = 15:1 ( <i>Hs4</i> <sup>+</sup> vs. <i>Hs4</i> <sup>-</sup> ) <sup>b</sup>
<i>Hs1::Hs4</i>	206178	38	36	2	7.89	0.06*
<i>Hs1::Hs4</i>	206181	37	34	3	5.63	0.22*
<i>Hs1::Hs4</i>	206182	37	23	14	3.25*	N.A.
<i>Hs1::Hs4</i>	206184	40	31	9	0.13*	N.A.
<i>35S::Hs4</i>	226882	39	26	13	1.44*	N.A.
<i>35S::Hs4</i>	226883	3	2	1	0.11*	N.A.
<i>35S::Hs4</i>	226885	40	34	6	2.13*	N.A.
<i>35S::Hs4</i>	226886	37	29	8	0.23*	N.A.

<sup>a</sup> H<sub>0</sub>, null hypothesis for one transgene integration

<sup>b</sup> H<sub>0</sub>, null hypothesis for two transgene integrations

\*  $\alpha = 0.05$

**Supplementary Table 9:** Germination rates of transgenic Arabidopsis T<sub>3</sub> lines.

Genotype	T <sub>3</sub> seed code	# of seeds sown	# of seeds germinated	Germination rate [%]
<i>35S::Hs4</i>	228921	10	10	100
	228924	12	12	100
	228934	12	4	33
	228936	10	10	100
	228944	12	12	100
	228956	11	11	100
<i>Hs1::Hs4</i>	210636	12	4	33
	210637	8	8	100
	210654	11	10	91
	210659	11	9	82
	210678	11	10	91
wild type	Col-0	11	8	73

**Supplementary Table 10:** Results of the preliminary semi-sterile *in vivo* experiment. Plants of the Hs1::*Hs4* transgenic line 210637 and Col-0 were inoculated with 250 *H. schachtii* larvae in semi-sterile sand-soil-filled plastic tubes in a sterilized climate chamber. Developing females were counted at 28 dpi.

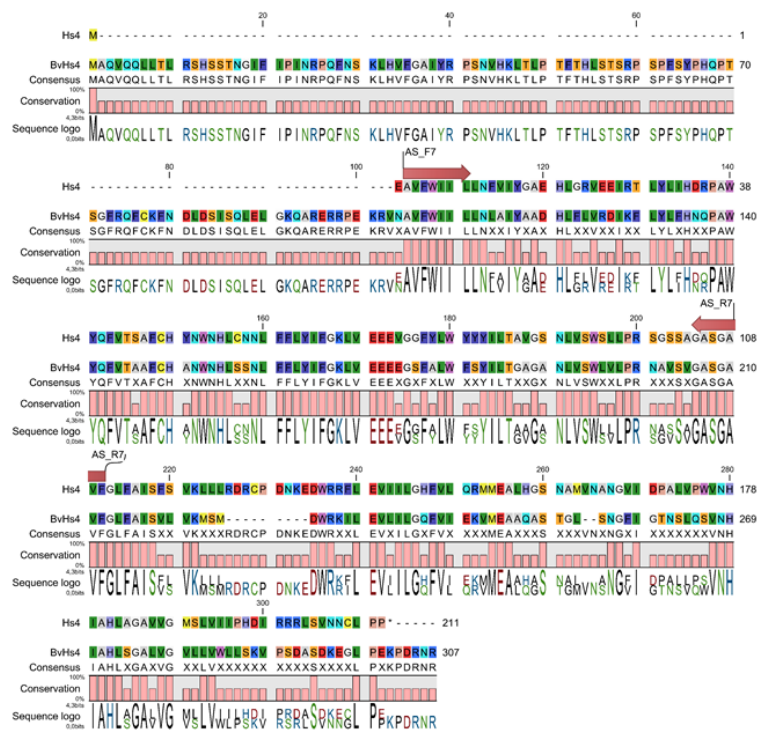
Genotype	T <sub>3</sub> seed code	Biological replicate	# developing females
Hs1:: <i>Hs4</i>	210637	1	24
		2	5
		3	14
		4	13
		5	14
wild type	Col-0	1	46
		2	42
		3	40
		4	70
		5	65
		6	32

**Supplementary Table 11:** Overview of the experiment to study syncytia under the electron microscope. The number of plants investigated, the syncytia embedded, and finally analyzed in the transgenic lines 228934 (35S::*Hs4*) and 210637 (Hs1::*Hs4*) and the wild type Col-0 are given. Plants were cultured in sterile 6-well plates and inoculated with 250 *H. schachtii* J2 larvae. N.A. indicates roots or syncytia not available or analyzed.

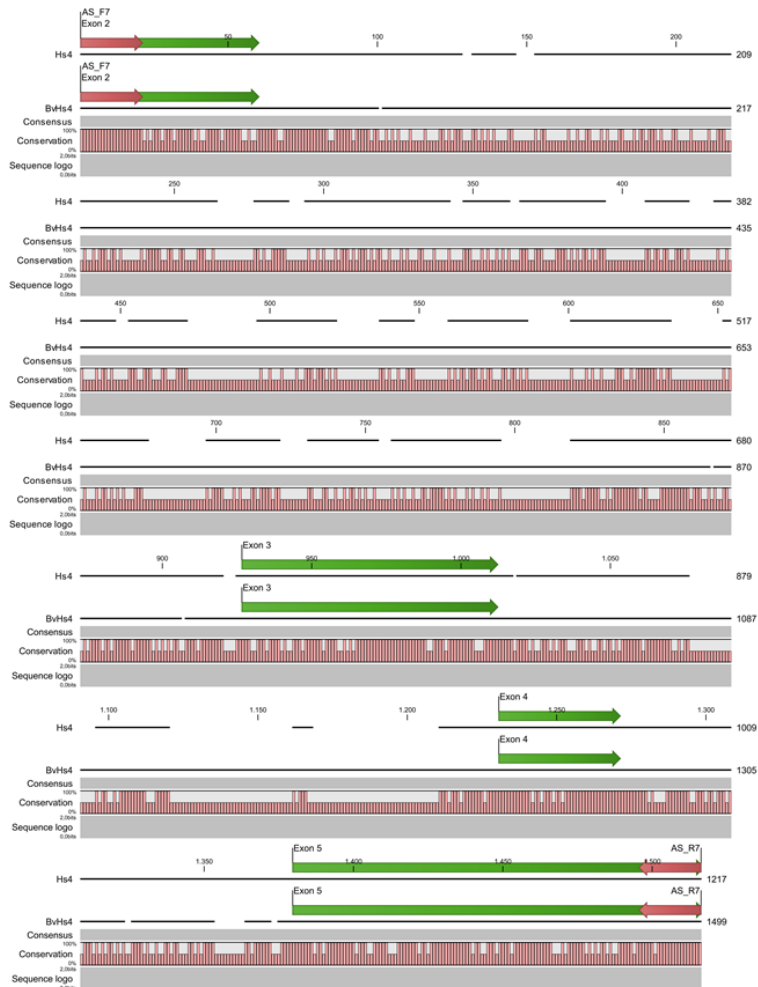
sampling point	5 dpi			8 dpi			9 dpi			11 dpi			26 dpi		
seed code	228 934	210 637	Col-0												
# plants investigated	10	14	12	9	13	11	6	N.A.	6	9	13	11	N.A.	6	6
# syncytia embedded	0	1	0	0	1	1	2	N.A.	5	4	4	3	N.A.	4	5
# syncytia analyzed (# layers investigated)	N.A.	1 (2)	N.A.	N.A.	1	N.A.	1	N.A.	1	2	2 (1-2)	N.A.	N.A.	2	2

## 9.2 Supplementary Figures

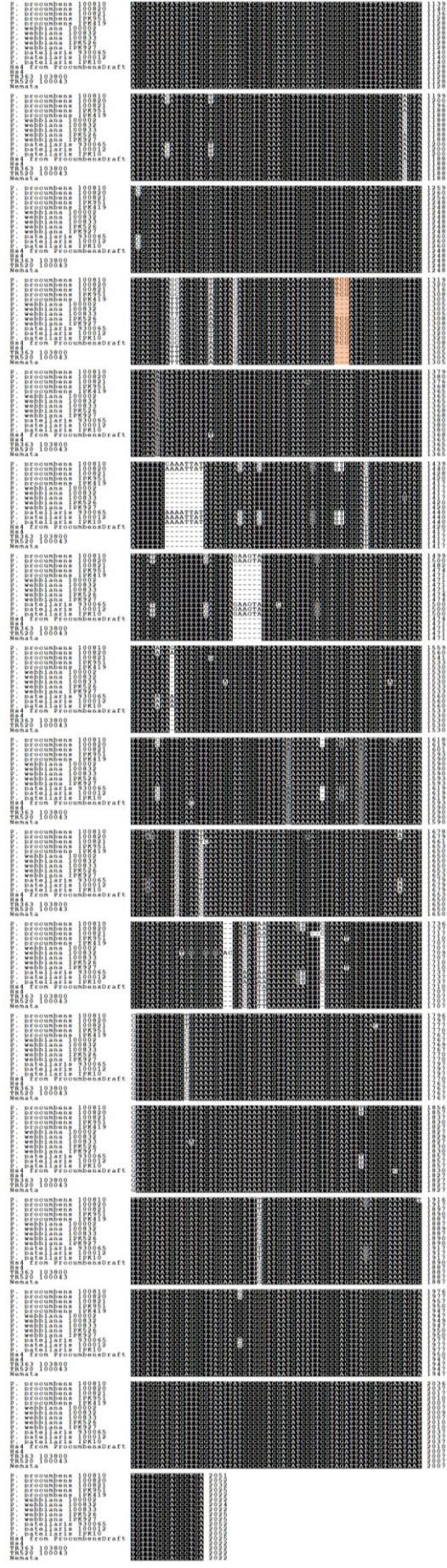
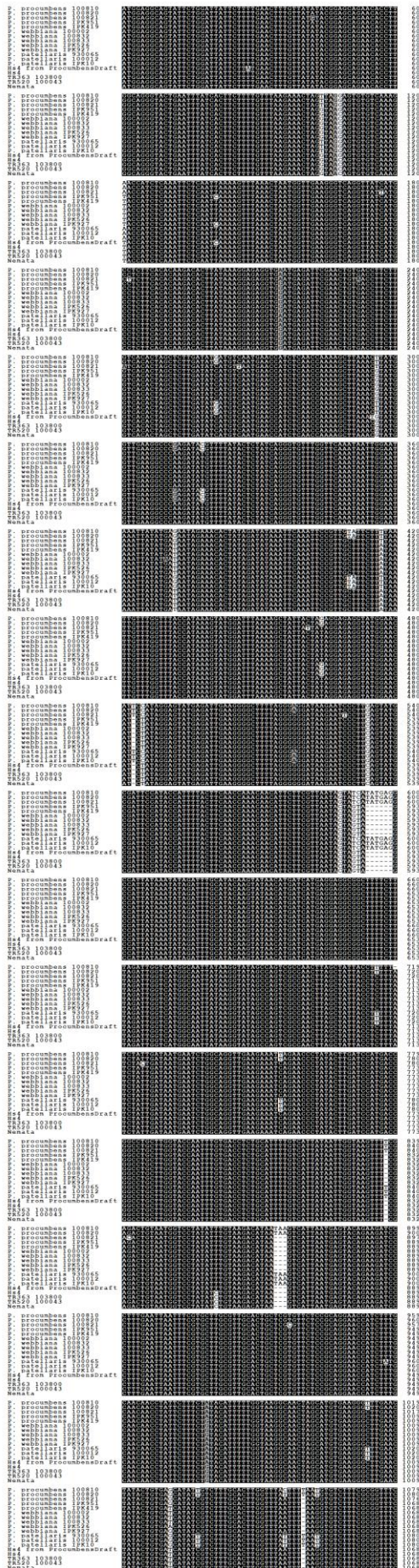
**A**



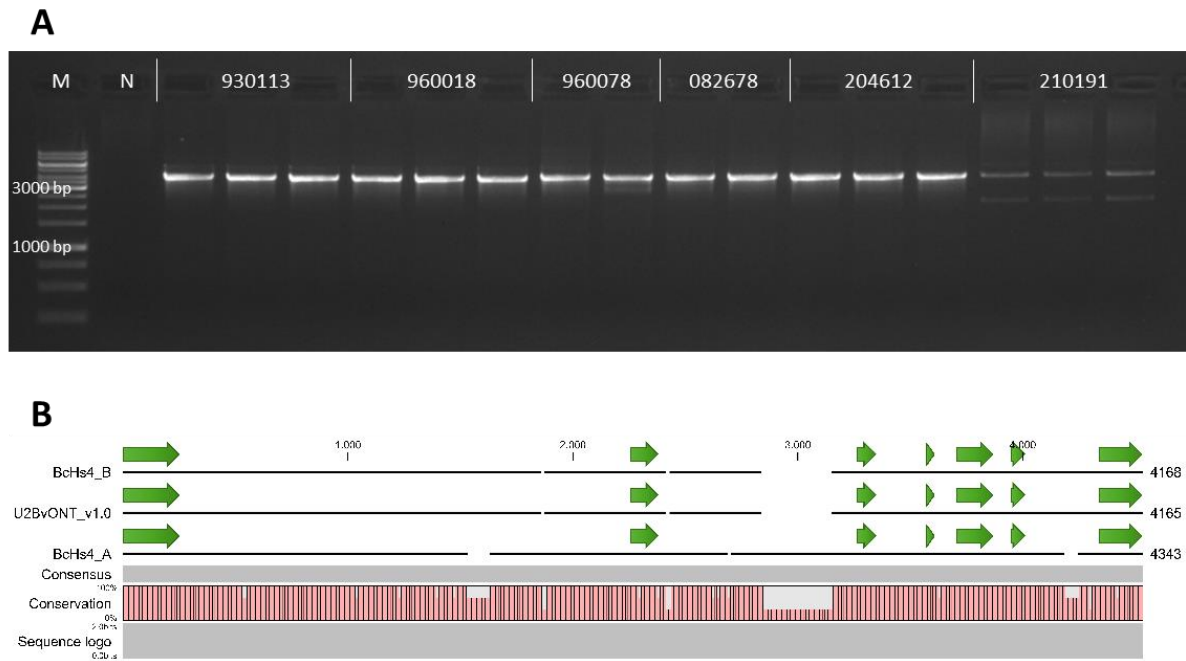
**B**



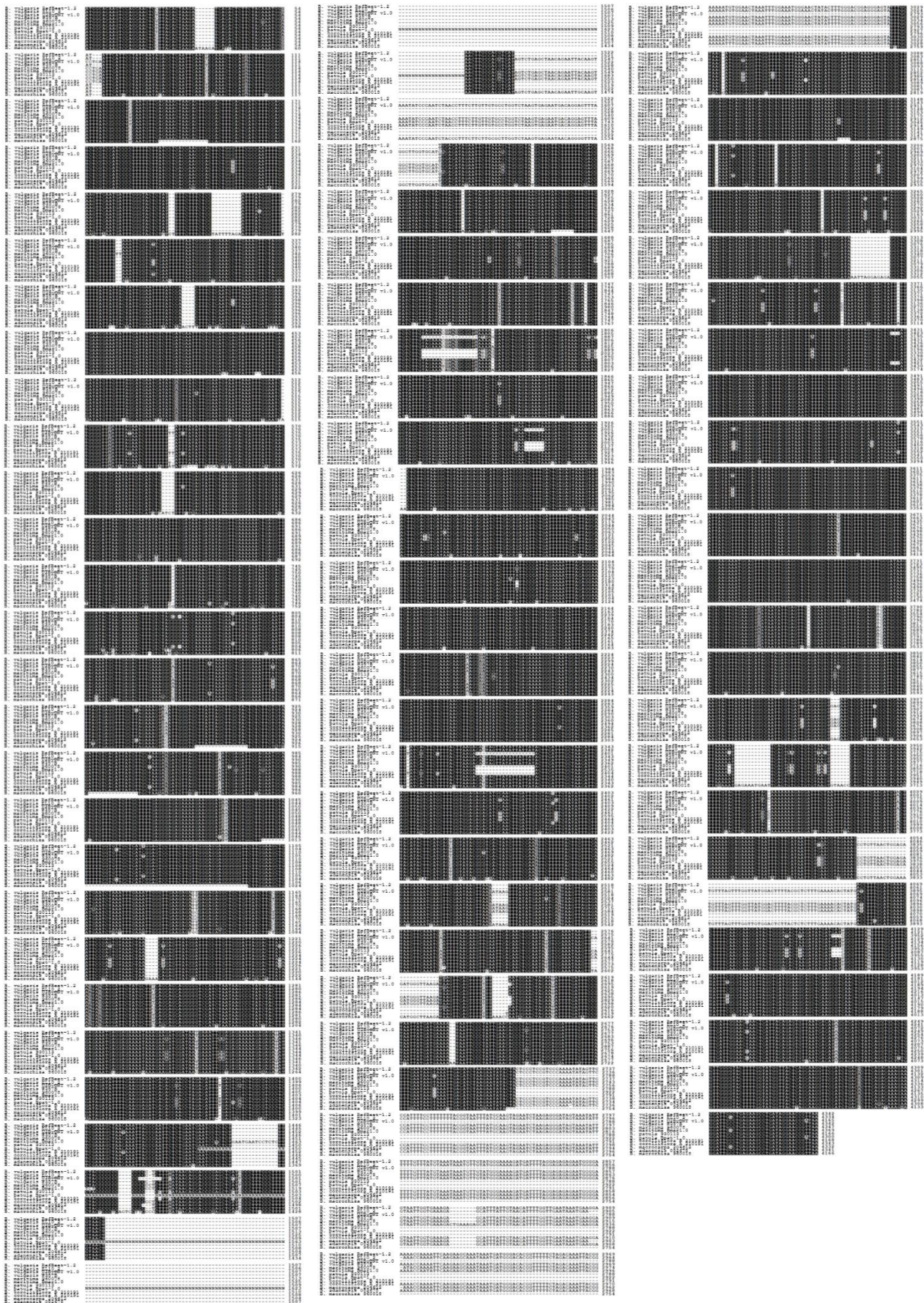
**Supplementary Figure 1:** Location of the AS\_F7/AS\_R7 primers. (A) The primers are designed to bind in a region conserved between Hs4 and BvHs4 proteins. (B) At the sequence level, single bases differ, resulting in a wobble base integrated into the reverse primer. The conservation level between the two sequences is illustrated by the “Conservation” bars at the bottom of the sequences. Bars of full height indicate the presence of the same amino acid or nucleotide, respectively, in both sequences, while halved bars indicate that only one of the sequences contains the according amino acid or nucleotide. The graphics were created using the CLC Main Workbench 20.



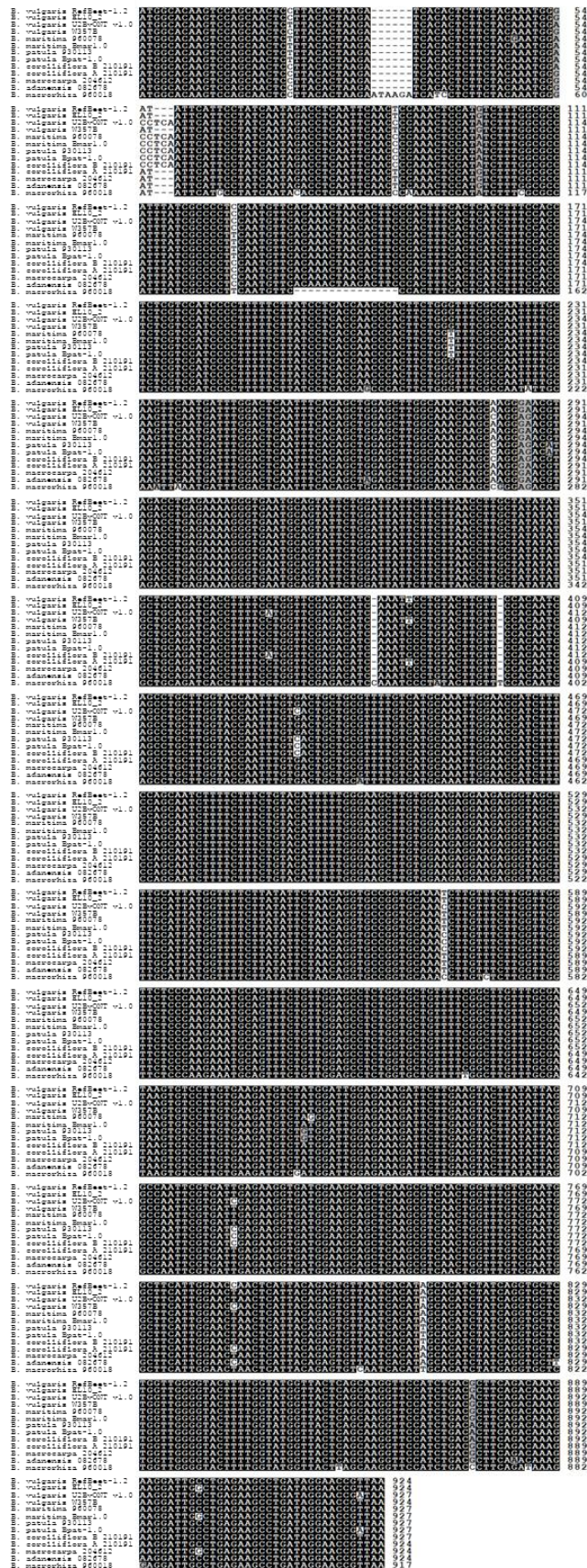
**Supplementary Figure 2:** Alignment of genomic sequences of *Hs4* and its homologs from different *Patellifolia* species and accessions. The orange box highlights the exonic insertion/deletion in *Patellifolia* species. The graphic was created using pyBoxshade v. 1.2 (mdbaron42 2021).



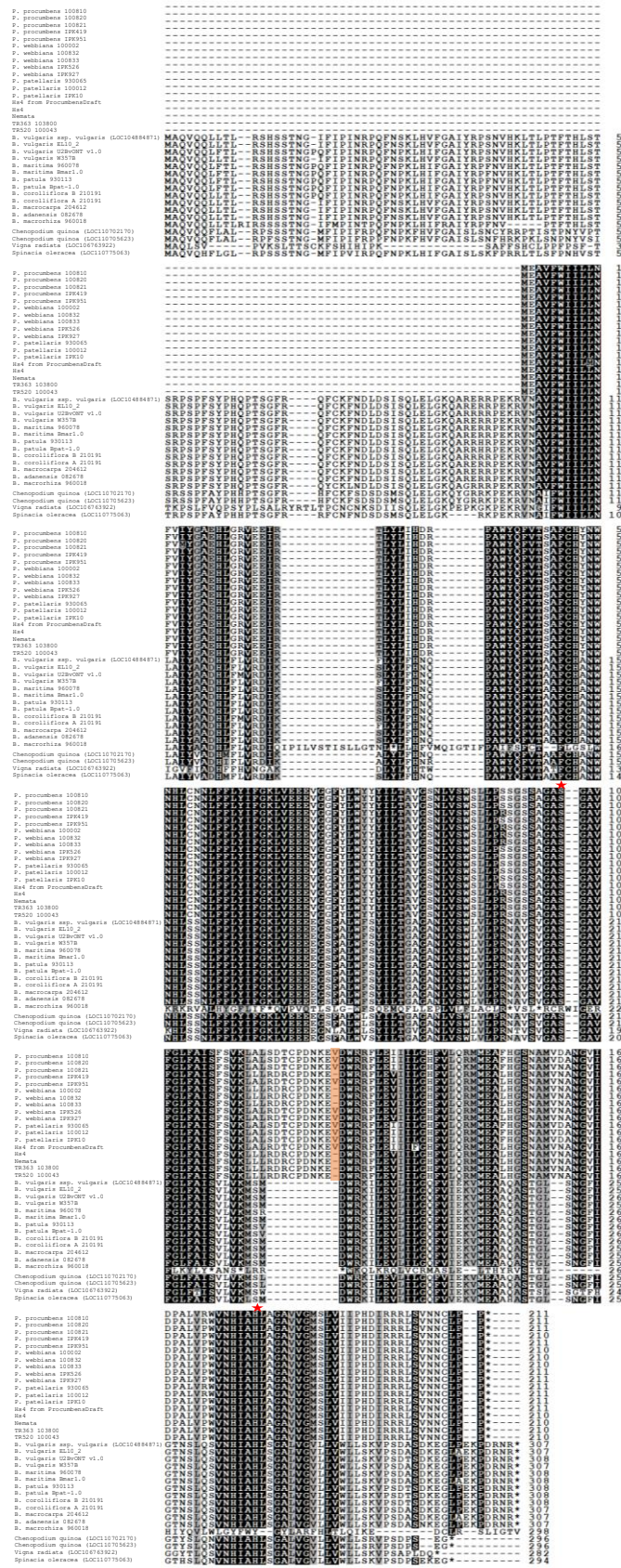
**Supplementary Figure 3:** Analysis of *BvHs4* homologs. (A) Agarose gel electrophoresis (1 %, 90V, 30 min) of a PCR amplifying the whole *BvHs4* homolog from *B. patula* (930113), *B. macrorhiza* (960018), *B. vulgaris* ssp. *maritima* (960078), *B. macrocarpa* (204612) and *B. corolliflora* (210191). (B) Alignment of two *BvHs4* homolog sequences derived from *B. corolliflora* and the reference sequence of the tolerant sugar beet cultivar U2Bv.



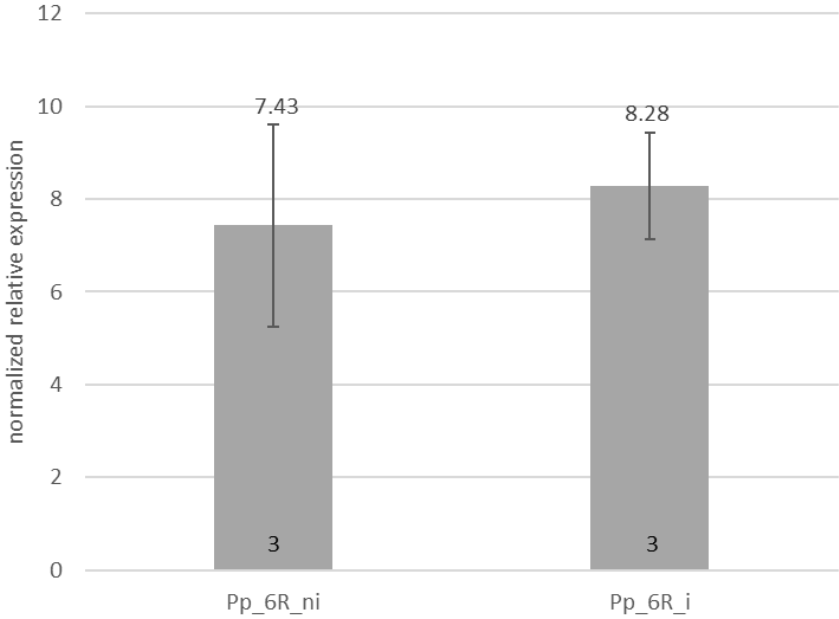
**Supplementary Figure 4:** Alignment of genomic sequences of *BvHs4* from RefBeet-1.2 and its homologs from different *Beta* species and accessions. The graphic was created using pyBoxshade v. 1.2 (mdbaron42 2021).



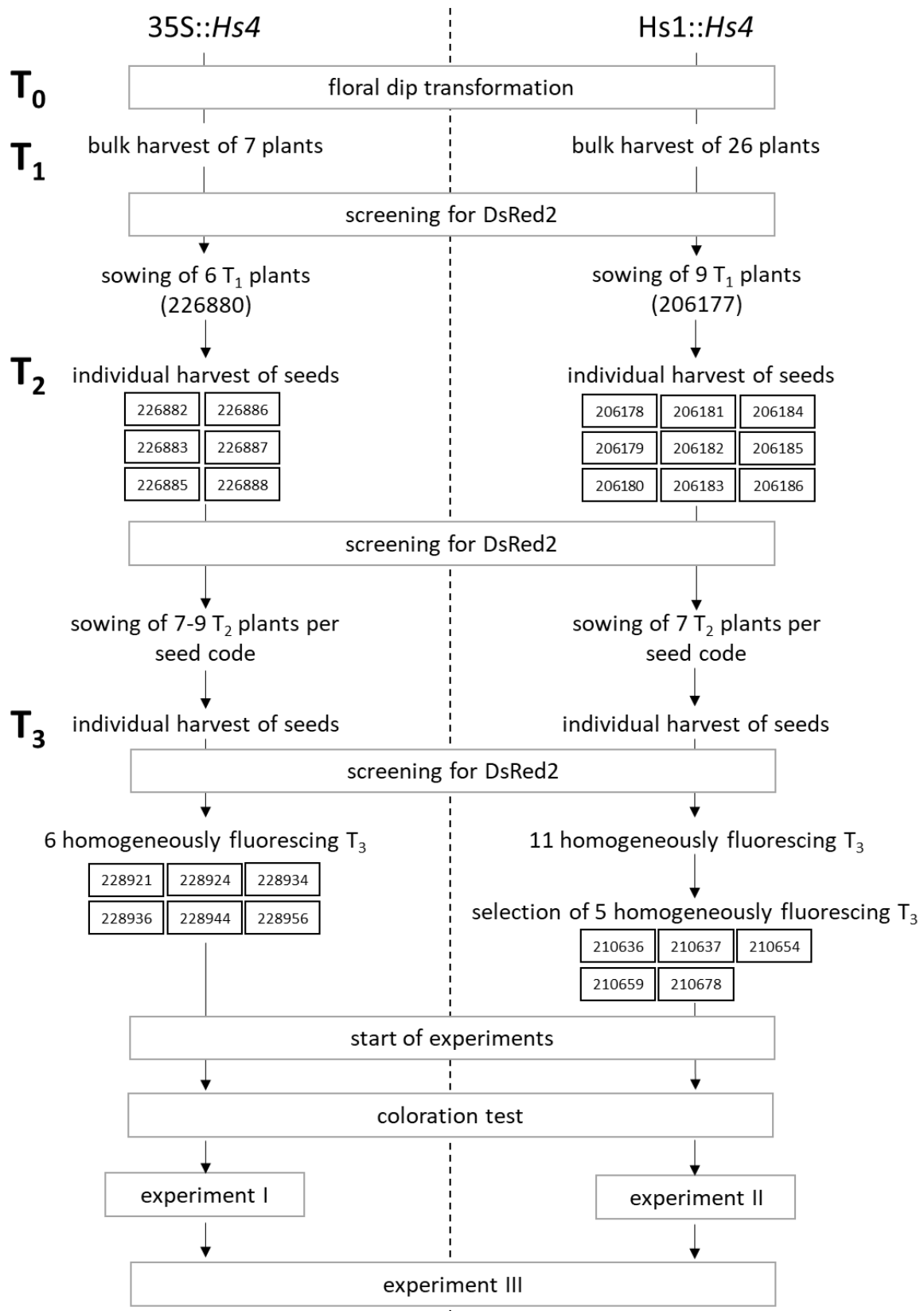
**Supplementary Figure 5:** Alignment of protein-coding sequences of *BvHs4* and its homologs from different *Beta* species and accessions. The graphic was created using pyBoxshade v. 1.2 (mdbaron42 2021).



**Supplementary Figure 6:** Alignment of polypeptide sequences of Hs4, BvHs4, and their homologs. The orange box highlights the additional amino acid present in some *Patellifolia* species and accessions. The active sites (S106 and H181; as in Kumar et al. 2021) are indicated with red stars. Quinoa (*Chenopodium quinoa*), mung bean (*Vigna radiata*), and spinach (*Spinacia oleracea*) were used as outgroups. The graphic was created using pyBoxshade v. 1.2 (mdbaron42 2021).

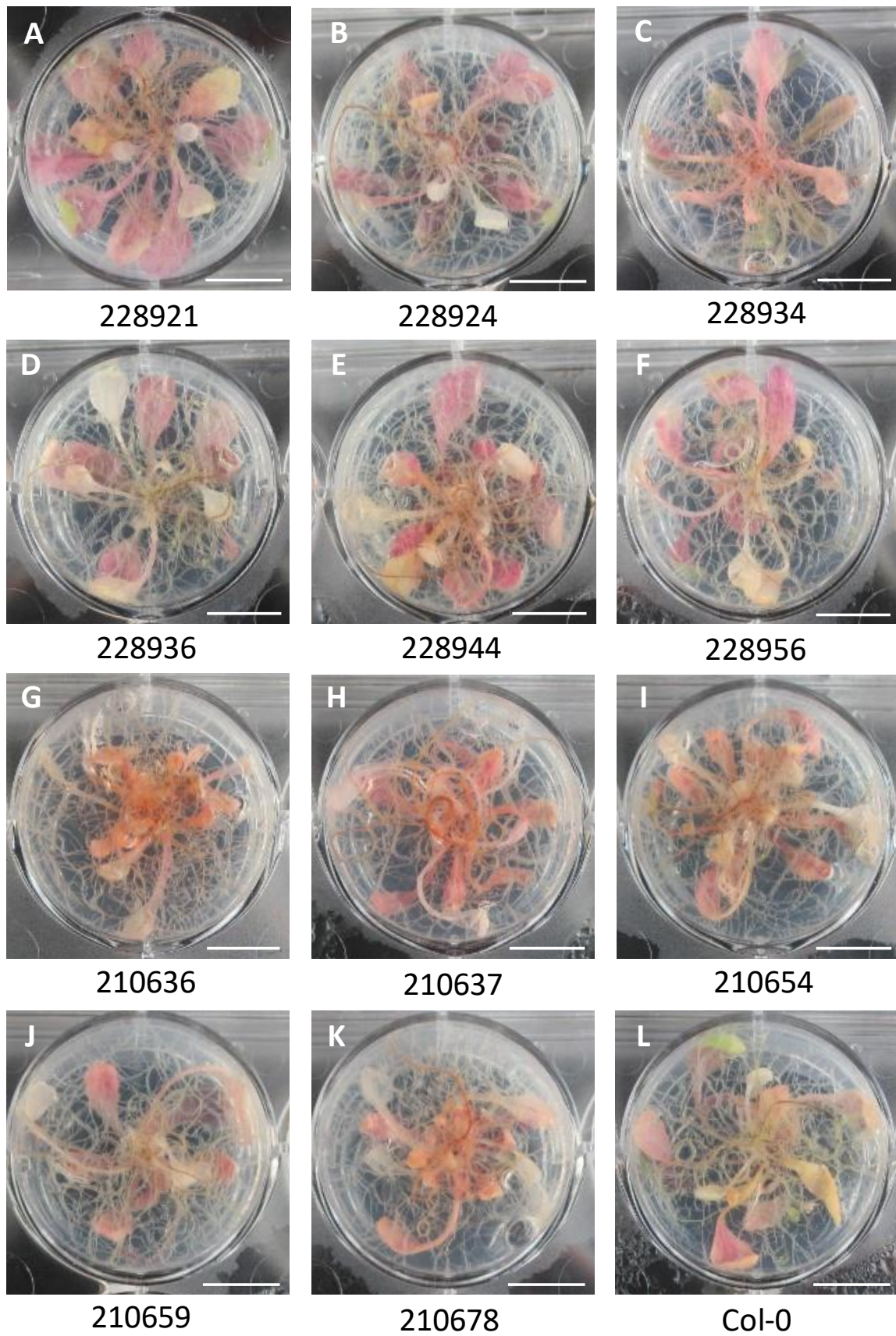


**Supplementary Figure 7:** Expression of *Hs1* in non-inoculated (ni) and inoculated (i) *P. procumbens* roots 28 dpi as determined by RT-qPCR (primer: AS\_Hs1\_F/AS\_Hs1\_R; reference gene: *GAPDH*). The number of biological replicates is given at the bottom of each bar. The mean expression is shown above each bar.



**Supplementary Figure 8:** Schematic workflow of the Arabidopsis transformation, the generation of the  $T_3$  lines, and the experiments I-III conducted under sterile *in vitro* conditions.

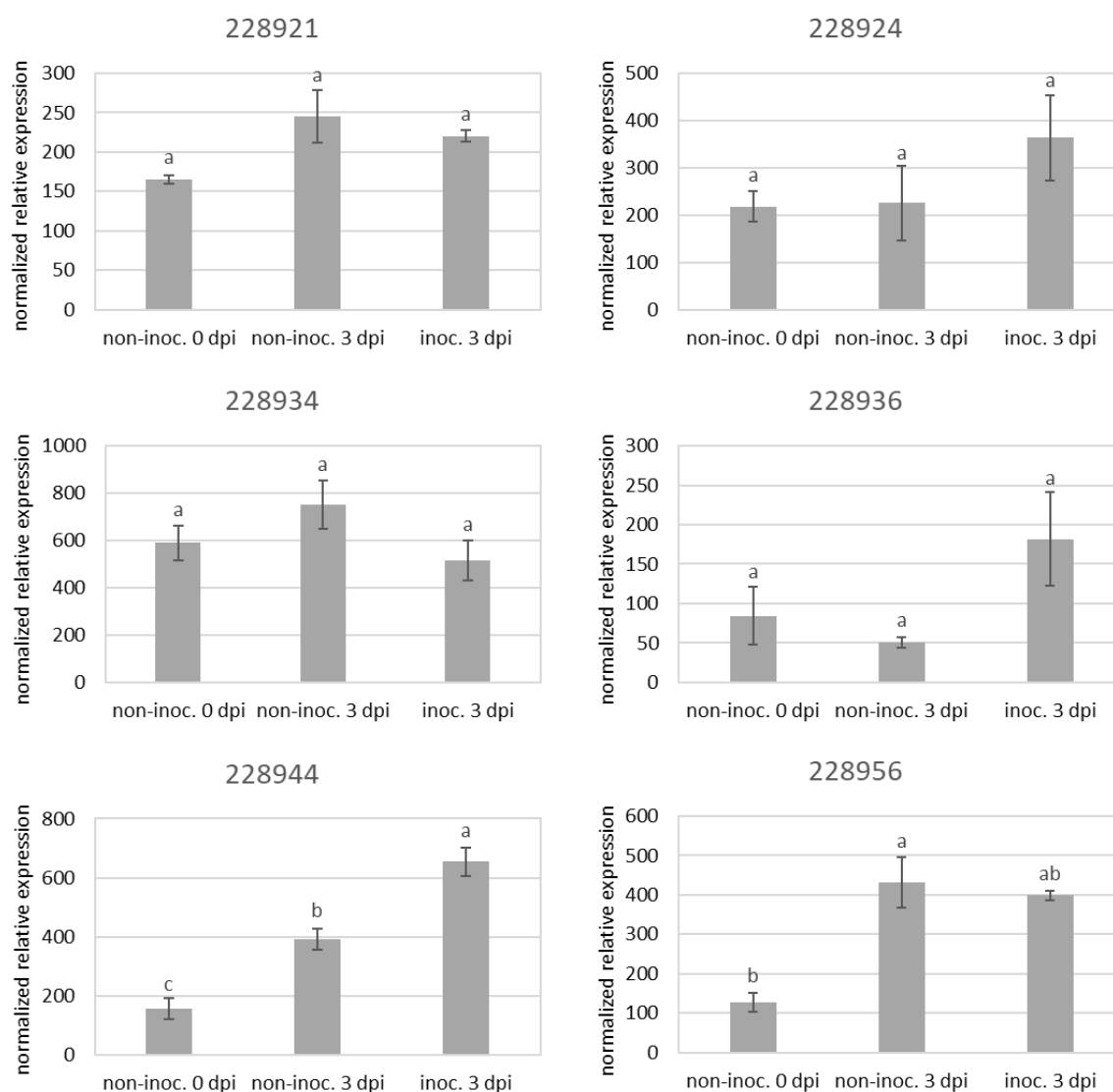




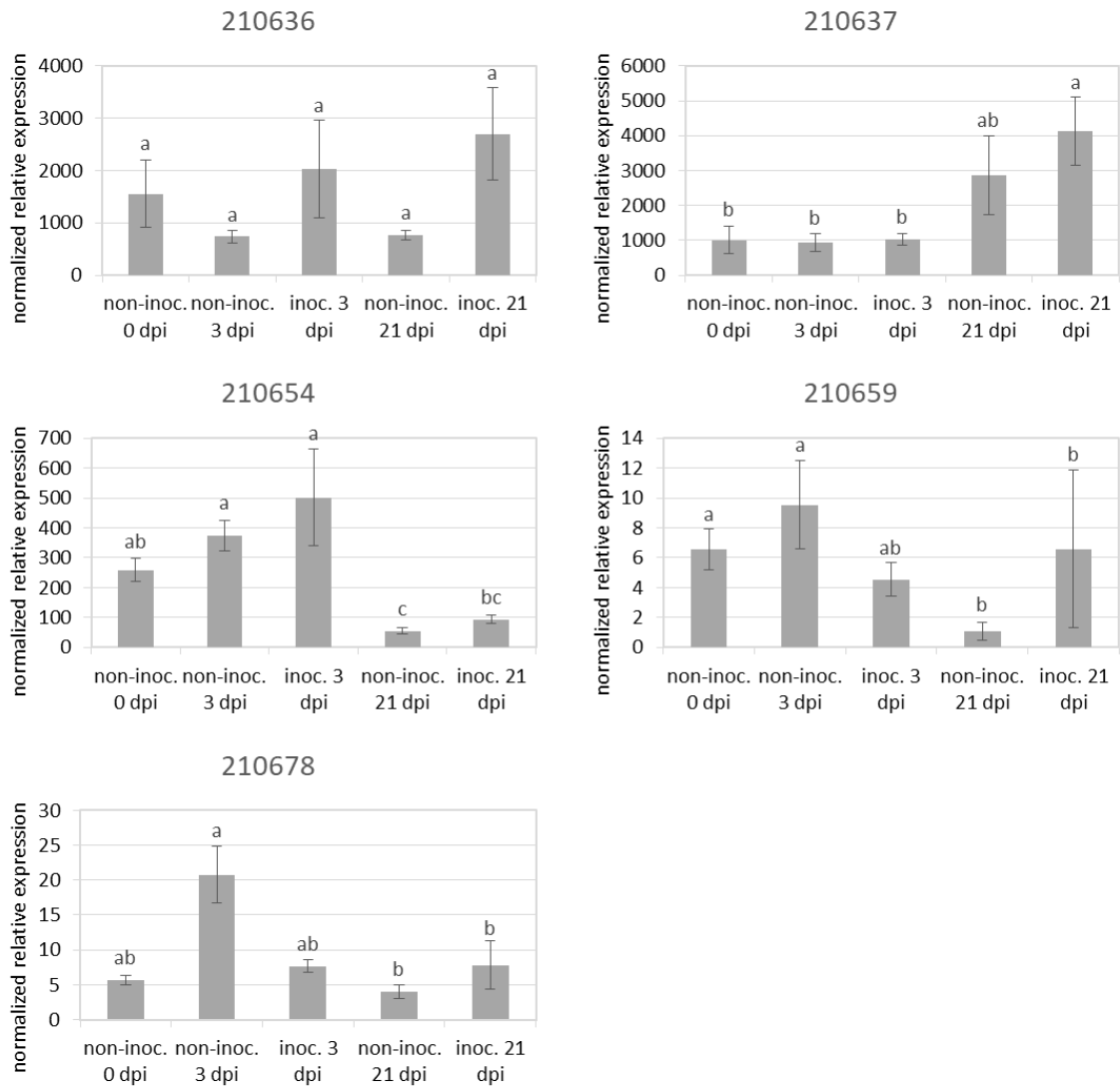
**Supplementary Figure 10:** Root and leaf colors of six 35S::Hs4 (A-F) and five Hs1::Hs4 (G-K) transgenic Arabidopsis lines compared to Col-0 (L) at 21 days post-inoculation in 6-well plates. Bars: 1 cm.



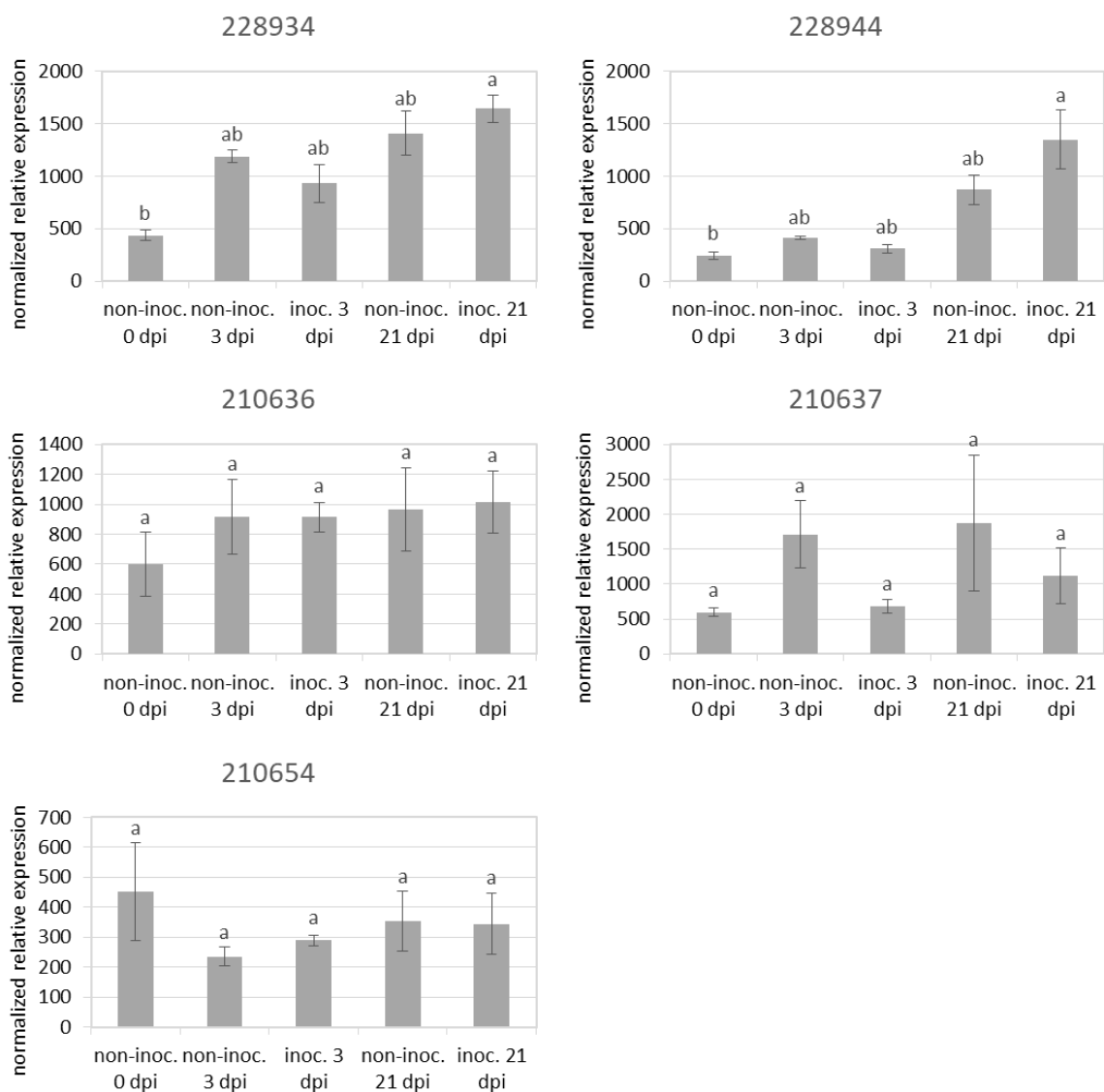
**Supplementary Figure 11:** Pink root color of the 35S::*Hs4* transgenic line 228934 at three weeks post-inoculation. The arrows highlight the pink coloration in young roots and points of emerging lateral roots. Bar: 1000  $\mu$ m.



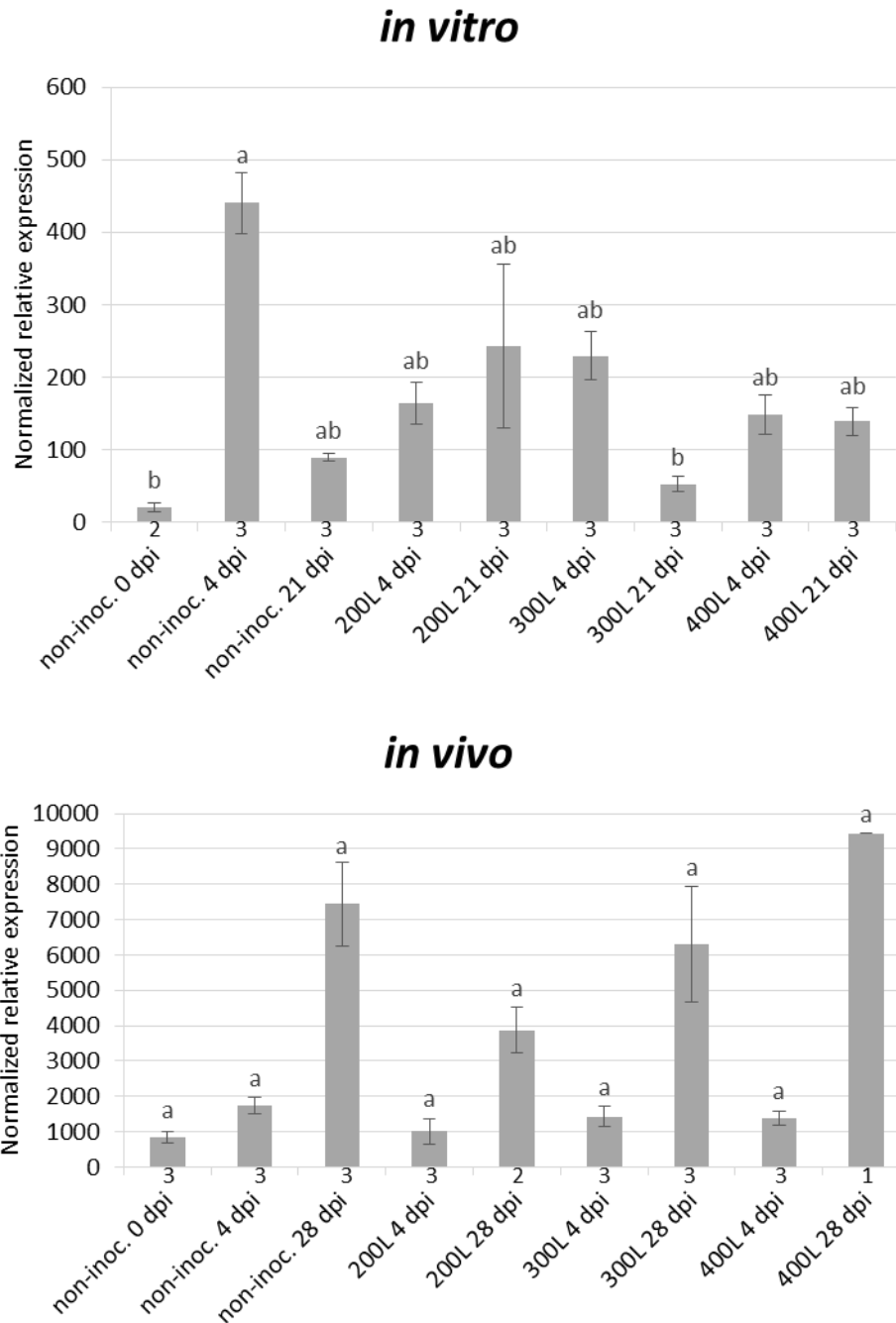
**Supplementary Figure 12:** Expression of *Hs4* in six different 35S::*Hs4*-transgenic Arabidopsis lines before inoculation (non-inoc. 0 dpi), and 3 dpi in non-inoculated (non-inoc.) and inoculated (inoc.) plant roots as determined by RT-qPCR (primer: AK\_F7/AK\_R5; reference gene: *GAPDH*) in experiment I. The plants were cultivated in sterile 6-well plates. Three biological replicates per time point were used (exception: 2 replicates for 228956 inoc. 3 dpi). Statistical significances were calculated using a one-way ANOVA, followed by the Tukey HSD Test. Standard deviations are given as SEM.



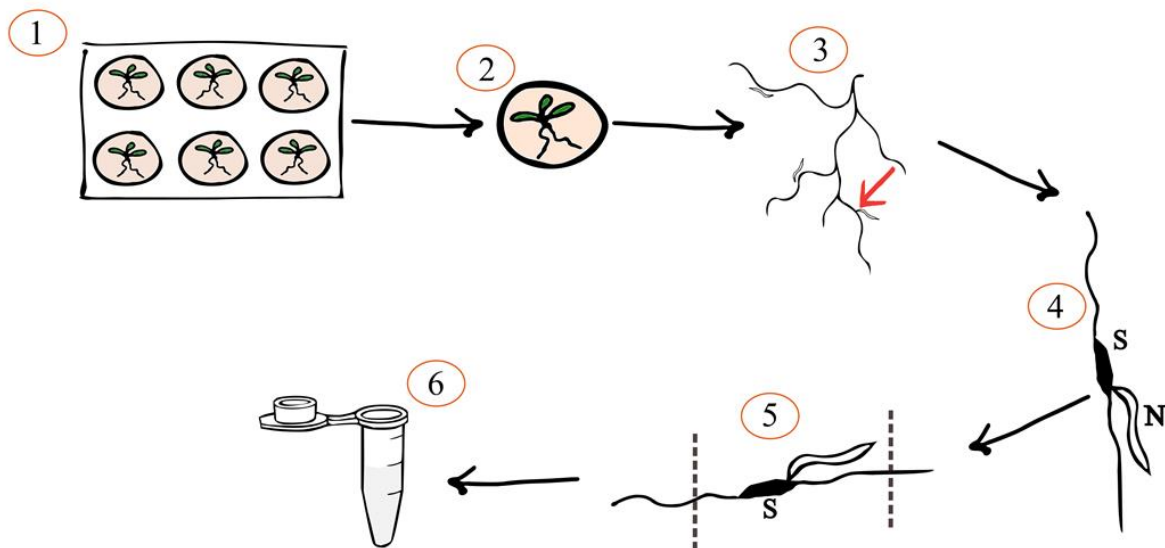
**Supplementary Figure 13:** Expression of *Hs4* in five *Hs1::Hs4* transgenic *Arabidopsis* lines before inoculation (non-inoc. 0 dpi), 3 dpi, and 21 dpi in non-inoculated (non-inoc.) and inoculated (inoc.) plant roots as determined by RT-qPCR (primer: AK\_F7/AK\_R5; reference gene: *GAPDH*) in experiment II. The plants were cultivated in sterile 6-well plates. Five biological replicates for the non-inoculated and ten replicates for the inoculated samples were used per time point. Statistical significances were calculated using a one-way ANOVA, followed by the Tukey HSD Test. Standard deviations are given as SEM.



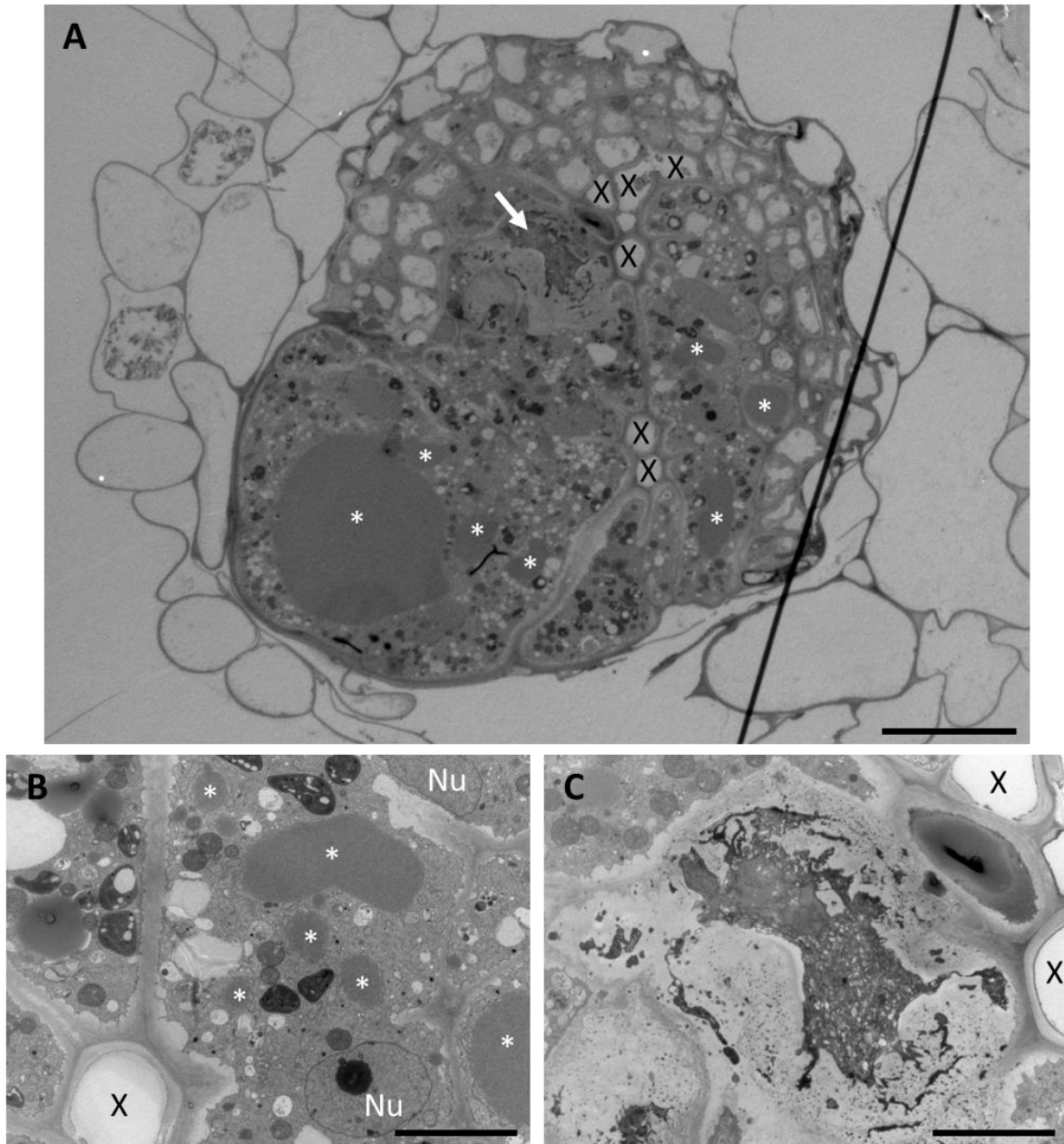
**Supplementary Figure 14:** Expression of *Hs4* in two 35S::*Hs4* and three Hs1::*Hs4* transgenic Arabidopsis lines before inoculation (non-inoc. 0 dpi), 3 dpi, and 21 dpi in non-inoculated (non-inoc.) and inoculated (inoc.) plant roots as determined by RT-qPCR (primer: AK\_F7/AK\_R5; reference gene: *GAPDH*) in experiment III. The plants were cultivated in sterile 6-well plates. Three biological replicates were used per time point. Statistical significances were calculated using the Kruskal-Wallis rank sum test, followed by a Hochberg-corrected Dunn test. Standard deviations are given as SEM.



**Supplementary Figure 15:** Expression of *Hs4* in the Hs1::*Hs4* transgenic line 210637 under sterile *in vitro* and non-sterile *in vivo* conditions as determined by RT-qPCR (primer: AK\_F7/AK\_R5; reference gene: *GAPDH*). The plants were inoculated with different larval densities (200, 300, 400 L). The number of biological replicates is indicated at the bottom of the bars. Statistical significances were calculated using the Kruskal-Wallis rank sum test, followed by a Hochberg-corrected Dunn test. Standard deviations are given as SEM.



**Supplementary Figure 16:** Schematic workflow for taking samples of syncytia for electron microscopy. (1) The Arabidopsis plants were cultured and inoculated in 6-well plates. (2) Starting one day after the inoculation, every plant was examined individually under a stereomicroscope. (3) Root regions with nematodes probing or adhering to the roots were marked (red arrow). (4) Every day the roots were examined until a developing syncytium (S) with an adhering nematode (N) could be identified. (5) The root was carefully excavated from the medium and the syncytium was generously excised (dotted lines). (6) Sampled syncytia from one genotype and sampling point were collected jointly in a tube with a 0.5 % glutaraldehyde solution.



**Supplementary Figure 17:** Transmission electron microscopic analysis of the syncytium from line 228934 at 11 dpi depicted in Figure 22 at a second position appr. 30  $\mu\text{m}$  deeper. (A) Overview of the whole root and the syncytium. The syncytium is stretching over half the root's cross-section. The syncytium contains large membrane aggregations (asterisks). A putatively necrotic region is visible along the upper syncytial border (arrow). The section has a fold in the right half. Bar: 20  $\mu\text{m}$ . X: xylem. (B) Membrane aggregations (asterisks) of different sizes in a syncytial cell. Bar: 5  $\mu\text{m}$ . Nu: nucleus, X: xylem. (C) Detail of the necrotic region at the border of the syncytium. It does not contain identifiable organelles and has porous, electron-translucent cell walls. Bar: 5  $\mu\text{m}$ .

## 10 References

- Akita K, Kobayashi M, Sato M, Kutsuna N, Ueda T, Toyooka K, Nagata N, Hasezawa S, Higaki T (2017) Cell wall accumulation of fluorescent proteins derived from a trans-Golgi cisternal membrane marker and paramural bodies in interdigitated *Arabidopsis* leaf epidermal cells. *Protoplasma* 254:367–377. <https://doi.org/10.1007/s00709-016-0955-1>
- Ali MA, Abbas A (2016) Analysis of reporter proteins *GUS* and *DsRed* driven under the control of CaMV35S promoter in syncytia induced by beet cyst nematode *Heterodera schachtii* in *Arabidopsis* roots. *Advancements in Life Sciences* 3:89–96
- Ali MA, Abbas A, Kreil DP, Bohlmann H (2013) Overexpression of the transcription factor RAP2.6 leads to enhanced callose deposition in syncytia and enhanced resistance against the beet cyst nematode *Heterodera schachtii* in *Arabidopsis* roots. *BMC Plant Biology* 13:47. <https://doi.org/10.1186/1471-2229-13-47>
- Anjam MS, Shah SJ, Matera C, Róžańska E, Sobczak M, Siddique S, Grundler FMW (2020) Host factors influence the sex of nematodes parasitizing roots of *Arabidopsis thaliana*. *Plant, Cell & Environment* 43:1160–1174. <https://doi.org/10.1111/pce.13728>
- Anwer MA, Anjam MS, Shah SJ, Hasan MS, Naz AA, Grundler FMW, Siddique S (2018) Genome-wide association study uncovers a novel QTL allele of AtS40-3 that affects the sex ratio of cyst nematodes in *Arabidopsis*. *Journal of Experimental Botany* 69:1805–1814. <https://doi.org/10.1093/jxb/ery019>
- Arabidopsis Genome Initiative (2000) Analysis of the genome sequence of the flowering plant *Arabidopsis thaliana*. *Nature* 408:796–815. <https://doi.org/10.1038/35048692>
- Aspden JL, Wallace EW, Whiffin N (2023) Not all exons are protein coding: Addressing a common misconception. *Cell Genomics* 3:100296. <https://doi.org/10.1016/j.xgen.2023.100296>
- Bayless AM, Zapotocny RW, Han S, Grunwald DJ, Amundson KK, Bent AF (2019) The *rhl1-a* (*Rhl1* low-copy) nematode resistance source harbors a copia-family retrotransposon within the *Rhl1*-encoded  $\alpha$ -SNAP gene. *Plant Direct* 3:1–19. <https://doi.org/10.1002/pld3.164>
- Bertioli DJ, Smoker M, Burrows PR (1999) Nematode-Responsive Activity of the Cauliflower Mosaic Virus 35S Promoter and Its Subdomains. *Molecular Plant-Microbe Interactions* 12:189–196
- Biancardi E, Panella LW, McGrath JM (eds) (2020) *Beta maritima: The Origin of Beets*. Springer International Publishing, Cham. <https://doi.org/10.1007/978-3-030-28748-1>
- Blanca G, Cabezudo B, Cueto Romero M, Torre C, Salazar-Mendias C (2011) *Flora Vasculare de Andalucía Oriental*, 2nd edn. Universidades de Almería, Granada, Jaén y Málaga, Granada, Spain
- Bleve-Zacheo T, Zacheo G (1987) Cytological studies of the susceptible reaction of sugarbeet roots to *Heterodera schachtii*. *Physiological and Molecular Plant Pathology* 30:13–25. [https://doi.org/10.1016/0885-5765\(87\)90079-8](https://doi.org/10.1016/0885-5765(87)90079-8)

## References

- Böckenhoff A, Grundler FMW (1994) Studies on the nutrient uptake by the beet cyst nematode *Heterodera schachtii* by *in situ* microinjection of fluorescent probes into the feeding structures in *Arabidopsis thaliana*. *Parasitology* 109:249–255. <https://doi.org/10.1017/S003118200007637X>
- Bohlmann H, Wieczorek K (2015) Infection Assay of Cyst Nematodes on Arabidopsis Roots. *Bio-protocol* 5:e1596. <https://doi.org/10.21769/BioProtoc.1596>
- Bosemark NO (1979) Genetic Poverty of the sugarbeet in Europe. In: Zeven AC (ed) *Proceedings of the Conference Broadening the Genetic Base of Crops*, Wageningen, Netherlands, 3 - 7 July, 1978. Centre for Agricultural Publishing and Documentation, Wageningen, pp 29–35
- Cai D, Kleine M, Kifle S, Harloff HJ, Sandal NN, Marcker KA, Klein-Lankhorst RM, Salentijn EM, Lange W, Stiekema WJ, Wyss U, Grundler FM, Jung C (1997) Positional cloning of a gene for nematode resistance in sugar beet. *Science (New York, N.Y.)* 275:832–834. <https://doi.org/10.1126/science.275.5301.832>
- Cai D, Thureau T, Tian Y, Lange T, Yeh K-W, Jung C (2003) Sporamin-mediated resistance to beet cyst nematodes (*Heterodera schachtii* Schm.) is dependent on trypsin inhibitory activity in sugar beet (*Beta vulgaris* L.) hairy roots. *Plant Molecular Biology* 51:839–849
- Camacho C, Coulouris G, Avagyan V, Ma N, Papadopoulos J, Bealer K, Madden TL (2009) BLAST+: architecture and applications. *BMC Bioinformatics* 10:421. <https://doi.org/10.1186/1471-2105-10-421>
- Cameron DD, Neal AL, van Wees SCM, Ton J (2013) Mycorrhiza-induced resistance: more than the sum of its parts? *Trends in Plant Science* 18:539–545. <https://doi.org/10.1016/j.tplants.2013.06.004>
- Capistrano G (2009) A candidate sequence for the nematode resistance gene *Hs1-2* in sugar beet, Christian-Albrechts University of Kiel
- Cardoza V, Stewart CN (2003) Increased *Agrobacterium*-mediated transformation and rooting efficiencies in canola (*Brassica napus* L.) from hypocotyl segment explants. *Plant Cell Reports* 21:599–604. <https://doi.org/10.1007/s00299-002-0560-y>
- Chen R-G, Zhang L-Y, Zhang J-H, Zhang W, Wang X, Ouyang B, Li H-X, Ye Z-B (2006) Functional Characterization of *Mi*, a Root-knot Nematode Resistance Gene from Tomato (*Lycopersicon esculentum* L.). *Journal of Integrative Plant Biology* 48:1458–1465
- Chitwood DJ, Lusby WR (1991) Metabolism of plant sterols by nematodes. *Lipids* 26:619–627. <https://doi.org/10.1007/BF02536426>
- Chopra D, Hasan MS, Matera C, Chitambo O, Mendy B, Mahlitz S-V, Naz AA, Szumski S, Janakowski S, Sobczak M, Mithöfer A, Kyndt T, Grundler FMW, Siddique S (2021) Plant parasitic cyst nematodes redirect host indole metabolism via NADPH oxidase-mediated ROS to promote infection. *New Phytologist* 232:318–331. <https://doi.org/10.1111/nph.17559>

- Clark RM, Wagler TN, Quijada P, Doebley J (2006) A distant upstream enhancer at the maize domestication gene *tb1* has pleiotropic effects on plant and inflorescent architecture. *Nature Genetics* 38:594–597. <https://doi.org/10.1038/ng1784>
- Clontech Laboratories, Inc. (2003) Living Colors® User Manual Volume II. Protocol No. PT3404-1. <https://web.stanford.edu/class/chem184/materials/livingcolors>
- Clough SJ, Bent AF (1998) Floral dip: a simplified method for *Agrobacterium* -mediated transformation of *Arabidopsis thaliana*. *The Plant Journal* 16:735–743. <https://doi.org/10.1046/j.1365-313x.1998.00343.x>
- Cole TCH, Hilger HH, Stevens P (2019) Angiosperm phylogeny poster (APP) – Flowering plant systematics, 2019. <https://doi.org/10.7287/peerj.preprints.2320v6>
- Cook R (1977) The Relationship Between Feeding and Fecundity of Females of *Heterodera Avenae*. *Nematologica* 23:403–410. <https://doi.org/10.1163/187529277X00129>
- Curtis GJ (1968) Observations of fruit shape and other characters in the species of the section *Patellares*, genus *Beta*. *Euphytica* 17:485–491. <https://doi.org/10.1007/BF00056252>
- d'Angelo P (2023) Hugin - Panorama photo stitcher
- Daub M (2021) The beet cyst nematode (*Heterodera schachtii*): an ancient threat to sugar beet crops in Central Europe has become an invisible actor. In: Sikora RA, Desaegeer J, Molendijk L (eds) Integrated nematode management: state-of-the-art and visions for the future, 1st edn. CABI, UK, pp 394–399. <https://doi.org/10.1079/9781789247541.0055>
- Daub M (2020) Effect of Winter Oilseed Rape Cropping on the Development of the Sugar Beet Cyst Nematode, *Heterodera schachtii*, and Control of Volunteer Plants as a Trap Crop Method. *Agronomy* 10:355. <https://doi.org/10.3390/agronomy10030355>
- Davies LJ, Lilley CJ, Paul Knox J, Urwin PE (2012) Syncytia formed by adult female *Heterodera schachtii* in *Arabidopsis thaliana* roots have a distinct cell wall molecular architecture. *New Phytologist* 196:238–246. <https://doi.org/10.1111/j.1469-8137.2012.04238.x>
- De Block M, De Brouwer D, Tenning P (1989) Transformation of *Brassica napus* and *Brassica oleracea* Using *Agrobacterium tumefaciens* and the Expression of the *bar* and *neo* Genes in the Transgenic Plants. *Plant Physiology* 91:694–701. <https://doi.org/10.1104/pp.91.2.694>
- Decraemer W, Coomans A, Baldwin J (2013) 1. Morphology of Nematoda. Volume 2 Nematoda. De Gruyter, pp 1–60. <https://doi.org/10.1515/9783110274257.1>
- Dellaporta SL, Wood J, Hicks JB (1983) A plant DNA miniprep: Version II. *Plant Molecular Biology Reporter* 1:19–21. <https://doi.org/10.1007/BF02712670>
- Demars BG, Boerner RE (1996) Vesicular arbuscular mycorrhizal development in the Brassicaceae in relation to plant life span. *Flora* 191:179–189. [https://doi.org/10.1016/S0367-2530\(17\)30711-9](https://doi.org/10.1016/S0367-2530(17)30711-9)
- Directorate-General for Agriculture, Rural Development (2024) Sugar. European Commission - Agriculture and rural development. [https://agriculture.ec.europa.eu/farming/crop-productions-and-plant-based-products/sugar\\_en](https://agriculture.ec.europa.eu/farming/crop-productions-and-plant-based-products/sugar_en)

## References

- Dirksen P, Marsh SA, Braker I, Heitland N, Wagner S, Nakad R, Mader S, Petersen C, Kowallik V, Rosenstiel P, Félix M-A, Schulenburg H (2016) The native microbiome of the nematode *Caenorhabditis elegans*: gateway to a new host-microbiome model. *BMC Biology* 14:38. <https://doi.org/10.1186/s12915-016-0258-1>
- Dohm JC, Minoche AE, Holtgräwe D et al (2014) The genome of the recently domesticated crop plant sugar beet (*Beta vulgaris*). *Nature* 505:546–549. <https://doi.org/10.1038/nature12817>
- Dorn K (2022) *Beta vulgaris* W357B genome. Zenodo. <https://zenodo.org/records/5911852>. Accessed 21 June 2024. <https://doi.org/10.5281/zenodo.5911852>
- Eberlein C, Heuer H, Westphal A (2020) Biological Suppression of Populations of *Heterodera schachtii* Adapted to Different Host Genotypes of Sugar Beet. *Frontiers in Plant Science* 11:812. <https://doi.org/10.3389/fpls.2020.00812>
- Elashry AM, Habash SS, Vijayapalani P, Brocke-Ahmadinejad N, Blümel R, Seetharam A, Schoof H, Grundler FMW (2020) Transcriptome and Parasitome Analysis of Beet Cyst Nematode *Heterodera schachtii*. *Scientific Reports* 10:3315. <https://doi.org/10.1038/s41598-020-60186-0>
- Elhady A, Topalović O, Heuer H (2021) Plants Specifically Modulate the Microbiome of Root-Lesion Nematodes in the Rhizosphere, Affecting Their Fitness. *Microorganisms* 9. <https://doi.org/10.3390/microorganisms9040679>
- Elling AA (2013) Major Emerging Problems with Minor Meloidogyne Species. *Phytopathology* 103:1092–1102. <https://doi.org/10.1094/PHYTO-01-13-0019-RVW>
- Eysholdt-Derzsó E, Renziehausen T, Frings S et al (2023) Endoplasmic reticulum-bound ANAC013 factor is cleaved by RHOMBOID-LIKE 2 during the initial response to hypoxia in *Arabidopsis thaliana*. *Proceedings of the National Academy of Sciences of the United States of America* 120:e2221308120. <https://doi.org/10.1073/pnas.2221308120>
- Ferris H (2010) Contribution of Nematodes to the Structure and Function of the Soil Food Web. *Journal of Nematology* 42:63–67
- Fischer HE (1989) Origin of the ‘Weisse Schlesische Rübe’ (white Silesian beet) and resynthesis of sugar beet. *Euphytica* 41:75–80. <https://doi.org/10.1007/BF00022414>
- Fleig L, Bergbold N, Sahasrabudhe P, Geiger B, Kaltak L, Lemberg MK (2012) Ubiquitin-Dependent Intramembrane Rhomboid Protease Promotes ERAD of Membrane Proteins. *Molecular Cell* 47:558–569. <https://doi.org/10.1016/j.molcel.2012.06.008>
- Food and Agriculture Organization of the United Nations (2024) FAOSTAT. FAO. <https://www.fao.org/faostat/en/#data/QCL/visualize>. Accessed 30 July 2024
- Ford-Lloyd BV, Williams JT (1975) A revision of *Beta* section *Vulgares* (Chenopodiaceae), with new light on the origin of cultivated beets. *Botanical Journal of the Linnean Society* 71:89–102. <https://doi.org/10.1111/j.1095-8339.1975.tb02448.x>
- Freeman M (2009) Rhomboids: 7 years of a new protease family. *Seminars in Cell & Developmental Biology* 20:231–239. <https://doi.org/10.1016/j.semcdb.2008.10.006>

- Frese L, Bülow, Castro S, Duarte C, Iriondo JM, Lohwasser U, Loureiro J, Maxted N, Nachtigall M, Nobrega H, Pinheiro de Carvalho, M. Â. A., Santos Guerra A, Romeiras MM, Rubio ML, Rey E (2017a) Genetic diversity of *Patellifolia* species (GeDiPa)
- Frese L, Ford-Lloyd B (2020) Taxonomy, Phylogeny, and the Genepool. In: Biancardi E, Panella LW, McGrath JM (eds) *Beta maritima: The Origin of Beets*. Springer International Publishing, Cham, pp 121–151. [https://doi.org/10.1007/978-3-030-28748-1\\_6](https://doi.org/10.1007/978-3-030-28748-1_6)
- Frese L, Nachtigall M, Iriondo JM, Rubio Teso ML, Duarte MC, Pinheiro de Carvalho, Miguel Ângelo A. (2019) Genetic diversity and differentiation in *Patellifolia* (Amaranthaceae) in the Macaronesian archipelagos and the Iberian Peninsula and implications for genetic conservation programmes. *Genetic Resources and Crop Evolution* 66:225–241. <https://doi.org/10.1007/s10722-018-0708-4>
- Frese L, Bülow L, Nachtigall M, Rubio Teso ML, Duarte MC, Rey E, Iriondo Alegría JM (2017b) Genetic diversity of *Patellifolia patellaris* from the Iberian Peninsula, a crop wild relative of cultivated beets. *Euphytica* 213:187. <https://doi.org/10.1007/s10681-017-1942-0>
- Friso G, van Wijk KJ (2015) Posttranslational Protein Modifications in Plant Metabolism. *Plant Physiology* 169:1469–1487. <https://doi.org/10.1104/pp.15.01378>
- Froger A, Hall JE (2007) Transformation of Plasmid DNA into *E. coli* Using the Heat Shock Method. *Journal of Visualized Experiments: JoVE* 253. <https://doi.org/10.3791/253>
- Fuller VL, Lilley CJ, Urwin PE (2008) Nematode resistance. *New Phytologist* 180:27–44. <https://doi.org/10.1111/j.1469-8137.2008.02508.x>
- Ghaemi R, Pourjam E, Safaie N, Verstraeten B, Mahmoudi SB, Mehrabi R, Meyer T de, Kyndt T (2020) Molecular insights into the compatible and incompatible interactions between sugar beet and the beet cyst nematode. *BMC Plant Biology* 20:483. <https://doi.org/10.1186/s12870-020-02706-8>
- Goddijn OJ, Lindsey K, van der Lee FM, Klap JC, Sijmons PC (1993) Differential gene expression in nematode-induced feeding structures of transgenic plants harbouring promoter-gusA fusion constructs. *The Plant Journal: For Cell and Molecular Biology* 4:863–873. <https://doi.org/10.1046/j.1365-313x.1993.04050863.x>
- Golden AM (1959) Susceptibility of several Beta species to the sugar beet nematode (*Heterodera schachtii*) and root knot nematodes (*Meloidogyne* spp.). *Journal of Sugarbeet Research* 10:444–447. <https://doi.org/10.5274/jsbr.10.5.441>
- Golinowski W, Grundler FMW, Sobczak M (1996) Changes in the structure of *Arabidopsis thaliana* during female development of the plant-parasitic nematode *Heterodera schachtii*. *Protoplasma* 194:103–116. <https://doi.org/10.1007/BF01273172>
- Golinowski W, Sobczak M, Kurek W, Grymaszewska G (1997) The Structure of Syncytia. In: Fenoll C, Grundler FMW, Ohl SA (eds) *Cellular and Molecular Aspects of Plant-Nematode Interactions*. Springer Netherlands, Dordrecht, pp 80–97. [https://doi.org/10.1007/978-94-011-5596-0\\_7](https://doi.org/10.1007/978-94-011-5596-0_7)

## References

- Goverse A, Smant G (2014) The Activation and Suppression of Plant Innate Immunity by Parasitic Nematodes. *Annual Review of Phytopathology* 52:243–265.  
<https://doi.org/10.1146/annurev-phyto-102313-050118>
- Goverse A, Bird D (2011) The Role of Plant Hormones in Nematode Feeding Cell Formation. In: Jones J, Gheysen G, Fenoll C (eds) *Genomics and Molecular Genetics of Plant-Nematode Interactions*. Springer Netherlands, Dordrecht, pp 325–347.  
[https://doi.org/10.1007/978-94-007-0434-3\\_16](https://doi.org/10.1007/978-94-007-0434-3_16)
- Grundler FMW, Sobczak M, Lange S (1997) Defence responses of *Arabidopsis thaliana* during invasion and feeding site induction by the plant–parasitic nematode *Heterodera glycines*. *Physiological and Molecular Plant Pathology* 50:419–429.  
<https://doi.org/10.1006/pmpp.1997.0100>
- Grundler FM, Sobczak M, Golinowski W (1998) Formation of wall openings in root cells of *Arabidopsis thaliana* following infection by the plant-parasitic nematode *Heterodera schachtii*. *European Journal of Plant Pathology* 104:545–551.  
<https://doi.org/10.1023/A:1008692022279>
- Grunewald W, Cannoot B, Friml J, Gheysen G (2009a) Parasitic Nematodes Modulate PIN-Mediated Auxin Transport to Facilitate Infection. *PLoS Pathogens* 5:e1000266.  
<https://doi.org/10.1371/journal.ppat.1000266>
- Grunewald W, van Noorden G, van Isterdael G, Beeckman T, Gheysen G, Mathesius U (2009b) Manipulation of Auxin Transport in Plant Roots during *Rhizobium* Symbiosis and Nematode Parasitism. *The Plant Cell* 21:2553–2562.  
<https://doi.org/10.1105/tpc.109.069617>
- Hallgren J, Tsigirgos KD, Pedersen MD, Armenteros JJA, Marcatili P, Nielsen H, Krogh A, Winther O (2022) DeepTMHMM predicts alpha and beta transmembrane proteins using deep neural networks. *bioRxiv*.  
<https://www.biorxiv.org/content/10.1101/2022.04.08.487609v1>. Accessed 14 August 2024. <https://doi.org/10.1101/2022.04.08.487609>
- Hallmann J, Daub M, Grundler F, Westphal A (2009) 150 Jahre *Heterodera schachtii*: Ein Überblick der frühen Arbeiten. *Journal für Kulturpflanzen* 61:429–439
- Hao Z, Fayolle L, van Tuinen D, Chatagnier O, Li X, Gianinazzi S, Gianinazzi-Pearson V (2012) Local and systemic mycorrhiza-induced protection against the ectoparasitic nematode *Xiphinema index* involves priming of defence gene responses in grapevine. *Journal of Experimental Botany* 63:3657–3672. <https://doi.org/10.1093/jxb/ers046>
- Harlan JR, Wet JMJ de (1971) Toward a Rational Classification of Cultivated Plants. *Taxon* 20:509–517. <https://doi.org/10.2307/1218252>
- Hartmann M-A, Benveniste P (1987) [58] Plant membrane sterols: Isolation, identification, and biosynthesis *Plant Cell Membranes*. Elsevier, pp 632–650.  
[https://doi.org/10.1016/0076-6879\(87\)48060-9](https://doi.org/10.1016/0076-6879(87)48060-9)
- Harveson RM, Jackson TA (2008) *Sugar Beet Cyst Nematode*. University of Nebraska-Lincoln
- Hawamda AIM, Reichert S, Ali MA, Nawaz MA, Austerlitz T, Schekahn P, Abbas A, Tenhaken R, Bohlmann H (2022) Characterization of an *Arabidopsis* Defensin-like

- Gene Conferring Resistance against Nematodes. *Plants* (Basel, Switzerland) 11:280. <https://doi.org/10.3390/plants11030280>
- Heijbroek W, Roelands AJ, Jong JH de (1983) Transfer of resistance to beet cyst nematode from *Beta patellaris* to sugar beet. *Euphytica* 32:287–298. <https://doi.org/10.1007/BF00021437>
- Heijbroek W, Mcfarlane JS, Doney DL (1977) Breeding for tolerance to beet-cyst eelworm *Heterodera schachtii* Schm. in sugarbeet. *Euphytica* 26:557–564. <https://doi.org/10.1007/BF00021681>
- Hellens R, Mullineaux P, Klee H (2000) Technical Focus: A guide to Agrobacterium binary Ti vectors. *Trends in Plant Science* 5:446–451. [https://doi.org/10.1016/S1360-1385\(00\)01740-4](https://doi.org/10.1016/S1360-1385(00)01740-4)
- Heller R, Schondelmaier J, Steinrücken G, Jung C (1996) Genetic localization of four genes for nematode (*Heterodera schachtii* Schm.) resistance in sugar beet (*Beta vulgaris* L.). *Theoretical and Applied Genetics* 92:991–997
- Hewezi T (2015) Cellular Signaling Pathways and Posttranslational Modifications Mediated by Nematode Effector Proteins. *Plant Physiology* 169:1018–1026. <https://doi.org/10.1104/pp.15.00923>
- Hewezi T, Howe PJ, Maier TR, Hussey RS, Mitchum MG, Davis EL, Baum TJ (2010) Arabidopsis Spermidine Synthase Is Targeted by an Effector Protein of the Cyst Nematode *Heterodera schachtii*. *Plant Physiology* 152:968–984. <https://doi.org/10.1104/pp.109.150557>
- Hewezi T, Howe P, Maier TR, Hussey RS, Mitchum MG, Davis EL, Baum TJ (2008) Cellulose Binding Protein from the Parasitic Nematode *Heterodera schachtii* Interacts with Arabidopsis Pectin Methylesterase: Cooperative Cell Wall Modification during Parasitism. *The Plant Cell* 20:3080–3093. <https://doi.org/10.1105/tpc.108.063065>
- Hoffmann CM (2010) Root Quality of Sugarbeet. *Sugar Tech* 12:276–287. <https://doi.org/10.1007/s12355-010-0040-6>
- Hoffmann CM, Kluge-Severin S (2011) Growth analysis of autumn and spring sown sugar beet. *European Journal of Agronomy* 34:1–9. <https://doi.org/10.1016/j.eja.2010.09.001>
- Hoffmann CM, Kenter C, Bloch D (2005) Sucrose concentration of sugar beet (*Beta vulgaris* L) in relation to sucrose storage. *Journal of the Science of Food and Agriculture* 85:459–465. <https://doi.org/10.1002/jsfa.2002>
- Höfgen R, Willmitzer L (1988) Storage of competent cells for Agrobacterium transformation. *Nucleic Acids Research* 16:9877
- Holbein J, Grundler FMW, Siddique S (2016) Plant basal resistance to nematodes: an update. *Journal of Experimental Botany* 67:2049–2061. <https://doi.org/10.1093/jxb/erw005>
- Holtmann B, Kleine M, Grundler FMW (2000) Ultrastructure and anatomy of nematode-induced syncytia in roots of susceptible and resistant sugar beet. *Protoplasma* 211:39–50. <https://doi.org/10.1007/BF01279898>

## References

- Holtmann B (2000) Die Histologie und Ultrastruktur der Resistenzreaktion von Zuckerrüben (*Beta vulgaris*) und Wildrüben (*Beta procumbens* und *Beta patellaris*) gegenüber dem Zystennematoden *Heterodera schachtii*, Christian-Albrechts-Universität Kiel
- Höwing T, Dann M, Hoefle C, Hückelhoven R, Gietl C (2017) Involvement of *Arabidopsis thaliana* endoplasmic reticulum KDEL-tailed cysteine endopeptidase 1 (AtCEP1) in powdery mildew-induced and AtCPR5-controlled cell death. *PloS One* 12:e0183870. <https://doi.org/10.1371/journal.pone.0183870>
- Höwing T, Huesmann C, Hoefle C, Nagel M-K, Isono E, Huckelhoven R, Gietl C (2014) Endoplasmic reticulum KDEL-tailed cysteine endopeptidase 1 of *Arabidopsis* (AtCEP1) is involved in pathogen defense. *Frontiers in Plant Science* 5. <https://doi.org/10.3389/fpls.2014.00058>
- Hu J, Rapoport TA (2016) Fusion of the endoplasmic reticulum by membrane-bound GTPases. *Seminars in Cell & Developmental Biology* 60:105–111. <https://doi.org/10.1016/j.semcdb.2016.06.001>
- Hugot J-P, Baujard P, Morand S (2001) Biodiversity in helminths and nematodes as a field of study: an overview. *Nematology* 3:199–208. <https://doi.org/10.1163/156854101750413270>
- Ibrahim M, Shi Y, Qiu H, Li B, Jabeen A, Li L, Liu H, Kube M, Xie G, Wang Y, Blondel C, Santiviago CA, Contreras I, Sun G (2012) Differential expression of *in vivo* and *in vitro* protein profile of outer membrane of *Acidovorax avenae* subsp. *avenae*. *PloS One* 7:e49657. <https://doi.org/10.1371/journal.pone.0049657>
- Jäger S (2012) Hybrid Assembly of Whole Genome Shotgun Sequences of Two Sugar Beet (*Beta vulgaris* L.) Translocation Lines Carrying the Beet Cyst Nematode Resistance Gene *Hsl-2* and Functional Analysis of Candidate Genes, Christian-Albrechts University of Kiel
- Jassem B (1992) Species relationship in the genus *Beta* as revealed by crossing experiments International Beta Genetic Resources Network: A report on the 2nd International Beta Genetic Resources Workshop held at the Institute for Crop Science and Plant Breeding, Braunschweig, Germany, 24 - 28 June 1991. IBPGR, Rome, pp 55–61
- Jaubert S, Laffaire J-B, Abad P, Rosso M-N (2002) A polygalacturonase of animal origin isolated from the root-knot nematode *Meloidogyne incognita*. *FEBS Letters* 522:109–112. [https://doi.org/10.1016/S0014-5793\(02\)02906-X](https://doi.org/10.1016/S0014-5793(02)02906-X)
- Jin J, Hewezi T, Baum TJ (2011) The *Arabidopsis* bHLH25 and bHLH27 transcription factors contribute to susceptibility to the cyst nematode *Heterodera schachtii*. *The Plant Journal* 65:319–328. <https://doi.org/10.1111/j.1365-313X.2010.04424.x>
- John A, Krämer M, Lehmann M et al (2024) Degradation of FATTY ACID EXPORT PROTEIN1 by RHOMBOID-LIKE PROTEASE11 contributes to cold tolerance in *Arabidopsis*. *The Plant Cell* 36:1937–1962. <https://doi.org/10.1093/plcell/koae011>
- Jones J, Gheysen G, Fenoll C (eds) (2011) Genomics and Molecular Genetics of Plant-Nematode Interactions. Springer Netherlands, Dordrecht
- Jones JT, Haegeman A, Danchin EGJ, Gaur HS, Helder J, Jones MGK, Kikuchi T, Manzanilla-López R, Palomares-Rius JE, Wesemael WML, Perry RN (2013) Top 10

- plant-parasitic nematodes in molecular plant pathology. *Molecular Plant Pathology* 14:946–961. <https://doi.org/10.1111/mpp.12057>
- Julkowska MM, Saade S, Agarwal G, Gao G, Pailles Y, Morton M, Awlia M, Tester M (2019) MVApp - Multivariate Analysis Application for Streamlined Data Analysis and Curation. *Plant Physiology* 180:1261–1276. <https://doi.org/10.1104/pp.19.00235>
- Jung C, Wricke G (1987) Selection of Diploid Nematode-Resistant Sugar Beet from Monosomic Addition Lines. *Plant Breeding* 98:205–214. <https://doi.org/10.1111/j.1439-0523.1987.tb01118.x>
- Jung C, Pillen K, Frese L, Fähr S, Melchinger AE (1993) Phylogenetic relationships between cultivated and wild species of the genus *Beta* revealed by DNA “fingerprinting”. *Theoretical and Applied Genetics* 86:449–457. <https://doi.org/10.1007/BF00838560>
- Jung C, Koch R, Fischer F, Brandes A, Wricke G, Herrmann RG (1992) DNA markers closely linked to nematode resistance genes in sugar beet (*Beta vulgaris* L.) mapped using chromosome additions and translocations originating from wild beets of the *Procumbentes* section. *Molecular and General Genetics MGG* 232:271–278. <https://doi.org/10.1007/BF00280006>
- Jung C, Kleine M, Fischer E, Herrmann RG (1990) Analysis of DNA from a *Beta procumbens* chromosome fragment in sugar beet carrying a gene for nematode resistance. *Theoretical and Applied Genetics* 79:663–672. <https://doi.org/10.1007/BF00226881>
- Jung C, Wehling P, Löptien H (1986) Electrophoretic Investigations on Nematode Resistant Sugar Beets. *Plant Breeding* 97:39–45. <https://doi.org/10.1111/j.1439-0523.1986.tb01299.x>
- Juvale PS, Baum TJ (2018) “Cyst-ained” research into *Heterodera* parasitism. *PLoS Pathogens* 14:e1006791. <https://doi.org/10.1371/journal.ppat.1006791>
- Kadereit G, Hohmann S, Kadereit J (2006) A synopsis of *Chenopodiaceae* subfam. *Betoideae* and notes on the taxonomy of *Beta*. *Willdenowia* 36. <https://doi.org/10.3372/wi.36.36101>
- Kenter C, Lukashyk P, Daub M, Ladewig E (2014) Population dynamics of *Heterodera schachtii* Schm. and yield response of susceptible and resistant sugar beet (*Beta vulgaris* L.) after cultivation of susceptible and resistant oilseed radish (*Raphanus sativus* L.). *Journal für Kulturpflanzen* 66:289–299. <https://doi.org/10.5073/JfK.2014.09.01>
- Kim YH, Riggs RD, Kim KS (1987) Structural Changes Associated with Resistance of Soybean to *Heterodera glycines*. *Journal of Nematology* 19:177–187
- Kim YH, Kim KS, Riggs RD (2012) Initial Subcellular Responses of Susceptible and Resistant Soybeans Infected with the Soybean Cyst Nematode. *The Plant Pathology Journal* 28:401–408. <https://doi.org/10.5423/PPJ.OA.04.2012.0054>
- Kleine M, Voss H, Cai D, Jung C (1998) Evaluation of nematode-resistant sugar beet (*Beta vulgaris* L.) lines by molecular analysis. *Theoretical and Applied Genetics* 97:896–904. <https://doi.org/10.1007/s001220050970>

## References

- Kleine M, Cai D, Elbl C, Herrmann RG, Jung C (1995) Physical mapping and cloning of a translocation in sugar beet (*Beta vulgaris* L) carrying a gene for nematode (*Heterodera schachtii*) resistance from *B. procumbens*. Theoretical and Applied Genetics 90:399–406. <https://doi.org/10.1007/BF00221982>
- Kniec-Wisniewska B, Krumpke K, Urantowka A, Sakamoto W, Pratje E, Janska H (2008) Plant mitochondrial rhomboid, AtRBL12, has different substrate specificity from its yeast counterpart. Plant Molecular Biology 68:159–171. <https://doi.org/10.1007/s11103-008-9359-8>
- Kong W, Wang M, Huang L, Wu F, Tao J, Mo B, Yu Y (2023) A high-efficient and naked-eye visible CRISPR/Cas9 system in *Arabidopsis*. Planta 257:30. <https://doi.org/10.1007/s00425-022-04060-5>
- Kranse OP, Ko I, Healey R, Sonawala U, Wei S, Senatori B, Batté F de, Zhou J, Eves-van den Akker S (2022) A low-cost and open-source solution to automate imaging and analysis of cyst nematode infection assays for *Arabidopsis thaliana*. Plant Methods 18:134. <https://doi.org/10.1186/s13007-022-00963-2>
- Kumar A (2020) Cloning of the beet cyst nematode resistance gene *Hs4* from the wild beet *Patellifolia procumbens*, Christian-Albrechts University of Kiel
- Kumar A, Harloff H-J, Melzer S, Leineweber J, Defant B, Jung C (2021) A rhomboid-like protease gene from an interspecies translocation confers resistance to cyst nematodes. New Phytologist 231:801–813. <https://doi.org/10.1111/nph.17394>
- Kus JV, Zaton K, Sarkar R, Cameron RK (2002) Age-Related Resistance in *Arabidopsis* Is a Developmentally Regulated Defense Response to *Pseudomonas syringae*. The Plant Cell 14:479–490. <https://doi.org/10.1105/tpc.010481>
- Labudda M, Rózańska E, Szewińska J, Sobczak M, Dzik JM (2016) Protease activity and phytocystatin expression in *Arabidopsis thaliana* upon *Heterodera schachtii* infection. Plant Physiology and Biochemistry 109:416–429. <https://doi.org/10.1016/j.plaphy.2016.10.021>
- Landwirtschaftlicher Informationsdienst Zuckerrübe by Pfeifer & Langen (2020) LIZ Ausfallraps-Manager. <https://www.liz-online.de/meldungen/meldung-ueberregional/liz-ausfallraps-manager-online0>
- Lange W, Bock T de (1994) Pre-Breeding for Nematode Resistance in Beet. Journal of Sugarbeet Research 31:13–26. <https://doi.org/10.5274/jsbr31.1.13>
- Lange W, Jung C, Heijbroek W (1990) Transfer of beet cyst nematode resistance from *Beta* species of the section *Patellares* to cultivated beet
- Lange W, Toxopeus H, Lubberts JH, Dolstra O, Harrewijn JL (1989) The development of Raparadish (x *Brassicoraphanus*, 2n=38), a new crop in agriculture. Euphytica 40:1–14. <https://doi.org/10.1007/BF00023291>
- Lange W, Bock TS de, van Geyt JP, Oléo M (1988) Monosomic additions in beet (*Beta vulgaris*) carrying extra chromosomes of *B. procumbens*. 2. Effects of the alien chromosomes on *in vivo* and *in vitro* plant development. TAG. Theoretical and applied genetics. Theoretische und angewandte Genetik 76:656–664. <https://doi.org/10.1007/BF00303509>

- Lange W, Müller J, Bock TSM de (1993) Virulence in the beet cyst nematode (*Heterodera schachtii*) versus some alien genes for resistance in beet. *Fundam. appl. Nematol.* 16:447–454
- Leibroek LB, Hofmann DM, Fuchs B, Birt A, Reinholz M, Guertler A, Frank K, Giunta RE, Egaña JT, Nickelsen J, Schenck TL, Moellhoff N (2022) In vitro and in vivo detection of microbial gene expression in bioactivated scaffolds seeded with cyanobacteria. *Lett Appl Microbiol* 75:401–409. <https://doi.org/10.1111/lam.13740>
- Leineweber J (2020) Funktionelle Analyse eines *Heterodera schachtii* Resistenzgens aus Zuckerrüben. Institut für Pflanzenbau und Pflanzenzüchtung, Christian-Albrechts-Universität zu Kiel
- Lelivelt CL, Krens FA (1992) Transfer of resistance to the beet cyst nematode (*Heterodera schachtii* Schm.) into the *Brassica napus* L. gene pool through intergeneric somatic hybridization with *Raphanus sativus* L. *TAG. Theoretical and applied genetics. Theoretische und angewandte Genetik* 83:887–894. <https://doi.org/10.1007/BF00226712>
- Lelivelt CLC, Lange W, Dolstra O (1993a) Intergeneric crosses for the transfer of resistance to the beet cyst nematode from *Raphanus sativus* to *Brassica napus*. *Euphytica* 68:111–120. <https://doi.org/10.1007/BF00024160>
- Lelivelt CLC, Leunissen EHM, Frederiks HJ, Helsper, J. P. F. G., Krens FA (1993b) Transfer of resistance to the beet cyst nematode (*Heterodera Schachtii* Schm.) from *Sinapis alba* L. (white mustard) to the *Brassica napus* L. gene pool by means of sexual and somatic hybridization. *Theoretical and Applied Genetics* 85:688–696. <https://doi.org/10.1007/BF00225006>
- Lelivelt CLC (1995) Attempted selection for partial resistance to the sugar beet cyst nematode, *Heterodera schachtii*, in *Brassica napus* L. *Fundam. appl. Nematol.* 18:11–15
- Lemberg MK, Freeman M (2007) Functional and evolutionary implications of enhanced genomic analysis of rhomboid intramembrane proteases. *Genome Research* 17:1634–1646. <https://doi.org/10.1101/gr.6425307>
- Lewellen RT, Pakish LM (2005) Performance of sugarbeet cyst nematode resistant cultivars and a search for sources of resistance 42:122–123
- Li H-Y, Yang G-D, Shu H-R, Yang Y-T, Ye B-X, Nishida I, Zheng C-C (2006) Colonization by the arbuscular mycorrhizal fungus *Glomus versiforme* induces a defense response against the root-knot nematode *Meloidogyne incognita* in the grapevine (*Vitis amurensis* Rupr.), which includes transcriptional activation of the class III chitinase gene *VCH3*. *Plant Cell Physiol* 47:154–163. <https://doi.org/10.1093/pcp/pci231>
- Liu J, Zhang J, Wei Y, Su W, Li W, Wang B, Peng D, Gheysen G, Peng H, Dai L (2024) The nematode effector calreticulin competes with the high mobility group protein OsHMGB1 for binding to the rice calmodulin-like protein OsCML31 to enhance rice susceptibility to *Meloidogyne graminicola*. *Plant, Cell & Environment* 47:1732–1746. <https://doi.org/10.1111/pce.14848>

## References

- Liu S, Kandath PK, Warren SD et al (2012) A soybean cyst nematode resistance gene points to a new mechanism of plant resistance to pathogens. *Nature* 492:256–260. <https://doi.org/10.1038/nature11651>
- Liu W, Xie Y, Ma J, Luo X, Nie P, Zuo Z, Lahrmann U, Zhao Q, Zheng Y, Zhao Y, Xue Y, Ren J (2015) IBS: an illustrator for the presentation and visualization of biological sequences. *Bioinformatics (Oxford, England)* 31:3359–3361. <https://doi.org/10.1093/bioinformatics/btv362>
- Loel J, Hoffmann CM (2014) Importance of growth stage and weather conditions for the winter hardiness of autumn sown sugar beet. *Field Crops Research* 162:70–76. <https://doi.org/10.1016/j.fcr.2014.03.007>
- Löptien H (1984) Breeding nematode-resistant beets. I. Development of resistant alien additions by crosses between *Beta vulgaris* L. and wild species of the section *Patellares* 92:208–220
- Lozano-Torres JL, Wilbers RHP, Gawronski P et al (2012) Dual disease resistance mediated by the immune receptor Cf-2 in tomato requires a common virulence target of a fungus and a nematode. *Proceedings of the National Academy of Sciences of the United States of America* 109:10119–10124. <https://doi.org/10.1073/pnas.1202867109>
- Manohar M, Tenjo-Castano F, Chen S, Zhang YK, Kumari A, Williamson VM, Wang X, Klessig DF, Schroeder FC (2020) Plant metabolism of nematode pheromones mediates plant-nematode interactions. *Nature Communications* 11:208. <https://doi.org/10.1038/s41467-019-14104-2>
- Manosalva P, Manohar M, Reuss SH von, Chen S, Koch A, Kaplan F, Choe A, Micikas RJ, Wang X, Kogel K-H, Sternberg PW, Williamson VM, Schroeder FC, Klessig DF (2015) Conserved nematode signalling molecules elicit plant defenses and pathogen resistance. *Nature Communications* 6:7795. <https://doi.org/10.1038/ncomms8795>
- Märländer B, Hoffmann C, Koch H-J, Ladewig E, Merkes R, Petersen J, Stockfisch N (2003) Environmental Situation and Yield Performance of the Sugar Beet Crop in Germany: Heading for Sustainable Development. *Journal of Agronomy and Crop Science* 189:201–226. <https://doi.org/10.1046/j.1439-037X.2003.00035.x>
- Martínez-Soto D, Ruiz-Herrera J (2016) Induced Resistance to *Ustilago maydis* in *Zea mays* Inoculated in Non-Sterile Conditions. *Int. J. Biotech. Well. Indus.* 5:51–59. <https://doi.org/10.6000/1927-3037.2016.05.02.4>
- Marzo C, Díaz AB, Caro I, Blandino A (2019) Chapter 4 - Status and Perspectives in Bioethanol Production From Sugar Beet. In: Ray RC, Ramachandran S (eds) *Bioethanol Production from Food Crops*. Academic Press, pp 61–79. <https://doi.org/10.1016/B978-0-12-813766-6.00004-7>
- Matz MV, Fradkov AF, Labas YA, Savitsky AP, Zaraisky AG, Markelov ML, Lukyanov SA (1999) Fluorescent proteins from nonbioluminescent Anthozoa species. *Nat Biotechnol* 17:969–973. <https://doi.org/10.1038/13657>
- Mazarei M, Lennon KA, Puthoff DP, Rodermeil SR, Baum TJ (2003) Expression of an Arabidopsis phosphoglycerate mutase homologue is localized to apical meristems, regulated by hormones, and induced by sedentary plant-parasitic nematodes. *Plant Molecular Biology* 53:513–530. <https://doi.org/10.1023/B:PLAN.0000019062.80459.80>

- McGrath JM, Funk A, Galewski P et al (2022) A contiguous *de novo* genome assembly of sugar beet EL10 (*Beta vulgaris* L.). DNA research: an international journal for rapid publication of reports on genes and genomes dsac033. <https://doi.org/10.1093/dnares/dsac033>
- McGrath JM, Panella L, Frese L (2011) Beta. In: Kole C (ed) Wild Crop Relatives: Genomic and Breeding Resources: Industrial Crops. Springer, Berlin, Heidelberg, pp 1–28. [https://doi.org/10.1007/978-3-642-21102-7\\_1](https://doi.org/10.1007/978-3-642-21102-7_1)
- McLean MD, Hoover GJ, Bancroft B, Makhmoudova A, Clark SM, Welacky T, Simmonds DH, Shelp BJ (2007) Identification of the full-length *HsI<sup>pro-1</sup>* coding sequence and preliminary evaluation of soybean cyst nematode resistance in soybean transformed with *HsI<sup>pro-1</sup>* cDNA. Canadian Journal of Botany 85:437–441. <https://doi.org/10.1139/B07-038>
- mdbaron42 (2021) pyBoxshade. GitHub
- Melillo MT, Leonetti P, Bongiovanni M, Castagnone-Sereno P, Bleve-Zacheo T (2006) Modulation of reactive oxygen species activities and H<sub>2</sub>O<sub>2</sub> accumulation during compatible and incompatible tomato–root-knot nematode interactions. New Phytologist 170:501–512. <https://doi.org/10.1111/j.1469-8137.2006.01724.x>
- Milford GFJ (1976) Sugar concentration in sugar beet: varietal differences and the effects of soil type and planting density on the size of the root cells. Annals of Applied Biology 83:251–257. <https://doi.org/10.1111/j.1744-7348.1976.tb00604.x>
- Molloy B, Shin DS, Long J et al (2024) The origin, deployment, and evolution of a plant-parasitic nematode effectorome. PLoS Pathogens 20:e1012395. <https://doi.org/10.1371/journal.ppat.1012395>
- Molloy B, Baum T, Eves-van den Akker S (2023) Unlocking the development- and physiology-altering ‘effector toolbox’ of plant-parasitic nematodes. Trends in Parasitology 39:732–738. <https://doi.org/10.1016/j.pt.2023.06.005>
- Müller J (1999) The economic importance of *Heterodera schachtii* in Europe. Helminthologia 36:205–213
- Müller J (1998) New pathotypes of the beet cyst nematode (*Heterodera schachtii*) differentiated on alien genes for resistance in beet (*Beta vulgaris*). Fundam. appl. Nematol. 21:519–526
- Müller J, Klinke A (1996) Selektion virulenter Populationen von *Heterodera schachtii* und ihre Nutzung zur Charakterisierung von Resistenzgenen in *Beta*-Rüben. Institut für Nematologie und Wirbeltierkunde: 50 Jahre Forschung am Standort Münster. Parley Buchverlag, Berlin-Dahlem, pp 102–116
- Müller J, Wyss U (1981) Entwicklung des Zystennematoden *Heterodera schachtii*. Institut für den Wissenschaftlichen Film 14
- Müller J, Rehbock K, Wyss U (1981) Growth of *Heterodera schachtii* with remarks on amounts of food consumed. Revue Nématol. 4:227–234
- Multamäki E, García de Fuentes A, Sieryi O, Bykov A, Gerken U, Ranzani AT, Köhler J, Meglinski I, Möglich A, Takala H (2022) Optogenetic Control of Bacterial Expression

## References

- by Red Light. *ACS Synth Biol* 11:3354–3367. <https://doi.org/10.1021/acssynbio.2c00259>
- Nachtigall M, Bülow L, Schubert J, Frese L (2016) Development of SSR markers for the genus *Patellifolia* (Chenopodiaceae). *Applications in Plant Sciences* 4:apps.1600040. <https://doi.org/10.3732/apps.1600040>
- Ng S, Ivanova A, Duncan O, Law SR, van Aken O, Clercq I de, Wang Y, Carrie C, Xu L, Kmiec B, Walker H, van Breusegem F, Whelan J, Giraud E (2013) A Membrane-Bound NAC Transcription Factor, ANAC017, Mediates Mitochondrial Retrograde Signaling in *Arabidopsis*. *The Plant Cell* 25:3450–3471. <https://doi.org/10.1105/tpc.113.113985>
- Nicol JM, Turner SJ, Coyne DL, Nijs L den, Hockland S, Maafi ZT (2011) Current Nematode Threats to World Agriculture. In: Jones J, Gheysen G, Fenoll C (eds) *Genomics and Molecular Genetics of Plant-Nematode Interactions*. Springer Netherlands, Dordrecht, pp 21–43. [https://doi.org/10.1007/978-94-007-0434-3\\_2](https://doi.org/10.1007/978-94-007-0434-3_2)
- Nielsen EL, Baltensperger DD, Kerr ED, Rife CL (2003) Host Suitability of Rapeseed for *Heterodera schachtii*. *Journal of Nematology* 35:35–38
- Noureddine Y, Mejias J, da Rocha M, Thomine S, Quentin M, Abad P, Favery B, Jaubert-Possamai S (2022) Copper microRNAs modulate the formation of giant feeding cells induced by the root knot nematode *Meloidogyne incognita* in *Arabidopsis thaliana*. *New Phytologist* 236:283–295. <https://doi.org/10.1111/nph.18362>
- Ødum MT, Teufel F, Thumuluri V, Almagro Armenteros JJ, Johansen AR, Winther O, Nielsen H (2024) DeepLoc 2.1: multi-label membrane protein type prediction using protein language models. *Nucleic Acids Research* 52:W215–W220. <https://doi.org/10.1093/nar/gkae237>
- Oostendorp M, Sikora RA (1989) Seed treatment with antagonistic rhizobacteria for the suppression of *Heterodera schachtii* early root infection of sugar beet. *Revue de Nématologie* 12:77–83
- Panella LW, Stevanato P, Pavli O, Skaracis G (2020) Source of Useful Traits. In: Biancardi E, Panella LW, McGrath JM (eds) *Beta maritima*. Springer International Publishing, Cham, pp 167–218. [https://doi.org/10.1007/978-3-030-28748-1\\_8](https://doi.org/10.1007/978-3-030-28748-1_8)
- Perry RN, Moens M, Jones JT, C.A.B. International (eds) (2018) *Cyst nematodes*. CAB International, Oxfordshire, UK, Boston, MA
- Pfaffl MW (2001) A new mathematical model for relative quantification in real-time RT-PCR. *Nucleic Acids Research* 29:e45–e45. <https://doi.org/10.1093/nar/29.9.e45>
- Pidkowich MS, Nguyen HT, Heilmann I, Ischebeck T, Shanklin J (2007) Modulating seed beta-ketoacyl-acyl carrier protein synthase II level converts the composition of a temperate seed oil to that of a palm-like tropical oil. *Proceedings of the National Academy of Sciences* 104:4742–4747. <https://doi.org/10.1073/pnas.0611141104>
- Pires D, Vicente CSL, Menéndez E, Faria JMS, Rusinque L, Camacho MJ, Inácio ML (2022) The Fight against Plant-Parasitic Nematodes: Current Status of Bacterial and Fungal Biocontrol Agents. *Pathogens* 11:1178. <https://doi.org/10.3390/pathogens11101178>

- Pogorelko GV, Juvale PS, Rutter WB, Hütten M, Maier TR, Hewezi T, Paulus J, van der Hoorn RAL, Grundler FMW, Siddique S, Lionetti V, Zobotina OA, Baum TJ (2019) Re-targeting of a plant defense protease by a cyst nematode effector. *The Plant Journal* 98:1000–1014. <https://doi.org/10.1111/tpj.14295>
- Pohlert T (2023) PMCMRplus: Calculate Pairwise Multiple Comparisons of Mean Rank Sums Extended. <https://CRAN.R-project.org/package=PMCMRplus>
- Poinar GO (2015) Chapter Two - The Geological Record of Parasitic Nematode Evolution. In: Baets K de, Littlewood DTJ (eds) *Advances in Parasitology*. Academic Press, pp 53–92. <https://doi.org/10.1016/bs.apar.2015.03.002>
- Qing X, Zhang YM, Sun S, Ahmed M, Lo W-S, Bert W, Holovachov O, Li H (2023) Phylogenomic Insights into the Evolution and Origin of Nematoda. *bioRxiv*. <https://www.biorxiv.org/content/10.1101/2023.12.13.571554v1>. Accessed 2 August 2024. <https://doi.org/10.1101/2023.12.13.571554>
- R Core Team (2024) R: A Language and Environment for Statistical Computing. R Foundation for Statistical Computing, Vienna, Austria. <https://www.R-project.org/>
- Reamon-Ramos SM, Wricke G (1992) A full set of monosomic addition lines in *Beta vulgaris* from *Beta webbiana*: morphology and isozyme markers. *Theoretical and Applied Genetics* 84:411–418. <https://doi.org/10.1007/BF00229501>
- Reeves PA, Richards CM (2022) A pan-genome data structure induced by pooled sequencing facilitates variant mining in heterogeneous germplasm. *Molecular Breeding* 42:36. <https://doi.org/10.1007/s11032-022-01308-6>
- Reeves PA, He Y, Schmitz RJ, Amasino RM, Panella LW, Richards CM (2007) Evolutionary Conservation of the FLOWERING LOCUS C-Mediated Vernalization Response: Evidence From the Sugar Beet (*Beta vulgaris*). *Genetics* 176:295–307. <https://doi.org/10.1534/genetics.106.069336>
- Reuther M, Lang C, Grundler FMW (2017) Nematode-tolerant sugar beet varieties - resistant or susceptible to the Beet Cyst Nematode *Heterodera schachtii*? *Sugar Industry/Zuckerindustrie* 142:277–284. <https://doi.org/10.36961/si18397>
- Reuther M, Lang C, Grundler F (2016) Die besten Pillen gegen Nematoden. *dlz agrarmagazin* 36–39
- Reynolds ES (1963) The use of lead citrate at high pH as an electron-opaque stain in electron microscopy. *J Cell Biol* 17:208–212. <https://doi.org/10.1083/jcb.17.1.208>
- Richardson KL (2018) Registration of Sugar Beet Germplasm Lines CN921-515 and CN921-516 with Sugar Beet Cyst Nematode Resistance from *Beta vulgaris* subsp. *maritima*. *Journal of Plant Registrations* 12:264–269. <https://doi.org/10.3198/jpr2017.09.0062crg>
- Rodríguez del Río Á, Minoche AE, Zwickl NF, Friedrich A, Liedtke S, Schmidt T, Himmelbauer H, Dohm JC (2019) Genomes of the wild beets *Beta patula* and *Beta vulgaris* ssp. *maritima*. *The Plant Journal* 99:1242–1253. <https://doi.org/10.1111/tpj.14413>

## References

- Rolland N, Bouchnak I, Moyet L, Salvi D, Kuntz M (2018) The Main Functions of Plastids. In: Maréchal E (ed) *Plastids: Methods and Protocols*. Springer US, New York, NY, pp 73–85. [https://doi.org/10.1007/978-1-4939-8654-5\\_5](https://doi.org/10.1007/978-1-4939-8654-5_5)
- Romeiras MM, Vieira A, Silva DN, Moura M, Santos-Guerra A, Batista D, Duarte MC, Paulo OS, Robillard T (2016) Evolutionary and Biogeographic Insights on the Macaronesian *Beta-Patellifolia* Species (Amaranthaceae) from a Time-Scaled Molecular Phylogeny. *PloS One* 11:e0152456. <https://doi.org/10.1371/journal.pone.0152456>
- Rota-Stabelli O, Daley AC, Pisani D (2013) Molecular Timetrees Reveal a Cambrian Colonization of Land and a New Scenario for Ecdysozoan Evolution. *Current Biology* 23:392–398. <https://doi.org/10.1016/j.cub.2013.01.026>
- Samuelian S, Kleine M, Ruyter-Spira CP, Klein-Lankhorst RM, Jung C (2004) Cloning and functional analyses of a gene from sugar beet up-regulated upon cyst nematode infection. *Plant Molecular Biology* 54:147–156. <https://doi.org/10.1023/B:PLAN.0000028776.30241.f3>
- Sandal NN, Salentijn EM, Kleine M, Cai D, Arens-de Reuver M, van Druten M, Bock TS de, Lange W, Steen P, Jung C, Marcker K, Stiekema WJ, Klein-Lankhorst RM (1997) Backcrossing of nematode-resistant sugar beet: a second nematode resistance gene at the locus containing *Hs1<sup>pro-1</sup>?* *Molecular Breeding* 3:471–480. <https://doi.org/10.1023/A:1009697119097>
- Savitsky H (1975) Hybridization between *Beta vulgaris* and *B. procumbens* and transmission of nematode (*Heterodera schachtii*) resistance to sugar beet. *Canadian Journal of Genetics and Cytology* 17:197–209. <https://doi.org/10.1139/g75-027>
- Savitsky H (1973) Meiosis in hybrids between *Beta vulgaris* L. and *Beta procumbens* Chr. Sm. and transmission of sugarbeet nematode resistance 74:241
- Sayers EW, Bolton EE, Brister JR et al (2022) Database resources of the national center for biotechnology information. *Nucleic Acids Research* 50:D20-D26. <https://doi.org/10.1093/nar/gkab1112>
- Schmidt T, Jung C, Heslop-Harrison JS, Kleine M (1997) Detection of alien chromatin conferring resistance to the beet cyst nematode (*Heterodera schachtii* Schm.) in cultivated beet (*Beta vulgaris* L.) using in situ hybridization. *Chromosome Research* 5:186–193. <https://doi.org/10.1023/A:1018447031020>
- Schratzberger M, Holterman M, van Oevelen D, Helder J (2019) A Worm’s World: Ecological Flexibility Pays Off for Free-Living Nematodes in Sediments and Soils. *BioScience* 69:867–876. <https://doi.org/10.1093/biosci/biz086>
- Schulte D, Cai D, Kleine M, Fan L, Wang S, Jung C (2006) A complete physical map of a wild beet (*Beta procumbens*) translocation in sugar beet. *Molecular Genetics and Genomics* 275:504–511. <https://doi.org/10.1007/s00438-006-0108-x>
- Scott AJ, Ford-Lloyd BV, Williams JT (1977) *Patellifolia*, nomen novum (Chenopodiaceae). *Taxon* 26:284. <https://doi.org/10.2307/1220567>
- Sharma SB (ed) (1998) *The Cyst Nematodes*. Springer Netherlands, Dordrecht. <https://doi.org/10.1007/978-94-015-9018-1>

- Siddique S, Radakovic ZS, Hiltl C et al (2022) The genome and lifestage-specific transcriptomes of a plant-parasitic nematode and its host reveal susceptibility genes involved in trans-kingdom synthesis of vitamin B5. *Nature Communications* 13:6190. <https://doi.org/10.1038/s41467-022-33769-w>
- Siddique S, Matera C, Radakovic ZS, Shamim Hasan M, Gutbrod P, Rozanska E, Sobczak M, Torres MA, Grundler FMW (2014) Parasitic Worms Stimulate Host NADPH Oxidases to Produce Reactive Oxygen Species That Limit Plant Cell Death and Promote Infection. *Science Signaling* 7. <https://doi.org/10.1126/scisignal.2004777>
- Sielemann K, Pucker B, Orsini E, Elashry A, Schulte L, Viehöver P, Müller AE, Schechert A, Weisshaar B, Holtgräwe D (2023a) Genomic characterization of a nematode tolerance locus in sugar beet. *BMC Genomics* 24:748. <https://doi.org/10.1186/s12864-023-09823-2>
- Sielemann K, Schmidt N, Guzik J, Kalina N, Pucker B, Viehöver P, Breitenbach S, Weisshaar B, Heitkam T, Holtgräwe D (2023b) Pangenome of cultivated beet and crop wild relatives reveals parental relationships of a tetraploid wild beet. *bioRxiv*. <https://www.biorxiv.org/content/10.1101/2023.06.28.546919v1>. Accessed 5 March 2024. <https://doi.org/10.1101/2023.06.28.546919>
- Sielemann K, Pucker B, Schmidt N, Viehöver P, Weisshaar B, Heitkam T, Holtgräwe D (2022) Complete pan-plastome sequences enable high resolution phylogenetic classification of sugar beet and closely related crop wild relatives. *BMC Genomics* 23:113. <https://doi.org/10.1186/s12864-022-08336-8>
- Sijmons PC, Atkinson HJ, Wyss U (1994) PARASITIC STRATEGIES OF ROOT NEMATODES AND ASSOCIATED HOST CELL RESPONSES. *Annual Review of Phytopathology* 32:235–259. <https://doi.org/10.1146/annurev.py.32.090194.001315>
- Sijmons PC, Grundler FM, Mende N von, Burrows PR, Wyss U (1991) *Arabidopsis thaliana* as a new model host for plant-parasitic nematodes. *The Plant Journal* 1:245–254. <https://doi.org/10.1111/j.1365-313X.1991.00245.x>
- Sikder MM, Vestergård M, Kyndt T, Topalović O, Kudjordjie EN, Nicolaisen M (2022) Genetic disruption of *Arabidopsis* secondary metabolite synthesis leads to microbiome-mediated modulation of nematode invasion. *ISME J* 16:2230–2241. <https://doi.org/10.1038/s41396-022-01276-x>
- Sikder MM, Vestergård M, Kyndt T, Kudjordjie EN, Nicolaisen M (2021) Phytohormones selectively affect plant parasitic nematodes associated with *Arabidopsis* roots. *New Phytologist* 232:1272–1285. <https://doi.org/10.1111/nph.17549>
- Simoni EB, Oliveira CC, Fraga OT, Reis PAB, Fontes EPB (2022) Cell Death Signaling From Endoplasmic Reticulum Stress: Plant-Specific and Conserved Features. *Frontiers in Plant Science* 13:835738. <https://doi.org/10.3389/fpls.2022.835738>
- Sobczak M, Golinowski W (2011) Cyst Nematodes and Syncytia. In: Jones J, Gheysen G, Fenoll C (eds) *Genomics and Molecular Genetics of Plant-Nematode Interactions*. Springer Netherlands, Dordrecht, pp 61–82. [https://doi.org/10.1007/978-94-007-0434-3\\_4](https://doi.org/10.1007/978-94-007-0434-3_4)

## References

- Sobczak M, Golinowski W, Grundler FMW (1999) Ultrastructure of feeding plugs and feeding tubes formed by *Heterodera schachtii*. *Nematology* 1:363–374. <https://doi.org/10.1163/156854199508351>
- Sobczak M, Golinowski W, Grundler FM (1997) Changes in the structure of *Arabidopsis thaliana* roots induced during development of males of the plant parasitic nematode *Heterodera schachtii*. *European Journal of Plant Pathology* 103:113–124. <https://doi.org/10.1023/A:1008609409465>
- Soulé S, Huang K, Mulet K, Mejias J, Bazin J, Truong NM, Kika JL, Jaubert S, Abad P, Zhao J, Favery B, Quentin M (2024) The root-knot nematode effector MiEFF12 targets the host ER quality control system to suppress immune responses and allow parasitism. *Molecular Plant Pathology* 25:e13491. <https://doi.org/10.1111/mpp.13491>
- Speckmann GJ, Bock TSM de (1982) The production of alien monosomic additions in *Beta vulgaris* as a source for the introgression of resistance to beet root nematode (*Heterodera schachtii*) from *Beta* species of the section *Patellares*. *Euphytica* 31:313–323. <https://doi.org/10.1007/BF00021646>
- Steele AE, Toxopeus H, Heijbroek W (1983) Susceptibility of plant selections to *Heterodera schachtii* and a race of *H. trifolii* parasitic on Sugarbeet in The Netherlands. *Journal of Nematology* 15:281–288
- Steele AE (1965) The host range of the sugar beet nematode, *Heterodera schachtii* Schmidt. *Journal of Sugarbeet Research* 13:573–603. <https://doi.org/10.5274/jsbr.13.7.573>
- Steiner AA (1968) Soilless Culture. Proceedings of the 6th colloquium of the International potash institute, Florence 324–341
- Stewart D (1950) Sugar Beet X *Beta Procumbens*, the F1 and Backcross Generations. American Society of Sugar Beet Technologists. <https://doi.org/10.5274/ASSBT.1952.176>
- Subbotin SA (2013) 7.19 Order Tylenchida Thorne, 1949 Volume 2 Nematoda. De Gruyter, pp 613–636. <https://doi.org/10.1515/9783110274257.613>
- Szota M (1995) Meiosis in species of sections *Procumbentes* and *Corollinae* and in interspecific hybrids within these sections and with sugarbeet (*Beta vulgaris* L.). (Mejoza gatunkow sekcji Procumbentes i Corollinae oraz miedzygatunkowych mieszanow w obrebie tych sekcji i z burakiem cukrowym (*Beta vulgaris* L.). *Hodowla Roślin, Aklimatyzacja i Nasiennictwo* 39:3–59
- Tamura K, Stecher G, Kumar S (2021) MEGA11: Molecular Evolutionary Genetics Analysis Version 11. *Molecular Biology and Evolution* 38:3022–3027. <https://doi.org/10.1093/molbev/msab120>
- Tang G-X, Knecht K, Yang X-F, Qin Y-B, Zhou W-J, Cai D (2011) A two-step protocol for shoot regeneration from hypocotyl explants of oilseed rape and its application for *Agrobacterium*-mediated transformation. *Biologia plant.* 55:21–26. <https://doi.org/10.1007/s10535-011-0003-0>
- Telford MJ, Boursat SJ, Economou A, Papillon D, Rota-Stabelli O (2008) The evolution of the Ecdysozoa. *Philosophical Transactions of the Royal Society B: Biological Sciences* 363:1529–1537. <https://doi.org/10.1098/rstb.2007.2243>

- Thomas EL, van der Hoorn RAL (2018) Ten Prominent Host Proteases in Plant-Pathogen Interactions. *International Journal of Molecular Sciences* 19:639. <https://doi.org/10.3390/ijms19020639>
- Thurau T, Ye W, Menkhau J, Knecht K, Tang G, Cai D (2010) Plant Nematode Control. *Sugar Tech* 12:229–237. <https://doi.org/10.1007/s12355-010-0056-y>
- Thurau T, Kifle S, Jung C, Cai D (2003) The promoter of the nematode resistance gene *HsI<sup>pro-1</sup>* activates a nematode-responsive and feeding site-specific gene expression in sugar beet (*Beta vulgaris* L.) and *Arabidopsis thaliana*. *Plant Molecular Biology* 52:643–660. <https://doi.org/10.1023/a:1024887516581>
- Tian Y (2003) PCR-based Cloning of the Second Nematode Resistance Gene *HsI-1<sup>pro-1</sup>* and Resistance Gene Analogues from Sugar Beet (*Beta vulgaris* L.), Christian-Albrechts University of Kiel
- Todd OE, Nielson AL, Fenwick A, Hanson LE, Richardson KL, Dorn KM (2024) Registration of sugar beet genetic stocks FC308 and FC309. *Journal of Plant Registrations* 18:187–196. <https://doi.org/10.1002/plr2.20345>
- Topalović O, Heuer H (2019) Plant-Nematode Interactions Assisted by Microbes in the Rhizosphere. *Curr Issues Mol Biol* 30:75–88. <https://doi.org/10.21775/cimb.030.075>
- Topalović O, Bak F, Santos S, Sikder MM, Sapkota R, Ekelund F, Nicolaisen MH, Vestergård M (2023) Activity of root-knot nematodes associated with composition of a nematode-attached microbiome and the surrounding soil microbiota. *FEMS Microbiology Ecology* 99:fiad091. <https://doi.org/10.1093/femsec/fiad091>
- Urban S, Dickey SW (2011) The rhomboid protease family: a decade of progress on function and mechanism. *Genome Biology* 12:231. <https://doi.org/10.1186/gb-2011-12-10-231>
- Urban S, Lee JR, Freeman M (2001) *Drosophila* Rhomboid-1 Defines a Family of Putative Intramembrane Serine Proteases. *Cell* 107:173–182. [https://doi.org/10.1016/S0092-8674\(01\)00525-6](https://doi.org/10.1016/S0092-8674(01)00525-6)
- Urwin PE, Møller SG, Lilley CJ, McPherson MJ, Atkinson HJ (1997) Continual Green-Fluorescent Protein Monitoring of Cauliflower Mosaic Virus 35S Promoter Activity in Nematode-Induced Feeding Cells in *Arabidopsis thaliana*. *Molecular Plant-Microbe Interactions* 10:394–400. <https://doi.org/10.1094/MPMI.1997.10.3.394>
- van Doorn WG, Beers EP, Dangl JL et al (2011) Morphological classification of plant cell deaths. *Cell Death & Differentiation* 18:1241–1246. <https://doi.org/10.1038/cdd.2011.36>
- van Geyt JPC, Lange W, Oleo M, Bock TSM de (1990) Natural variation within the genus *Beta* and its possible use for breeding sugar beet: A review. *Euphytica* 49:57–76. <https://doi.org/10.1007/BF00024131>
- van Geyt JPC, Oléo M, Lange W, Bock TSM de (1988) Monosomic additions in beet (*Beta vulgaris*) carrying extra chromosomes of *Beta procumbens*. 1. Identification of the alien chromosomes with the help of isozyme markers. *Theoretical and Applied Genetics* 76:577–586. <https://doi.org/10.1007/BF00260912>

## References

- Varadi M, Bertoni D, Magana P et al (2024) AlphaFold Protein Structure Database in 2024: providing structure coverage for over 214 million protein sequences. *Nucleic Acids Research* 52:D368-D375. <https://doi.org/10.1093/nar/gkad1011>
- Varadi M, Anyango S, Deshpande M et al (2022) AlphaFold Protein Structure Database: massively expanding the structural coverage of protein-sequence space with high-accuracy models. *Nucleic Acids Research* 50:D439-D444. <https://doi.org/10.1093/nar/gkab1061>
- Vasavada N (2016) Astatsa - Online Web Statistical Calculators. <https://astatsa.com/>
- Veronico P, Melillo MT, Saponaro C, Leonetti P, Picardi E, Jones JT (2010) A polygalacturonase-inhibiting protein with a role in pea defence against the cyst nematode *Heterodera goettingiana*. *Molecular Plant Pathology* 12:275–287. <https://doi.org/10.1111/j.1364-3703.2010.00671.x>
- Viglierchio DR (1960) Resistance in *Beta* species to the sugar beet nematode, *Heterodera schachtii*. *Experimental Parasitology* 10:389–395. [https://doi.org/10.1016/0014-4894\(60\)90075-8](https://doi.org/10.1016/0014-4894(60)90075-8)
- Wagner H, Gimbel E-M, Wricke G (1989) Are *Beta procumbens* Chr. Sm. and *Beta webbiana* Moq. Different Species? *Plant Breeding* 102:17–21. <https://doi.org/10.1111/j.1439-0523.1989.tb00309.x>
- Wang B, Yang X, Jia Y, Xu Y, Jia P, Dang N, Wang S, Xu T, Zhao X, Gao S, Dong Q, Ye K (2022) High-quality *Arabidopsis thaliana* Genome Assembly with Nanopore and HiFi Long Reads. *Genomics, Proteomics & Bioinformatics* 20:4–13. <https://doi.org/10.1016/j.gpb.2021.08.003>
- Wang J, Dhroso A, Liu X, Baum TJ, Hussey RS, Davis EL, Wang X, Korkin D, Mitchum MG (2021) Phytonematode peptide effectors exploit a host post-translational trafficking mechanism to the ER using a novel translocation signal. *New Phytologist* 229:563–574. <https://doi.org/10.1111/nph.16765>
- Watts A, Sankaranarayanan S, Watts A, Raipuria RK (2021) Optimizing protein expression in heterologous system: Strategies and tools. *Meta Gene* 29:100899. <https://doi.org/10.1016/j.mgene.2021.100899>
- Williams JT, Scott AJ, Ford-Lloyd BV (1976) *Patellaria*: A new genus in the Chenopodiaceae. *Feddes Repertorium* 87:289–292. <https://doi.org/10.1002/fedr.19760870502>
- Williamson V, Kumar A (2006) Nematode resistance in plants: the battle underground. *Trends in Genetics* 22:396–403. <https://doi.org/10.1016/j.tig.2006.05.003>
- Willig J-J, Guarneri N, van Loon T, Wahyuni S, Astudillo-Estévez IE, Xu L, Willemsen V, Goverse A, Sterken MG, Lozano-Torres JL, Bakker J, Smant G (2024) Transcription factor WOX11 modulates tolerance to cyst nematodes via adventitious lateral root formation. *Plant Physiology* kiae053. <https://doi.org/10.1093/plphys/kiae053>
- Willig J-J, Sonneveld D, van Steenbrugge JJM, Deurhof L, van Schaik CC, Teklu MG, Goverse A, Lozano-Torres JL, Smant G, Sterken MG, Dupuy L (2023) From root to shoot: quantifying nematode tolerance in *Arabidopsis thaliana* by high-throughput

- phenotyping of plant development. *Journal of Experimental Botany* 74:5487–5499. <https://doi.org/10.1093/jxb/erad266>
- Willig J-J, Guarneri N, van Steenbrugge JJM, Jong W de, Chen J, Goverse A, Lozano Torres JL, Sterken MG, Bakker J, Smant G (2022) The *Arabidopsis* transcription factor TCP9 modulates root architectural plasticity, reactive oxygen species-mediated processes, and tolerance to cyst nematode infections. *The Plant Journal* 112:1070–1083. <https://doi.org/10.1111/tpj.15996>
- Wojszko K, Różańska E, Sobczak M, Kuczerski K, Krępski T, Wiśniewska A (2023) The role of AtPP2-A3 and AtPP2-A8 genes encoding Nictaba-related lectin domains in the defense response of *Arabidopsis thaliana* to *Heterodera schachtii*. *Planta* 258:40. <https://doi.org/10.1007/s00425-023-04196-y>
- Wyss U, Grundler FMW (1992) Seminar: *Heterodera Schachtii* and *Arabidopsis Thaliana*, a Model Host-Parasite Interaction. *Nematologica* 38:488–493. <https://doi.org/10.1163/187529292X00450>
- Wyss U, Stender C, Lehmann H (1984) Ultrastructure of feeding sites of the cyst nematode *Heterodera schachtii* Schmidt in roots of susceptible and resistant *Raphanus sativus* L. var. *oleiformis* Pers. cultivars. *Physiological Plant Pathology* 25:21–37. [https://doi.org/10.1016/0048-4059\(84\)90015-8](https://doi.org/10.1016/0048-4059(84)90015-8)
- Wyss U (2002) Feeding Behavior of Plant-Parasitic Nematodes. In: Lee D (ed) *The Biology of Nematodes*. CRC Press, pp 233–260. <https://doi.org/10.1201/b12614-10>
- Wyss U (1992) Observations on the feeding behaviour of *Heterodera schachtii* throughout development, including events during moulting. *Fund. Appl. Nematol* 15
- Wyss U, Zunke U (1986) Observations on the behaviour of second stage juveniles of *Heterodera schachtii* inside host roots 9:153–165
- Xie Y, Liu B, Zhou Z, Gao K, Yin H, Zhao Y, Liu Q (2024) *PmHs1* monitors *Bsursaphelenchus xylophilus* infection and activates defensive response in resistant *Pinus massoniana*. *Plant, Cell & Environment* n/a:1–14. <https://doi.org/10.1111/pce.15025>
- Xue G, Wu W, Fan Y, Ma C, Xiong R, Bai Q, Yao X, Weng W, Cheng J, Ruan J (2024) Genome-wide identification, evolution, and role of SPL gene family in beet (*Beta vulgaris* L.) under cold stress. *BMC Genomics* 25:101. <https://doi.org/10.1186/s12864-024-09995-5>
- Yang Y, Chou H-L, Crofts AJ, Zhang L, Tian L, Washida H, Fukuda M, Kumamaru T, Oviedo OJ, Starkenburg SR, Okita TW (2018) Selective sets of mRNAs localize to extracellular paramural bodies in a rice *glup6* mutant. *Journal of Experimental Botany* 69:5045–5058. <https://doi.org/10.1093/jxb/ery297>
- Yoon J, Cho L-H, Tun W, Jeon J-S, An G (2021) Sucrose signaling in higher plants. *Plant Science* 302:110703. <https://doi.org/10.1016/j.plantsci.2020.110703>
- Yu MH (1984) Resistance to *Heterodera schachtii* in *Patellares* section of the genus *Beta*. *Euphytica* 33:633–640. <https://doi.org/10.1007/BF00021891>

## References

- Zamioudis C, Pieterse CMJ (2012) Modulation of host immunity by beneficial microbes. *Molecular Plant-Microbe Interactions*® 25:139–150. <https://doi.org/10.1094/MPMI-06-11-0179>
- Zhong X, Zhou Q, Cui N, Cai D, Tang G (2019) *BvcZR3* and *BvHsI<sup>pro-1</sup>* Genes Pyramiding Enhanced Beet Cyst Nematode (*Heterodera schachtii* Schm.) Resistance in Oilseed Rape (*Brassica napus* L.). *International Journal of Molecular Sciences* 20:1740. <https://doi.org/10.3390/ijms20071740>

## 11 Supplementary data provided only electronically

The following files and data are provided only electronically.

Folder name	Subfolder or file name	Content	Format
1. Chapter2_ BetaAndPatellifolia	1 SangerSequencing_ RawData	Sanger sequencing raw reads for 21 <i>Patellifolia</i> and <i>Beta</i> species/accessions sequenced	.ab1
	2 Assembled sequences	ORF, CDS, and protein sequences of 35 <i>Hs4</i> - and <i>BvHs4</i> -homologs assembled anew or retrieved from reference sequences	.clc
	3 Reference sequence	whole genomic annotated <i>Hs4</i> reference sequence obtained from A. Kumar and altered after sequencing	.clc
	4 Alignments	alignments of ORF, CDS, or protein sequences of the different homologs	.clc or .fas
	Expression across all <i>Patellifolia</i> and <i>Beta</i>	RT-qPCR data for all <i>Patellifolia</i> and <i>Beta</i> species/accessions	.xlsx
	Expression under nematode infestation	RT-qPCR data of different tissues at various developmental stages and with nematode infection of <i>P. procumbens</i> and <i>B. vulgaris</i> ; female count data	.xlsx
2. Chapter3_ Arabidopsis	FemaleCounts_ Arabidopsis	female count data of all Arabidopsis nematode inoculation experiments	.xlsx
	RT-qPCR_ Arabidopsis	RT-qPCR data for all Arabidopsis expression analyses	.xlsx
3. Chapter5_ Rapeseed	PhenotypicData	dates of transformation, transfer to soil, genotyping, flowering, etc. for all 66 rapeseed plants tested	.xlsx

## 12 Curriculum Vitae and Publications

### 12.1 Curriculum vitae

<b>Personal Data</b>	
Name	Annika Carolin Schildberg
Date of birth	29.04.1996
Place of birth	Speyer, Germany
Nationality	German
<b>Education</b>	
May 2021 – present	<b>Ph.D. student at the Plant Breeding Institute, Christian-Albrechts-University of Kiel, Germany</b> Thesis title: Studying the cyst nematode resistance gene <i>Hs4</i> in different genomic backgrounds
October 2018 – April 2021	<b>M. Sc. in AgriGenomics, Christian-Albrechts-University of Kiel, Germany</b> Thesis title: Overexpression and promoter studies of <i>SUPPRESSOR OF OVEREXPRESSION OF CONSTANS1</i> ( <i>Bna.SOC1.A05</i> ) in <i>Arabidopsis thaliana</i>
October 2015 – September 2018	<b>B. Sc. in Biology, University of Greifswald, Germany</b> Thesis title: Etablierung eines Mikrofluidsystems zur Untersuchung Zellkultur-basierter Endothelzellinfektionen mit <i>Streptococcus pneumoniae</i>

### 12.2 Oral and poster presentations

**Schildberg, A., Defant, B., Schneider, M., and Jung, C. (2022).** Unravelling the function of the cyst nematode resistance gene *Hs4* in different genomic backgrounds. Kiel Plant Center (KPC) Summer Event, 05.09.2022, Kiel, Germany. Poster presentation

**Schildberg, A. and Jung, C. (2023).** Unravelling the function of the cyst nematode resistance gene *Hs4* in different genomic backgrounds. 51st meeting of the Deutsche Phytomedizinische Gesellschaft (DPG) research group nematology, 08.-09.03.2023, Julius-Kühn-Institute, Braunschweig, Germany. Oral presentation

**Schildberg, A. and Jung, C. (2023).** Unravelling the function of the cyst nematode resistance gene *Hs4* in different genomic backgrounds. KPC Mini Symposium, 08.06.2023, Kiel, Germany. Oral presentation

**Schildberg, A. and Jung, C. (2024).** Unravelling the function of the cyst nematode resistance gene *Hs4* in different genomic backgrounds. German Plant Breeding Conference 2024 – Accelerating Crop Genetic Gain, 19.-21.03.2024, Geisenheim, Germany. Oral presentation

**Schildberg, A. and Jung, C. (2024).** Unravelling the function of the cyst nematode resistance gene *Hs4* in different genomic backgrounds. 35<sup>th</sup> Symposium of the European Society of Nematologists, 15.-19.04.2024, Córdoba, Spain. Oral presentation

### **13 Publications and declaration of own contribution**

I hereby declare that the chapters of this thesis are not yet published. They include the contributions of the doctoral candidate alone.

## 14 Acknowledgements

First, it must be acknowledged that the thesis was conducted under the supervision and supported financially by Prof. Dr. Christian Jung. I thank him for this opportunity and for his invaluable expertise and guidance on experimental design and research work.

I want to give a huge “thank you” to Birgit Defant and Maike Schneider for introducing me to ‘How to handle nematodes’, for their constant help, and for sticking with me through the ups and downs of lab work repetitions. I would also like to thank Brigitte Neidhardt-Olf and Ines Schütt who jumped in and helped when additional hands were required, and thank you to all the TAs for always having an open ear for my questions.

I would like to thank Dr. Siegbert Melzer for sharing his vast knowledge of conventional and non-conventional lab techniques with me and aiding me in trying to find explanations for unexplainable results.

Further, I would like to acknowledge the basic introduction to statistics given to me by Dr. Nazgol Emrani and the important lesson on the abysses of human social behavior taught.

A big thank you to Dr. Matthias Daub from the JKI for providing in-depth information about nematodes and the *H. betae* inoculum itself, even though this experiment’s results didn’t make it into this thesis. And thank you for sharing the pictures of the infested sugar beets!

Thank you also to Dr. Katja Richert-Pöggeler and Verena Maibaum from the electron microscopy of the JKI in Braunschweig who introduced me to the protocol for sample embedding, showed me how the sectioning devices worked and with whom I had a first glimpse at my very first embedded Arabidopsis roots, even though these test samples also did not make it into this thesis.

I am very grateful to Dr. Urska Repnik from the central microscopy of the CAU Kiel for making time to sit with me at the electron microscopes and analyze the Arabidopsis root samples, for showing me the beauty of electron microscopic images (especially Golgi!), for questioning aspects that were obvious to me, which ultimately made me dig deeper into the ultrastructural makeup of syncytia, for helping me clarify what we observed on the screen and for sharing and enjoying the moment of the first membrane aggregation discovery. I am also indebted to Ulrike Voigt who did a great job sectioning my embedded blocks and took notes so that I could follow up on what was happening and who was so excited when she learned she could identify the state of the syncytium already under the light microscope by its opaque or translucent appearance.

I would also like to acknowledge the Sanger sequencing service of the Institute of Clinical Molecular Biology in Kiel.

Thank you to my Mamma Mia-girls for always supporting me from the distance. A huge thank you goes to dear Tara for sharing her expertise in the English language with me!

I am incredibly thankful to my Ph.D. colleagues Amar, Ehsan, Kea, and Sarah, who had an open ear for my struggles and made the time at the institute much more enjoyable – even though all but one left it before I did. I would like to express my heartfelt gratitude, especially to Kea, who always tried to help me solve my frequent lab problems, who showed me how to transform rapeseed, shared her lab knowledge with me, made me laugh and laughed with me at the mess we were trapped in but also gave me a shoulder to cry on when it was necessary, and who became a really good friend during the past three and a half years.

Last but not least I want to thank my family, my best friend, and, most of all, my boyfriend, for always supporting me throughout my studies, keeping my back clear, and trying to understand what the heck I was actually doing. An amazingly huge thank you to my boyfriend

who was always in the direct fireline when I came home stressed from work but who managed to stick with me through the stressful and strenuous times of a B.Sc., M.Sc., and now a Ph.D. thesis!

Finally, I would like to thank the Walt Disney Animation Studios and Walt Disney Pictures for creating the ingeniously sappy rooster Heihei whose disbelief when finding himself out on the ocean made me think of my own situation more than once.